Shaping Nonlinearity in Reset Control Systems to Realize Complex-Order Controllers Application in Precision Motion Control

Karbasizadeh, Nima

DOI
10.4233/uuid:81a0f1cc-aba6-4cd5-8d8e-d6732c29ea2a

Publication date
2023

Document Version
Final published version

Citation (APA)
Karbasizadeh, N. (2023). *Shaping Nonlinearity in Reset Control Systems to Realize Complex-Order Controllers: Application in Precision Motion Control*. [Dissertation (TU Delft), Delft University of Technology]. https://doi.org/10.4233/uuid:81a0f1cc-aba6-4cd5-8d8e-d6732c29ea2a

Important note
To cite this publication, please use the final published version (if applicable).
Please check the document version above.

Shaping Nonlinearity in Reset Control Systems to Realize Complex-Order Controllers:

Application in Precision Motion Control

Shaping Nonlinearity in Reset Control Systems to Realize Complex-Order Controllers:

Application in Precision Motion Control

Dissertation

for the purpose of obtaining the degree of doctor
at Delft University of Technology
by the authority of the Rector Magnificus,
Prof.dr.ir. T.H.J.J. van der Hagen,
chair of the Board for Doctorates
to be defended publicly on 20 September 2023 at 10:00 o'clock.

by

Nima KARBASIZADEH ESFAHANI

Master of Science in Mechatronics Engineering, University of Tehran, Iran,
born in Esfahan, Iran.

This dissertation has been approved by the promotors.

Composition of the doctoral committee:

Rector Magnificus,	Chairperson
Prof. dr. ir. J.L. Herder,	Delft University of Technology (Promotor)
Dr. S.H. Hossein Nia Kani,	Delft University of Technology (Co-Promotor)
Independent members:	
Prof. dr. J.T. Gravdahl,	Norwegian University of Science and Technology
Dr. I. Tejdo,	University of Extremadura
Prof. dr. ir. T.A.E. Oomen,	Delft University of Technology & Eindhoven University of Technology
Prof. dr. ir. J.W. van Wingerden,	Delft University of Technology
Other members:	
Prof. dr. ir. M.F. Heertjes,	Eindhoven University of Technology & ASML

Keywords: Reset Control, Complex-Order Control, Shaping Nonlinearity, Precision Motion Control

Printed by: ProefschriftMaken || www.proefschriftmaken.nl

Front & Back: The concept created by Midjourney AI with the title of this dissertation as input.

Cover Layout: Ali Amoozandeh

ISBN 978-94-6384-484-0

An electronic version of this dissertation is available at
http://repository.tudelft.nl/.

To Delaram, Elaheh and Hamidreza,
For making me feel loved

CONTENTS

SUMMARY

This dissertation addresses the demand for faster, more precise, and robust controllers in the precision motion industry. Traditional linear controllers have limitations due to the waterbed effect and Bode's phase-gain relationship. To overcome these limitations, complex-order controllers are explored in this study. The dissertation focuses on shaping nonlinearities in reset controllers to realize complex-order behavior. Various methods and approaches are investigated, each contributing to the understanding and improvement of reset control systems for linear time-invariant systems.

The dissertation demonstrates that reset controllers exhibit first-order harmonic behavior, which can be advantageous in achieving complex-order behavior and enhancing controller performance compared to linear controllers. However, higher-order harmonics resulting from nonlinearities play a significant role and should not be neglected. The study explores methods to shape and manipulate these higher-order harmonics for improved performance.

Different approaches are categorized into two main categories: methods based on shaping the reset phase (ψ) and continuous reset (CR) methods. In the first category, ψ-shaping methods focus on manipulating ψ to achieve desirable non-linear behaviors. This includes the introduction of elements such as fractional-order lag elements and filters to shape ψ and suppress higher-order harmonics. The dissertation presents practical frameworks for analyzing and utilizing ψ-shaping concepts.

The second category, continuous reset methods, addresses both transient and steady-state performance. By introducing lead and lag elements as pre- and post-filters for reset elements, improvements in transient response are achieved. Additionally, CR methods preserve the first-order harmonic behavior while reducing higher-order harmonics across the entire frequency range. The dissertation highlights the advantages and trade-offs between ψ-shaping and CR methods, providing insights for selecting the appropriate approach based on application requirements.

Practical implementation aspects are also considered throughout the dissertation. Challenges such as noise amplification caused by lead elements in CR architectures are addressed, offering solutions through increased filter orders or observer-based filtering techniques. The dissertation demonstrates the effectiveness of the proposed approaches through implementation in industrial precision motion stages, showcasing the superiority of complex-order reset controllers over their linear counterparts.

Overall, this dissertation contributes to the understanding and practical implementation of reset controllers for realizing complex-order behavior in precision motion control. It provides insights into shaping nonlinearities, optimizing steady-state and transient performance, and selecting suitable architectures based on specific application needs. The findings and guidelines presented in this study offer valuable contributions to the precision motion industry and pave the way for further advancements in controller design and performance.

SAMENVATTING

Dit proefschrift gaat in op de vraag naar snellere, nauwkeurigere en robuustere regelaars voor precisiebewegingen. Traditionele lineaire regelaars hebben beperkingen door het waterbedeffect en Bode's fase-versterkingsrelatie. Om deze beperkingen te overwinnen worden in deze studie complexe-orde regelaars onderzocht. Het proefschrift richt zich op het vormen van niet-lineariteiten in reset-controllers om complex-orde gedrag te realiseren. Verschillende methoden en benaderingen worden onderzocht, die bijdragen aan het begrip en de verbetering van reset regelsystemen voor lineaire tijd-invariante systemen.

Het proefschrift toont aan dat reset-regelaars eerste-orde harmonisch gedrag vertonen, wat voordelig kan zijn voor het bereiken van complex-orde gedrag en het verbeteren van regelaarprestaties in vergelijking met lineaire regelaars. Hogere-orde harmonischen als gevolg van niet-lineariteiten spelen echter een belangrijke rol en mogen niet worden verwaarloosd. De studie onderzoekt methoden om deze hogere-orde harmonischen vorm te geven en te manipuleren voor betere prestaties.

De verschillende benaderingen worden ingedeeld in twee hoofdcategorieën: methoden gebaseerd op het vormen van de resetfase (ψ) en continue resetmethoden (CR). In de eerste categorie richten de methoden voor het vormen van de ψ zich op het manipuleren van de ψ om gewenst niet-lineair gedrag te bereiken. Dit omvat het invoeren van elementen zoals fractionele-orde vertragingselementen en filters om ψ te vorm te geven en hogere-orde harmonischen te onderdrukken. Het proefschrift presenteert praktische kaders voor het analyseren en toepassen van ψ-vormingsconcepten.

De tweede categorie, continue reset-methoden, behandelt zowel de prestaties voor transiënt en stationair gedrag. Door voor- en na-ijl elementen te introduceren als voor- en nafilters voor reset-elementen, worden verbeteringen in de transiente respons bereikt. Bovendien behouden CR-methoden het eerste-orde harmonische gedrag, terwijl hogere-orde harmonischen over het gehele frequentiebereik worden verminderd. De dissertatie belicht de voordelen en afwegingen tussen de methoden van ψ-shaping en CR, en biedt inzicht in de keuze van de juiste aanpak op basis van de toepassingseisen.

In het hele proefschrift worden ook praktische uitvoeringsaspecten behandeld. Uitdagingen zoals ruisversterking door voorijl elementen in CR-architecturen worden behandeld, waarbij oplossingen worden geboden door grotere filterorders of op waarnemers gebaseerde filtertechnieken. Het proefschrift demonstreert de effectiviteit van de voorgestelde benaderingen door implementatie in industriële precisiebewegingen, en toont de superioriteit van complexe-orde reset regelaars ten opzichte van hun lineaire tegenhangers.

In het algemeen draagt dit proefschrift bij aan het begrip en de praktische implementatie van reset controllers voor het realiseren van complex-orde gedrag in precisiebewegingen. Het biedt inzicht in het vormgeven van niet-lineariteiten, het optimaliseren van stabiele en voorbijgaande prestaties en het selecteren van geschikte architecturen op

basis van specifieke toepassingsbehoeften. De bevindingen en richtlijnen in deze studie leveren een waardevolle bijdrage aan de industrie van precisiebewegingen en effenen het pad voor verdere vooruitgang in het ontwerp en de prestaties van regelaars.

1

INTRODUCTION

The precision motion industry has an ever-increasing demand for faster, more precise, and more robust controllers. From the perspective of the frequency domain and loop-shaping technique, this demand has driven linear controllers to their inherent limits, namely, the waterbed effect and Bode's phase-gain relationship. Mathematically, complex-order transfer functions are not bound by Bode's phase-gain relationship. However, implementing them in practice is a challenge to solve. This dissertation will show how shaping nonlinearities in reset controllers contributes to realizing complex-order controllers with mainly for application in precision motion control.

1.1. COMPLEX-ORDER TRANSFER FUNCTIONS

A derivative of complex order can be defined in a variety of ways. But it is commonly indicated by the operator $D^{\alpha+j\beta}$, where $\alpha + j\beta \in \mathbb{C}$. The simplest corresponding transfer function in the Laplace domain will be $G(s) = s^{\alpha+j\beta}$. The frequency response of such a transfer function is given in [1].

$$20\log_{10}|G(j\omega)| = 20\alpha\log_{10}\omega + 20\log_{10}e^{-\frac{\beta\pi}{2}} \tag{1.1}$$

$$\angle G(j\omega) = \frac{\alpha\pi}{2} + \beta\log(10)\log_{10}\omega \tag{1.2}$$

$$\tag{1.3}$$

When $\alpha < 0$ and $\beta > 0$, the frequency response will show a negative gain slope and a positive phase slope, for which there is no practical implementation method in the linear domain. However, such frequency response is highly desirable, especially in precision motion control, since one can, for example, increase the bandwidth of the system without sacrificing the phase margin [2]. However, this complex-order transfer is not directly implementable. Approximations with linear transfer functions through methods like CRONE [3] often result in unstable poles or non-minimum phase zeros appearing in the controller [1]. Hence, recently researchers turned to nonlinear controllers for such approximation.

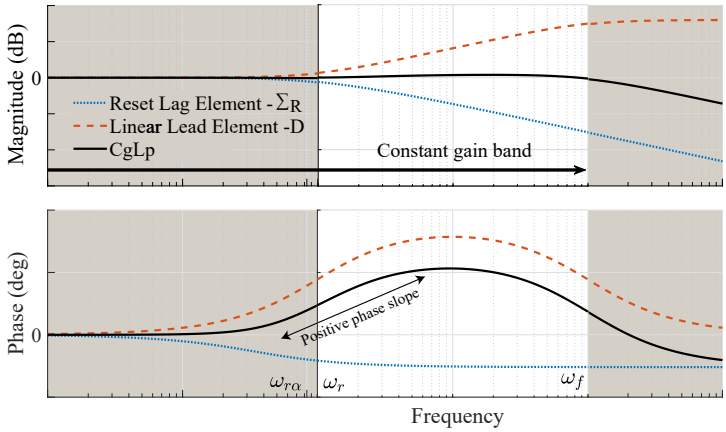

Figure 1.1: The concept of using combination of a reset lag and a linear lead element to form a CgLp element. The figure is from [10].

1.2. RESET CONTROL SYSTEMS

Reset control systems are one of the simplest nonlinear control systems used to approximate complex-order transfer functions. Reset controllers were first proposed by Clegg [4] in the form of a reset integrator that can improve the transient response of a control system. To address the drawbacks and exploit the benefits, the idea was later extended to more sophisticated elements such as "First-Order Reset Element" [5], [6] and "Second-Order Reset Element" [7] or using Clegg's integrator in the form of PI+CI [8] or resetting the state to a fraction of its current value, known as partial resetting [9]. However, most of the research done in reset control theory lacks either a frequency domain and loop-shaping perspective or industrial applicability.
Among different forms of reset control systems, the following is the most common

$$\sum_R = \begin{cases} \dot{x}_r(t) = A_r x_r(t) + B_r e(t), & \text{if } e(t) \neq 0 \\ x_r\left(t^+\right) = A_\rho x_r(t), & \text{if } e(t) = 0 \\ u(t) = C_r x_r(t) + D_r e(t) \end{cases} \tag{1.4}$$

where A_r, B_r, C_r, D_r denote the state space matrices of the Base Linear System (BLS) and the reset matrix is denoted by $A_\rho = \text{diag}(\gamma_1, ..., \gamma_n)$ which contains the reset coefficients for each state. $e(t)$ and $u(t)$ represent the input and output of the reset controller, respectively.

1.3. DESCRIBING FUNCTIONS

Because of its nonlinearity, the steady state response of a reset element to a sinusoidal input is not sinusoidal. Thus, its frequency response should be analyzed using approximations such as the Describing Function (DF) method [11]. However, the DF method only takes into account the first harmonic of the Fourier series decomposition of the output and neglects the effects of the higher-order harmonics. As shown in [12], this simpli-

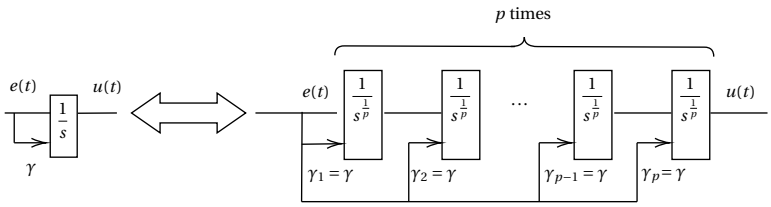

Figure 1.2: The concept of augmenting the reset state to shape the nonlinearities which is presented in Chaper 2

fication can sometimes be significantly inaccurate. To have more accurate information about the frequency response of nonlinear systems, a method called "Higher Order Sinusoidal Input Describing Function" (HOSIDF) has been introduced in [13]. This method was developed in [14] for reset elements. Throughout this dissertation, the HOSIDF equations for different situations are presented accordingly.

1.4. RESET CONTROL SYSTEMS AND COMPLEX-ORDER TRANSFER FUNCTIONS

Recently some steps have been taken to use the reset control in approximating complex-order transfer functions [1], [10]. One specific type of reset controller named "Constant in Gain, Lead in Phase" (CgLp), which is introduced in [10], has a constant gain over a tunable frequency range while providing phase lead. According to (1.1), such frequency domain behaviour resembles that of $s^{j\beta}$. Such an element can be created by multiplying a reset lag element and a linear lead element. Figure 1.1 depicts the frequency response of such an element. The advantageous phase lead of this element is due to the fact that the reset elements have a lower phase delay than their linear counterparts. The frequency response of this element does not follow Bode's phase-gain relationship. This element can partly replace the derivative action in a PID framework. However, this figure shows the approximate frequency response behaviour of CgLp based on Describing Function (DF) method. In this method, only the first harmonic of the Fourier transform of the response is considered, and higher-order harmonics are neglected. In some cases, this assumption can be inaccurate with regard to severe performance deterioration caused by higher-order harmonics [12].

1.5. RESEARCH OBJECTIVE: SHAPING NONLINEARITIES IN RESET CONTROL SYSTEMS

Higher-order harmonics directly result from nonlinearity in the reset control systems. Therefore, they cannot be totally eliminated, as the resultant system will be linear and therefore bound by the inherent limitations of linear systems. Nevertheless, the nonlinearity and, therefore, the higher-order harmonics in reset control systems can be shaped to minimise the disadvantages and maximise the advantages. This section will briefly introduce some sub-questions and methods for shaping the nonlinearity of reset control systems.

1

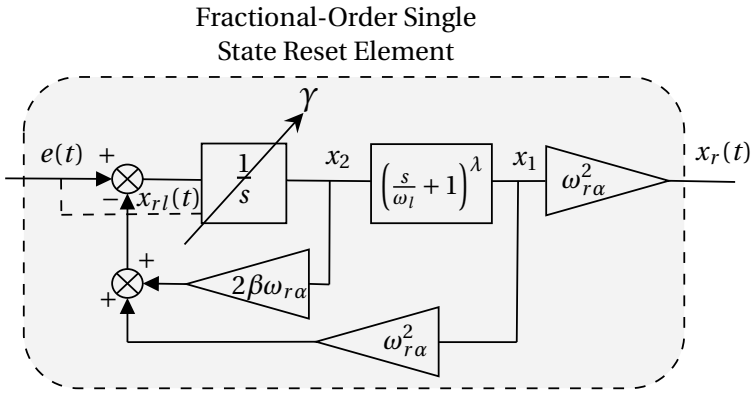

Figure 1.3: Block diagram of the a FOSRE element used in Chapter 3. $\gamma \in (0\ -1]$

1.5.1. SHAPING NONLINEARITY BY AUGMENTING THE RESET STATE

This concept is presented in Chapter 2 and chronologically is the first method used in this dissertation for this purpose. Although the idea was not investigated further, it showed a clear way forward, which is used in the following chapters. This chapter uses the the architecture shown in Fig. 1.2, in which the reset state is broken down into sub-states and then an optimization is used to determine the reset coefficient for these sub-states to keep the first-order harmonic intact and lower the magnitude of higher-order harmonics as much as possible. The study shows the feasibility of shaping nonlinearity. Furthermore, it shows that the sequence of the sub-states is of importance and the sub-states closer to the output of the element should be closer to linearity for a better result. This observation is further investigated and exploited in other parts of the dissertation.

1.5.2. SHAPING NONLINEARITY BY PHASE SHAPING THE RESET CONDITION

In Chapter 3, 4 and 5, architectures for reset controllers are introduced which rely on the concept of shaping the reset condition for shaping nonlinearities in reset controllers. These studies use the following definition for the reset control system

$$\sum_R = \begin{cases} \dot{x}_r(t) = A_r x_r(t) + B_r e(t), & \text{if } x_{rl}(t) \neq 0 \\ x_r\left(t^+\right) = A_\rho x_r(t), & \text{if } x_{rl}(t) = 0 \\ u(t) = C_r x_r(t) + D_r e(t) \end{cases} \tag{1.5}$$

It should be noted that the reset condition is not the zero-crossing of the input to the reset element but a different signal named $x_{rl}(t)$. These studies show that assuming a sinusoidal input to the element, $\psi(\omega) := \angle \frac{X_r(j\omega)}{X_{rl}(j\omega)}$ changes the behaviour of the element, where X_r, X_{rl} stand for Laplace transform of $x_r(t)$ and $x_{rl}(t)$. In the special case of $\psi(\omega) = 0$, $x_{rl}(t) = 0$ implies $x_r(t) = 0$. Then it implies that at the reset instant, $x_r(t^+) = x_r(t) = 0$. It means that the after-reset state value is the same as the current state value, and practically, the reset action has no effect, and the system always remains in the linear regime; thus, higher-order harmonics will be zero at all frequencies satisfying $\psi(\omega) = 0$. These researches also study $\psi(\omega) \neq 0$ and how it affects the behaviour of

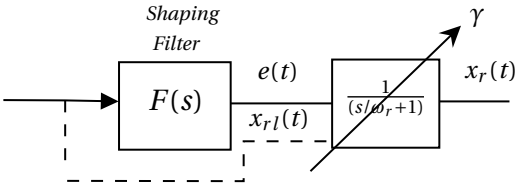

Figure 1.4: The architecture used in Chapter 4 for shaping the phase $\psi(\omega)$. Arrow indicates the resetting action.

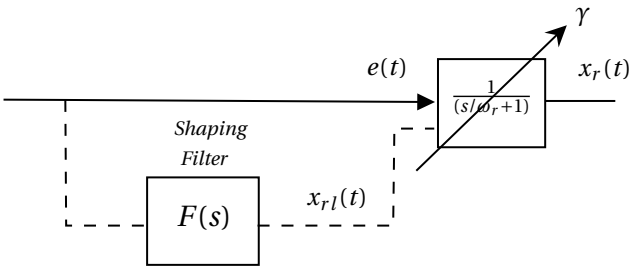

Figure 1.5: The architecture used in Chapter 5 for shaping the phase $\psi(\omega)$. Arrow indicates the resetting action.

the system.

The shaping of the phase $\psi(\omega)$ is done in different ways in these chapters. Chapter 3, introduces a fractional-order reset element that has a single resetting state. The element is named Fractional-Order Single State Reset Element (FOSRE). This chapter shows how the extra tunability of a fractional-order element helps achieve $\psi(\omega) = 0$ at a desired frequency. The architecture used in this chapter is presented in Fig. 1.3.

In turn, Chapter 4 introduces a simpler architecture and a more systematic approach to shape $\psi(\omega)$. In this chapter, the focus of shaping is to confine the nonlinearity of the reset control system to a desired range of frequencies. In other words, the higher-order harmonics can be band-passed using this method. The suggested architecture is shown in Fig. 1.4. The tuning method for shaping filter, $F(s)$ to achieve such an objective is also introduced in Chapter 4.

Chapter 5 uses a shaping filter to shape $\psi(\omega)$. Figure 1.5 shows the block diagram of the architecture used in Chapter 5. In Chapter 5, a method of tuning is introduced for the shaping filter, $F(s)$, which allows different phase slopes to be achieved. In other words, with a combination of this element and a linear lead filter, an approximation of $s^{j\beta}$ can be achieved for a desired value of β.

1.5.3. SHAPING NONLINEARITY BY PRE- AND POST-FILTERING A RESET ELEMENT: CONTINUOUS RESET (CR) STRUCTURE

Another important common property of all reset elements in the literature is the discontinuity of the output signal. This property is a cause for the presence of high-frequency content in the signals and other practical issues, such as large jumps in control signals that can saturate actuators. The concept of pre- and post-filtering (see Fig. 1.6) appears in the signal processing literature [15] and in the context of nonlinear control

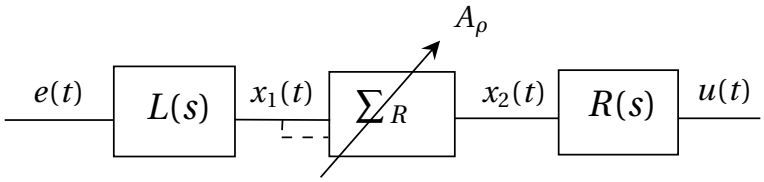

Figure 1.6: The architecture used in Chapter 6 for shaping nonlinearity in reset controllers.

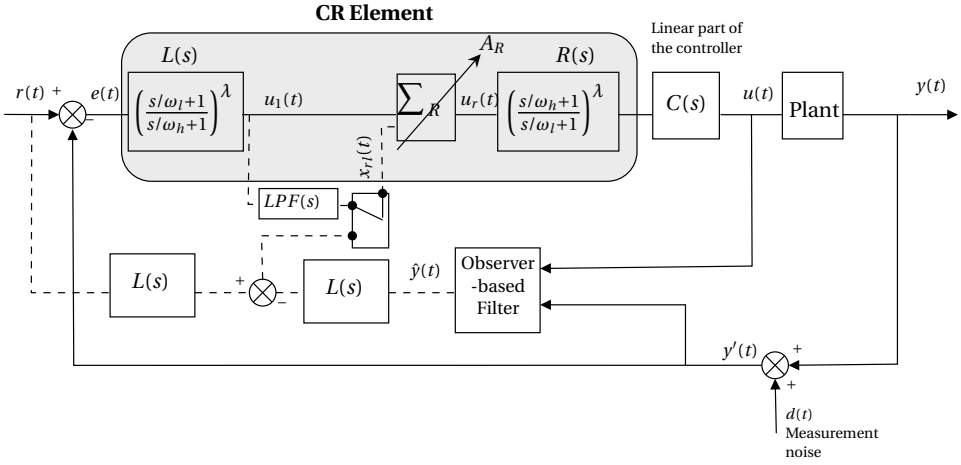

Figure 1.7: The concept of using higher-order lead and lag element and an observer-based filter in CR CgLp to have less amplification of high-frequency content of noisy reset signal.

elements, [16], [17]. Unlike [16], which focuses on studying amplitude-dependent nonlinearity, [17] explores a reset-like control that is independent of amplitude. Chapter 6 employs a strategy similar to that in [17] to preserve the first harmonic. However, it demonstrates the opposite requirement for the prefilter, advocating that it be a lead filter instead of the low-pass filter used in [17]. The utilization of a lag pre-filter, as in [17], can indeed enhance noise rejection but will also lead to an increase in higher-order harmonics [18]. On the other hand, as proposed in Chapter 7.3, employing a lead pre-filter yields both reduced higher-order harmonics and improved transient response. This results in a lag post-filter, which makes the output of the reset element continuous.

In this architecture $L(s) = \frac{s/\omega_l+1}{s/\omega_h+1}$ and $R(s) = \frac{1}{s/\omega_l+1}$. By taking $\omega_l < \omega_h$ and a large enough ω_h one can see that in the linear domain $R(s)$ and $L(s)$ would cancel each other. However, this is not the case for nonlinear controllers, such as reset controllers. In the closed loop, assuming that $e(t)$ is the closed-loop error due to the lead behavior of $L(s)$, the system will reset not only based on the error but also on its derivative, which can drastically improve the transient behavior of the system. Furthermore, it is shown that in this architecture, the presence of a lag filter, i.e. $R(s)$, reduces the higher-order harmonics of the controller while keeping the desirable almost first-harmonic intact.
The improvement in transient response achieved in the CR architecture, especially in terms of overshoot, paves the way for the exploit of different possibilities. Chapter 7

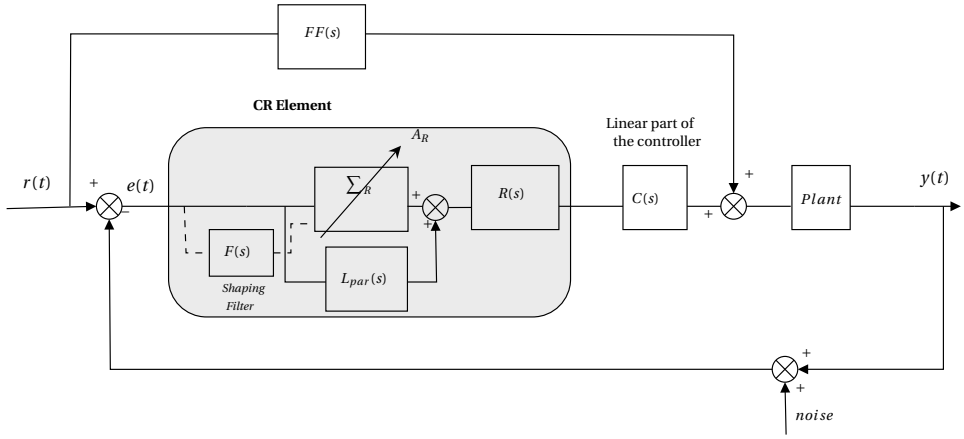

Figure 1.8: Closed-loop architecture containing parallel CR architecture.

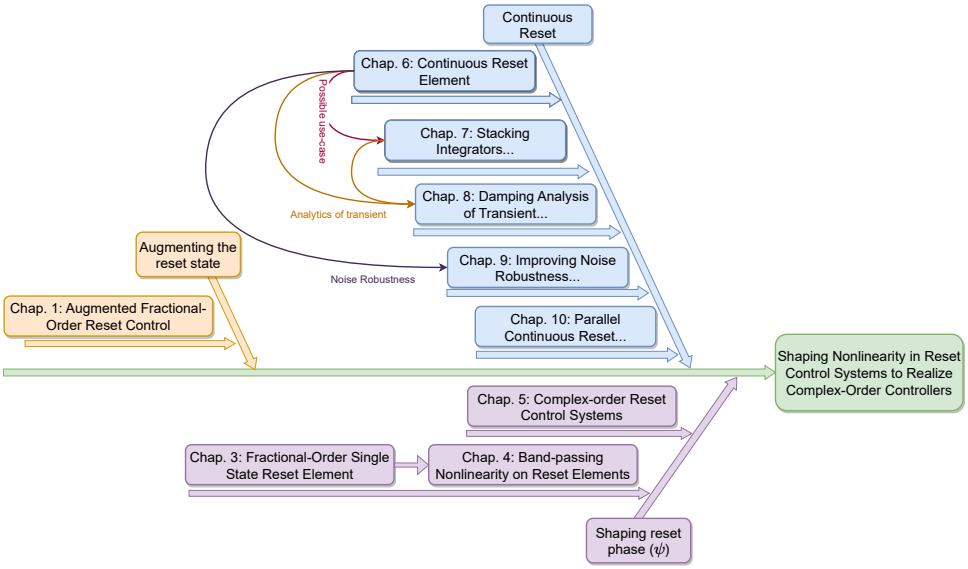

Figure 1.9: The overview of the chapters in the dissertation.

investigates the possibility of stacking integrates for stronger disturbance rejection in lower frequencies while keeping overshoot low and even at zero level.
The transient response study, which is performed in Chapter 6 and 7 is numerical since an general analytical approach will become too complex. However, an analytical approach for a special case can always shed light for better understanding, this is done in Chapter 8. This chapter shows how the damping of the system changes by using continuous reset architecture.
The main drawback of such an architecture is the fact that $L(s)$ will amplify the high-

frequency content of the noise in the closed-loop error signal, which can create unwanted excessive reset instants. Such problems can be solved by using the solutions and architecture proposed in Chapter 9. This architecture is shown in Fig. 1.7 which uses a higher-order lead and lag element and an observer-based filter to prevent excessive resets.

However, in many precision motion applications, the presence of a feed-forward controller will take care of the transient tracking response, and the feedback loop is mainly responsible for disturbance rejection. In such cases, a parallel equivalent of $L(s)$ can be put in parallel to reset element instead of series. This will prevent $L(s)$ from creating excessive resets while keeping the benefit $R(s)$. Figure 1.8 shows such a configuration. Chapter 10 will study this configuration in detail and also presents a case in which such a scheme is implemented in an industrial precision motion stage and a significant improvement was achieved.

All chapters in this dissertation are self-contained and independently readable; however, in order to have a better overview and their connection in terms of answering the main research question, one can refer to the diagram presented in Fig. 1.9.

BIBLIOGRAPHY

[1] D. Valério, N. Saikumar, A. A. Dastjerdi, N. Karbasizadeh, and S. H. HosseinNia, "Reset control approximates complex order transfer functions", *Nonlinear Dynamics*, vol. 97, no. 4, pp. 2323–2337, 2019.

[2] N. Saikumar, D. Valério, and S. H. HosseinNia, "Complex order control for improved loop-shaping in precision positioning", *arXiv preprint arXiv:1907.09249*, 2019.

[3] A. Oustaloup, "La Commade CRONE: Commande Robuste d'Ordre Non Entier", in *Hermes*, Hermés, 1991, ISBN: 9782866012892.

[4] J. Clegg, "A nonlinear integrator for servomechanisms", *Transactions of the American Institute of Electrical Engineers, Part II: Applications and Industry*, vol. 77, no. 1, pp. 41–42, 1958.

[5] I. Horowitz and P. Rosenbaum, "Non-linear design for cost of feedback reduction in systems with large parameter uncertainty", *International Journal of Control*, vol. 21, no. 6, pp. 977–1001, 1975.

[6] K. Krishnan and I. Horowitz, "Synthesis of a non-linear feedback system with significant plant-ignorance for prescribed system tolerances", *International Journal of Control*, vol. 19, no. 4, pp. 689–706, 1974.

[7] L. Hazeleger, M. Heertjes, and H. Nijmeijer, "Second-order reset elements for stage control design", in *2016 American Control Conference (ACC)*, IEEE, 2016, pp. 2643–2648.

[8] A. Baños and A. Vidal, "Definition and tuning of a PI+ CI reset controller", in *2007 European Control Conference (ECC)*, IEEE, 2007, pp. 4792–4798.

[9] O. Beker, C. Hollot, Y. Chait, and H. Han, "Fundamental properties of reset control systems", *Automatica*, vol. 40, no. 6, pp. 905–915, 2004.

[10] N. Saikumar, R. Sinha, and S. H. Hoseinnia, "'constant in gain lead in phase'element-application in precision motion control", *IEEE/ASME Transactions on Mechatronics*, 2019.

[11] Y. Guo, Y. Wang, and L. Xie, "Frequency-domain properties of reset systems with application in hard-disk-drive systems", *IEEE Transactions on Control Systems Technology*, vol. 17, no. 6, pp. 1446–1453, 2009.

[12] N. Karbasizadeh, A. A. Dastjerdi, N. Saikumar, D. Valerio, and S. H. HosseinNia, *Benefiting from linear behaviour of a nonlinear reset-based element at certain frequencies*, 2020. arXiv: 2004.03529 [eess.SY].

[13] P. Nuij, O. Bosgra, and M. Steinbuch, "Higher-order sinusoidal input describing functions for the analysis of non-linear systems with harmonic responses", *Mechanical Systems and Signal Processing*, vol. 20, no. 8, pp. 1883–1904, 2006.

[14] N. Saikumar, K. Heinen, and S. H. HosseinNia, "Loop-shaping for reset control systems: A higher-order sinusoidal-input describing functions approach", *Control Engineering Practice*, vol. 111, p. 104 808, 2021.

[15] A. Oppenheim, R. Schafer, and T. Stockham, "Nonlinear filtering of multiplied and convolved signals", *IEEE Transactions on Audio and Electroacoustics*, vol. 16, no. 3, pp. 437–466, 1968. DOI: 10.1109/TAU.1968.1161990.

[16] M. F. Heertjes, X. G. Schuurbiers, and H. Nijmeijer, "Performance-improved design of n-pid controlled motion systems with applications to wafer stages", *IEEE Transactions on Industrial Electronics*, vol. 56, no. 5, pp. 1347–1355, 2009.

[17] M. F. Heertjes, S. J. Van Den Eijnden, W. M. H. Heemels, and H. Nijmeijer, "A solution to gain loss in hybrid integrator-gain systems", in *2021 IEEE Conference on Control Technology and Applications (CCTA)*, IEEE, 2021, pp. 1179–1184.

[18] C. Cai, A. A. Dastjerdi, N. Saikumar, and S. HosseinNia, "The optimal sequence for reset controllers", in *2020 European Control Conference (ECC)*, 2020, pp. 1826–1833. DOI: 10.23919/ECC51009.2020.9143690.

2

AUGMENTED FRACTIONAL-ORDER RESET CONTROL

Linear controllers such as PID possess fundamental limitations, seen through the waterbed effect. Reset control has been found to be able to overcome these limitations while still maintaining the simplicity and ease of use of PID control due to its compatibility with the loop shaping method. However, the resetting action also gives rise to higher-order harmonics, which hinders consistent realization of the aforementioned expected improvement. In this paper, a fractional-order augmented state analogue of the reset integrator is investigated. This analogue is composed of a series of augmented states that each possess unique reset values, providing the same first-order harmonic behavior but reduced higher-order harmonics magnitude compared to the reset integrator. The optimal number of augmented states along with the corresponding tuning values is investigated. To validate the improvement, the reset integrator and the optimal fractional order analogue are tuned to equally improve disturbance rejection of a high precision 1 DOF positioning stage while maintaining the stability level, with both designed to overcome linear control. From simulation and experimental results, it was found that the novel fractional-order augmented state analogue gives rise to disturbance rejection performance that is closer to the desired and expected improvement, compared to the traditional reset integrator.

2.1. INTRODUCTION

PID control scheme has become the most used controller in many industries even if it is new or high tech[1], [2] due to its robustness and ease of use through the loop shaping method. However, being inherently linear, it suffers from fundamental limitations, which are the waterbed effect and Bode's gain phase relation [3], [4]. Reset control is

This chapter is published as:
A. Sebastian, N. Karbasizadeh, N. Saikumar, and S. H. HosseinNia, "Augmented Fractional-order Reset Control: Application in Precision Mechatronics," 2021 IEEE/ASME International Conference on Advanced Intelligent Mechatronics (AIM), Delft, The Netherlands, 2021, pp. 231-238, doi: 10.1109/AIM46487.2021.9517368.
The author of this dissertation has contributed to the content and supervision of this paper.

a nonlinear control technique which has gained increasing attention due to its compatibility with frequency domain techniques for design and analysis, which are popular within industry.

In reset control, the controller states are reset when a predefined condition is satisfied. The first reset element introduced was a Clegg Integrator (CI) in 1958 [5], which is an integrator whose state is reset to zero when the input is zero. Using a pseudo-linear frequency response description of nonlinear filters called the Describing Function (DF) [6], the frequency response of the CI is obtained, which reveals a gain behavior similar to the linear integrator but with only -38° phase lag. This is advantageous, since this violates Bode's gain phase relationship, allowing improved performance without sacrificing stability. The idea of a reset has also been extended to elements such as First Order Reset Element (FORE) [7], [8] and Second order Reset Element (SORE) [9]. These elements have been successfully applied to meet various objectives such as reducing phase lag [10], broadband phase compensation [11], improving servomotor performance [12], and improving mid-frequency disturbance rejection [13].

The frequency response of the reset controllers can be approximated using the aforementioned DF method [6]. However, since it is an approximation, the advantages described previously are not always seen in practice. This is because the higher-order harmonics present in the output of the nonlinear reset controllers are not considered by the DF method. These higher-order harmonics are analyzed in open loop through HOSIDF method [14] and recently in closed loop [15]. There exists a need to reduce the higher-order harmonics such that the output is dominated by the first harmonic, which makes the benefit of reset control predicted by the DF consistently realizable. This paper presents a novel augmented analogue for the reset integrator with the aim of obtaining the same first-harmonic behavior while reducing the higher order harmonics.

The paper is structured as follows. Section II of this paper introduces reset control. Section III examines the fractional order augmented state reset integrator and the benefits it possesses over the traditional reset integrator. Section IV gives an illustrative example of the benefits of using the augmented state reset integrator through simulation and experimental validation of disturbance rejection on a precision positioning system. Conclusions and possible future work are outlined in Section V.

2.2. RESET CONTROL

2.2.1. DEFINITION

A single-input single-output (SISO) reset controller (denoted Σ_{RC}) is defined as

$$\Sigma_{RC} := \begin{cases} \dot{x}(t) = A_r x(t) + B_r e(t) & \text{if } e(t) \neq 0 \\ x\left(t^+\right) = A_\rho x(t) & \text{if } e(t) = 0 \\ u(t) = C_r x(t) + D_r e(t) & \end{cases} \tag{2.1}$$

where $x(t)$ are the states and A_r, B_r, C_r and D_r are the matrices corresponding to its state-space representation. These are referred to as the base linear system of the controller. $e(t)$ and $u(t)$ are the input and output of the controller, respectively. A_ρ is a diagonal matrix that dictates the after-reset values of the states.

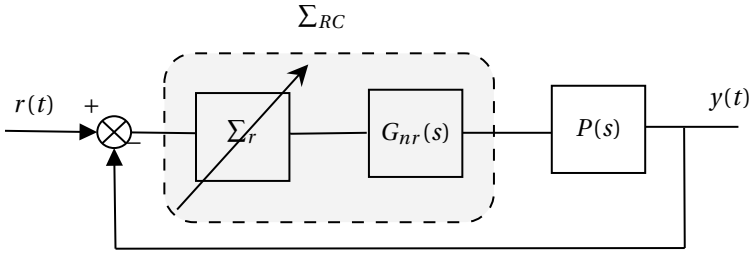

Figure 2.1: Block diagram of a reset controller RC with a plant P.

Theorem 1. *[16] The reset controller defined by (2.1) with a sinusoidal input has a $\frac{2\pi}{\omega}$ periodic solution that is globally asymptotically stable for all $\omega > 0$ if and only if*

$$|\lambda(A_\rho e^{\Delta})| < 1 \tag{2.2}$$

where $\Delta \in \mathbb{R} > 0$. This theorem consequently constrains each member of the diagonal of A_ρ to be between -1 and 1.

2.2.2. RESET SYSTEMS STABILITY

Fig. 2.1 shows a reset controller Σ_{RC} with a plant P. As shown in the figure, the reset controller can be decomposed into a reset part Σ_r and a non-reset part G_{nr}. Let n_r and n_{nr} therefore denote the number of reset and non-reset states of Σ_{RC} respectively.

Theorem 2. *[17] The reset control system depicted in Fig. (2.1) is quadratically stable if and only if the H_β condition holds, i.e. there exists a $\beta \in \mathbb{R}^{n_r}$ and a positive definite matrix $P_r \in \mathbb{R}^{n_r \times n_r}$ such that the transfer function*

$$Z_\beta(s) := \begin{bmatrix} \beta C_p & 0_{n_r \times n_{nr}} & P_r \end{bmatrix} (sI - A_{cl})^{-1} \begin{bmatrix} 0_{n_p} \\ 0_{n_{nr} \times n_r} \\ I_{n_r} \end{bmatrix} \tag{2.3}$$

is strictly positive real. And

$$A_\rho^T P_\rho A_\rho - P_\rho \leq 0. \tag{2.4}$$

Here A_{cl} is the closed loop A matrix of Fig. 2.1 defined as:

$$A_{cl} = \begin{bmatrix} A_p & B_p C_{RC} \\ -B_{RC} C_p & A_{RC} \end{bmatrix}$$

in which (A_p, B_p, C_p) are the state space matrices of Σ_p, and (A_{RC}, B_{RC}, C_{RC}) are the state space matrices of Σ_{RC}.

2.2.3. DESCRIBING FUNCTION

Describing Function (DF) is a pseudo-linear approximation of the frequency response of non-linear elements like reset controllers. Since it only considers the first harmonic of the output, expected experimental results based on loop shaping are not seen [11].

Reference [6] developed the concept of higher-order sinusoidal input describing function (HOSIDF), which is further developed by [14] specifically for reset elements. The HOSIDF formula for reset elements is as shown:

$$
\begin{aligned}
H_n(\omega) &= \begin{cases} C_r(j\omega I - A_r)^{-1}(I + j\Theta(\omega))B_r + D_r, & n = 1 \\ C_r(j\omega n I - A_r)^{-1} j\Theta(\omega) B_r, & \text{odd } n > 2 \\ 0, & \text{even } n \geq 2 \end{cases} \\
\Theta(\omega) &= -\frac{2\omega^2}{\pi}\Delta(\omega)[\Gamma(\omega) - \Lambda^{-1}(\omega)] \\
\Lambda(\omega) &= \omega^2 I + {A_r}^2 \\
\Delta(\omega) &= I + e^{\frac{\pi}{\omega}A_r} \\
\Delta_\rho(\omega) &= I + A_\rho e^{\frac{\pi}{\omega}A_r} \\
\Gamma(\omega) &= \Delta_\rho^{-1}(\omega) A_\rho \Delta(\omega) \Lambda^{-1}(\omega)
\end{aligned}
\tag{2.5}
$$

where $H_n(\omega)$ is the n^{th} harmonic describing function for sinusoidal input with frequency ω. Therefore, the DF is a special case of HOSIDF with $n = 1$.

2.3. AUGMENTED FRACTIONAL-ORDER STATE RESET INTEGRATOR

Fractional calculus generalizes integration and differentiation to real or complex number powers. There exist multiple accepted definitions of fractional differentiation. The notation $D^\alpha x(t)$, $k \in [0,1]$ in this paper will refer to the Caputo definition defined in [18].

2.3.1. AUGMENTED SYSTEM OF FRACTIONAL ORDER RESET INTEGRATOR

A fractional order reset integrator is defined as:

$$
\begin{aligned}
D^\alpha x(t) &= e(t) \\
x(t^+) &= \gamma x(t) \\
u(t) &= x(t)
\end{aligned}
\tag{2.6}
$$

where $\alpha \in [0,1]$.

The fractional order integrator is implemented through the CRONE approximation [19] with its poles being reset, defined by:

$$
s^\alpha \approx \gamma P \prod_{m=1}^{N} \frac{1 + \frac{s}{\omega_{z,m}}}{1 + \frac{s}{\omega_{p,m}}} \qquad A_\rho
\tag{2.7}
$$

with

$$
\omega_{z,m} = \omega_l \left(\frac{\omega_n}{\omega_l}\right)^{\frac{2m-1-\alpha}{2N}}
$$

$$
\omega_{p,m} = \omega_1 \left(\frac{\omega_h}{\omega_l}\right)^{\frac{2m-1+\alpha}{2N}}
$$

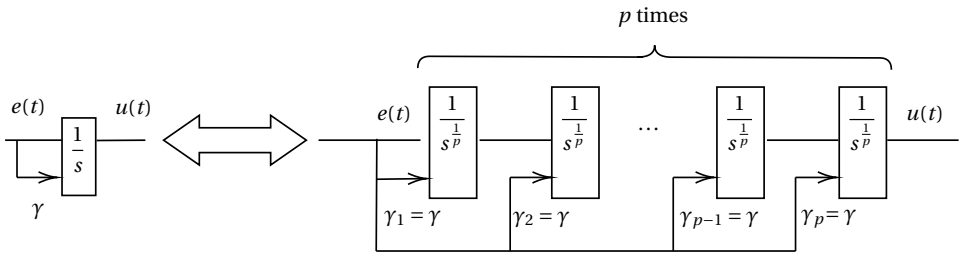

Figure 2.2: Illustration of equivalence between cascade of fractional order integrators and an integer reset integrator. The arrows indicate that the reset of each element is with respect to the input to the cascade i.e. $e(t)$

where $\alpha \in (0,1)$, N is the number of real stable poles and real minimum phase zeros, $[\omega_l, \omega_h]$ is the frequency range where the approximation is valid, and P is a parameter to tune the gain of the approximation. A_ρ is a reset matrix that corresponds to the reset of the fractional order integrator γ.

2.3.2. AUGMENTED SYSTEM OF INTEGER ORDER RESET INTEGRATOR

The integer-order state reset integrator is obtained by setting $k = 1$ in (2.6). The augmented fractional order form of this case is given by:

$$\begin{aligned} D^q \chi(t) &= \mathbf{A}\mathscr{X}(t) + \mathbf{B}e(t) \\ \mathscr{X}(t^+) &= \mathbf{A}_\rho \mathscr{X}(t) \\ u(t) &= \mathbf{C}\mathscr{X}(t) \end{aligned} \tag{2.8}$$

where,

$$\mathbf{A} = \begin{bmatrix} \mathbf{0} & \boldsymbol{I} \\ \mathbf{0} & \mathbf{0} \end{bmatrix}, \quad \mathbf{A}_\rho = \gamma \boldsymbol{I}$$

$$\mathbf{B} = \begin{bmatrix} 0 \\ \vdots \\ 1 \end{bmatrix}, \mathbf{C} = \begin{bmatrix} 1 & \dots & 0 \end{bmatrix}$$

Here $\mathscr{X} = [x_1, x_2 \dots x_p]^T$ is a vector of the augmented states and $p = \frac{1}{q}$, where $p \in \mathbb{Z}^+$.

2.3.3. EQUIVALENCE OF CASCADED FRACTIONAL ORDER RESET INTEGRATORS WITH AUGMENTED INTEGER ORDER RESET INTEGRATOR

Remark 1. *Consider Fig. 2.2. The cascade of p fractional order reset integrators in series is equivalent to the augmented form of an integer reset integrator with* $q = \frac{1}{p}$.

Proof. Consider the k^{th} fractional-order reset integrator, with $1 \le k \le p$. The state-space

representation becomes:

$$D^{1/p}x_k(t) = e_k(t) \tag{2.9}$$
$$x_k(t^+) = \gamma_k x_k(t)$$
$$u_k(t) = x_k(t)$$

With $e_1(t) = e(t)$, $e_k = u_{k-1}$ and $u_p(t) = u(t)$, the combined state space of the cascade is simplified to:

$$D^{1/p}\begin{bmatrix} x_1(t) \\ \vdots \\ x_p(t) \end{bmatrix} = \begin{bmatrix} \mathbf{0} & \mathbf{0} \\ \boldsymbol{I} & \mathbf{0} \end{bmatrix}\begin{bmatrix} x_1(t) \\ \vdots \\ x_p(t) \end{bmatrix} + \begin{bmatrix} 1 \\ \vdots \\ 0 \end{bmatrix} e(t) \tag{2.10}$$

$$u(t) = \begin{bmatrix} 0 & \dots & 1 \end{bmatrix}\begin{bmatrix} x_1(t) \\ \vdots \\ x_p(t) \end{bmatrix}$$

where $x_2 = x_1/D^{1/p}$, $x_3 = x_2/D^{1/p}$, $\dots$, $x_p = x_{p-1}/D^{1/p}$.

Reverse the ordering of the state vector above such that x_p becomes in the first entry. With $q = 1/p$ and $\mathbf{A}_\rho = \gamma \boldsymbol{I}$, this results in a state space equal to (2.8). Therefore equivalence is proven and the augmented system is a valid replacement of the integer-order reset integrator.

□

Remark 2. *[20] Let the reset control system Σ_{RC} in Fig. 2.1 be composed first of a reset element Σ_r followed by a linear element G_{nr}. The higher order harmonics gain of Σ_{RC} is smaller than Σ_r if G_{nr} is a linear lag element:*

$$|H_n(j\omega)|_{\Sigma_{RC}} \leq |H_n(j\omega)|_{\Sigma_r}, \quad \textit{odd } n > 1 \tag{2.11}$$

Remark 3. *Consider a reset integrator with reset value γ. With $-1 < \gamma \leq 1$, the following relation holds:*

$$-90^\circ \leq \angle H_1(j\omega) < 0^\circ \tag{2.12}$$

where -90° corresponds to $\gamma = 1$ (linear integrator) and 0° corresponds to $\gamma = -1$.

Remark 3 also holds for the fractional order reset integrator of (2.6), with the lower limit changed to $-90k^\circ$.
Equation (2.10) is the analogue of the reset integrator if $\gamma_k = \gamma, \forall\, k$. It therefore follows that not only the first- but also higher-order harmonics are similar. However, it is desired to reduce the higher order harmonics while maintaining the first-order harmonic behavior. Considering Remarks 2 and 3, this could be achieved through a combination of $\gamma_1, \dots, \gamma_p$ that does not necessarily satisfy the aforementioned restriction on γ_k. More specifically, from Remark 2, there could be an advantage in making later fractional integrators more linear. Therefore, the goal of this paper is to design $\gamma_1, ..., \gamma_p$ such that the first harmonic is the same as that of the reset integrator while simultaneously possessing lower higher-order harmonic gain.

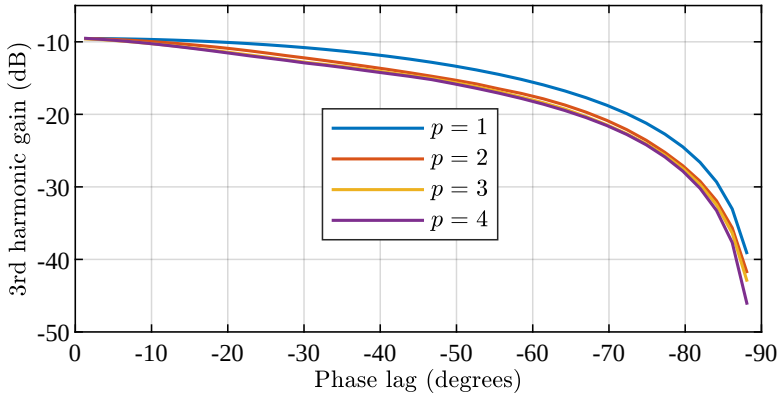

Figure 2.3: 3rd order harmonic gain at $\omega = 100$ rad/s of various p values, for different provided phase lag.

This goal is described in an optimization problem as shown:

$$\min_{\gamma_{Aug}=[\gamma_1,\gamma_2,\ldots,\gamma_p]} |H_n(\gamma_{Aug}, j\omega)|_{Aug} \tag{2.13}$$

$$\forall \text{ odd } n > 1, \forall \omega \in [\omega_l, \omega_h]$$

subject to

$$|H_1(\gamma_{Aug}, j\omega)|_{Aug} = |H_1(\gamma, j\omega)|_{\text{RI}}$$
$$\angle H_1(\gamma_{Aug}, j\omega)_{Aug} = \angle H_1(\gamma, j\omega)_{\text{RI}}$$

where Aug refers to the fractional order analogue of the reset integrator and RI stands for Reset Integrator. For simplicity, the optimization will be run for $p = 2, 3$ and 4 and the reductions in the magnitude of higher order harmonics will be compared. In addition, non-zero values of γ for RI will also be considered.

2.3.4. RESULTS

Tables 2.1 and 2.2 show the third order harmonic gain for different reset values of the reset integrator and its respective augmented fractional order analogue for $p = 2, 3$ and 4. Instead of the different reset values, by using Remark 3, the horizontal axis of Fig. 2.3 alternatively shows the phase lag that the reset integrator provides, which is matched by the novel augmented fractional order analogue. Tables 2.1 and 2.2 show the reset values of the augmented states for each value of p and the optimal reset values. Some observations:

- For all p and phase lag values, the integrator near the end of the cascade is more linear than those near the start, which satisfies Remark 2.
- As the required phase lag decreases, the reset value of the integrators near the end of the cascade is not fully linear. Taking into account Remark 2, this indicates that the starting integrators cannot provide all the required phase lag reduction, and thus the integrators near the end provide some support in this regard.

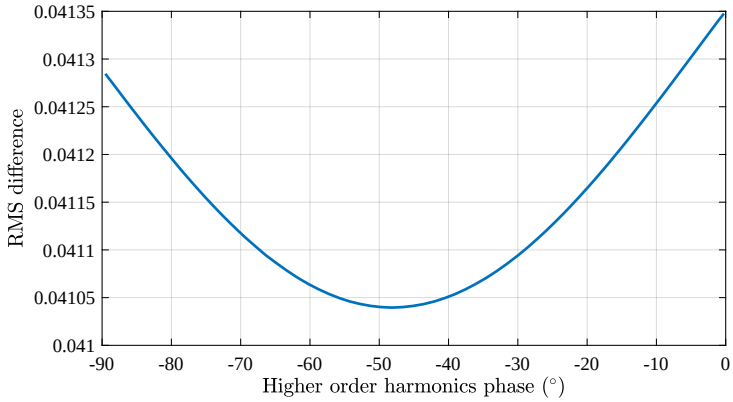

Figure 2.4: Higher order harmonics phase vs. RMS error of reset integrator with $\gamma = 0$.

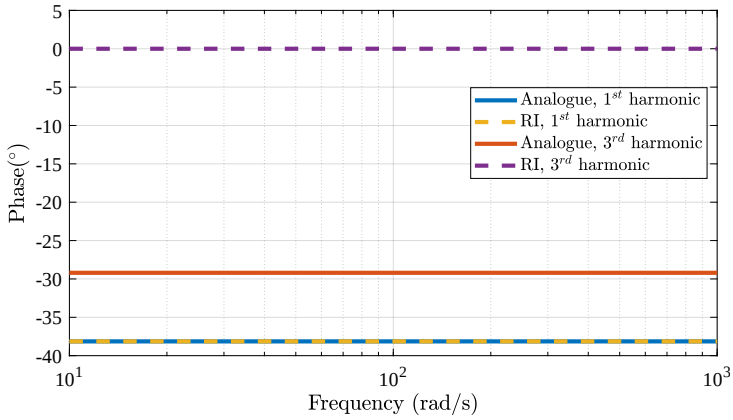

Figure 2.5: Phase plot of 1st and 3rd harmonic of the RI vs. augmented fractional-order analogue.

- There is more reduction of the third-order harmonic for larger phase lag. Thus, there exists a trade-off between obtaining a larger reduced phase-lag advantage and the corresponding third-harmonic gain reduction.
- The further reduction in the third harmonic gain by going from $p = 2$ to $p = 3$ or $p = 4$ is insignificant compared to the reduction from the original reset integrator to the case $p = 2$. Therefore, it is recommended to use $p = 2$ in implementation.

2.3.5. NON-ZERO HIGHER ORDER HARMONIC PHASE

In this subsection it will be shown how the non-zero higher-order harmonics phase of the augmented fractional-order state analogue could be of benefit.

The time domain output of a reset element given a sinusoidal input $\sin(\omega t)$ is:

$$u(t) = \sum_{n=1}^{\infty} A_n \sin(n\omega t + \phi_n), \text{ odd } n \geq 1 \tag{2.14}$$

Table 2.1: Reset values and 3rd harmonic gain at $\omega = 100$ rad/s of each augmented state for various p values, the subscripts for the various γ correspond to Fig. 2.2.

Reset Integrator		
γ	Equivalent phase lag (°)	3^{rd} harmonic gain (dB)
-0.8	-5.00	-9.57
-0.4	-18.60	-10.00
0	-38.15	-11.63
0.4	-61.38	-15.94
0.8	-81.95	-26.62

Augmented analogue, $p = 2$				
γ	Equivalent phase lag (°)	γ_2	γ_1	3^{rd} harmonic gain (dB)
-0.8	-5.00	-0.98	-0.74	-9.71
-0.4	-18.60	-0.98	-0.11	-10.83
0	-38.15	-0.97	0.66	-13.56
0.4	-61.38	-0.38	1.00	-18.44
0.8	-81.95	0.59	1.00	-29.32

The above emphasizes that not only the gain but the higher-order harmonics phase also influence the output of the reset element.

To investigate this, the RMS difference between the time-domain response of the reset integrators and the ideal response is computed, where the ideal response is the response of the reset integrator with all the higher-order harmonic gains eliminated. Fig. 2.4 shows this RMS difference for different values of the higher-order harmonic phase. At -48.5° there exists a minimum of the RMS difference. The reset integrator, however, has zero higher order harmonics phase and so this minimum cannot be achieved.

In contrast, the augmented fractional-order state analogue has a negative higher-order harmonic phase. For instance, the third harmonic phase is shown in Fig. 2.5 for $p = 2$. Therefore in addition to lower higher-order harmonics gain, the augmented fractional-order state analogue also possesses a beneficial higher-order harmonics phase behavior.

2.4. ILLUSTRATIVE EXAMPLE

For validation in performance improvement of a system that utilizes the augmented fractional state analogue, four controllers are designed and studied in simulation and in practice. This section compares the results of the disturbance rejection performance between a parallel PID (termed PI+D) and three other parallel PID respectively in series with a linear integrator, the Clegg Integrator, and an augmented fractional state analogue of the Clegg Integrator with $p = 2$.

Table 2.2: Reset values and 3rd harmonic gain at ω = 100 rad/s of each augmented state for various p values, the subscripts for the various γ correspond to Fig. 2.2. (Cont'd)

Augmented analogue, $p = 3$					
γ	Equivalent phase lag (°)	γ_3	γ_2	γ_1	3rd harmonic gain (dB)
-0.8	-5.00	-0.97	-0.97	-0.66	-9.80
-0.4	-18.60	-0.95	-0.95	0.27	-11.25
0	-38.15	-0.75	-0.71	1.00	-13.72
0.4	-61.38	-0.6	0.48	1.00	-18.55
0.8	-81.95	0.35	1.00	1.00	-29.68

Augmented analogue, $p = 4$						
γ	Equivalent phase lag (°)	γ_4	γ_3	γ_2	γ_1	3rd harmonic gain (dB)
-0.8	-5.00	-0.94	-0.92	-0.87	-0.64	-9.81
-0.4	-18.60	-0.95	-0.92	-0.87	0.53	-11.34
0	-38.15	-0.97	-0.82	0.18	1.00	-13.73
0.4	-61.38	-0.43	-0.23	1.00	1.00	-18.60
0.8	-81.95	0.16	1.00	1.00	1.00	-30.20

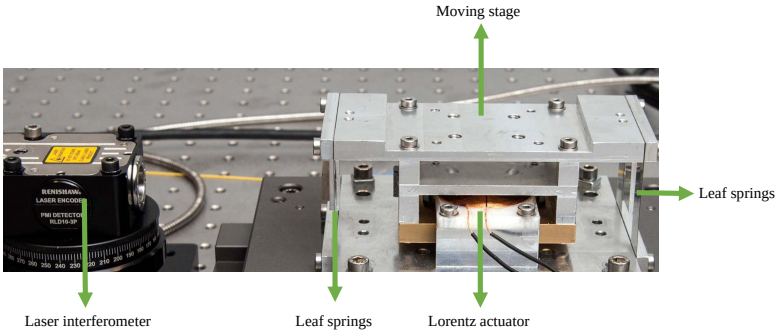

Figure 2.6: The custom-designed precision stage used for experiments.

PLANT

The plant use for this validation is a flexure-guided stage actuated by a Lorentz actuator as shown in Fig. 2.6, with Fig. 2.7 describing its identified frequency response and additionally a fitted second order transfer function. The position of the plant is sensed using a laser interferometer with a resolution of 10 nm, with a sampling period of 100μs.
The fitted transfer function is as follows:

$$G(s) = \frac{3.038e4}{s^2 + 0.7413s + 243.3} \tag{2.15}$$

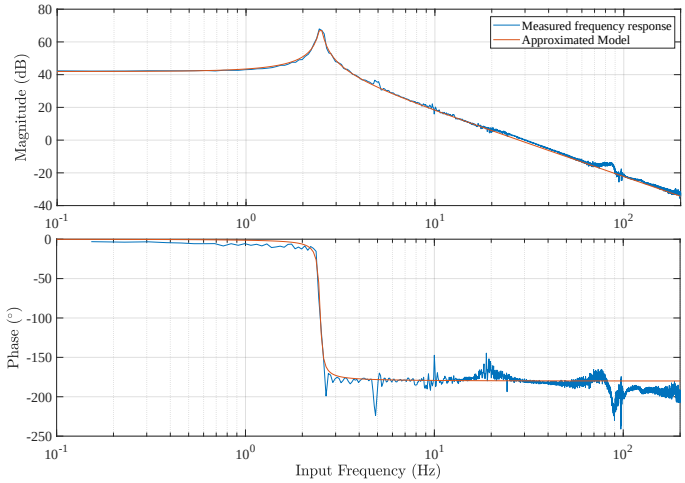

Figure 2.7: Identified frequency response of the stage.

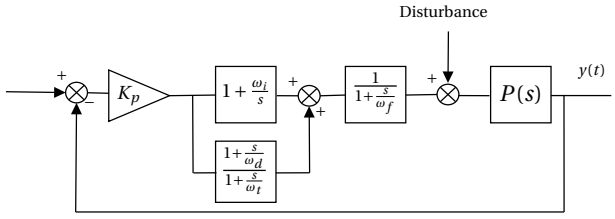

(a) PI+D

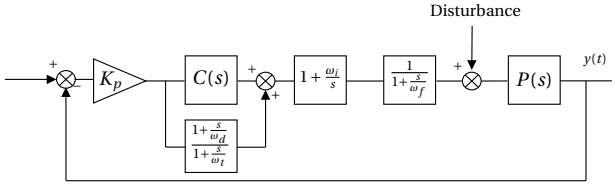

$$C(s) = 1 + \frac{\omega_i}{s} \Longrightarrow (PI + D)PI$$

$$C(s) = 1 + \frac{\omega_i}{s}^{\gamma=0} \Longrightarrow (PCI + D)PI$$

$$C(s) = 1 + \frac{\omega_i}{s}^{\gamma_{CI_{Aug}}=[-0.97,0.66]} \Longrightarrow (PCI_{Aug} + D)PI$$

(b) Control schemes used for the adapted PI+D controllers

Figure 2.8: Validation control scheme definitions. Disturbance refers to an applied sinusoidal disturbance input.

CONTROL STRATEGY

Four sets of controllers are designed with a bandwidth of 100 Hz: a parallel PID controller (PI+D), a parallel PID with an extra tamed integrator ((PI+D)PI), a parallel PID

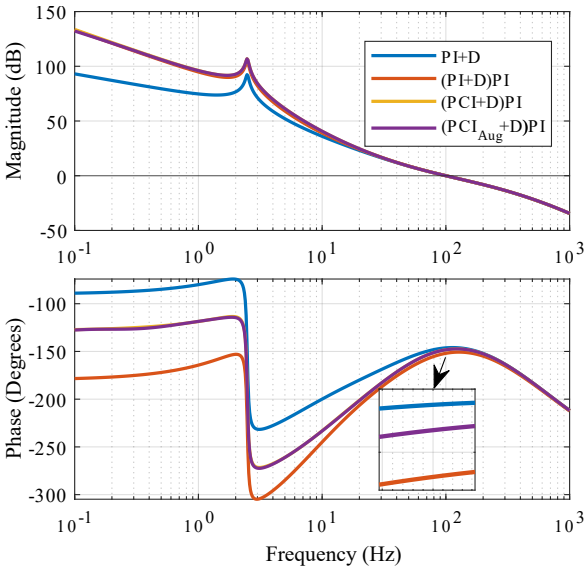

Figure 2.9: Open loop frequency response of control scheme in Fig. 2.8. The gain and phase of (PCI+D)PI (yellow) is below that of (PCI_{Aug}+D)PI (purple).

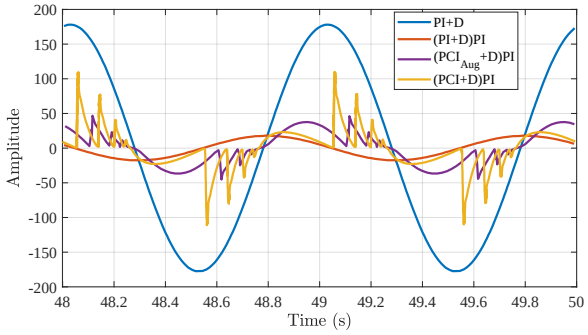

Figure 2.10: Response of control scheme in Fig. 2.8 to a 1 Hz disturbance, using each of the four different extra controllers.

with an extra tamed Clegg Integrator ((PCI+D)PI), and a parallel PID with an extra tamed augmented fractional order analogue of Clegg Integrator ((PCI_{Aug}+D)PI). Fig. 2.8 depicts the details of these controllers. As shown in Fig. 2.9, the (PI+D)PI controller is capable of outperforming PI+D in terms increased gain at low frequencies, resulting in better disturbance rejection, however, with the trade-off of phase margin reduction. Considering the reduced phase lag advantage of a Clegg Integrator, it is assumed that the (PCI + D) PI controller could be tuned to have less phase margin reduction while still maintaining the gain behavior of (PI+D)PI, which is indeed the case as shown in yellow and blue in Fig. 2.9. To verify this result, Fig. 2.10 shows the simulation result of the disturbance rejection performance on the input of 1 Hz disturbance. Contrary to expected

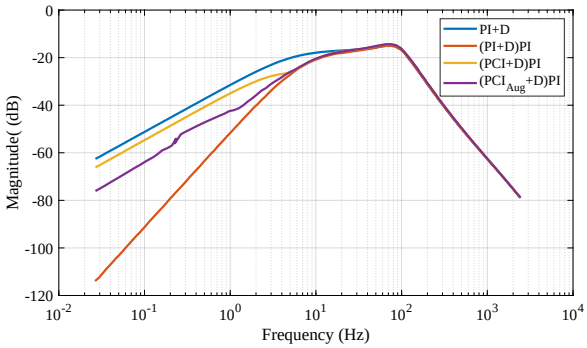

Figure 2.11: Process sensitivity plot based on (2.16).

performance from Fig. 2.9, the simulation plot shows (PCI+D)PI performing far worse compared to (PI+D)PI; this is because Fig. 2.9 shows only the first order harmonic.

To reduce the effects of the higher-order harmonics, the augmented fractional-order analogue replaces the Clegg Integrator (giving the controller (PCI_{Aug} + D) PI), with tuned open-loop performance shown in purple in Fig. 2.9. The simulation result is also shown in purple in Fig. 2.10. From these figures it is observed that the phase margin of (PCI+D)PI is still maintained, while the jump size in Fig. 2.10 reduced in magnitude, making the maximum amplitude of the response now closer to (PI+D)PI.

To see whether this improvement exists over a range of frequencies, a process sensitivity function is constructed. To capture the higher-order harmonics in the process sensitivity function plot for the controllers with reset elements, a new process sensitivity function is defined as:

$$S(\omega) = \frac{max(|e(t)|)}{|D|} \quad \text{for } t \geq t_{ss} \tag{2.16}$$

where t_{ss} is the time it takes for the response to become steady state and periodic, $y(t)$ is the output, and D is the amplitude of the sinusoidal disturbance input. This function is found by simulating the closed-loop system with a disturbance input for increasing, closely spaced ω. The plot is shown in Fig. 2.11. Here it is seen that compared to (PCI+D)PI, (PCI_{Aug}+D)PI's performance is closer to (PI+D)PI up to approximately 4 Hz, from which the performance of all the reset controllers is now able to match (PI+D)PI.

It is also noted that the higher stability level of the (PCI+D)PI and the (PCI_{Aug}+D)PI compared to (PI+D)PI and PI+D, which was implied by their higher phase margin from Fig. 2.9, was also taken by using the Descibing function. Therefore, this means that the true stability level may not be the same as what the DF predicted in this figure. To check that the higher stability level indeed truly exist, the peak of the step response is examined, with a lower overshoot indicating higher stability. This is shown in Fig. 2.12. This confirms that a higher stability level has indeed been achieved.

STABILITY CHECK USING H_β CONDITION

To further confirm the stability of the fractional order analogue, the H_β condition described in Section II is also applied on the control scheme of Fig. 2.8. By solving the

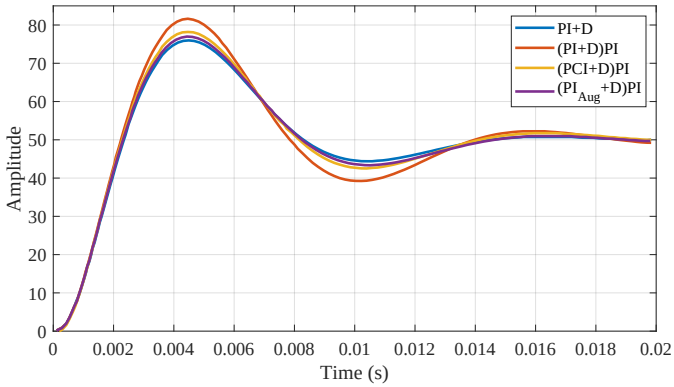

Figure 2.12: Step response of each controller.

Table 2.3: Experiment results. The amplitude of the disturbance sinusoidal input is 6528 (10 nm) and the step input size is 1000 (10 nm).

Sin Dist.	max($\|y(t)\|$)			
Hz	PI+D	(PI+D)PI	(PCI+D)PI	(PCI$_{Aug}$+D)PI
0.1	21	3	14	13
0.2	32	3	25	20
0.3	56	4	37	35
0.4	74	5	49	40
0.5	93	7	61	46
0.6	110	8	72	62
0.7	127	12	84	69
0.8	146	14	96	78
0.9	163	13	107	85
1	178	19	116	89
2	341	68	206	146
3	476	137	263	250
4	582	216	296	290
Step Dist.	max($\|y(t)\|$)			
1000	1492	1611	1515	1516

condition using a YALMIP Sedumi solver [21], a positive definite matrix P_r was indeed found, further confirming that the fractional order analogue is indeed stable.

2.5. EXPERIMENT RESULTS

To validate the results of the closed-loop simulation, an experiment is conducted. Disturbances of selected frequencies are chosen and the amplitude of the plant response is recorded. To check the stability level, a step input is also applied.

Table 2.3 shows the maximum error of the plant controlled by each of the four different controllers in steady state. It is seen that the trend in the simulation result is confirmed, with the (PCI$_{\text{Aug}}$+D)PI outperforming (PCI+D)PI and PI+D in the frequency region predicted by the simulation in Fig. 2.11. In addition, the step response of the (PCI+D)PI and the (PCI$_{\text{Aug}}$+D)PI also exhibit a similar overshoot value, indicating that the increased stability level predicted by simulation is also seen in the experiment.

2.6. CONCLUSION

Reset controller is a subset of nonlinear controllers that overcomes the fundamental limitations of linear controllers, while still retaining the advantage of linear controllers in that the loop shaping method is applicable through the Describing Function method. However, the description function does not take into account higher-order harmonics, which makes the actual output of the reset controlled system sometimes deviate from that predicted using the description function. It is then desired to minimize the role of these higher-order harmonics on influencing the output.

The Augmented Fractional-Order Reset Integrator Analogue is a promising method in achieving this goal. By resetting the fractional states of the reset integrator to determined optimal values, it has been shown that there is a higher-order harmonics reduction that may not seem huge in open-loop, however, results in significant closed-loop performance improvement. Then a recommendation was made as to the reset values of the fractional states required for a particular tolerable phase lag. Furthermore, the nonzero higher order harmonics phase that the augmented fractional-order reset integrator analogue possess was shown to be promising in further improving the output of the reset integrator.

For future work, it is recommended to develop a tuning rule for the state space representation of the augmented fractional-order analogue such that the higher order harmonics phase can be manipulated to obtain the optimal reduction in the RMS difference discussed in Section 2.3.5, while still maintaining reduced higher order harmonic gains. A final recommendation is to also investigate resetting the fractional elements with respect to their own respective inputs as opposed to the error; there may be aspects of the intermediate signals that could bring about more higher order harmonic reductions.

BIBLIOGRAPHY

[1] T. Samad, S. Mastellone, P. Goupil, A. van Delft, A. Serbezov, and K. Brooks, "Ifac industry committee update, initiative to increase industrial participation in the control community", in *Newsletters April 2019*, IFAC, 2019.

[2] E. Mortazavian, Z. Wang, and H. Teng, "Thermal-kinetic-mechanical modeling of laser powder deposition process for rail repair", in *ASME 2019 International Mechanical Engineering Congress and Exposition*, American Society of Mechanical Engineers Digital Collection, 2019.

[3] R. M. Schmidt, G. Schitter, and J. van Eijk, *The design of high performance mechatronics*. 2014, ISBN: 9781607508250.

[4] A. Barreiro and A. Bãnos, "Reset control systems", in *RIAI - Revista Iberoamericana de Automatica e Informatica Industrial*, 2012, ch. 1, pp. 11–17. DOI: 10.1016/j.riai.2012.09.007.

[5] J. C. Clegg, "A nonlinear integrator for servomechanisms", *Transactions of the American Institute of Electrical Engineers, Part II: Applications and Industry*, 2013, ISSN: 0097-2185. DOI: 10.1109/tai.1958.6367399.

[6] P. W. Nuij, O. H. Bosgra, and M. Steinbuch, "Higher-order sinusoidal input describing functions for the analysis of non-linear systems with harmonic responses", *Mechanical Systems and Signal Processing*, vol. 20, no. 8, pp. 1883–1904, 2006, ISSN: 08883270. DOI: 10.1016/j.ymssp.2005.04.006.

[7] I. Horowitz and P. Rosenbaum, "Non-linear design for cost of feedback reduction in systems with large parameter uncertainty", *International Journal of Control*, vol. 21, no. 6, pp. 977–1001, 1975, ISSN: 13665820. DOI: 10.1080/00207177508922051.

[8] L. Zaccarian, D. Nešić, and A. R. Teel, "First order reset elements and the Clegg integrator revisited", in *Proceedings of the American Control Conference*, 2005. DOI: 10.1109/acc.2005.1470016.

[9] H. N. L.Hazeleger M. Heertjes, "Second-order reset elements for stage control design", *Proceedings of the American Control Conference*, vol. 2016-July, pp. 2643–2648, Jul. 2016, ISSN: 07431619. DOI: 10.1109/ACC.2016.7525315.

[10] M. F. Heertjes, K. G. Gruntjens, S. J. Van Loon, N. Kontaras, and W. P. Heemels, "Design of a variable gain integrator with reset", in *Proceedings of the American Control Conference*, 2015, ISBN: 9781479986842. DOI: 10.1109/ACC.2015.7171052.

[11] N. Saikumar, R. K. Sinha, and S. Hassan Hosseinnia, "'Constant in Gain Lead in Phase' Element-Application in Precision Motion Control", *IEEE/ASME Transactions on Mechatronics*, 2019, ISSN: 1941014X. DOI: 10.1109/TMECH.2019.2909082. arXiv: 1805.12406.

[12] S. H. HosseinNia, I. Tejado, and B. M. Vinagre, "Fractional-order reset control: Application to a servomotor", *Mechatronics*, vol. 23, no. 7, pp. 781–788, 2013, ISSN: 09574158. DOI: 10.1016/j.mechatronics.2013.03.005.

[13] Y. Li, G. Guo, and Y. Wang, "Nonlinear mid-frequency disturbance compensation in hard disk drives", in *IFAC Proceedings Volumes (IFAC-PapersOnline)*, 2005, ISBN: 008045108X.

[14] N. Saikumar, K. Heinen, and S. H. HosseinNia, *Loop-shaping for reset control systems – a higher-order sinusoidal-input describing functions approach*, 2020. arXiv: 2008.10908 [eess.SY].

[15] A. Dastjerdi, N. Saikumar, D. Valerio, and H. Hassan, "Closed-loop frequency analyses of reset systems", 2020. [Online]. Available: https://arxiv.org/abs/2001.10487.

[16] Y. Guo, Y. Wang, and L. Xie, "Frequency-domain properties of reset systems with application in hard-disk-drive systems", *IEEE Transactions on Control Systems Technology*, vol. 17, no. 6, pp. 1446–1453, 2009, ISSN: 10636536. DOI: 10.1109/TCST.2008.2009066.

[17] O. Beker, C. V. Hollot, Y. Chait, and H. Han, "Fundamental properties of reset control systems", *Automatica*, vol. 40, no. 6, pp. 905–915, 2004, ISSN: 00051098. DOI: 10.1016/j.automatica.2004.01.004.

[18] M. Caputo, "Linear Models of Dissipation whose Q is almost Frequency Independent-II", *Geophysical Journal of the Royal Astronomical Society*, 1967, ISSN: 1365246X. DOI: 10.1111/j.1365-246X.1967.tb02303.x.

[19] A. Oustaloup and M. Bansard, "First generation CRONE control", in *Proceedings of the IEEE International Conference on Systems, Man and Cybernetics*, 1993, ISBN: 0780309111. DOI: 10.1109/icsmc.1993.384861.

[20] C. Cai, A. A. Dastjerdi, N. Saikumar, and S. H. HosseinNia, "The optimal sequence for reset controllers", in *2020 European Control Conference (ECC)*, 2020, pp. 1826–1833. DOI: 10.23919/ECC51009.2020.9143690.

[21] J. Löfberg, "YALMIP: A toolbox for modeling and optimization in MATLAB", in *Proceedings of the IEEE International Symposium on Computer-Aided Control System Design*, 2004, pp. 284–289. DOI: 10.1109/cacsd.2004.1393890.

3

FRACTIONAL-ORDER SINGLE STATE RESET ELEMENT

This paper proposes a fractional-order reset element whose architecture allows suppression of non-linear effects for a range of frequencies. Suppressing the nonlinear effects of a reset element for the desired frequency range while maintaining it for the rest is beneficial, especially when it is used in the framework of a "Constant in gain, Lead in phase" (CgLp) filter. CgLp is a newly introduced nonlinear filter, bound to circumvent the well-known linear control limitation – the waterbed effect. The ideal behaviour of such a filter in the frequency domain is unity gain while providing a phase lead for a broad range of frequencies. However, CgLp's ideal behaviour is based on the describing function, which is a first-order approximation that neglects the effects of the higher-order harmonics in the output of the filter. Although CgLp is fundamentally a nonlinear filter, its nonlinearity is not required for all frequencies. Thus, in this paper, it is shown that using the proposed reset element architecture, CgLp gets closer to its ideal behaviour for a range of frequencies, and its performance will be improved accordingly.

3.1. INTRODUCTION

PID is still the workhorse of the industry when it comes to the term "control". However, in some fields, particularly, precision motion control, there is an increasingly high demand for more precise, faster, and more robust controllers. The "waterbed effect" is the fundamental and well-known limitation of linear controllers that prevents them from meeting these demands simultaneously [1]. In terms of steady-state precision, increasing the system gain at lower frequencies while decreasing it at higher frequencies will improve the performance of the system. This is according to a well-known frequency-based controller design method, known as loop shaping [2]. However, according to Bode's gain-

This chapter is published as:
N. Karbasizadeh, N. Saikumar and S. H. HosseinNia, "Fractional-order single state reset element," in Nonlinear Dynamics, vol. 104, pp. 413-327, 2021, doi: 10.1007/s11071-020-06138-9.

phase relationship for linear systems and frequency response of the differentiator part of PID, this desire is in contradiction with the stability of the systems. In other words, improving the performance of the system in terms of precision, speed, or stability will be at the cost of deteriorating at least one of the other two.

Nonlinear controllers can be used to circumvent this limitation. Among all of the different types of nonlinearities used by researchers to this end, a relatively simple one was first used by Clegg [3] in his special integrator. The idea was to reset the value of the integrator whenever its input crosses zero. Clegg showed that his integrator benefits from a phase lead with respect to its linear counterpart. This category of controllers, thereafter called reset controllers, have been further developed and more sophisticated elements such as First Order Reset Element (FORE) in [4], [5], Generalised FORE (GFORE) in [6] and Second-Order Reset Element (SORE) in [7]. These reset elements were used in different capacities such as phase lag reduction, decreasing sensitivity peak, narrowband and broadband phase compensation, control of positioning systems with friction, see [8]–[15]. The stability of reset elements has also been investigated in the literature [16], [17].

In almost all the reset elements studied in the literature, all the coupled states of the reset element reset [7], [18], [19]. In other words, there is no coupling between a reset and a non-reset state in the architecture of a reset element. However, in [20], it was shown that coupling a reset state and a linear one in an architecture of a SORE can cause the element, called "Second-Order Single State Reset Element"(SOSRE), to exhibit a linear behaviour in terms of steady-state sinusoidal response at a certain frequency. It was also shown that this phenomenon could be used to the benefit of improving steady-state precision of the overall controller at that certain frequency. However, this architecture cannot be used to suppress higher-order harmonics in a broad range of frequencies.

A new reset-based architecture was recently proposed by [18], which has a constant gain while providing phase lead in a broad range of frequencies. This architecture, named "Constant in gain, Lead in phase" (CgLp), can completely replace or take up a significant portion of derivative duties in the framework of PID. In its ideal behaviour, this element robustly stabilises the system by providing the phase lead required in the bandwidth region; however, unlike the derivative part of PID, it does not violate the loop-shaping requirements. Nevertheless, this ideal behaviour is based on the assumptions of the describing function (DF) method, which is a first-order approximation, neglecting higher-order harmonics in the output of a nonlinear element. As will be shown in this paper, the DF approximation can be totally unreliable in the cases where the magnitude of higher-order harmonics are relatively large. In some cases, the magnitudes of higher-order harmonics can be even larger than the first-order one.

Fractional order derivatives and integrals have been used for control designs such as fractional PID [21]–[24] or CRONE control [25]–[27]. Recently, fractional-order elements have also been used within reset elements [19], [28]–[30] in order to approximate complex-order behaviour.

The main contribution of this paper is to use the concept of fractional order calculus within reset elements to suppress the nonlinear effects, i.e., higher-order harmonics. As an extension to SOSRE, this paper couples a fractional-order integrator with a reset one which creates the ability to selectively higher-order harmonics, in a range of frequencies where nonlinearity does not have a clear benefit. In the framework of CgLp, nonlinear-

ity is mainly used to create phase lead in the crossover frequency region; however, it is shown that it can have ill effects for other regions, especially, lower frequencies which are important for tracking performance. Moreover, the nonlinear architecture proposed in this paper can be tuned to behave completely linear at a particular frequency, which means higher-order harmonics will be zero. Suppressing higher-order harmonics at lower frequencies and eliminating them at a particular frequency will improve the performance of the system in terms of steady-state tracking precision.
The remainder of this paper is organised as follows. The second section presents the preliminaries. The following one introduces and discusses the architecture of the introduced element. The fourth section will investigate the benefits of the architecture in suppressing higher-order harmonics at a wide range of frequencies. The following will introduce an illustrative example and verify the discussions in simulation. Finally, the paper concludes with some remarks and recommendations about ongoing work.

3.2. PRELIMINARIES

In this section, the preliminaries of this study will be discussed.

3.2.1. GENERAL RESET CONTROLLER

Following is a general form of a rest controller [31]:

$$\sum_R := \begin{cases} \dot{x}_r(t) = Ax_r(t) + Be(t) & \text{if } e(t) \neq 0, \\ x_r(t^+) = A_\rho x_r(t) & \text{if } e(t) = 0, \\ u(t) = Cx_r(t) + De(t) \end{cases} \tag{3.1}$$

where A, B, C, D are the state space matrices of the base linear system and $A_\rho = \text{diag}(\gamma_1, ..., \gamma_n)$ is called the reset matrix. This contains the reset coefficients for each state which are denoted by $\gamma_1, ..., \gamma_n$. The controller's input and output are represented by $e(t)$ and $u(t)$, respectively. In the special case of $A_\rho = I$, no reset will occur and the result is called the "base linear system".

3.2.2. H_β CONDITION

The quadratic stability of the closed loop reset system when the base linear system is stable can be examined by the following condition [32], [33].

Theorem 3. *There exists a constant $\beta \in \Re^{n_r \times 1}$ and positive definite matrix $P_\rho \in \Re^{n_r \times n_r}$, such that the restricted Lyapunov equation*

$$P > 0, \quad A_{cl}^T P + P A_{cl} < 0 \tag{3.2}$$

$$B_0^T P = C_0 \tag{3.3}$$

has a solution for P, where C_0 and B_0 are defined by

$$C_0 = \begin{bmatrix} \beta C_p & 0_{n_r \times n_{nr}} & P_\rho \end{bmatrix}, \qquad B_0 = \begin{bmatrix} 0_{n_p \times n_r} \\ 0_{n_{nr} \times n_r} \\ I_{n_r} \end{bmatrix}. \tag{3.4}$$

And

$$A_\rho^T P_\rho A_\rho - P_\rho \leq 0 \tag{3.5}$$

A_{cl} is the closed-loop A matrix. n_r is the number of states being reset and n_{nr} is the number of non-resetting states, and n_p is the number of states for the plant. A_p, B_p, C_p, D_p are

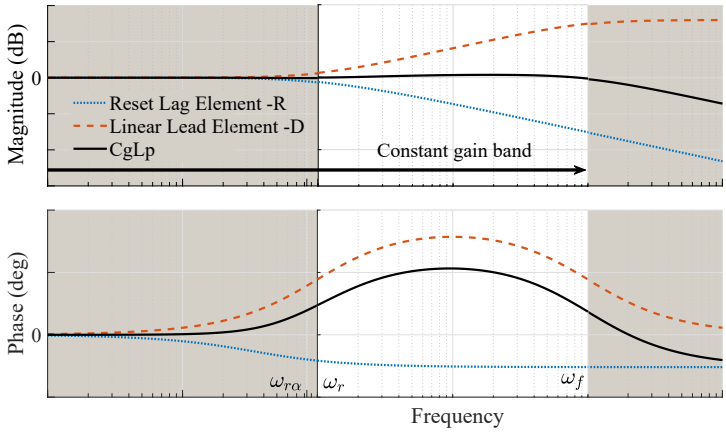

Figure 3.1: The concept of using combination of a reset lag and a linear lead element to form a CgLp element. The figure is adopted from [18].

the state space matrices of the plant.

3.2.3. DESCRIBING FUNCTIONS

Because of its nonlinearity, the steady state response of a reset element to a sinusoidal input is not sinusoidal. Thus, its frequency response should be analysed using approximations such as the Describing Function (DF) method [6]. However, the DF method only takes the first harmonic of Fourier series decomposition of the output into account and neglects the effects of the higher-order harmonics. As shown in [20], this simplification can sometimes be significantly inaccurate. To have more accurate information about the frequency response of nonlinear systems, a method called "Higher Order Sinusoidal Input Describing Function" (HOSIDF) has been introduced in [34]. This method was developed in [35], [36] for reset elements defined by (3.1) as follows:

$$
\begin{aligned}
G_n(\omega) &= \begin{cases} C(j\omega I - A)^{-1}(I + j\Theta_D(\omega))B + D & n = 1 \\ C(j\omega n I - A)^{-1} j\Theta_D(\omega) B & \text{odd } n > 2 \\ 0 & \text{even } n \geq 2 \end{cases} \\
\Theta_D(\omega) &= -\frac{2\omega^2}{\pi}\Delta(\omega)[\Gamma_r(\omega) - \Lambda^{-1}(\omega)] \\
\Lambda(\omega) &= \omega^2 I + A^2 \\
\Delta(\omega) &= I + e^{\frac{\pi}{\omega}A} \\
\Delta_r(\omega) &= I + A_\rho e^{\frac{\pi}{\omega}A} \\
\Gamma_r(\omega) &= {\Delta_r}^{-1}(\omega) A_\rho \Delta(\omega) \Lambda^{-1}(\omega)
\end{aligned}
\tag{3.6}
$$

where $G_n(\omega)$ is the n^{th} harmonic describing function for sinusoidal input with frequency of ω.

3.2.4. CGLP

According to [18], CgLp is a broadband phase compensation element whose first harmonic gain behaviour is constant while providing a phase lead. Originally, two architectures for CgLp are suggested using FORE or SORE, both consisting in a reset lag element in series with a linear lead filter, namely R and D. For FORE CgLp:

$$R(s) = \frac{1}{s/\omega_{r\alpha} + 1}, \quad A_\rho \qquad D(s) = \frac{s/\omega_r + 1}{s/\omega_f + 1} \tag{3.7}$$

For SORE CgLp:

$$R(s) = \frac{1}{(s/\omega_{r\alpha})^2 + (2s\beta/\omega_{r\alpha}) + 1}, \quad A_\rho \tag{3.8}$$

$$D(s) = \frac{(s/\omega_r)^2 + (2s\beta/\omega_r) + 1}{(s/\omega_f)^2 + (2s/\omega_f) + 1}$$

In (3.7) and (3.8), $\omega_{r\alpha} = \omega_r/\alpha$, α is a tuning parameter accounting for a shift in corner frequency of the filter due to resetting action, β is the damping coefficient and $[\omega_r, \omega_f]$ is the frequency range where the CgLp will provide the required phase lead. The arrow indicates that the states of element are reset according to A_ρ; i.e. are multiplied by A_ρ when the reset condition is met.

The main idea behind the CgLp is taking the phase advantage of a reset lag element over its linear counterpart and using it in combination with a corresponding lead element to create a broadband phase lead. Ideally, the gain of the reset lag element should be cancelled out by the gain of the corresponding linear lead element, which create a constant gain behaviour. The concept is depicted in Fig. 3.1.

It can be seen that since this idea is based on DF approximation, the ideal behaviour of CgLp will not be achieved when DF is not a reliable approximation, i.e., when the higher-order harmonics are relatively large and not negligible. Nevertheless, the main idea of CgLp is not restricted to FORE and SORE by nature and can be generalized to any reset lag and linear lead filter. This paper uses fractional ones to reduce higher-order harmonics in a large range of frequencies and consequently create a CgLp element that has close-to-ideal behaviour in a larger range of frequencies.

3.2.5. SECOND-ORDER SINGLE STATE RESET ELEMENT (SOSRE)

This reset element is a special case of a SORE, in which only one integrator resets in a specific architecture. This element is presented in [20] and is used in the framework of a CgLp as the reset lag element. The state-space representation and the reset matrix of the element is as follows:

$$A = \begin{bmatrix} 0 & 1 \\ -\omega_{r\alpha}^2 & -2\beta\omega_{r\alpha} \end{bmatrix}, B = \begin{bmatrix} 0 \\ 1 \end{bmatrix}, C = \begin{bmatrix} \omega_{r\alpha} & 0 \end{bmatrix}, D = [0],$$
$$A_\rho = \begin{bmatrix} 1 & 0 \\ 0 & \gamma \end{bmatrix}. \tag{3.9}$$

As shown in [20], assuming a sinusoidal input at frequency $\omega_{r\alpha}$ to a SOSRE, the steady-state output will be a sinusoidal with the same frequency and no phase shift; thus, the

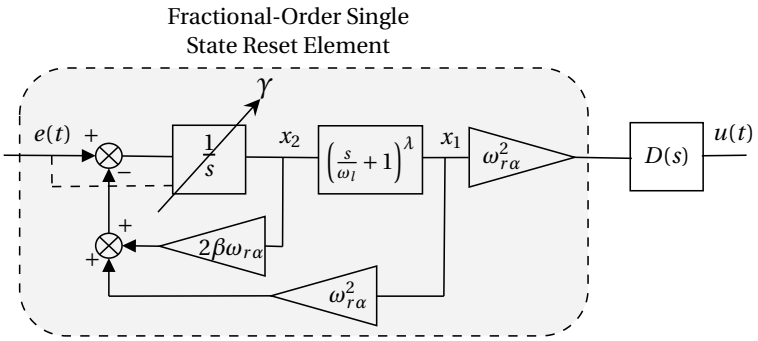

Figure 3.2: Block diagram of the a FOSRE CgLp. $\lambda \in (0 \quad -1]$.

magnitude of higher-order harmonics at $\omega_{r\alpha}$ is zero.

3.2.6. FRACTIONAL ORDER CALCULUS AND CRONE APPROXIMATION OF s^λ

Fractional order calculus developed by generalizing the integration and differentiation to non-integer order operators. Behaviour of such an element should be approximated for application in control. This paper uses the CRONE approximation of s^λ, $\lambda \in \Re^-$, which creates fractional behaviour using real stable poles and real minimum phase zeros for this purpose. The approximation is valid in a frequency range of $[\omega_l, \omega_h]$. Referring to [37], the approximation will be:

$$s^\lambda \approx C \prod_{m=1}^{N} \frac{1+\frac{s}{\omega_{z,m}}}{1+\frac{s}{\omega_{p,m}}} \tag{3.10}$$

$$\omega_{z,m} = \omega_l \left(\frac{\omega_h}{\omega_l}\right)^{\frac{2m-1-\lambda}{2N}} \tag{3.11}$$

$$\omega_{p,m} = \omega_l \left(\frac{\omega_h}{\omega_l}\right)^{\frac{2m-1+\lambda}{2N}} \tag{3.12}$$

where N is number poles and zeros and for an acceptable approximation it should be one unit more than the number of decades in approximation. CRONE ensures that the poles and zeros are placed in the same distance in logarithmic scale. C is the tuning parameter to adjust the gain of the approximation. Considering the range where the approximation is valid, CRONE is actually approximating the $\left(\frac{\frac{s}{\omega_l}+1}{\frac{s}{\omega_h}+1}\right)^\lambda$. Assuming a large enough ω_h, in this paper the CRONE is used to approximate $\left(\frac{s}{\omega_l}+1\right)^\lambda$.

3.3. FRACTIONAL-ORDER SINGLE STATE RESET ELEMENT (FOSRE)

This sections introduces a new structure for reset elements in the framework of CgLp and discusses the architecture, frequency response, and its superiority over FORE and SORE in the framework of CgLp.

3.3.1. ARCHITECTURE

The architecture of the FOSRE is similar to that of the SORE with the difference being that the second linear integrator is replaced by a fractional one, and only the first integrator, which is a integer one, is reset. Figure 3.2 shows the block diagram of the element. The following defines the FOSRE (the reset lag element) and its corresponding lead element to form a CgLp.

$$FOSRE(s) = \frac{1}{(s/\omega_l + 1)^{-\lambda}\left(s/\omega_{r\alpha}^2 + 2\beta/\omega_{r\alpha}\right) + 1} \qquad A_\rho \tag{3.13}$$

$$D(s) = \frac{(s/\omega_l + 1)^{-\lambda}\left(s/\omega_r^2 + 2\beta/\omega_r\right) + 1}{(s/\omega_f)^2 + (2s/\omega_f) + 1}$$

A matching state space representation of FOSRE with the architecture of Fig. 3.2 is as follows:

$$\begin{aligned} A &= \begin{bmatrix} -2\beta\omega_{r\alpha} & 0_{1\times N} \\ \overline{B}_{N\times 1} & \overline{A}_{N\times N} \end{bmatrix} - \omega_{r\alpha}^2 \begin{bmatrix} 1 \\ 0_{N\times 1} \end{bmatrix} \times \begin{bmatrix} \overline{D}_{1\times 1} & \overline{C}_{1\times N} \end{bmatrix}, \\ B &= \begin{bmatrix} 1 \\ 0_{N\times 1} \end{bmatrix}, \quad C = \omega_{r\alpha}^2 \begin{bmatrix} \overline{D}_{1\times 1} & \overline{C}_{1\times N} \end{bmatrix}, \quad D = 0 \\ A_\rho &= \mathrm{diag}(\gamma, \underbrace{1, ..., 1}_{N}) \end{aligned} \tag{3.14}$$

where $\overline{A}$, $\overline{B}$, $\overline{C}$ and $\overline{D}$ are state space matrices of the CRONE approximation of $\left(\frac{s}{\omega_l} + 1\right)^\lambda$.

3.3.2. LINEAR BEHAVIOUR OF FOSRE AT A CERTAIN FREQUENCY

The architecture of FOSRE, along with the non-identical reset of its states, creates a peculiar phenomenon which can be used to the benefit of the performance of the system.

Lemma 1. *Reset control system Eq. (3.1) in open-loop has a globally asymptotically stable $2\pi/\omega$-periodic solution under sinusoid input with arbitrary frequency, $\omega > 0$ if and only if*

$$\left|\lambda\left(A_\rho e^{A\delta}\right)\right| < 1 \quad \forall \delta \in \Re^+ \tag{3.15}$$

where $\lambda(.)$ stands for eigenvalues [6].

Remark 4. *Let us define*

$$\psi(\omega) := \angle \frac{X_2(j\omega)}{E(j\omega)} \quad \text{for } A_\rho = I. \tag{3.16}$$

Assuming a sinusoidal input, $\sin(\omega_{lb} t)$, to a reset element, the reset action will have no effect on the steady-state response, and thus the reset element can be regarded as a linear system in terms of steady-state response at that certain frequency if:

$$\psi(\omega_{lb}) = 0. \tag{3.17}$$

The proof of this is trivial, since the reset element under such circumstances will reset its output when its output is at zero, resulting in no change from the reset action. Figure 3.3 shows an example of this situation, where the steady-state output of the base

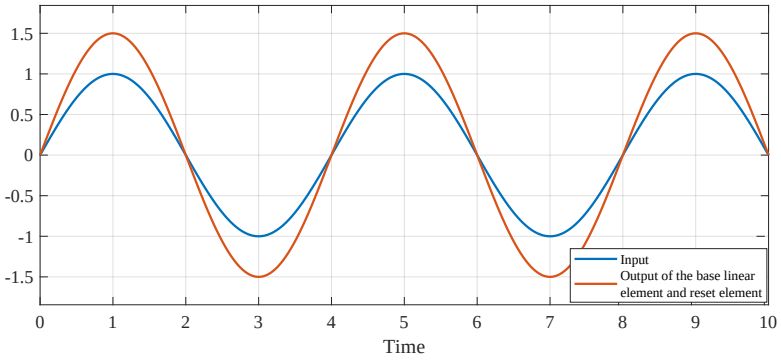

Figure 3.3: Assuming that the output of the base linear element for a reset element has no phase shift with respect to its input, the output of the reset element itself will match the base linear element output at steady state.

linear element and the reset element itself will be the same. Under such circumstances, the reset element can be regarded as a linear element at that certain frequency in terms of steady-state output.

Remark 5. *Assuming a sinusoidal input,* $\sin(\omega_{lb}t)$*, to a reset element where* $\psi(\omega_{lb}) = 0$*, the higher-order harmonics will be zero.*

Since the reset action does not have an effect in steady-state, the steady-state output is sinusoidal. Such an output can be completely described by first harmonic of the Fourier series, and all higher-order harmonics are zero.
For the case of an FOSRE, if $e(t) = \sin(\omega_{lb}t)$, the reset action of the first integrator will be of no effect if:

$$\psi(\omega_{lb}) = 0 \Rightarrow$$

$$\angle \frac{1}{j\omega_{lb}/\omega_{r\alpha}^2 + 2\beta/\omega_{r\alpha} + \left(j\omega_{lb}/\omega_l + 1\right)^{\lambda}} = 0 \Rightarrow$$

$$\omega_{lb} = -\omega_{r\alpha}^2 \left(\frac{\omega_{lb}^2}{\omega_l^2} + 1\right)^{\frac{\lambda}{2}} \sin\left(\lambda \tan^{-1}\left(\frac{\omega_{lb}}{\omega_l}\right)\right). \tag{3.18}$$

Thus, FOSRE exhibits a linear behaviour at a frequency, ω_{lb}, which depends on $\omega_{r\alpha}$, β, ω_l and λ.

3.3.3. HOSIDF OF FOSRE CGLP

Reset elements are nonlinear elements because of the discontinuity in their state values and output. This discontinuity or, in other terms, jumps creates higher-order terms in Fourier decomposition of the output. These jumps also create large peaks in the controller's output, which is a known characteristic for reset elements.
There are many situations where the system's behaviour is not predictable based on DF. As an example, for the mass-spring-damper systems with a resonance peak at ω_n, the 3^{rd} HOSIDF of the open-loop system has a peak at $\omega_n/3$ and the 5^{th} HOSIDF has a peak

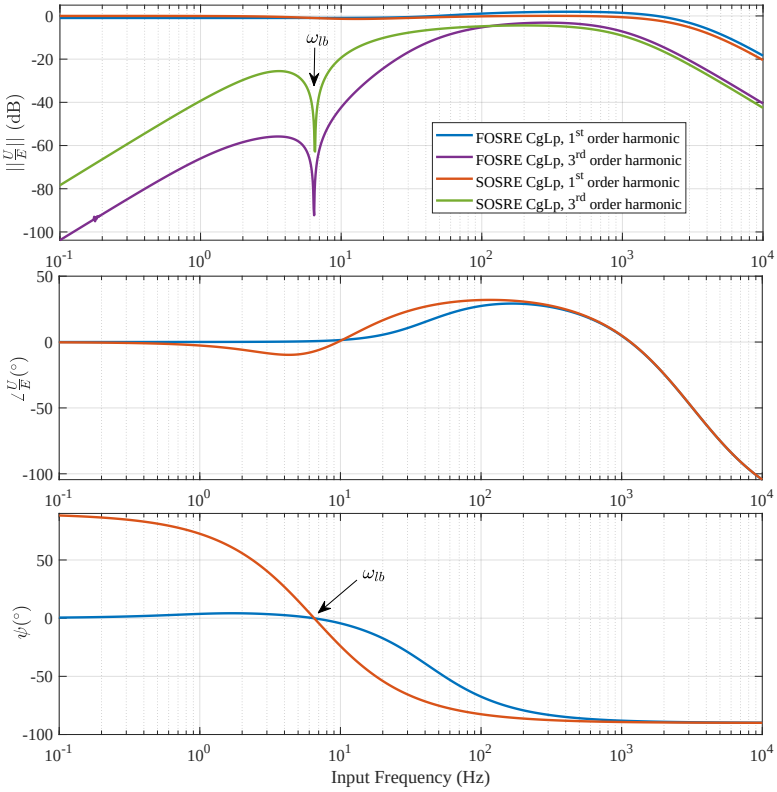

Figure 3.4: HOSIDF comparison of a SOSRE and a FOSRE CgLp along with corresponding ψ which is $\angle\frac{X_2}{E}$ of the base linear system. For FOSRE CgLp, $\omega_{r\alpha} = 3.18$ Hz, $\beta = 1, \alpha = 0.94, \omega_l = 0.8$ Hz, $\lambda = -0.1$, and $\gamma = 0.2$. For SOSRE CgLp, $\omega_{r\alpha} = 6.5$ Hz, $\beta = 1, \alpha = 1.12$ and $\gamma = 0.2$.

at $\omega_n/5$ and so on. If the resonance peak of the system is large enough, higher-order harmonics will probably dominate the first one at $\omega_n/3, \omega_n/5, \ldots$. (See [20], [35]). Therefore, it can be concluded that the smaller the higher-order harmonics are, the closer the system is to what it is designed for.

The main benefit of using FOSRE is that tuning its parameters, one can reduce higher-order harmonics at a range of frequency where nonlinearity not only does not have a clear benefit but also deteriorates the tracking precision of the system.

In [20], it was shown that the elimination of higher-order harmonics using the concept of Remark 4 at one frequency in a SOSRE CgLp element results in the improvement of steady-state tracking precision. While FOSRE enjoys the same benefit, the HOSIDF analysis in this section shows that the structure of FOSRE allows the reduction of the higher-order harmonics at a wider range of frequencies.

In FOSRE, the concept of Remark 4 can be generalised. According to Remark 4, when ψ is zero, the higher-order harmonics will be zero. On top of that, it can be seen empirically that the closer ψ is to zero, the smaller the gain of the higher-order harmonics. Figure 3.4 shows this relation by comparing the HOSIDF of FOSRE and a SOSRE CgLp along with

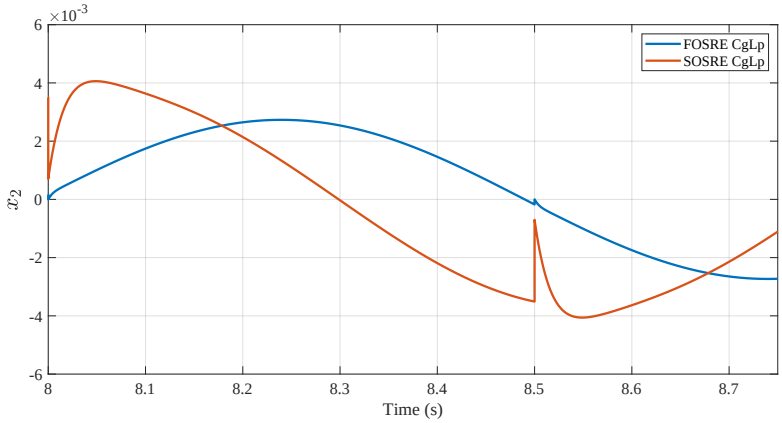

Figure 3.5: Comparing x_2 of the FOSRE CgLp and SOSRE CgLp for an input of $\sin(2\pi t)$.

their ψ plot. All the even harmonics are zero for reset elements and Fig. 3.4 only depicts the 1st and the 3rd harmonic for the sake of clarity of the figure since all the other odd harmonics will follow the same trend as the 3rd one and are descending with respect to their order.
Three main conclusions can be drawn from this figure.

- Both of the ψ plots cross zero between 6 and 7 Hz and correspondingly higher-order harmonics will be zero at ω_{lb} which validates Remark 4 and 5.
- For the range of 0.1 till 500 Hz, ψ of FOSRE CgLp is closer to zero than that of SOSRE CgLp, correspondingly, its magnitude of higher-order harmonics is smaller than that of SOSRE CgLp.
- As ψ approaches more negative values, the phase advantage of CgLp elements increases. Therefore, when comparing two CgLp elements, especially between 10 and 100 Hz, the closer value of ψ to zero results in a smaller phase advantage.

The same line of reasoning has been tested and is valid comparing any two FOSRE CgLp elements. The relation between ψ and higher-order harmonics can be justified by considering the fact that the closer ψ to zero is, the smaller the jumps of the reset element will be. Furthermore, the biggest jump, and thus, the largest higher-order harmonics will happen when $\psi = \pm 90°$. This concept is shown in Fig. 3.5, by comparing the time response of x_2 in FOSRE CgLp and SOSRE CgLp to a sinusoidal input of 1 Hz. It is readily obvious that due to the smaller value of ψ in the FOSRE CgLp at this frequency, the jumps are smaller and thus justifies the smaller magnitude of higher-order harmonics.
According to the aforementioned discussion, the graph ψ contains important information about higher-order harmonics and phase advantage created by CgLp elements, and hence can be used to tune the FOSRE parameters so that the FOSRE CgLp element has a closer-to-ideal behaviour.
The following section will discuss the effect of FOSRE parameters on the ψ plot and thus higher-order harmonics.

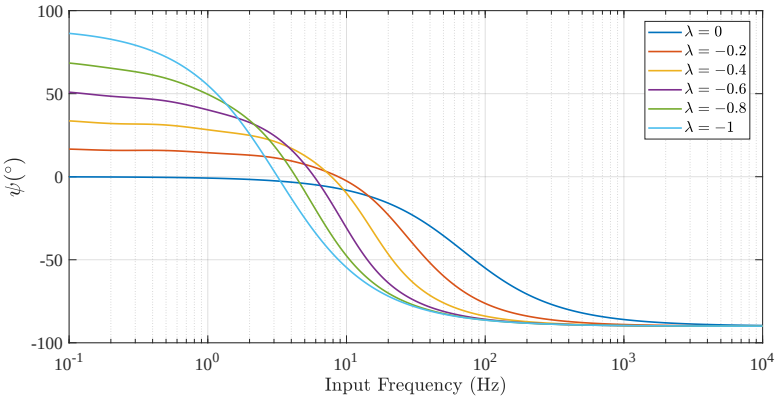

Figure 3.6: The effect of λ on ψ in FOSRE. $\omega_{r\alpha} = 3.18$ Hz, $\beta = 1$ and $\omega_l = 0.001$ Hz.

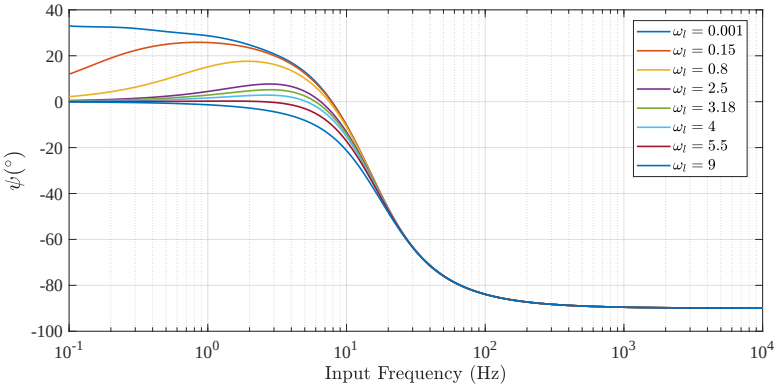

Figure 3.7: The effect of ω_l on ψ in FOSRE. $\omega_{r\alpha} = 3.18$ Hz, $\beta = 1$ and $\lambda = -0.4$.

3.4. SUPPRESSING HIGHER-ORDER HARMONICS AT LOW FREQUENCIES

The main advantage of FOSRE over SOSRE is that the nonlinearity effects, i.e., the higher-order harmonics, can be suppressed at low frequencies. This can be done by manipulating the value of ψ at lower frequencies. This is made possible for FOSRE by two additional parameters, namely λ and ω_l. The effects of these two parameters on the ψ plot are discussed below.

The effect of λ on higher-order harmonics and the phase advantage created by a FOSRE can be depicted by plotting ψ versus the input frequency for different values of λ. See Fig. 3.6. As λ approaches -1, ψ deviates more from zero in lower frequencies, indicating larger higher-order harmonics at low frequencies and thus deterioration of tracking precision. Nevertheless, ψ will approach $-90°$ faster; in turn, the phase advantage of the CgLp element will be available in a wider frequency range. For example, designing a controller for 100 Hz bandwidth, a FOSRE depicted in Fig. 3.6 with $\lambda = -0.2$ will have

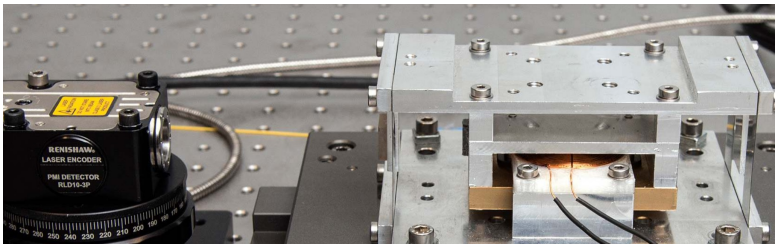

Figure 3.8: The stage whose transfer function is used for simulation.

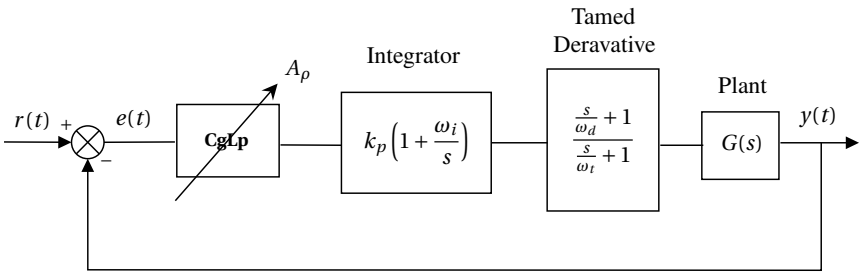

Figure 3.9: Designed control architecture to compare the performance of two sets of controllers.

less phase margin compared to the one with $\lambda = -0.8$. Notice that ω_{lb} varies with λ and for $\lambda = 0$, $\omega_{lb} = 0$, which means that FOSRE will not show linear behaviour for such a configuration.
Changing λ, suppressing higher-order harmonics comes at the cost of losing phase advantage. However, by tuning ω_l, one can circumvent this limitation. Figure 3.7 shows the plot of ψ for different values of ω_l when $\lambda = -0.4$. Increasing ω_l to a certain point, ψ becomes closer to zero for frequencies below ω_{lb}, while it will not cause loss of phase advantage in the crossover frequency region. It should be noted that ω_{lb} according to (3.18), depends on ω_l.
The ideal tracking performance of a CgLp will occur at ω_{lb} where higher-order harmonics are zero, and hence the tracking error can be accurately calculated using DF. If tracking at a certain frequency is important for a system, one may consider designing ω_{lb} to match that frequency. Otherwise, as suggested in [20], ω_{lb} can be designed to match and cancel out the peak of the 3rd order harmonic.

3.4.1. TUNING GUIDELINES

Tuning of FOSRE can be done through optimisation or several iterations of trial and error. The first parameter to choose is ω_{lb}. As mentioned above, this frequency can be a working frequency of the system or a peak of the 3rd harmonic. The cost function to minimize is $\psi(\omega)$ in the range of lower frequencies up to ω_{lb}. Denoting the crossover frequency as ω_c, one can follow the following steps as a rule of thumb to achieve a favourable configuration:

Table 3.1: Parameters of the designed controllers. All frequencies are in Hz.

Controller	ω_i	ω_d	ω_t	ω_f	$\omega_{r\alpha}$	β	γ	λ	ω_l
PID	15	32	705	1500	N/A	N/A	N/A	N/A	N/A
SOSRE No. 1	15	100	225	1500	2	1	0.2	N/A	N/A
SOSRE No. 2	15	100	225	1500	0.8	1	0.2	N/A	N/A
FOSRE No. 1	15	100	225	1500	2	1	0.2	-0.4	2.5
FOSRE No. 2	15	100	225	1500	1.2	1	0.2	-0.4	1.3

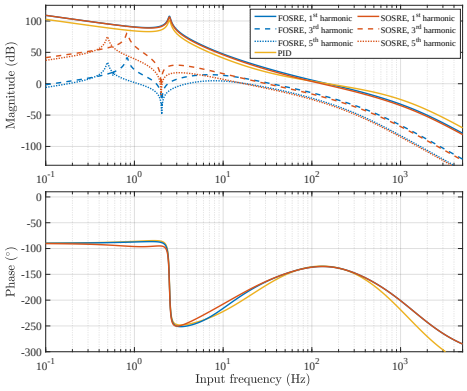

(a) Set No.1: Controllers designed to behave linearly at 2 Hz

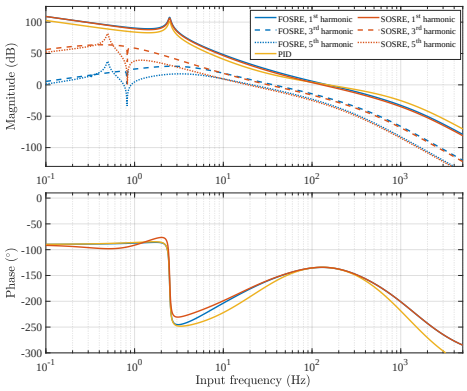

(b) Set No.2: Controllers designed to behave linearly at 0.8 Hz to cancel the 3rd order harmonic peak

Figure 3.10: HOSIDF of open loop for 3 systems designed based on a SOSRE CgLp, FOSRE CgLp and a PID.

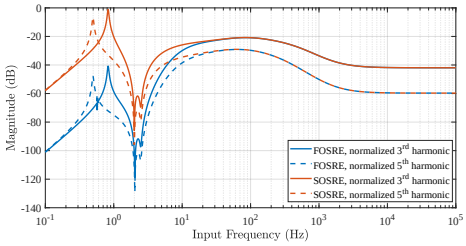

(a) Set No.1: Controllers designed to behave linearly at 2 Hz

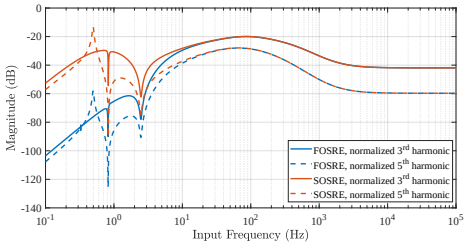

(b) Set No.2: Controllers designed to behave linearly at 0.8 Hz to cancel 3rd order harmonic peak

Figure 3.11: Normalized magnitude of higher-order harmonics with respect to first-order one for FOSRE and SOSRE.

1. **Choose** ω_{lb}.
2. **Set** λ **to be** -0.1**.**
3. **Set** β **to be** 1**.**

4. **Optimise ω_l and $\omega_{r\alpha}$ to minimise $|\psi(\omega)|$ at frequencies lower than ω_{lb}, constrained to $\psi(\omega_{lb}) = 0$.**

5. **Is $\psi(\omega_c) < -85°$? If yes, proceed to 7, if not, decrease β by** 0.1.

6. **Is $\beta = 0$? if yes, decrease λ by** -0.1 **and return to 3, if not, return to 4.**

7. **Choose γ in** $[-1 \quad 1)$ **to achieve the phase margin required.**

3

3.5. AN ILLUSTRATIVE EXAMPLE

In order to validate the increase in performance of the system in terms of steady-state tracking by suppressing the higher-order harmonics, three controllers were designed and studied in simulation. This section presents the results of the comparison of an FOSRE CgLp with an SOSRE CgLp and a PID.

3.5.1. PLANT

The plant which is simulated is a custom-designed precision stage that is actuated with the use of a Lorentz actuator. This stage is linearly guided using two flexures to attach the Lorentz actuator to the base of the stage and actuated at the center of the flexures. With a laser encoder, the position of the fine stage is read out with 10nm resolution. A picture of the setup can be found in Fig. 3.8. The identified transfer function for the plant is:

$$G(s) = \frac{3.038e4}{s^2 + 0.7413s + 243.3}. \tag{3.19}$$

This plant has a relatively high resonance peak around 2.5 Hz, which will cause high peaks in higher-order harmonics at frequencies below 1 Hz.

3.5.2. CONTROLLER DESIGN APPROACH

Two sets of controllers have been designed, each containing a FOSRE CgLp, a SOSRE CgLp and a PID. All controllers have designed a bandwidth of 150 Hz and 45° of phase margin considering a sensitivity peak below 6 dB criteria for robustness.

In set No. 1, assuming a main working frequency of 2 Hz, FOSRE CgLp and SOSRE CgLp are designed in such a way that they have $\omega_{lb} = 2$ Hz. This means that the reset controllers will behave linearly in terms of steady-state output and will generate no higher-order harmonics at the said frequency. In set No. 2, reset controllers are designed to have $\omega_{lb} = 0.8$ Hz, which is the frequency of the peak of the third harmonic. Considering the discussion in Section 3.4, parameters of the FOSRE are chosen in a manner that ψ stays as close as possible to zero in frequencies below ω_{lb}. Moreover, such a design is not possible for SOSRE. Figure 3.9 and Table 3.1 show the closed-loop block diagram and the parameters for each controller.

In order to be able to verify the stability of the reset systems through the so-called H_β condition, a relatively weak derivate has been added to the design of CgLp's to provide a phase margin of 5° for the base-linear system. Thus, the CgLp's are providing the remaining 40° required.

The HOSIDF analysis of the open loop of the designed system sets is presented in Fig. 3.10. As expected, SOSRE CgLp's produce larger higher-order harmonics at low frequencies than the FOSRE ones, while they both have the same first-order DF and provide the same

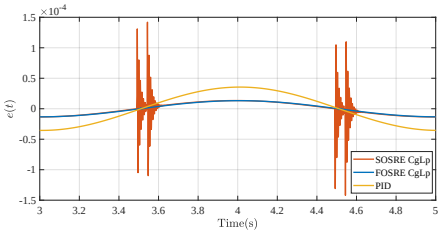

(a) Systems in set No. 1, $r(t) = \sin(\pi t)$

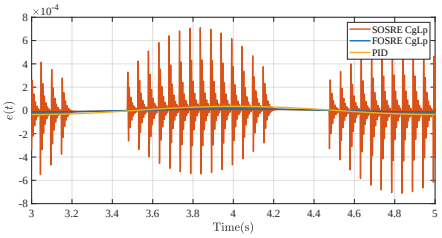

(b) Systems in set No. 2, $r(t) = \sin(\pi t)$

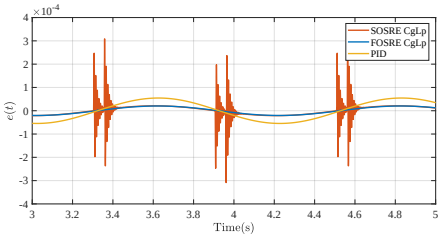

(c) Systems in set No. 1, $r(t) = \sin(1.6\pi t)$

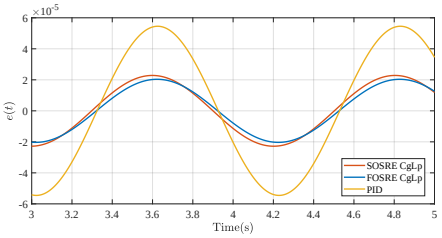

(d) Systems in set No. 2, $r(t) = \sin(1.6\pi t)$

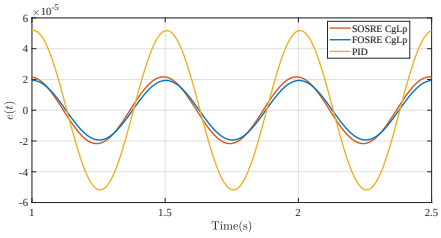

(e) Systems in set No. 1, $r(t) = \sin(4\pi t)$

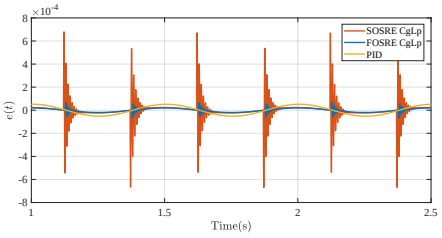

(f) Systems in set No. 2, $r(t) = \sin(4\pi t)$

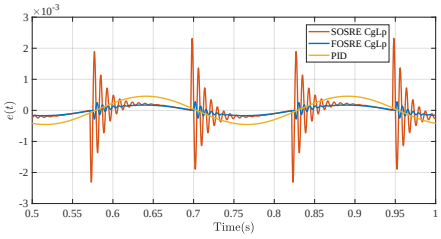

(g) Systems in set No. 1, $r(t) = \sin(8\pi t)$

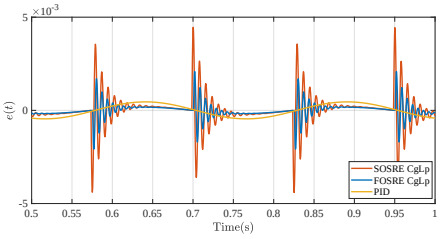

(h) Systems in set No. 2, $r(t) = \sin(8\pi t)$

Figure 3.12: The steady-state error of designed systems for tacking sinusoidal inputs.

phase margin. The presence of large higher-order harmonics can jeopardise the tracking performance of the controller, as it invalidates the assumption of design based on DF. To better clarify the frequencies at which the tracking performance is weak and where it is the ideal, one can refer to normalised magnitude of higher-order harmonics with

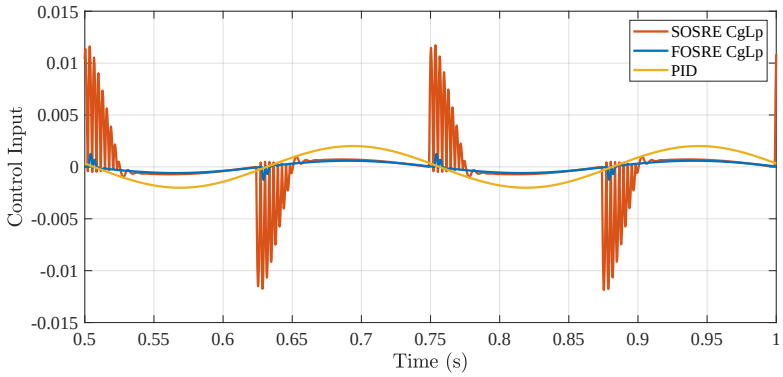

Figure 3.13: Control input of controllers in set No.1 for $r(t) = \sin(8\pi t)$.

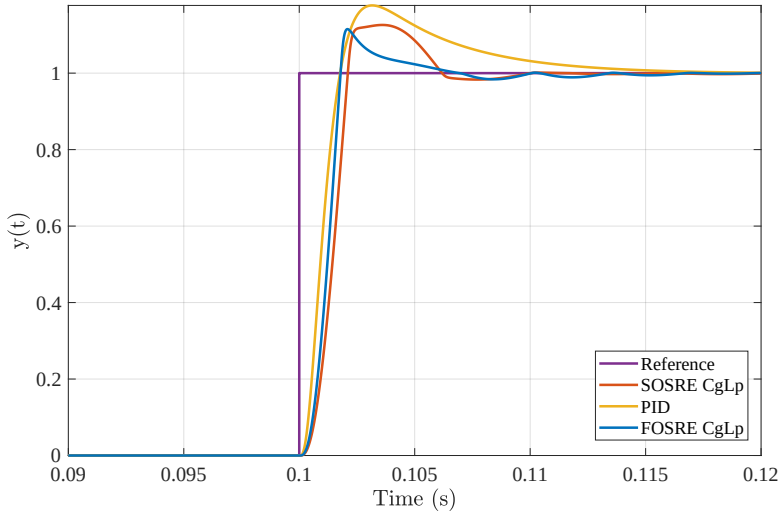

Figure 3.14: Step responce of controllers in set No. 1.

respect to the first order harmonics in Fig. 3.11. According to this figure, one can predict that the lower values of this plot indicate closer-to-ideal behavior for CgLp. As a rule of thumb, if the normalised magnitude if higher-order harmonics are below -40 dB, their effect is negligible, provided that their magnitude is different enough to prevent their constructive behaviour from deteriorating the performance.
Referring to Figs. 3.10 and 3.11, it is clearly shown that using the FOSRE architecture in CgLp framework, higher-order harmonics can be suppressed at lower frequencies while maintaining them at the crossover frequency region to provide the required phase margin. Notice that the normalised higher-order harmonics are almost 0 dB at their peaks for SOSRE, which shows that they are almost equal to the first-order one.
Furthermore, it is shown that at ω_{lb}, the higher-order harmonics will be zero, and this can be used to cancel out the higher-order harmonics peaks, as shown in Fig. 3.10b.

Table 3.2: RMS and IAE of steady state error for controllers in set No. 1 for tracking the sinusoidal references of 0.5, 0.8, 2 and 4 Hz.

Frequency	0.5 Hz		0.8 Hz		2 Hz		4 Hz	
Metric	RMS	IAE	RMS	IAE	RMS	IAE	RMS	IAE
FOSRE CgLp	9.36e-6	1.68e-5	1.47e-5	2.68e-5	1.36e-5	1.84e-5	1.31e-4	5.99e-5
SOSRE CgLp	1.62e-5	2.22e-5	3.64e-5	4.30e-5	1.53e-5	2.07e-5	4.76e-4	1.44e-4
PID	2.51e-5	4.52e-5	3.96e-5	7.21e-5	3.66e-5	4.94e-5	3.21e-4	1.44e-4

Table 3.3: RMS and IAE of steady state error for controllers in set No. 2 for tracking the sinusoidal references of 0.5, 0.8, 2 and 4 Hz.

Frequency	0.5 Hz		0.8 Hz		2 Hz		4 Hz	
Metric	RMS	IAE	RMS	IAE	RMS	IAE	RMS	IAE
FOSRE CgLp	9.37e-6	1.68e-5	1.47e-5	2.68e-5	1.60e-5	2.11e-5	3.95e-4	1.15e-4
SOSRE CgLp	1.47e-4	1.63e-4	1.64e-5	2.99e-5	9.34e-5	6.13e-5	8.72e-4	2.28e-4
PID	2.51e-5	4.52e-5	3.96e-5	7.21e-5	3.65e-5	4.94e-5	3.21e-4	1.44e-4

To validate the performance of the controllers in closed-loop, a simulation has been performed in the Simulink environment of Matlab for tracking four sinusoidal waves of 0.5, 0.8, 2 and 4 Hz. The resulting error plots are depicted in Fig. 3.12. Furthermore, the Root Mean Square (RMS) and Integral Absolute Error (IAE) for steady-state error is presented in Table 3.2 and 3.3. The plots and tables verify that if the higher-order harmonics are small enough, the reset controllers outperform the linear controller in terms of steady-state tracking error. A SOSRE CgLp designed for a system with a high resonance peak can outperform PID around ω_{lb}; however, it has difficulties at other frequencies. Nevertheless, FOSRE CgLp because of its much smaller higher-order harmonics has a much wider range of superiority, about 1.5 decades in this particular example.

Since the direct relation of higher-order harmonics and tracking performance can be observed, it should be noted that 0.5 and 0.8 Hz are the degenerate cases for reset controllers, however, designing ω_{lb} to match and cancel out the peaks, the ideal tracking performance based on DF can be achieved. See Fig. 3.12d.

In order to compare the control actions of the designed controllers, the control input for controllers in set No.1 is depicted for a sinusoidal input of 4 Hz in Fig. 3.13. Reset controllers are known for having large peaks in their control actions, however, according to Fig. 3.13, FOSRE CgLp shows smaller peaks due to reduced higher-order harmonics. The same holds for other frequencies and controllers in set No. 2, however they are not depicted for the sake of brevity.

At last, the step response for designed controllers in set No. 1 is shown in Fig. 3.14. FOSRE and SOSRE CgLp show smaller overshoot and approximately the same settling time compared to PID. Controllers in set No. 2, show approximately the same step response.

3.6. CONCLUSION

This paper presented an architecture, named FOSRE, for reset elements based on a fractional-order integrator and the concept of having only one resetting integrator. It was shown that using this architecture in framework of CgLp; the higher-order harmonics can be suppressed at lower frequencies based on tuning the phase difference of input and output of the base linear system of the element. It was shown that at a particular frequency at which the mentioned phase difference is zero, no higher-order harmonics would be produced, and the reset system would behave as a linear one in terms of steady-state output. Using this architecture, one can achieve the same phase margin as CgLp's introduced in the literature while increasing their tracking performance. The closed-loop performance of the FOSRE CgLp was compared with a SOSRE one and a PID in two different designs in simulation, and its superiority was validated.

It was shown that one peak of higher-order harmonics could be canceled out using the linear behaviour concept. However, this opens an opportunity for future research on architectures that can behave linearly at more than one frequency, as there are multiple peaks in higher-order harmonics. As ongoing work, the performance of the FOSRE CgLp is being studied in the presence of noise and disturbance and afterwards in a practical setup.

BIBLIOGRAPHY

[1] J. Maclejowski, *Multivariate feedback design*, 1989.

[2] R. M. Schmidt, G. Schitter, and A. Rankers, *The Design of High Performance Mechatronics-: High-Tech Functionality by Multidisciplinary System Integration*. Ios Press, 2014.

[3] J. Clegg, "A nonlinear integrator for servomechanisms", *Transactions of the American Institute of Electrical Engineers, Part II: Applications and Industry*, vol. 77, no. 1, pp. 41–42, 1958.

[4] I. Horowitz and P. Rosenbaum, "Non-linear design for cost of feedback reduction in systems with large parameter uncertainty", *International Journal of Control*, vol. 21, no. 6, pp. 977–1001, 1975.

[5] L. Zaccarian, D. Nesic, and A. R. Teel, "First order reset elements and the clegg integrator revisited", in *Proceedings of the 2005, American Control Conference, 2005.*, IEEE, 2005, pp. 563–568.

[6] Y. Guo, Y. Wang, and L. Xie, "Frequency-domain properties of reset systems with application in hard-disk-drive systems", *IEEE Transactions on Control Systems Technology*, vol. 17, no. 6, pp. 1446–1453, 2009.

[7] L. Hazeleger, M. Heertjes, and H. Nijmeijer, "Second-order reset elements for stage control design", in *2016 American Control Conference (ACC)*, IEEE, 2016, pp. 2643–2648.

[8] D. Wu, G. Guo, and Y. Wang, "Reset integral-derivative control for hdd servo systems", *IEEE Transactions on Control Systems Technology*, vol. 15, no. 1, pp. 161–167, 2006.

[9] Y. Li, G. Guo, and Y. Wang, "Nonlinear mid-frequency disturbance compensation in hdds", in *Proc. 16th IFAC Triennial World Congr.*, 2005, pp. 151–156.

[10] Y. Li, G. Guo, and Y. Wang, "Reset control for midfrequency narrowband disturbance rejection with an application in hard disk drives", *IEEE Transactions on Control Systems Technology*, vol. 19, no. 6, pp. 1339–1348, 2010.

[11] H. Li, C. Du, and Y. Wang, "Optimal reset control for a dual-stage actuator system in hdds", *IEEE/ASME Transactions on Mechatronics*, vol. 16, no. 3, pp. 480–488, 2011.

[12] A. Palanikumar, N. Saikumar, and S. H. HosseinNia, "No more differentiator in PID: Development of nonlinear lead for precision mechatronics", in *2018 European Control Conference (ECC)*, IEEE, 2018, pp. 991–996.

[13] N. Saikumar, R. K. Sinha, and S. H. HosseinNia, "Resetting disturbance observers with application in compensation of bounded nonlinearities like hysteresis in piezo-actuators", *Control Engineering Practice*, vol. 82, pp. 36–49, 2019.

[14] A. Bisoffi, R. Beerens, W. Heemels, H. Nijmeijer, N. van de Wouw, and L. Zaccarian, "To stick or to slip: A reset pid control perspective on positioning systems with friction", *Annual Reviews in Control*, 2020.

[15] R. Beerens, A. Bisoffi, L. Zaccarian, W. Heemels, H. Nijmeijer, and N. van de Wouw, "Reset integral control for improved settling of pid-based motion systems with friction", *Automatica*, vol. 107, pp. 483–492, 2019.

[16] S. van Loon, K. Gruntjens, M. Heertjes, N. van de Wouw, and W. Heemels, "Frequency-domain tools for stability analysis of reset control systems", *Automatica*, vol. 82, pp. 101–108, 2017.

[17] O. Beker, C. Hollot, Q. Chen, and Y. Chait, "Stability of a reset control system under constant inputs", in *Proceedings of the 1999 American Control Conference (Cat. No. 99CH36251)*, IEEE, vol. 5, 1999, pp. 3044–3045.

[18] N. Saikumar, R. Sinha, and S. H. Hoseinnia, "'constant in gain lead in phase'element-application in precision motion control", *IEEE/ASME Transactions on Mechatronics*, 2019.

[19] D. Valério, N. Saikumar, A. A. Dastjerdi, N. Karbasizadeh, and S. H. HosseinNia, "Reset control approximates complex order transfer functions", *Nonlinear Dynamics*, vol. 97, no. 4, pp. 2323–2337, 2019.

[20] N. Karbasizadeh, A. A. Dastjerdi, N. Saikumar, D. Valerio, and S. H. HosseinNia, *Benefiting from linear behaviour of a nonlinear reset-based element at certain frequencies*, 2020. arXiv: 2004.03529 [eess.SY].

[21] I. Podlubny, "Fractional-order systems and $PI^{\lambda}D^{\mu}$-controllers", *IEEE Transactions on Automatic Control*, vol. 44, no. 1, pp. 208–214, 1999.

[22] A. A. Dastjerdi, B. M. Vinagre, Y. Chen, and S. H. HosseinNia, "Linear fractional order controllers; a survey in the frequency domain", *Annual Reviews in Control*, 2019.

[23] M. F. Silva, J. T. Machado, and A. Lopes, "Fractional order control of a hexapod robot", *Nonlinear Dynamics*, vol. 38, no. 1-4, pp. 417–433, 2004.

[24] S. Ladaci and A. Charef, "On fractional adaptive control", *Nonlinear Dynamics*, vol. 43, no. 4, pp. 365–378, 2006.

[25] A. Oustaloup and M. Bansard, "First generation crone control", in *Proceedings of IEEE Systems Man and Cybernetics Conference-SMC*, IEEE, vol. 2, 1993, pp. 130–135.

[26] A. Oustaloup, B. Mathieu, and P. Lanusse, "Second generation crone control", in *Proceedings of IEEE Systems Man and Cybernetics Conference-SMC*, IEEE, vol. 2, 1993, pp. 136–142.

[27] P. Melchior, A. Poty, and A. Oustaloup, "Motion control by ZV shaper synthesis extended for fractional systems and its application to crone control", *Nonlinear dynamics*, vol. 38, no. 1-4, pp. 401–416, 2004.

[28] S. H. HosseinNia, I. Tejado, and B. M. Vinagre, "Fractional-order reset control: Application to a servomotor", *Mechatronics*, vol. 23, no. 7, pp. 781–788, 2013.

[29] D. Valério and J. S. da Costa, "Fractional reset control", *Signal, Image and Video Processing*, vol. 6, no. 3, pp. 495–501, 2012.

[30] N. Saikumar, D. Valério, and S. H. HosseinNia, "Complex order control for improved loop-shaping in precision positioning", *arXiv preprint arXiv:1907.09249*, 2019.

[31] Y. Guo, L. Xie, and Y. Wang, *Analysis and Design of Reset Control Systems*. Institution of Engineering and Technology, 2015, ISBN: 1849197032, 9781849197038.

[32] O. Beker, C. Hollot, Y. Chait, and H. Han, "Fundamental properties of reset control systems", *Automatica*, vol. 40, no. 6, pp. 905–915, 2004.

[33] Y. Guo, L. Xie, and Y. Wang, *Analysis and design of reset control systems*. Institution of Engineering and Technology, 2015.

[34] P. Nuij, O. Bosgra, and M. Steinbuch, "Higher-order sinusoidal input describing functions for the analysis of non-linear systems with harmonic responses", *Mechanical Systems and Signal Processing*, vol. 20, no. 8, pp. 1883–1904, 2006.

[35] K. Heinen, "Frequency analysis of reset systems containing a clegg integrator", M.S. thesis, Delft University of Technology, 2018.

[36] A. A. Dastjerdi, N. Saikumar, D. Valerio, and S. H. HosseinNia, *Closed-loop frequency analyses of reset systems*, 2020.

[37] A. Oustaloup, "La Commade CRONE: Commande Robuste d'Ordre Non Entier", in *Hermes*, Hermés, 1991, ISBN: 9782866012892.

4

BAND-PASSING NONLINEARITY IN RESET ELEMENTS

This paper addresses nonlinearity in reset elements and its effects. Reset elements are known for having less phase lag based on describing function analysis compared to their linear counterparts; however, they are nonlinear elements and produce higher-order harmonics. This paper investigates the steady-state higher-order harmonics for reset elements with one resetting state and proposes an architecture and a method of design that allows for band-passing the nonlinearity and its effects, namely, higher-order harmonics and phase advantage. The nonlinearity of reset elements is not entirely useful for all frequencies, e.g., they are useful for reducing phase lag at cross-over frequency region; however, higher-order harmonics can compromise tracking and disturbance rejection performance at lower frequencies. Using the proposed "phase shaping" method, one can selectively suppress the nonlinearity of a single-state reset element in a desired range of frequencies and allow the nonlinearity to provide its phase benefit in a different desired range of frequencies. This can be especially useful for the reset elements in the framework of the "Constant in gain, Lead in phase" (CgLp) filter, which is a newly introduced nonlinear filter, bound to circumvent the well-known linear control limitation – the waterbed effect.

4.1. INTRODUCTION

The growing demand on precision, bandwidth and robustness of controllers in fields like precision motion control are pushing linear control to its limits [1]. Fundamental limits of linear controllers, namely Bode's phase gain relationship or Bode's sensitivity integral theorem, a.k.a., "the waterbed effect" [2], have caused researchers and industries to change course toward nonlinear control to circumvent these limitations [3]. Reset

This chapter is published as:
N. Karbasizadeh, A. A. Dastjerdi, N. Saikumar and S. H. HosseinNia, "Band-Passing Nonlinearity in Reset Elements," in IEEE Transactions on Control Systems Technology, vol. 31, no. 1, pp. 333-343, Jan. 2023, doi: 10.1109/TCST.2022.3178043.

control is one of those non-linear techniques that has gained significant prominence in recent times [4], [5] especially in the field of precision motion control.
The reset control technique was first introduced by Clegg [6] as a nonlinear integrator, and its advantage was described in [7] in terms of reducing phase lag compared to its linear counterparts. The main idea of a reset control is to reset a subset of controller states when a predefined reset condition is met. More sophisticated reset elements have been developed over the years, namely, the First-Order Reset Element (FORE) [8], Generalized First-Order Reset Element (GFORE) [9] and the Second-Order Reset Element (SORE) [10]. These reset elements were used in different capacities, such as phase lag reduction, decrease in the sensitivity peak, narrowband and broadband phase compensation, guarantee of exponential convergence and approximation of complex order behaviour [11]–[19]. Furthermore, they have been used for different applications, especially precision motion control [20]. A new reset-based architecture was recently proposed by [21], which has a constant gain while providing phase lead in a broad range of frequencies. This architecture, named “Constant in gain, Lead in phase” (CgLp), can completely replace or take up a significant portion of derivative duties in the framework of PID. The stability of reset elements is studied in the literature from different aspects [22], [23].
Being a nonlinear controller, reset elements produce higher-order harmonics, which in turn makes the reset control two-edged. While it is capable of overcoming linear control limitations, the existence of higher-order harmonics can compromise the performance of the system [24]. Recently researchers found that the Describing Function (DF) method for analyzing reset elements in frequency domain [9] is insufficient, as it neglects the effect of higher-order harmonics. A generalised form of the DF method which accounts for higher-order harmonics called the Higher-Order Sinusoidal Input Describing Function (HOSIDF) [25] was adopted for reset elements in [26], [27]. In the literature, efforts are made to reduce the adverse effects of higher-order harmonics in one frequency or by tuning the parameters of the reset element or finding the optimal sequence of elements [24], [28]–[32]. However, to the best of the authors’ knowledge, there is no systematic approach in the literature for deliberately reducing higher-order harmonics to a desired upper bound in a range of frequencies.
The main benefit of reset elements is the reduction of phase lag relative to their linear counterparts. This characterization is beneficial in cross-over frequency region and has no clear benefit at other frequencies. Furthermore, higher-order harmonics compromise the performance of the system in terms of tracking precision and disturbance rejection, which is basically discussed in loop-shaping method at lower frequencies [30], [33]. Thus, providing a method to band-pass the nonlinearity and, in turn, higher-order harmonics seems logical to help keep the positive edge of reset elements while limiting its negative edge.
The main contribution of this paper is the investigation of higher-order harmonics in reset elements with one resetting state and the proposal of an architecture and a method of design called "phase shaping" to allow for band-passing nonlinearity in reset elements. In other words, using the proposed architecture and phase shaping method, one can create a reset element, e.g., a Clegg integrator, a FORE or a CgLp, which is nonlinear in a range of frequencies while it acts linear in terms of steady-state response at other fre-

quencies. Meaning that the element will limit its phase benefits to where it is needed and will have reduced higher-order harmonics at other frequencies. The paper also investigates the performance of the proposed element in the framework of CgLp and shows that, using the proposed method, the performance of the CgLp element will be significantly improved.
The remainder of this paper is organized as follows. The second section presents the preliminaries. The following section introduces and discusses the architecture of the proposed reset element and investigates its HOSIDF. The fourth section will propose the design and tuning method called phase-shaping. The following will introduce an illustrative example and verify the discussions in practice. Finally, the paper concludes with some remarks and recommendations about ongoing work.

4.2. PRELIMINARIES

This section will discuss the preliminaries of this study.

4.2.1. GENERAL RESET CONTROLLER

Following is a general form of a reset controller [34]:

$$\sum_R := \begin{cases} \dot{x}_r(t) = A_r x_r(t) + B_r e(t), & \text{if } e(t) \neq 0 \\ x_r(t^+) = A_\rho x_r(t), & \text{if } e(t) = 0 \\ u(t) = C_r x_r(t) + D_r e(t) \end{cases} \tag{4.1}$$

where $\sum_R$ is the reset controller and A_r, B_r, C_r, D_r are the state space matrices of the base linear system and $A_\rho = \text{diag}(\gamma_1, ..., \gamma_n)$ is called the reset matrix. This matrix contains the reset coefficients for each state, which are denoted by $\gamma_1, ..., \gamma_n$. $x_r(t^+)$ represents the value of the reset state exactly after the reset action. The controller input and output are represented by $e(t)$ and $u(t)$, respectively.

4.2.2. H_β CONDITION

The quadratic stability of the closed loop reset system when the base linear system is stable can be examined by the following condition [5], [35].

Theorem 4. *There exists a constant $\beta \in \Re^{n_r \times 1}$ and positive definite matrix $P_\rho \in \Re^{n_r \times n_r}$, such that the restricted Lyapunov equation*

$$P > 0, \quad A_{cl}^T P + P A_{cl} < 0 \tag{4.2}$$

$$B_0^T P = C_0 \tag{4.3}$$

has a solution for P, where C_0 and B_0 are defined by

$$C_0 = \begin{bmatrix} \beta C_p & 0_{n_r \times n_{nr}} & P_\rho \end{bmatrix}, \qquad B_0 = \begin{bmatrix} 0_{n_p \times n_r} \\ 0_{n_{nr} \times n_r} \\ I_{n_r} \end{bmatrix}. \tag{4.4}$$

and

$$A_\rho^T P_\rho A_\rho - P_\rho \leq 0 \tag{4.5}$$

where A_{cl} is the closed-loop A-matrix. n_r is the number of states that are reset and n_{nr} is the number of non-resetting states, and n_p is the number of states for the plant. A_p, B_p, C_p, D_p are the state space matrices of the plant.

4.2.3. DESCRIBING FUNCTIONS

Because of its nonlinearity, the steady state response of a reset element to a sinusoidal input is not sinusoidal. Therefore, its frequency response should be analyzed using approximations such as the Describing Function (DF) method [9]. However, the DF method only takes the first harmonic of Fourier series decomposition of the output into account and neglects the effects of the higher-order harmonics. As shown in [24], this simplification can sometimes be significantly inaccurate. To have more accurate information about the frequency response of nonlinear systems, a method called "Higher Order Sinusoidal Input Describing Function" (HOSIDF) has been introduced in [25]. This method was developed in [26], [27] for reset elements defined by Eq. (4.1) as follows:

$$
\begin{aligned}
G_n(\omega) &= \begin{cases} C_r(j\omega I - A_r)^{-1}(I + j\Theta(\omega))B_r + D_r, & n = 1 \\ C_r(j\omega n I - A_r)^{-1} j\Theta(\omega) B_r, & \text{odd } n > 2 \\ 0, & \text{even } n \geq 2 \end{cases} \\
\Theta(\omega) &= -\frac{2\omega^2}{\pi}\Delta(\omega)[\Gamma(\omega) - \Lambda^{-1}(\omega)] \\
\Lambda(\omega) &= \omega^2 I + {A_r}^2 \\
\Delta(\omega) &= I + e^{\frac{\pi}{\omega}A_r} \\
\Delta_\rho(\omega) &= I + A_\rho e^{\frac{\pi}{\omega}A_r} \\
\Gamma(\omega) &= \Delta_\rho^{-1}(\omega) A_\rho \Delta(\omega) \Lambda^{-1}(\omega)
\end{aligned}
\tag{4.6}
$$

where $G_n(\omega)$ is the n^{th} harmonic describing function for sinusoidal input with frequency ω.

According to definition of reset elements in open-loop in Eq. (4.1), assuming $e(t) = \sin(\omega t)$, the reset condition will be $\sin(t) = 0$ and the reset instants will be $t_k = \frac{k\pi}{\omega}$. However, if by changing the architecture of reset element, one can manage to change the resetting condition to the following:

$$
\sum_R := \begin{cases} \dot{x}_r(t) = A_r x_r(t) + B_r e(t), & \text{if } \sin(\omega t - \varphi) \neq 0 \\ x_r(t^+) = A_\rho x_r(t), & \text{if } \sin(\omega t - \varphi) = 0 \\ u(t) = C_r x_r(t) + D_r e(t), & \end{cases}
\tag{4.7}
$$

means that the signal that determines the reset instances is phase shifted by φ. In other words, if one changes the reset instants, $t_k = \frac{k\pi+\varphi}{\omega}$, while maintaining the input, $e(t)$, the HOSIDF will change to [27]:

$$
\begin{aligned}
G_{\varphi n}(\omega) &= \begin{cases} C_r(A_r - j\omega I)^{-1}\Theta_\varphi(\omega) \\ \qquad + C_r(j\omega I - A_r)^{-1}B_r + D_r, & n = 1 \\ C_r(A_r - j\omega n I)^{-1}\Theta_\varphi(\omega), & \text{odd } n > 2 \\ 0 & \text{even } n \geq 2 \end{cases} \\
\Theta_\varphi(\omega) &= \frac{-2j\omega e^{-j\varphi}}{\pi}\Omega(\omega)\left(\omega I \cos(\varphi) + A_r \sin(\varphi)\right)\Lambda^{-1}(\omega)B \\
\Omega(\omega) &= \Delta(\omega) - \Delta(\omega)\Delta_\rho^{-1}(\omega)A_\rho\Delta(\omega).
\end{aligned}
\tag{4.8}
$$

Later in the paper it will be discussed later in the paper that Eq. (4.8) can be used to obtain the HOSIDF of the proposed architecture, where the phase shift, φ, is implemented

in a set of frequencies.

4.2.4. CGLP

According to [21], CgLp is a broadband phase compensation element whose first-harmonic gain behaviour is constant while providing a phase lead. Originally, two architectures for CgLp are suggested using FORE or SORE, both consisting in a reset lag element in series with a linear lead filter, namely $\sum_R$ and D. For FORE CgLp:

$$\sum_R = \frac{1}{s/\omega_{r\alpha}+1}, \quad A_\rho \qquad D(s) = \frac{s/\omega_r + 1}{s/\omega_f + 1} \tag{4.9}$$

The arrow indicates that the states of element are reset according to A_ρ; i.e. are multiplied by A_ρ when the reset condition is met, see Eq. (4.1). For SORE CgLp:

$$\sum_R = \frac{1}{(s/\omega_{r\alpha})^2 + (2s\beta/\omega_{r\alpha}) + 1}, \quad A_\rho \tag{4.10}$$

$$D(s) = \frac{(s/\omega_r)^2 + (2s\beta/\omega_r) + 1}{(s/\omega_f)^2 + (2s/\omega_f) + 1}$$

In (4.9) and (4.10), $\omega_{r\alpha} = \omega_r/\alpha$, α is a tuning parameter accounting for a shift in corner frequency of the filter due to resetting action, β is the damping coefficient and $[\omega_r, \omega_f]$ is the frequency range where the CgLp will provide the required phase lead.
The main idea behind the CgLp is taking the phase advantage of reset lag element over its linear counter part and use it in combination with a corresponding lead element to create broadband phase lead. Ideally, the gain of the reset lag element should be cancelled out by the gain of the corresponding linear lead element, which creates a constant gain behaviour. The concept is depicted in Fig. 4.1.

4.3. A SINGLE STATE RESET ELEMENT INCLUDING A SHAPING FILTER

This paper proposes an architecture for reset elements with only one resetting state including a shaping filter. This section will analyse the HOSIDF of such an element and its specific properties. The block diagram of the proposed element is presented in Fig. 4.2b.
HOSIDF of this element can be found using Eq. (4.6) with

$$A_\rho = \text{diag}(\underbrace{1,\ldots,1}_{n_F+n_K}, \gamma, \underbrace{1,\ldots,1}_{n_T})$$

where n_F, n_K and n_T are number of states for linear filters $F(s), K(s)$ and $T(s)$, respectively.
However, in this paper, Eq. (4.8) will be used, since it will reveal more useful information. Let's define:

$$\psi(\omega) := \angle \frac{X_1(j\omega)}{E(j\omega)} \quad \text{for } \gamma = 1. \tag{4.11}$$

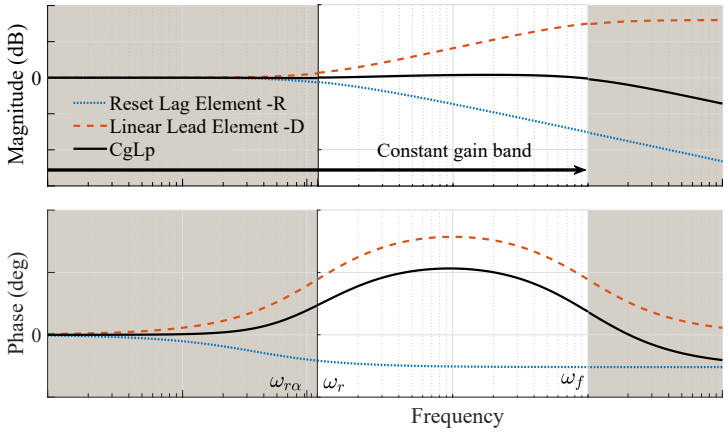

Figure 4.1: The concept of using combination of a reset lag and a linear lead element to form a CgLp element. The figure is from [21].

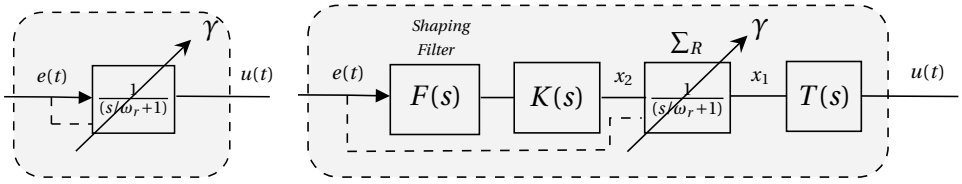

(a) A conventional FORE

(b) A single state reset element including a shaping filter

Figure 4.2: Block diagrams of a conventional FORE and a single state reset element including a shaping filter proposed by this paper.

It is to be noted that ψ is defined in a linear context and is based on base linear system and $X_1(j\omega)$ and $E(j\omega)$ are the Fourier transform of the signals $x_1(t)$ and $e(t)$ in Fig. 4.2b.

Theorem 5. *The higher-order harmonics of the architecture in Fig. 4.2b is an exponential function of* $\psi(\omega)$.

$$H_n(\omega) = f(n,\omega)(1-e^{-j2\psi}) \tag{4.12}$$

where

$$f(n,\omega) = C_r(A_r - j\omega nI)^{-1}\frac{\omega e^{-j\tan^{-1}(\frac{\omega}{\omega_r})}}{\pi\sqrt{1+\left(\frac{\omega}{\omega_r}\right)^2}}\Big((1-\gamma)$$
$$\left(1+\gamma e^{\frac{-\pi\omega_r}{\omega}}\right)^{-1}\left(1+e^{\frac{-\pi\omega_r}{\omega}}\right)\Big). \tag{4.13}$$

Proof. Let's temporarily denote $Q(s) := F(s)K(s)$. For HOSIDF analysis, $e(t) = \sin(\omega t)$; thus,

$$x_2(t) = \left|Q(j\omega)\right|\sin(\omega t + \phi(\omega)) \tag{4.14}$$

where $\phi(\omega) = \angle Q(j\omega)$. From block diagram of Fig. 4.2b we have

$$\phi(\omega) = \psi(\omega) + \tan^{-1}\left(\frac{\omega}{\omega_r}\right) \tag{4.15}$$

It can be readily seen that input to the $\sum_R$ is $x_2(t)$ while the resetting condition is determined by $e(t)$, which have a phase difference. One can find the n^{th} harmonic, $H_n(\omega)$, by the following equation:

$$H_n(\omega) = Q(j\omega)G_{\varphi n}(\omega)T(jn\omega) \tag{4.16}$$

where $G_{\varphi n}$ can be obtained using Eq. (4.8) using

$$\varphi = \phi(\omega) = \psi(\omega) + \tan^{-1}\left(\frac{\omega}{\omega_r}\right). \tag{4.17}$$

For $\sum_R$, in this paper, we have

$$A_r = -\omega_r, B_r = \omega_r, C_r = 1, D_r = 0, A_\rho = \gamma. \tag{4.18}$$

Using Eqs. (4.8), (4.17) and (4.18), after some simplifications we have

$$G_{\varphi n}(\omega) = \begin{cases} f(n,\omega)\left(1 - e^{-j2\psi}\right) \\ \qquad + C_r\left(j\omega I - A_r\right)^{-1}B_r + D_r, & n = 1 \\ f(n,\omega)\left(1 - e^{-j2\psi}\right), & \text{odd } n > 2 \\ 0 & \text{even } n \geq 2 \end{cases} \tag{4.19}$$

□

Remark 6. *Let's define*

$$\omega_{lb} := \{\omega | \psi(\omega) = 0\}. \tag{4.20}$$

According to Eqs. (4.19) and (4.8),

$$G_{\varphi n}(\omega_{lb}) = \begin{cases} C(j\omega_{lb}I - A_r)^{-1}B_r + D_r, & n = 1 \\ 0 & n \geq 2 \end{cases} \tag{4.21}$$

Remark 6 shows that for each frequency in ω_{lb}, all the higher-order harmonics will be zero, in other words, the element will act as its base linear system in terms of steady state output. By way of explanation, when ψ is zero, the reset element, $\sum_R$, will reset its state to zero when the state value is already zero. Hence, the resetting action has no effect in steady state response. Fig. 4.3 depicts this situation. Obviously, in this situation, there exists no phase advantage for the reset element.

Remark 7. *For a fixed value of ω, ω_r and γ, the maximum of the magnitude of higher-order harmonics will occur when $\psi(\omega) = \frac{(k+1)\pi}{2}, k \in \mathbb{Z}$.*

Remark 8. *For $\omega > 10\omega_r$, the phase of the first harmonic of the reset element can be approximated by*

$$\angle G_{\varphi 1}(\omega) \approx \tan^{-1}\left(\frac{U\sin(2\psi) - 1}{2U\sin^2(\psi)}\right) \tag{4.22}$$

where

$$U = \frac{2(1-\gamma)}{\pi(1+\gamma)}.$$

Thus, the phase of the first harmonic of the reset element for $\omega > 10\omega_r$, only depends on ψ and γ.

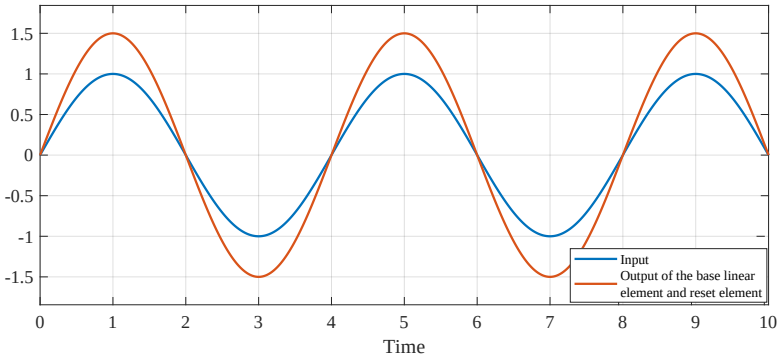

Figure 4.3: Assuming that the output of the base linear element ($x_1(t)$ for $\gamma = 1$) for a reset element has no phase shift with respect to its input ($e(t)$), the output of the reset element itself ($x_1(t)$ for $\gamma \neq 1$) will match the base linear element output at steady state.

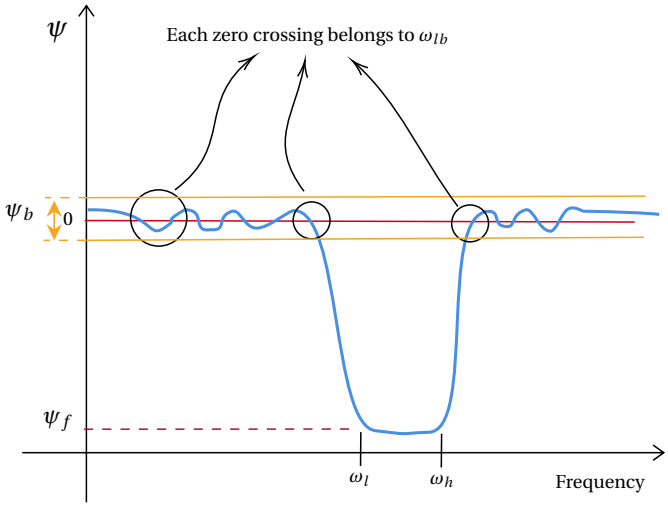

Figure 4.4: Desired shape of phase for $\psi(\omega)$ for band-passing nonlinearity.

Remark 8 implies that at a frequency that is at least one decade higher than ω_r, different combinations of ψ and γ may result in the same first-harmonics phase for the reset element. Meanwhile, ψ and γ also affect the magnitude of the higher harmonics, as indicated in Eq. (4.19). Thus, in solving an optimization problem, one can find the best combination of ψ and γ for a desired first-harmonic phase and minimum higher-order harmonics magnitude.

4.4. PHASE SHAPING METHOD

Theorem 5 and its following remarks, constitute the main idea of phase shaping method for band-passing nonlinearity in reset elements. Previous discussions revealed that the nonlinearity in reset element and its two immediate consequences, namely, the phase

advantage and higher-order harmonics, are dependent on $\psi(\omega)$. The proposed architecture in this paper allows for shaping this phase difference, ψ, and consequently nonlinearity in a reset element.
From Fig. 4.2b, we have

$$\psi(\omega) = \angle\big(F(j\omega)K(j\omega)R(j\omega)\big) \tag{4.23}$$

where $R(s)$ represents the base-linear element for $\sum_R$. Let

$$K(s) = \frac{R^{-1}(s)}{s/\omega_f + 1} = \frac{s/\omega_r + 1}{s/\omega_f + 1} \tag{4.24}$$

which is the inverse of the $R(s)$ multiplied to a low-pass filter to make it proper. For a large enough ω_f,

$$\psi(\omega) = \angle F(j\omega). \tag{4.25}$$

Shaping $\psi(\omega)$ is now reduced to shaping the phase of $F(s)$. If one designs $F(s)$ to have a phase plot as depicted in Fig. 4.4, the following will happen according to Theorem 5 and its following remarks:

- Each zero crossing frequency belongs to ω_{lb}, where reset element produces no higher-order harmonics at steady state. These frequencies will be seen as higher-order harmonic notches in the HOSIDF.
- For frequencies outside $[\omega_l, \omega_h]$, one can determine the upper bound of nonlinearity by determining ψ_b. For a small enough ψ_b, higher-order harmonics can be approximated to zero. There will be no phase advantage for the reset element at these frequencies.
- For frequencies in $[\omega_l, \omega_h]$, the reset element will produce high-order harmonics and will have phase advantage.
- ψ_f and γ determine the phase advantage of the reset element in $[\omega_l, \omega_h]$.

It can be concluded that by this design, the nonlinearity of the reset element is band-passed in $[\omega_l, \omega_h]$. The details on how to design $F(s)$ to have this phase behaviour will be discussed in the next section.

4.4.1. BAND-PASSED CGLP

In order to create a band-passed CgLp, let

$$T(s) = F^{-1}(s) \tag{4.26}$$

then we have

$$\begin{aligned} H_n(\omega) &= \begin{cases} K(j\omega)G_{\varphi n}(\omega), & n = 1 \\ F(j\omega)K(j\omega)G_{\varphi n}(\omega)F^{-1}(jn\omega) & n > 1 \end{cases} \\ \varphi(\omega) &= \angle F(j\omega) + \tan^{-1}\left(\frac{\omega}{\omega_r}\right) \end{aligned} \tag{4.27}$$

where $F(s)$ and $K(s)$ should be designed based on the guidelines of the phase shaping method. As mentioned above, it should be noted that the reset action will cause a shift in corner frequency of $R(s)$ [21]. In order to account for this frequency shift an additional filter of

$$W(s) = \frac{(s/\omega_{r\alpha} + 1)}{(s/\omega_r + 1)} \tag{4.28}$$

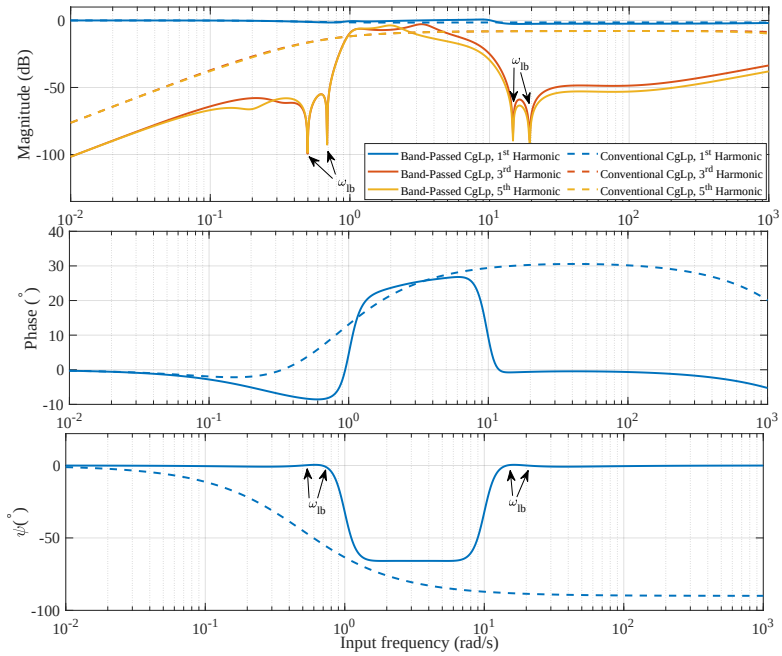

Figure 4.5: Comparison of HOSIDF of a band-passed CgLp with a conventional one, along with their ψ plot. $\omega_r = 0.5$ rad/s and γ is 0.2 and 0.35 for band-passed CgLp and conventional one, respectively.

can be used in $T(s)$.

$$T(s) = F^{-1}(s)W(s). \tag{4.29}$$

In order to verify the discussion, a CgLp element has been band-passed in $[1,10]$ rad/s. HOSIDF analysis of the band-passed CgLp is compared with a conventional one in Fig. 4.5. Both CgLps have $\omega_r = 0.5$ rad/s, γ is chosen to get approximately the same phase advantage. As expected, the shaped ψ has made higher-order harmonics zero at frequencies in ω_{lb} and almost zero at other frequencies outside $[1,10]$ rad/s. The phase advantage is also limited to the specified band. It should be noted that by changing the ψ shape in $[\omega_l, \omega_h]$, one can change the shape of the phase advantage. This can be useful in creating properties such as iso-damping behaviour [36]–[38].

4.4.2. BAND-PASSED CLEGG INTEGRATOR AND BAND-PASSED FORE

Following the same design approach and by letting

$$T(s) = \frac{F^{-1}(s)}{s} \tag{4.30}$$

one can create a band-passed Clegg integrator. Likewise, a band-passed FORE can be created by

$$T(s) = \frac{F^{-1}(s)}{s/\omega_{rr} + 1} \tag{4.31}$$

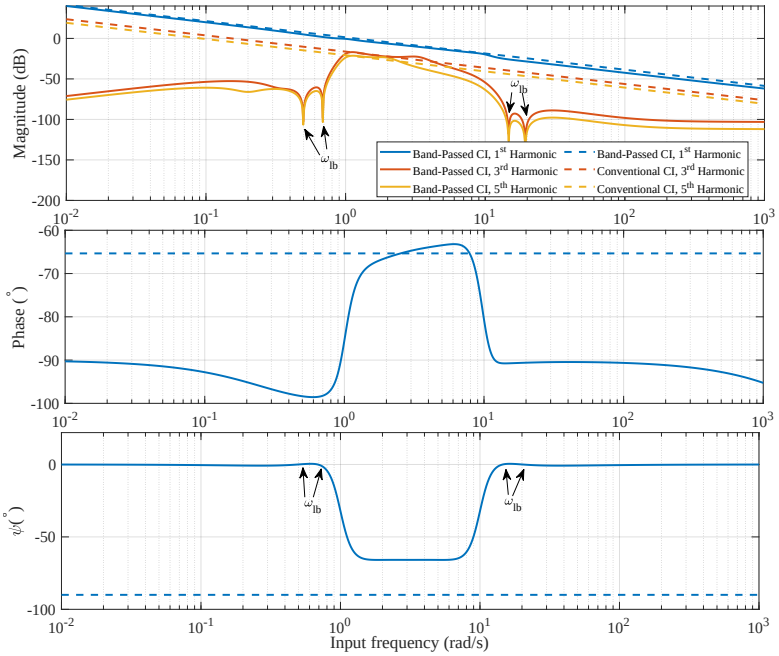

Figure 4.6: Comparison of HOSIDF of a band-passed Clegg integrator with a conventional one, along with their ψ plot. γ is 0.2 and 0.47 for the band-passed Clegg Integrator and the conventional one, respectively. For band-passed Clegg, $\omega_r = 0.5$ rad/s.

Figs. 4.6 and 4.7 compares the HOSIDF of a band-passed Clegg integrator and a band-passed FORE with their conventional counterparts. Both reset elements are band-passed in $[1, 10]$ rad/s. As aforementioned, reset elements are usually known and used for their phase lag reduction compared to their linear counterparts [8], [39], [40]. Phase lag reduction is mainly useful in the cross-over frequency region and in other regions it does not have a clear benefit. Thus, due to the ill effect of higher-order harmonics especially for tracking and disturbance rejection, the proposed method is useful to band-pass the nonlinearity of these reset elements and its consequent benefits and ill effects to the cross-over frequency region.

4.5. DESIGNING THE SHAPING FILTER

This section proposes a method to design the shaping filter $F(s)$, so that its phase mimics the schematic shape of Fig. 4.4. The first parameter to consider is ψ_f, which affects the phase of the reset element. Assuming that the nonlinearity of the reset element is bandpassed in the cross-frequency region, if ω_r is less than $\omega_c/10$, where ω_c is the cross-frequency, one can choose a combination of γ and ψ_f according to Eq. (4.22) to achieve the desired first-harmonic phase of the reset element in ω_c.
The suggested architecture for the shaping filter consists of a lag filter, a notch, and an

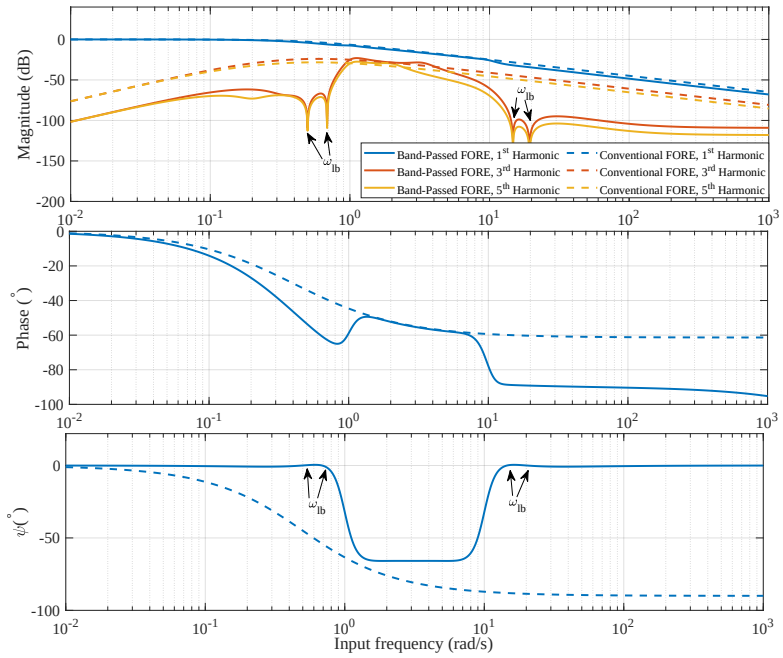

Figure 4.7: Comparison of HOSIDF of a band-passed CgLp with a conventional one, along with their ψ plot. $\omega_r = 0.5$ rad/s and γ is 0.2 and 0.4 for band-passed CgLp and conventional one, respectively. For band-passed Clegg, $\omega_{rr} = 0.5$ rad/s.

anti-notch filter. The notch and the anti-notch filters should be placed at ω_h and ω_l, respectively. Since it is necessary for the phase of the shaping filter to reach a certain value in the passing band, this method requires a flat phase behaviour that is not an integer multiple of 90°. This is achievable using fractional lag filters; thus, the poles and zeros of the lag filter can be placed according to the CRONE approximation guidelines for a fractional order element [41]. Such a placement will simplify the calculations.
The CRONE approximation is

$$\left(\frac{s/\omega_l+1}{s/\omega_h+1}\right)^{\lambda} \approx C \prod_{m=1}^{N} \frac{1+\frac{s}{\omega_{z,m}}}{1+\frac{s}{\omega_{p,m}}} \tag{4.32}$$

$$\omega_{z,m} = \omega_l \left(\frac{\omega_h}{\omega_l}\right)^{\frac{2m-1-\lambda}{2N}} \tag{4.33}$$

$$\omega_{p,m} = \omega_l \left(\frac{\omega_h}{\omega_l}\right)^{\frac{2m-1+\lambda}{2N}} \tag{4.34}$$

where $\lambda \in \Re^-$ and N is number of poles and zeros. CRONE ensures that the poles and zeros are placed in equal distance in logarithmic scale. C is the tuning parameter to adjust the gain of the approximation. However, in this paper, only the phase behaviour of this filter is of interest, since the first-order gain behaviour of this element will be canceled out according to Eq. (4.27). Thus, for the sake of simplicity one can use $C = 1$.

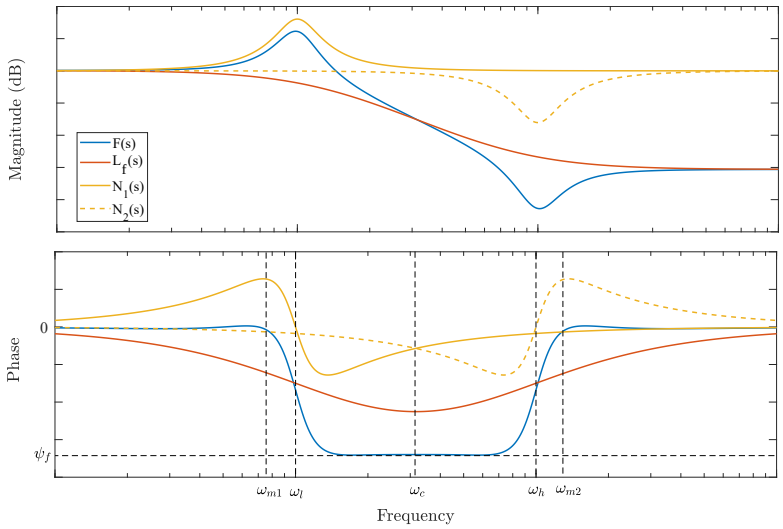

Figure 4.8: Bode diagram of the composition of $F(s)$.

The proposed design of shaping filter is

$$F(s) = N_1(s)L_f(s)N_2(s) \tag{4.35}$$

$$L_f(s) = \left(\frac{s/\omega_l + 1}{s/\omega_h + 1}\right)^{\lambda} \tag{4.36}$$

$$N_1(s) = \frac{(s/\omega_l)^2 + s/\omega_l + 1}{(s/\omega_l)^2 + s/(q\omega_l) + 1} \tag{4.37}$$

$$N_2(s) = \frac{(s/\omega_h)^2 + s/(q\omega_h) + 1}{(s/\omega_h)^2 + s/\omega_h + 1} \tag{4.38}$$

Thus, there are two parameters to tune, namely, λ and q. According to Fig. 4.8 and criteria mentioned in Section 4.4 for the shaping filter, two constraints can be introduced to find the appropriate value for λ and q.

$$\angle F(j\omega_c) = \psi_f \tag{4.39}$$

$$\angle F(j\omega_{m1}) = \angle F(j\omega_{m2}) = \varepsilon_1 \tag{4.40}$$

where ε_1 is a small positive value and

$$\omega_{m1} \in (0, \omega_l) \mid \frac{d}{d\omega}\angle N_1(j\omega_{m1}) = 0 \tag{4.41}$$

$$\omega_{m2} \in (\omega_h, +\infty) \mid \frac{d}{d\omega}\angle N_2(j\omega_{m2}) = 0 \tag{4.42}$$

Equation (4.40) ensures that phase of shaping filter remains close to zero and crosses the zero line two time before ω_l and two times after ω_h. By symmetry, constraints will be simplified to

$$\angle L_f(j\omega_c) + 2\angle N_1(j\omega_c) = \psi_f \tag{4.43}$$

$$\angle L_f(j\omega_{m1}) + \angle N_1(j\omega_{m1}) = \varepsilon_2. \tag{4.44}$$

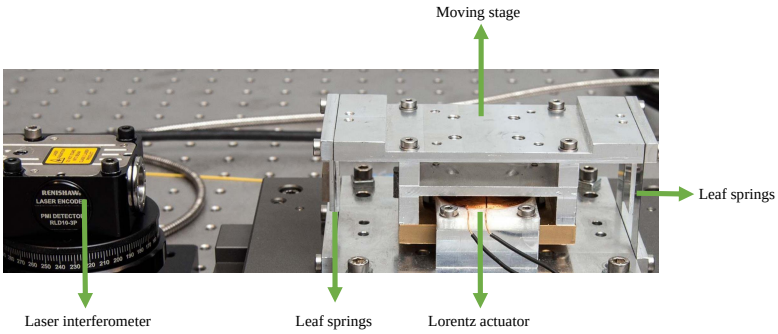

Figure 4.9: The custom-designed precision stage used for comparison of controllers performance.

As a rule of thumb, one can choose $\varepsilon_2 = \pi/180$ rad/s.
In this paper, without loss of generality, it is assumed that the band-passing range is one decade, i.e., $\omega_h = 10\omega_l$ and the equations are derived in the following.
Assuming $\omega_h = 10\omega_l$, we have $\omega_c = \sqrt{10}\omega_l$, thus

$$\angle L_f(j\omega_c) \approx \lambda\left(\tan^{-1}\left(\sqrt{10}\right) - \tan^{-1}\left(\frac{1}{\sqrt{10}}\right)\right) \tag{4.45}$$

$$\angle N_1(j\omega_c) = \tan^{-1}\left(\frac{\sqrt{10}}{9q}\right) - \tan^{-1}\left(\frac{\sqrt{10}}{9}\right) \tag{4.46}$$

$$\angle L_f(j\omega_{m1}) = \lambda\left(\tan^{-1}(\zeta) - \tan^{-1}(\zeta/10)\right) \tag{4.47}$$

$$\angle N_1(j\omega_{m1}) = \tan^{-1}\left(\frac{\zeta}{1-\zeta^2}\right) - \tan^{-1}\left(\frac{\zeta/q}{1-\zeta^2}\right) \tag{4.48}$$

where

$$\zeta = \frac{\omega_{m1}}{\omega_l} = \frac{\sqrt{2}}{2}\sqrt{\frac{2q+1-\sqrt{1+4q}}{q}}. \tag{4.49}$$

4.6. AN ILLUSTRATIVE EXAMPLE

In order to illustrate the application of the proposed architecture and method in precision motion control, three controllers have been designed and their performance has been compared. The three controllers are a band-passed CgLp, a conventional CgLp designed based on the guidelines of [21] and a PID.

4.6.1. PLANT

The plant which is used for practical implementation is a custom-designed precision stage that is actuated with the use of a Lorentz actuator. This stage is linearly guided using two flexures to attach the Lorentz actuator to the base of the stage and actuated at the center of the flexures. With a laser encoder, the position of the precision stage is read out with 10 nm resolution. A picture of the setup can be found in Fig. 4.9. The identified transfer function for the plant is:

$$G(s) = \frac{3.038 \times 10^4}{s^2 + 0.7413s + 243.3} \tag{4.50}$$

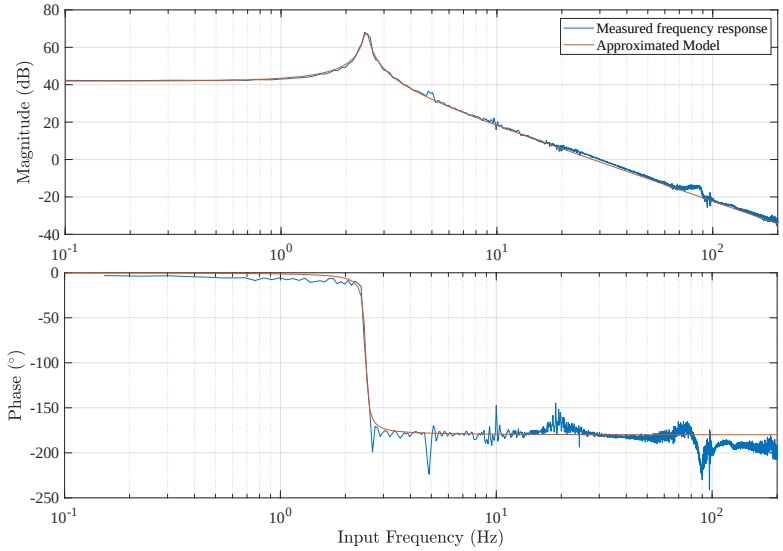

Figure 4.10: Measured frequency response of the plant and corresponding identified model.

Generally precision motion setups can be modeled as mass-spring-damper systems as this is the case for this setup. Fig. 4.10 shows the measured frequency response and that of the identified model.

4.6.2. CONTROLLER DESIGN APPROACH

Controllers are designed for a bandwidth of $\omega_c = 100$ Hz and phase margin of 40°. The block diagram of the closed-loop system for CgLps is presented in Fig. 4.11. The tamed differentiator [33] is designed such that the linear part of the controller provides 10° of PM for the system and the CgLps are designed to provide the remaining 30°. The main reason for the existence of the tamed differentiator for CgLp controllers is stabilizing the base linear system, which is one of the necessary conditions for stability using the H_β theorem. For the case of PID controller, the whole required PM is provided through tamed differentiator.

Table 4.1 shows the parameters for the designed controllers. Fig. 4.12 shows the open-loop HOSIDF analysis for them including the plant. As expected, CgLp controllers show a higher first-order harmonic gain than PID in lower frequencies while they have the same phase margin as PID. However, due to the design method presented in this paper, the band-passed CgLp shows a significant decrease in higher-order harmonics compared to the conventional one. Consequently, one can expect an improvement in the precision in the results of band-passed CgLp.

The reset controllers have been checked for the H_β condition as presented in Theorem 4. Both reset controllers satisfy the condition, thus, their quadratic closed-loop stability is guaranteed.

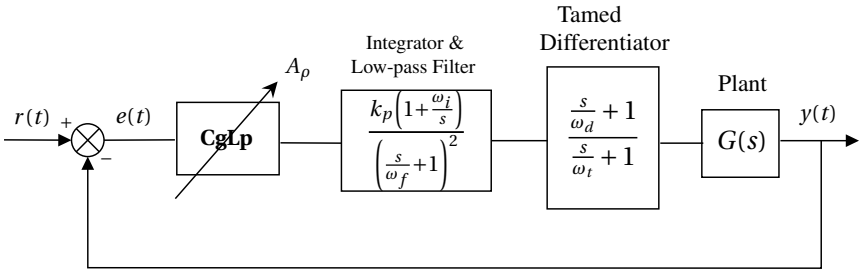

Figure 4.11: Designed control architecture to compare the performance of the controllers.

Table 4.1: Parameters of the designed controllers. Frequencies are in Hz.

Controller	ω_i	ω_d	ω_t	ω_f	ω_r	γ	ψ	λ	q
Band-passed CgLp	10	60.6	165	1000	5	-0.05	$-57.34°$	-0.69	2.21
FORE CgLp	10	60.6	165	1000	5	0.25	N/A	N/A	N/A
PID	10	27.0	370	1000	N/A	N/A	N/A	N/A	N/A

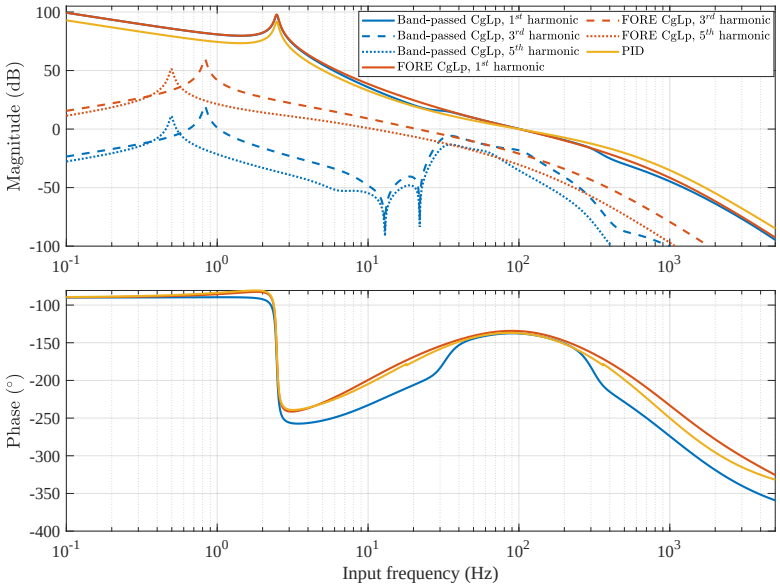

Figure 4.12: Open loop HOSIDF analysis of the designed controllers including the plant. At lower frequencies, the first-harmonic gain of band-passed CgLp and FORE CgLp are on top of each other.

4.6.3. PRACTICAL IMPLEMENTATION

In order to validate the theories, architectures, and methods discussed, the designed controllers have been implemented in practice and their performance has been compared. Implementation was carried out using the National Instruments CompactRIO

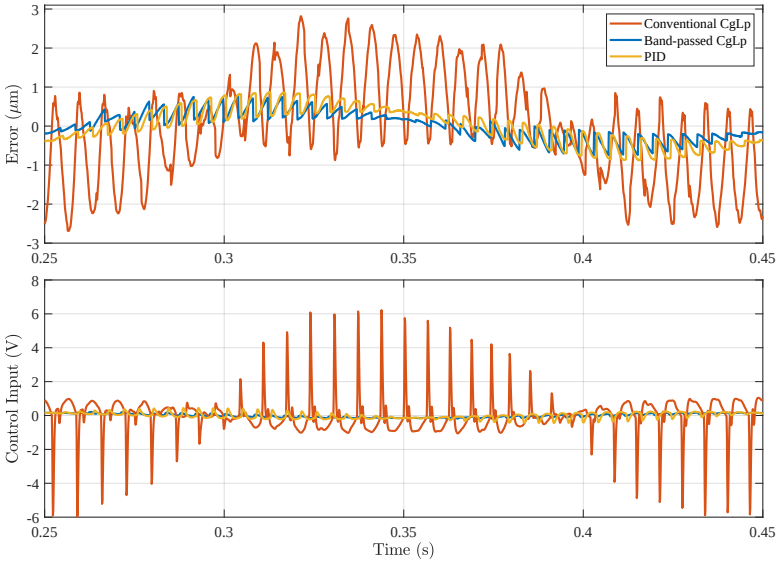

Figure 4.13: Error and control input of designed controllers, measured in practice for a sinusoidal input of 5 Hz and amplitude of 0.2 mm.

instrument with a sampling frequency of 10 kHz. The overall order of controller for PID, FORE CgLp and Band-passed CgLp are 3, 5 and 16, respectively. Since high-end hardware for implementing the controller is used, the high-order of band-passed CgLp is feasible to implement, which is the case for most precision motion control system hardware.

Sinusoidal tracking of different frequencies and different amplitudes has been tested in practice for three designed controllers. Fig. 4.13 shows the error and control input of three controllers to follow a 5 Hz sinusoidal input with amplitude of 200 μm.

As shown in Fig. 4.13, band-passed CgLp has better steady-state precision than PID as it could be predicted referring to Fig. 4.12. However, conventional CgLp, due to the presence of higher-order harmonics, cannot live up to the expectation of first-order DF. The Root Mean Square (RMS) of error for controllers are 0.346 μm, 1.32 μm and 0.465 μm for the band-passed CgLp, the conventional one and PID, respectively. The figures show a reduction of 25.7% and 74% in RMS of steady state error for the band-passed CgLp with respect to PID and the conventional CgLp.

Fig. 4.13 also reveals another interesting characteristic of the band-passed CgLp. Reset controllers are known to have large peaks in control input that can saturate the actuator. However, the band-passed CgLp due to limited nonlinearity shows much smaller control input compared to that of conventional CgLp. The maximum control inputs for controllers are 0.297 V, 6.980 V, and 0.448 V for the band-passed CgLp, the conventional one, and PID, respectively.

The main contribution of this paper and designing band-passed CgLp is to limit nonlinearity to a range of frequencies and reduce it in other frequencies. Thus, it is expected that the band-passed CgLp has lower higher-order harmonics than the conventional one

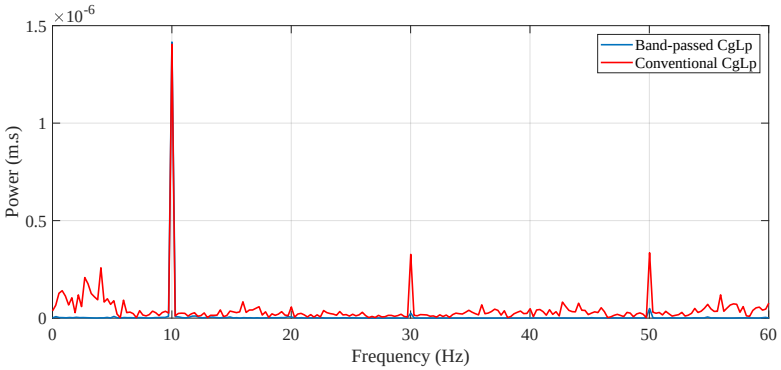

Figure 4.14: The single-sided FFT spectrum of steady-state error for a sinusoidal input of 10 Hz. The amplitude of reference is 71.43 μm.

in the range of [0.1 30] Hz. This was also verified in practical implementation, as it is shown in the single-sided spectrum of Fast Fourier Transform (FFT) of steady-state error for a sinusoidal input of 10 Hz, presented in Fig. 4.14. From the figure it can be observed that the 3$^{\text{rd}}$ and the 5$^{\text{th}}$ harmonics, which are at 30 and 50 Hz, are significantly lower for band-passed CgLp. The same holds for other sinusoidal inputs with frequencies in [0.1 30] Hz, however, they are not presented for the sake of brevity.

Furthermore, in order to have a broader view of tracking performance of designed controllers, L_2 and L_∞ norm of their steady-state error for sinusoidal inputs of amplitude 71.43 μm and frequencies of 1 to 24 Hz in steps of 1 Hz is depicted in Fig. 4.15. The figure clearly shows a significant decrease in the steady-state error for band-passed CgLp with respect to the conventional one, indicating the adverse effect of higher-order harmonics in lower frequencies for tracking precision. Due to large peaks present in control input of the conventional CgLp, tracking sinusoidal waves of frequencies larger than 10 Hz was not possible due to actuator saturation. Furthermore, the L_∞ norm (RMS) of error for band-passed CgLp is lower than PID in almost the entire frequency range till 17 Hz. By resorting to Fig. 4.12, one can notice that from 17 Hz, the higher-order harmonics will increase for band-passed CgLp and decrease again at 22 Hz. The same trend holds for Fig. 4.15. At very low frequencies, i.e., 1 to 3 Hz, higher-order harmonics of band-passed CgLp are relatively high and thus the steady-state error. A possible suggestion to improve performance at these frequencies is to design a shaping filter such that a frequency within this range, e.g. 2 Hz, is included in ω_{lb}. This will reduce the higher-order harmonics in this range.

Remark 6 suggests that for every frequency in ω_{lb}, higher-order harmonics will be zero. However, in practice due to practical challenges like discretization, quantization, and delay, it is expected that this claim does not hold completely. In other words, one can expect a decrease in higher-order harmonics to drop for frequencies in ω_{lb}. Table 4.2 presents the 1$^{\text{st}}$, 3$^{\text{rd}}$, 5$^{\text{th}}$ and 7$^{\text{th}}$ harmonics of steady-state error for sinusoidal inputs of 21, 22, and 23 Hz, where 22 Hz is in ω_{lb}. The harmonics are obtained using the FFT method. The significant drop in higher-order harmonics is observable for 22 Hz.

At last, in order to evaluate the performance of the proposed band-passed CgLp con-

Table 4.2: Harmonics of steady-state error for sinusoidal inputs of 21, 22 and 23 Hz. Columns 2 through 5 shows harmonics in m and in columns 5 till 8, harmonics are normalised by the amplitude of input and presented in dB.

Freq. (Hz)	1^{st} (m)	3^{rd} (m)	5^{th} (m)	7^{th} (m)	1^{st} (dB)	3^{rd} (dB)	5^{th} (dB)	7^{th} (dB)
21	5.45×10^{-6}	4.54×10^{-7}	1.97×10^{-7}	7.23×10^{-8}	-22.33	-43.93	-51.15	-59.89
22	6.54×10^{-6}	1.92×10^{-7}	1.11×10^{-7}	3.80×10^{-8}	-20.75	-51.40	-56.10	-65.48
23	7.50×10^{-6}	1.64×10^{-6}	5.33×10^{-7}	1.22×10^{-7}	-19.56	-32.77	-42.52	-55.31

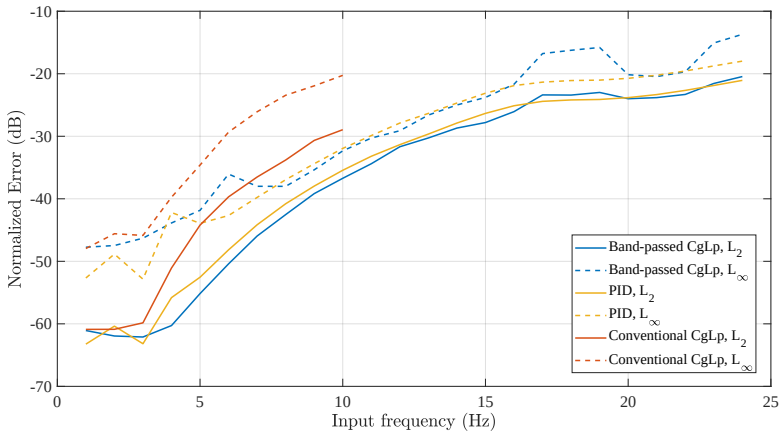

Figure 4.15: L_2 and L_∞ norm of normalized steady-state error for sinusoidal inputs with amplitude of 71.43 μm and frequencies of 1 to 24 Hz with step of 1 Hz. The error is normalized with respect to amplitude of input.

troller for multi-sinusoidal tracking, an input constituted of 3 sinusoidal wave was used. The reference which was used is

$$r(t) = 10^{-5}\left(1.5\sin(2\pi 13t) + 2.5\sin(2\pi 7t) + 5\sin(2\pi 5t)\right). \tag{4.51}$$

Fig. 4.16 shows the error and control input for three designed controllers. The band-passed CgLp still shows less steady-state error with respect to other controllers and no large peak in control input.

4.7. CONCLUSION

This paper investigated the nonlinearity and higher-order harmonics for reset elements with one resetting state. A new architecture was introduced which allowed for band-passing nonlinearity in a range of frequency and selectively reducing higher-order harmonics in a range of frequencies. After developing the HOSIDF analysis of the proposed architecture, a method called “phase shaping” was proposed for the design and tuning of the introduced architecture. It was shown that first-order reset elements such as Clegg integrator, FORE or CgLp can be band-passed using the proposed architecture and method.

It was discussed that nonlinearity and higher-order harmonics can be beneficial in some range of frequencies such as a cross-over frequency region for increasing the phase mar-

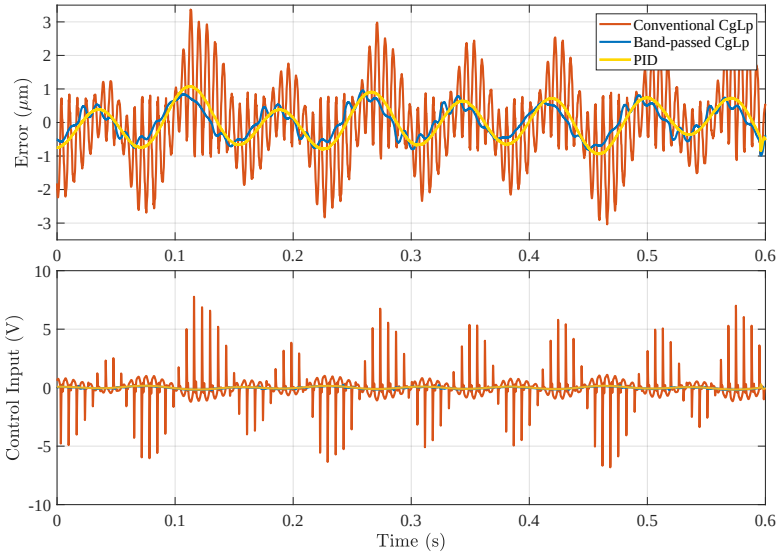

Figure 4.16: Error and control input compared for 3 designed controllers for the input of Eq. (4.51). The error RMS is 0.463 μ m, 1.17 μ m and 0.535 μ m for bandpassed CgLp, conventional CgLp, and PID, respectively. The maximum steady-state error for controllers is 1.13 μm, 3.47 μm and 1.18 μm.

gin and can be harmful at others like lower frequencies. In the phase shaping method, the approach to eliminate nonlinearity at one frequency was also introduced, which is useful for systems with a single important working frequency.

In order to validate the architecture, method, and developed theories, 3 controllers were designed to control a precision positioning stage. The controllers were a band-passed CgLp, a conventional one, and a PID. It was validated in practice that higher-order harmonics for band-passed CgLp at lower frequencies are much lower than the conventional one. Moreover, it was shown that there is a clear relation between the reduction of higher harmonics at lower frequencies and the tracking precision of the system. It was verified in practice that a poorly designed conventional CgLp which performs poorly compared to PID, can outperform or at least equally perform compared to PID in terms of precision in a certain range of frequencies when the nonlinearity of conventional CgLp is band-passed using the phase shaping method presented in the paper. In other words, while the main contribution of this paper was not to outperform the PID controller, but rather to improve the performance of CgLp controllers, the current controller shows the potential to outperform the linear controllers and overcome their limitations. However, the optimal tuning of reset elements using the phase-shaping method is a subject for further studies.

Since the phase shaping method is capable of shaping the phase benefit of the reset element, one may suggest shaping the phase benefit to achieve other characteristics such as iso-damping behaviour for the system or constant gain and positive phase slope. Furthermore, in this paper, only the band-passed CgLp was studied in detail; the investigation of band-passed Clegg and FORE are considered future works.

BIBLIOGRAPHY

[1] S. P. Boyd and C. H. Barratt, *Linear controller design: limits of performance*. Citeseer, 1991, vol. 7.

[2] J. Maclejowski, *Multivariate feedback design*, 1989.

[3] M. F. Heertjes, H. Butler, N. Dirkx, *et al.*, "Control of wafer scanners: Methods and developments", in *2020 American Control Conference (ACC)*, IEEE, 2020, pp. 3686–3703.

[4] A. Baños and A. Barreiro, *Reset control systems*. Springer Science & Business Media, 2011.

[5] Y. Guo, L. Xie, and Y. Wang, *Analysis and design of reset control systems*. Institution of Engineering and Technology, 2015.

[6] J. Clegg, "A nonlinear integrator for servomechanisms", *Transactions of the American Institute of Electrical Engineers, Part II: Applications and Industry*, vol. 77, no. 1, pp. 41–42, 1958.

[7] K. Krishnan and I. Horowitz, "Synthesis of a non-linear feedback system with significant plant-ignorance for prescribed system tolerances", *International Journal of Control*, vol. 19, no. 4, pp. 689–706, 1974.

[8] I. Horowitz and P. Rosenbaum, "Non-linear design for cost of feedback reduction in systems with large parameter uncertainty", *International Journal of Control*, vol. 21, no. 6, pp. 977–1001, 1975.

[9] Y. Guo, Y. Wang, and L. Xie, "Frequency-domain properties of reset systems with application in hard-disk-drive systems", *IEEE Transactions on Control Systems Technology*, vol. 17, no. 6, pp. 1446–1453, 2009.

[10] L. Hazeleger, M. Heertjes, and H. Nijmeijer, "Second-order reset elements for stage control design", in *2016 American Control Conference (ACC)*, IEEE, 2016, pp. 2643–2648.

[11] D. Wu, G. Guo, and Y. Wang, "Reset integral-derivative control for hdd servo systems", *IEEE Transactions on Control Systems Technology*, vol. 15, no. 1, pp. 161–167, 2006.

[12] Y. Li, G. Guo, and Y. Wang, "Nonlinear mid-frequency disturbance compensation in hdds", in *Proc. 16th IFAC Triennial World Congr.*, 2005, pp. 151–156.

[13] Y. Li, G. Guo, and Y. Wang, "Reset control for midfrequency narrowband disturbance rejection with an application in hard disk drives", *IEEE Transactions on Control Systems Technology*, vol. 19, no. 6, pp. 1339–1348, 2010.

[14] H. Li, C. Du, and Y. Wang, "Optimal reset control for a dual-stage actuator system in hdds", *IEEE/ASME Transactions on Mechatronics*, vol. 16, no. 3, pp. 480–488, 2011.

[15] A. Palanikumar, N. Saikumar, and S. H. HosseinNia, "No more differentiator in PID: Development of nonlinear lead for precision mechatronics", in *2018 European Control Conference (ECC)*, IEEE, 2018, pp. 991–996.

[16] C. Weise, K. Wulff, and J. Reger, "Fractional-order memory reset control for integer-order lti systems", in *2019 IEEE 58th Conference on Decision and Control (CDC)*, IEEE, 2019, pp. 5710–5715.

[17] N. Saikumar, R. K. Sinha, and S. H. HosseinNia, "Resetting disturbance observers with application in compensation of bounded nonlinearities like hysteresis in piezo-actuators", *Control Engineering Practice*, vol. 82, pp. 36–49, 2019.

[18] C. Weise, K. Wulff, and J. Reger, "Extended fractional-order memory reset control for integer-order lti systems and experimental demonstration", in *IFAC World Congress 2020*, IFAC, 2020.

[19] D. Valério, N. Saikumar, A. A. Dastjerdi, N. Karbasizadeh, and S. H. HosseinNia, "Reset control approximates complex order transfer functions", *Nonlinear Dynamics*, vol. 97, no. 4, pp. 2323–2337, 2019.

[20] M. Heertjes, K. Gruntjens, S. Van Loon, N. Van De Wouw, and W. Heemels, "Experimental evaluation of reset control for improved stage performance", *IFAC-PapersOnLine*, vol. 49, no. 13, pp. 93–98, 2016.

[21] N. Saikumar, R. Sinha, and S. H. Hoseinnia, "'constant in gain lead in phase'element-application in precision motion control", *IEEE/ASME Transactions on Mechatronics*, 2019.

[22] S. Van Loon, K. Gruntjens, M. F. Heertjes, N. van de Wouw, and W. Heemels, "Frequency-domain tools for stability analysis of reset control systems", *Automatica*, vol. 82, pp. 101–108, 2017.

[23] O. Beker, C. Hollot, Q. Chen, and Y. Chait, "Stability of a reset control system under constant inputs", in *Proceedings of the 1999 American Control Conference (Cat. No. 99CH36251)*, IEEE, vol. 5, 1999, pp. 3044–3045.

[24] N. Karbasizadeh, A. A. Dastjerdi, N. Saikumar, D. Valerio, and S. H. HosseinNia, *Benefiting from linear behaviour of a nonlinear reset-based element at certain frequencies*, 2020. arXiv: 2004.03529 [eess.SY].

[25] P. Nuij, O. Bosgra, and M. Steinbuch, "Higher-order sinusoidal input describing functions for the analysis of non-linear systems with harmonic responses", *Mechanical Systems and Signal Processing*, vol. 20, no. 8, pp. 1883–1904, 2006.

[26] N. Saikumar, K. Heinen, and S. H. HosseinNia, "Loop-shaping for reset control systems: A higher-order sinusoidal-input describing functions approach", *Control Engineering Practice*, vol. 111, p. 104 808, 2021.

[27] A. A. Dastjerdi, N. Saikumar, D. Valerio, and S. H. HosseinNia, *Closed-loop frequency analyses of reset systems*, 2020.

[28] M. S. Bahnamiri, N. Karbasizadeh, A. A. Dastjerdi, N. Saikumar, and S. H. HosseinNia, "Tuning of CgLp based reset controllers: Application in precision positioning systems", *IFAC-PapersOnLine*, vol. 53, no. 2, pp. 8997–9004, 2020. DOI: 10.1016/j.ifacol.2020.12.2017. [Online]. Available: https://doi.org/10.1016/j.ifacol.2020.12.2017.

[29] A. A. Dastjerdi and S. H. Hosseinnia, "A frequency-domain tuning method for a class of reset control systems", *IEEE Access*, vol. 9, pp. 40 950–40 962, 2021. DOI: 10.1109/ACCESS.2021.3064812.

[30] N. Karbasizadeh, N. Saikumar, and S. Hossein Nia Kani, "Fractional-order single state reset element", English, *Nonlinear Dynamics*, vol. 104, no. 1, pp. 413–427, 2021, ISSN: 0924-090X. DOI: 10.1007/s11071-020-06138-9.

[31] C. Cai, A. A. Dastjerdi, N. Saikumar, and S. HosseinNia, "The optimal sequence for reset controllers", in *2020 European Control Conference (ECC)*, 2020, pp. 1826–1833. DOI: 10.23919/ECC51009.2020.9143690.

[32] A. Sebastian, N. Karbasizadeh, N. Saikumar, and S. H. HosseinNia, "Augmented fractional-order reset control: Application in precision mechatronics", in *2021 IEEE/ASME International Conference on Advanced Intelligent Mechatronics (AIM)*, 2021, pp. 231–238. DOI: 10.1109/AIM46487.2021.9517368.

[33] R. M. Schmidt, G. Schitter, and A. Rankers, *The design of high performance mechatronics-: high-Tech functionality by multidisciplinary system integration*. Ios Press, 2020.

[34] Y. Guo, L. Xie, and Y. Wang, *Analysis and Design of Reset Control Systems*. Institution of Engineering and Technology, 2015, ISBN: 1849197032, 9781849197038.

[35] O. Beker, C. Hollot, Y. Chait, and H. Han, "Fundamental properties of reset control systems", *Automatica*, vol. 40, no. 6, pp. 905–915, 2004.

[36] A. A. Dastjerdi, N. Saikumar, and S. H. HosseinNia, "Tuning guidelines for fractional order pid controllers: Rules of thumb", *Mechatronics*, vol. 56, pp. 26–36, 2018, ISSN: 0957-4158. DOI: https://doi.org/10.1016/j.mechatronics.2018.10.004. [Online]. Available: http://www.sciencedirect.com/science/article/pii/S0957415818301612.

[37] Y. Chen, C. Hu, and K. L. Moore, "Relay feedback tuning of robust pid controllers with iso-damping property", in *42nd IEEE International Conference on Decision and Control (IEEE Cat. No. 03CH37475)*, IEEE, vol. 3, 2003, pp. 2180–2185.

[38] Y. Luo, Y. Chen, and Y. Pi, "Experimental study of fractional order proportional derivative controller synthesis for fractional order systems", *Mechatronics*, vol. 21, no. 1, pp. 204–214, 2011.

[39] L. Zaccarian, D. Nesic, and A. R. Teel, "First order reset elements and the clegg integrator revisited", in *Proceedings of the 2005, American Control Conference, 2005.*, IEEE, 2005, pp. 563–568.

[40] S. H. HosseinNia, I. Tejado, and B. M. Vinagre, "Fractional-order reset control: Application to a servomotor", *Mechatronics*, vol. 23, no. 7, pp. 781–788, 2013.

[41] A. Oustaloup, "La Commade CRONE: Commande Robuste d'Ordre Non Entier", in *Hermes*, Hermés, 1991, ISBN: 9782866012892.

5

COMPLEX-ORDER RESET CONTROL SYSTEM

According to the well-known loop shaping method for the design of controllers, the performance of the controllers in terms of step response, steady-state disturbance rejection, and noise attenuation and robustness can be improved by increasing the gain at lower frequencies and decreasing it at higher frequencies and increasing the phase margin as much as possible. However, the inherent properties of linear controllers, the Bode's phase-gain relation, create a limitation. In theory, a complex-order transfer function can break the Bode's gain-phase relation; however, such a transfer function cannot be directly implemented and should be approximated. This paper proposes a reset element and a tuning method to approximate a Complex-Order Controller (CLOC) and, through a simulation example, shows the benefits of using such a controller.

5.1. INTRODUCTION

The increasing demands for speed and accuracy from the high-tech industry, especially in the field of precision motion control, have pushed the linear controllers to their inherent limitations, namely Bode's gain-phase relationship and waterbed effect [1]–[3]. The well-known limitations pose a trade-off between tracking and steady-state precision on one side and bandwidth, stability margins, and transient response properties on the other.

From the perspective of the loop-shaping technique, the industry-standard method for controller design in the frequency domain, one needs to break this gain-phase relationship to break the trade-off. This was first recognized in complex-order derivatives used in the third generation CRONE technique [4], [5]. However, such a derivative, which can

This chapter is published as:
N. Karbasizadeh and S. H. HosseinNia, "Complex-order Reset Control System," 2022 IEEE/ASME International Conference on Advanced Intelligent Mechatronics (AIM), Sapporo, Japan, 2022, pp. 427-433, doi: 10.1109/AIM52237.2022.9863350.

potentially show a negative gain slope with a corresponding positive increasing phase, is unfortunately not practically implementable in the linear domain. Existing attempts in the literature for approximating such behaviour resulted in unstable poles, non-minimum phase zeros or poor approximation of gain behaviour among other issues [6], [7].
The impossibility of achieving implementable complex-order behaviour in linear systems has made researchers and industries interested in nonlinear control methods that are industry-compatible in design and implementation. One of such interesting concepts is reset control, which was first introduced by Clegg [8]. In [9], [10], a method is introduced to approximate Complex Order Controllers (CLOC) using reset control, which consists of multiple reset states, making the system unnecessarily complicated and can potentially deteriorate the precision performance of the system.
Based on the analysis of the Description Function (DF), it is established that the reset integrator proposed by Clegg reduces the phase lag of the integrator by 52°. Although this already breaks the Bode's gain-phase relation for linear control systems, there are concerns while using Clegg's Integrator (CI) in practice, namely, the accuracy of DF approximation, limit cycle, etc. [11]. To address the drawbacks and exploit the benefits, the idea was later extended to more sophisticated elements such as "First-Order Reset Element" [12], [13] and "Second-Order Reset Element" [14] or using Clegg's integrator in the form of PI+CI [15] or resetting the state to a fraction of its current value, known as partial resetting [16].
One of recent studies introduces a new reset element called "Constant-in-Gain, Lead-in-Phase" (CgLp) [17]. DF analysis of this element shows that it can provide broadband phase lead while maintaining constant gain. This element is used in the literature to replace some part of the differentiation action in PID controllers as it will help improve the precision of the system according to the concept of loop shaping [17]–[20]. Despite the fact that the analysis and designs focus on describing functions without taking higher-order harmonics into account, significant tracking and steady-state precision improvements are reported.
The main contribution of this paper is to propose a reset controller to approximate a complex-order transfer function. This reset controller is based on the CgLp structure with a shaped reset signal. The CgLp used has only one resetting state, which reduces the complications of multiple resetting states. The shaping filter and its tuning method for the reset signal will be introduced to tune the slope of gain and phase as in a complex-order transfer function. This paper also shows the benefits of using such a reset controller in step responses and steady-state precision over a linear PID controller in simulation.
The remainder of the paper is organized as follows. Section II presents the preliminaries of the study. Section III introduces the reset element to approximate the complex-order transfer function. Section IV will show an illustrative example and, finally, the paper will be closed with conclusions and future work tips.

5.2. PRELIMINARIES

This section will discuss the preliminaries of this study.

5.2.1. GENERAL RESET CONTROLLER

The general form of a SISO reset controllers used in this study is as following:

$$\sum_R := \begin{cases} \dot{x}_r(t) = A_r x_r(t) + B_r e(t), & \text{if } e(t) \neq 0 \\ x_r(t^+) = A_\rho x_r(t), & \text{if } e(t) = 0 \\ u(t) = C_r x_r(t) + D_r e(t) \end{cases} \tag{5.1}$$

where A_r, B_r, C_r, D_r denote the state space matrices of the Base Linear System (BLS) and the reset matrix is denoted by $A_\rho = \text{diag}(\gamma_1, ..., \gamma_n)$ which contains the reset coefficients for each state. $e(t)$ and $u(t)$ represent the input and output of the reset controller, respectively.

5.2.2. DESCRIBING FUNCTIONS

Describing function analysis is a well-known approach in the literature for the approximation of the frequency response of nonlinear systems such as reset controllers [21]. However, the DF method only takes into account the first harmonic of the Fourier series decomposition of the output and neglects the effects of the higher-order harmonics. This simplification can be significantly inaccurate under certain circumstances [19]. The "Higher-Order Sinusoidal Input Describing Function" (HOSIDF) method has been introduced in [22] to provide more accurate information about the frequency response of nonlinear systems by investigating higher-order harmonics of the Fourier series decomposition. In other words, in this method, the nonlinear element will be replaced by a virtual harmonic generator.

By definition, describing functions are calculated for sinusoidal inputs. Thus, assuming $e(t) = \sin(\omega t)$, HOSIDF method was developed in [23], [24] for reset elements defined by (5.1) as follows:

$$\begin{aligned} H_n(\omega) &= \begin{cases} C_r(j\omega I - A_r)^{-1}(I + j\Theta(\omega))B_r + D_r, & n = 1 \\ C_r(j\omega n I - A_r)^{-1} j\Theta(\omega) B_r, & \text{odd } n > 2 \\ 0, & \text{even } n \geq 2 \end{cases} \\ \Theta(\omega) &= -\frac{2\omega^2}{\pi}\Delta(\omega)[\Gamma(\omega) - \Lambda^{-1}(\omega)] \\ \Lambda(\omega) &= \omega^2 I + {A_r}^2 \\ \Delta(\omega) &= I + e^{\frac{\pi}{\omega}A_r} \\ \Delta_\rho(\omega) &= I + A_\rho e^{\frac{\pi}{\omega}A_r} \\ \Gamma(\omega) &= \Delta_\rho^{-1}(\omega) A_\rho \Delta(\omega) \Lambda^{-1}(\omega) \end{aligned} \tag{5.2}$$

where $H_n(\omega)$ is the n^{th} harmonic describing function for sinusoidal input with the frequency of ω. It should be noted that according to [21], the convergence and asymptotic stability of the reset elements in open loop are guaranteed when $|\lambda(A_\rho)| < 1$, where $\lambda(A_\rho)$ stands for the eigenvalues of the matrix A_ρ.

5.2.3. DESCRIBING FUNCTIONS WITH SHAPED RESET SIGNAL

In a conventional reset element, the reset condition is based on the input of the reset element, i.e., $e(t)$. However, one can use a signal other than the input for the reset condition. If the reset signal is denoted by $x_{rl}(t)$, the reset condition will change to $x_{rl}(t) = 0$.

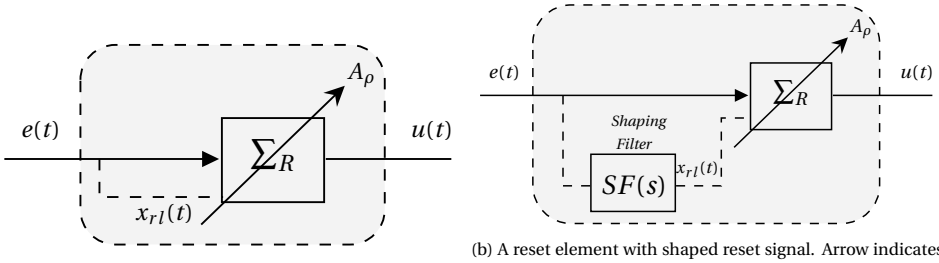

(a) A conventional reset element. Arrow indicates the resetting action. The resetting action is determined by $x_{rl}(t)$ which is not equal to $e(t)$, i.e., the resetting condition is equal to $e(t)$, i.e., the resetting condition is $x_{rl}(t) = e(t) = 0$.

(b) A reset element with shaped reset signal. Arrow indicates the resetting action. The resetting action is determined by $x_{rl}(t)$ which is not equal to $e(t)$, i.e., the resetting condition is $x_{rl}(t) = 0$.

Figure 5.1: A conventional reset element vs. a reset element with a shaped reset signal.

This paper creates a reset signal by filtering $e(t)$ and is thus named a shaped reset signal. Assuming $e(t) = \sin(\omega t)$ for HOSIDF analysis purposes, the reset instants will be $t_k = \frac{k\pi}{\omega}$. However, if one creates $x_{rl}(t)$ such that it has φ phase shift compared to $e(t)$, or in other terms,

$$\sum_R := \begin{cases} \dot{x}_r(t) = A_r x_r(t) + B_r e(t), & \text{if } \sin(\omega t + \varphi) \neq 0 \\ x_r(t^+) = A_\rho x_r(t), & \text{if } \sin(\omega t + \varphi) = 0 \\ u(t) = C_r x_r(t) + D_r e(t), \end{cases} \tag{5.3}$$

it means that the reset instants will become $t_k = \frac{k\pi+\varphi}{\omega}$, while maintaining the input $e(t)$. In this case, the HOSIDF will change to [24]:

$$\begin{aligned} G_{\varphi n}(\omega) &= \begin{cases} C_r(A_r - j\omega I)^{-1}\Theta_\varphi(\omega) \\ \qquad + C_r(j\omega I - A_r)^{-1}B_r + D_r, & n = 1 \\ C_r(A_r - j\omega n I)^{-1}\Theta_\varphi(\omega), & \text{odd } n > 2 \\ 0 & \text{even } n \geq 2 \end{cases} \\ \Theta_\varphi(\omega) &= \frac{-2j\omega e^{j\varphi}}{\pi}\Omega(\omega)\left(\omega I\cos(\varphi) - A_r\sin(\varphi)\right)\Lambda^{-1}(\omega)B_r \\ \Omega(\omega) &= \Delta(\omega) - \Delta(\omega)\Delta_\rho^{-1}(\omega)A_\rho\Delta(\omega). \end{aligned} \tag{5.4}$$

The above indicates that first- and higher-order describing functions can be changed by shaping the reset signal. Fig. 5.1 shows a conventional reset element vs. a reset element with a shaped reset signal. It has to be noted that for $x_{rl}(t)$, only zero-crossings matter and thus, ideally, its gain does not have any effect on the system.

5.2.4. H_β CONDITION

H_β condition [16], despite being conservative, has gained attention among different criteria for stability of reset control systems [11], [25], [26], because of simplicity and frequency domain applicability. In [27], the H_β condition has been reformulated such that the frequency response functions of the controllers and the plant can be used directly. This method especially includes the case where the reset element is not the first element in the loop.

5.2.5. FREQUENCY RESPONSE OF $s^{\alpha+j\beta}$

A derivative of complex order can be defined in a variety of ways [28]–[30], but it is commonly indicated by the operator $D^{\alpha+j\beta}$. It makes no difference which one is utilized for the purpose of this paper, as long as the Laplace transform of a derivative of order $\alpha + j\beta \in \mathbb{C}$ generates a complex power of the Laplace variable s:

$$\mathscr{L}\left[D^{\alpha+j\beta} f(t)\right] = s^{\alpha+j\beta}\mathscr{L}[f(t)] \tag{5.5}$$

The initial conditions for Laplace are also irrelevant for this paper, since the frequency response of the the simplest corresponding complex-order transfer function is under consideration, i.e., $G(s) = s^{\alpha+j\beta}$. The frequency response is given by [9]:

$$\begin{aligned} G(j\omega) &= j^{\alpha}\omega^{\alpha} j^{j\beta}\omega^{j\beta} \\ &= \left(\cos\frac{\alpha\pi}{2} + j\sin\frac{\alpha\pi}{2}\right)\omega^{\alpha} \\ &\times e^{-\frac{\beta\pi}{2}}(\cos(\beta\log\omega) \\ &+ j\sin(\beta\log\omega)) \end{aligned} \tag{5.6}$$

$$\begin{aligned} 20\log_{10}|G(j\omega)| &= 20\log_{10}\left(\omega^{\alpha}e^{-\frac{\beta\pi}{2}}\right) \\ &= 20\alpha\log_{10}\omega + 20\log_{10}e^{-\frac{\beta\pi}{2}} \end{aligned} \tag{5.7}$$

$$\begin{aligned} \arg G(j\omega) &= \angle\left\{\left(\cos\frac{\alpha\pi}{2} + j\sin\frac{\alpha\pi}{2}\right)\right. \\ &\left.\times[\cos(\beta\log\omega) + j\sin(\beta\log\omega)]\right\} \\ &= \frac{\alpha\pi}{2} + \beta\log(10)\log_{10}\omega \end{aligned} \tag{5.8}$$

When $\alpha < 0$ and $\beta > 0$, the frequency response will show a negative gain slope and a positive phase slope, for which there is no practical implementation method in linear domain. However, such frequency response is highly desirable especially in precision motion control since one can for example increase the bandwidth of the system without sacrificing the phase margin [10].

5.3. APPROXIMATING THE COMPLEX-ORDER BEHAVIOUR USING CGLP

$G(s) = s^{\alpha+j\beta}$ is a complex-order transfer function that can be written as $G(s) = s^{\alpha}s^{j\beta}$. There is a large literature on the approximation s^{α} for any noninteger $\alpha \in \mathbb{R}$, with the CRONE approximation being one of the more well-known methods. The novelty, on the other hand, lies in the approximation of $s^{j\beta}$. According to (5.6) to (5.8), for $\beta > 0$, such a transfer function should show constant gain behaviour while having a positive phase slope of $\beta\log(10)$.

CgLp is a reset element that shows a DF behaviour similar to required. This element creates a unity gain with phase lead in a desired range of frequencies. CgLp can be created using a first-order reset lag filter $\sum_R$, a.k.a. FORE, in series with a corresponding linear

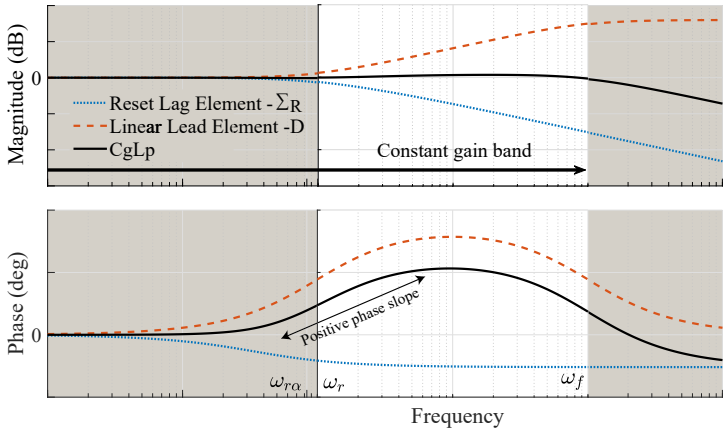

Figure 5.2: The concept of using combination of a reset lag and a linear lead element to form a CgLp element. The figure is from [17].

5

first-order lead filter $D(s)$ having the same cut-off frequency as given below.

$$\sum_R = \frac{1}{s/\omega_r + 1}^{\gamma}, \qquad D(s) = \frac{s/\omega_{r\kappa} + 1}{s/\omega_f + 1} \tag{5.9}$$

where $\omega_{r\kappa} = \kappa\omega_r$, κ is a tuning parameter accounting for a shift in corner frequency of the filter due to resetting action, and $[\omega_r, \omega_f]$ is the frequency range where the CgLp will provide the required phase lead [17]. The arrow indicates the resetting action as described in (5.1), i.e., the element's state is multiplied by γ when the reset condition is met.

While the gains of the reset lag element and the linear lead cancel each other to create a unity gain, a phase lead is created due to reduced phase lag in the reset lag filter compared to its linear counterpart. The concept is presented in Fig. 5.2.

Fig. 5.2 shows that within a frequency range, CgLp shows a unity gain and a positive phase slope that resembles the frequency response of $s^{j\beta}$. Although the phase slope can be tuned by tuning γ (since decreasing γ increases the created phase lead), the range of achievable slopes and the range of frequencies for which the slope is constant are limited.

An approach to gain more freedom in shaping the positive phase slope in the CgLp element is to shape the phase of the reset element without affecting the gain. In [31] a method called "Phase Shaping" is presented to shape the phase of a reset controller. The method is based on the fact that according to (5.4), one can shape the first and higher-order describing function of a reset element by changing φ. In [31], the objective of changing φ is achieved through putting a shaping filter on the input signal of the reset element while maintaining the reset signal the same.

However, in this paper, the objective is achieved by using the shaping filter on the reset signal itself, as depicted in Fig. 5.1b. In this configuration, one can see that

$$\varphi = \angle SF(j\omega). \tag{5.10}$$

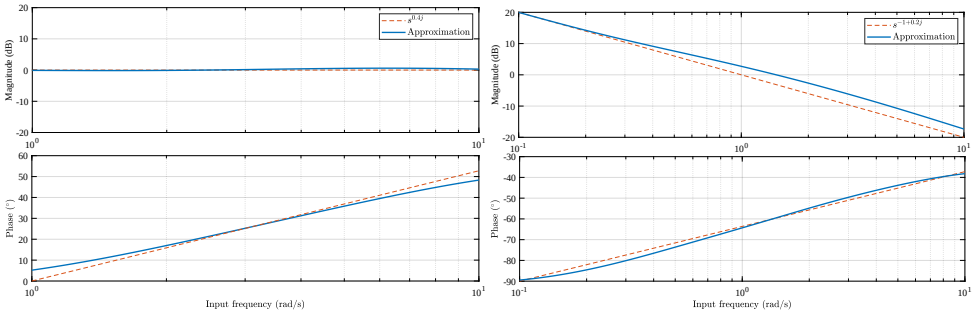

(a) Frequency response of $s^{0.4j}$ and its DF approximation using CgLp in the range of $[1,10]$ rad/s. $N = M = 4$, $\zeta = 3.72$ and $\eta = 21.37$.

(b) Frequency response of $s^{-1+0.2j}$ and its DF approximation using CgLp in the range of $[0.1,10]$ rad/s. $N = M = 7$, $\zeta = 2.93$ and $\eta = 4.30$.

Figure 5.3: A conventional reset element vs. a reset element with a shaped reset signal.

If $\sum_R$ is a FORE as presented in (5.9), and by defining

$$\psi := -\varphi - \tan^{-1}\left(\frac{\omega}{\omega_r}\right), \tag{5.11}$$

one can conclude the following points, following the same logic and procedure as presented in [31]:

- If

$$\varphi = -\tan^{-1}\left(\frac{\omega}{\omega_r}\right) \Rightarrow \psi = 0, \tag{5.12}$$

  then in the steady-state, the resetting action will not affect the output since the reset action will occur when the output of the base linear system (BLS) is already zero. Thus, the $x(t) = x(t^+) = 0$ at the time of reset. In this case, all the higher-order harmonics will be zero because the system is completely acting linear in steady state, and obviously, the phase advantage from the resetting action disappears. Furthermore, if one uses such an element to form a CgLp, the element's phase will remain at zero, since the linear lead will cancel out both gain and phase of the reset element.

- As $\psi \to -90°$, the resetting action will create its benefit, and the reset element will provide a greater phase advantage.

- The phase advantage created by the reset element is dependent on ω_r, γ and ψ, and for frequencies larger enough than ω_r, i.e., $\omega > 10\omega_r$, it only depends on γ and ψ.

According to the points mentioned above, for each value of $\gamma \in [-1,1]$, one can shape the reset element's phase advantage and, thus, the CgLp's phase by shaping ψ. In other words, by designing the shaping filter, $SF(s)$, one can achieve the desired phase slope for the CgLp.

5.4. DESIGN OF THE SHAPING FILTER

Let

$$SF(s) = Q(s)K(s) \quad \text{and} \quad K(s) = \frac{1}{s/\omega_r + 1}. \tag{5.13}$$

Thus according to (5.10) and (5.11),

$$\psi = -\angle SF(s) - \tan^{-1}\left(\frac{\omega}{\omega_r}\right) = -\angle Q(s). \tag{5.14}$$

Now the shaping ψ and thus the phase advantage of CgLp has been reduced to shaping $\angle Q(s)$.
The requirements for $SF(s)$ can be categorized into three regions:

- At the lower frequency region, which is critical for sinusoidal tracking and disturbance rejection performance, the higher-order harmonics should be reduced as much as possible [18], [19], [31], [32]. Meaning that ψ and thus $\angle Q(s)$ should remain as close to 0°.
- In cross-over frequency region that will be presented as $[\omega_l, \omega_h]$, $\angle Q(s)$ should increase to 90° for CgLp to create phase advantage. Moreover, the increase slope should be tuned for CgLp to maintain a positive phase slope of $\beta \log(10)$.
- In the higher frequency region, the gain of $SF(s)$ should have a negative slope to attenuate the high frequency content of the reset signal and thus avoid excessive reset action due to noise. It has already been taken care of by the presence of $K(s)$.

To achieve a $Q(s)$ with tunable phase slope, one may refer to [33], where it introduces a variation of the CRONE approximation as follows.

$$\begin{aligned} Q(s) &= \frac{\prod_{n=1}^{M}\left(1+\frac{s}{\omega_{zn}}\right)}{\prod_{n=1}^{N}\left(1+\frac{s}{\omega_{pn}}\right)} \\ \omega_{zj+1} &= \zeta\omega_{zj}, \quad j = 1,2,\ldots,M-1 \\ \omega_{pi+1} &= \eta\omega_{pi}, \quad i = 1,2,\ldots,N-1 \end{aligned} \tag{5.15}$$

where the slope of phase within the range of approximation is

$$\mathfrak{S} = \frac{\pi}{2}\frac{1}{\log_{10}\zeta} - \frac{\pi}{2}\frac{1}{\log_{10}\eta} \text{ rad/decade} \tag{5.16}$$

Although $\mathfrak{S}$ is directly related to β, a numerical optimization problem should be solved to find η and ζ for a desired β. For the approximation to happen in the range of $[\omega_l, \omega_h]$, one should choose $\omega_{z1} = \omega_{p1} = \omega_l$ and choose N and M accordingly to cover the whole range of frequencies.

5.5. COMPLEX-ORDER TAMED DIFFERENTIATION

One possible application of a complex-order function is to use a complex-order tamed differentiation element instead of linear tamed differentiator [2] in motion control. For this purpose, without loss of generality, consider a mass system controlled by using a control loop presented in Fig. 5.4. Following the steps below, one can design a CLOC

1. Choose ω_c.

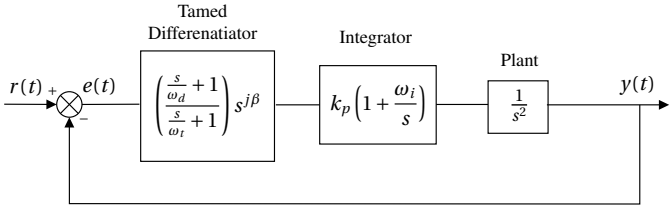

(a) Control loop for position control of a mass system. For PID, $\beta = 0$ and for CLOC $\beta = 0.3$.

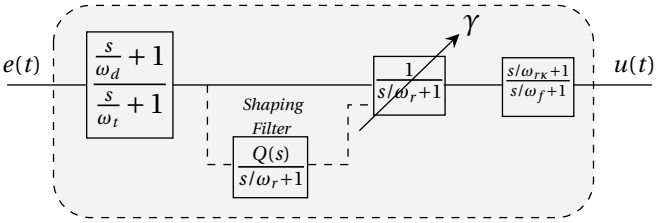

(b) Block diagram for approximating $\left(\frac{\frac{s}{\omega_d}+1}{\frac{s}{\omega_t}+1}\right)s^{j\beta}$. Approximation will be done in the range of $[\omega_l, \omega_h]$.

Figure 5.4: Block diagram for closed-loop control of a mass system using integer and complex-order tamed differentiator and approximation of complex-order tamed differentiator using reset control.

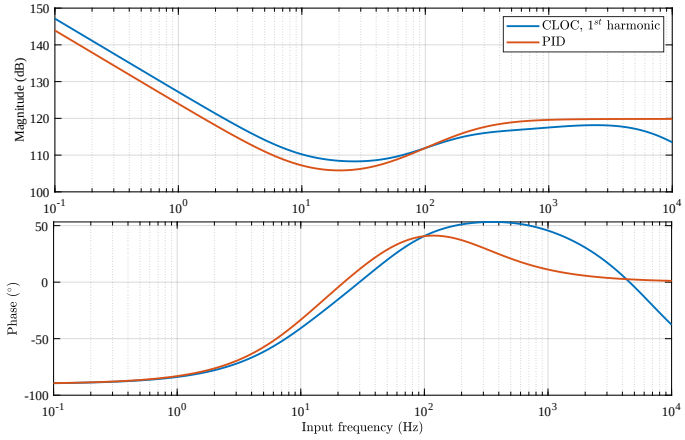

Figure 5.5: The Bode diagram of PID and the DF of CLOC.

2. Set $\omega_d = \omega_c/1.5$, $\omega_t = 1.5\omega_c$ and $\omega_i = \omega_c/10$.
3. Choose the frequency range in which the positive slope phase should be present and set ω_l and ω_h accordingly.
4. Choose β.
5. Find ζ and η using (5.4), (5.8) and (5.16) by optimization.

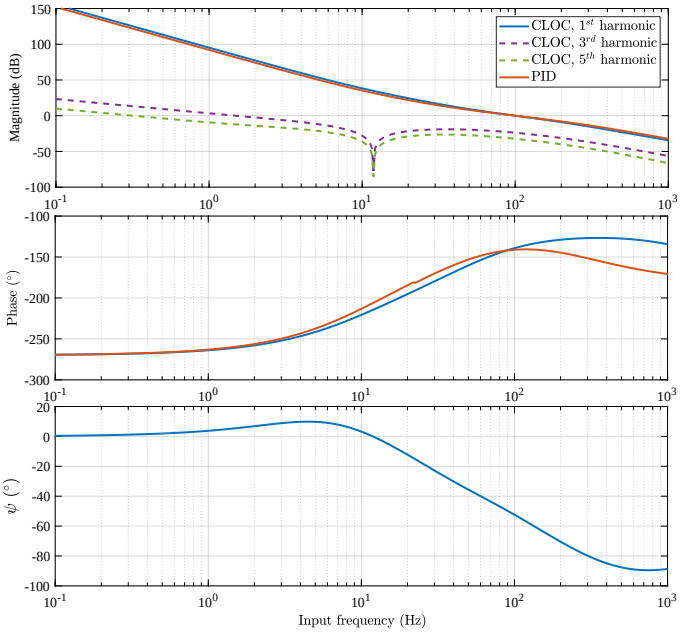

Figure 5.6: Open-loop Bode diagram of PID and HOSIDF of CLOC including plant.

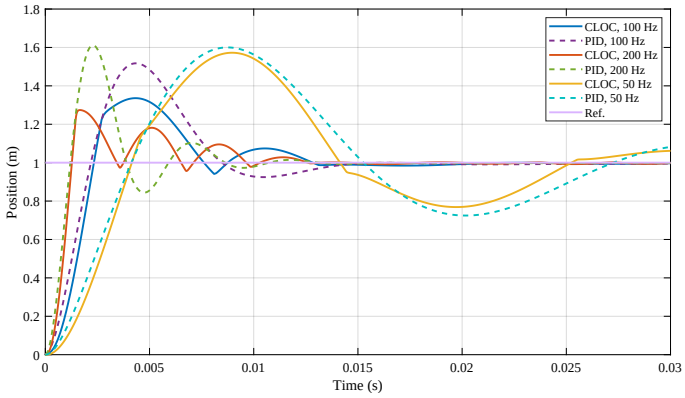

Figure 5.7: Step response of the CLOC and PID for bandwidth of 50 Hz, 100 Hz and 200 Hz.

6. Choose M and N s.t. according to (5.15), $\omega_{zM} \geq \omega_h$ and $\omega_{pN} \geq \omega_h$.
7. Set $\omega_r = \omega_l$ and $\omega_f = 10\omega_h$.
8. Choose $\gamma \in (-1, 1)$ s.t. the required phase margin is achieved. If not achievable, go to step 4 and correct β accordingly.

Step 2 ensures that the BLS is stable as a necessary condition for H_β. It should be noted that according to waterbed effect, increasing the linear differentiation band will reduce

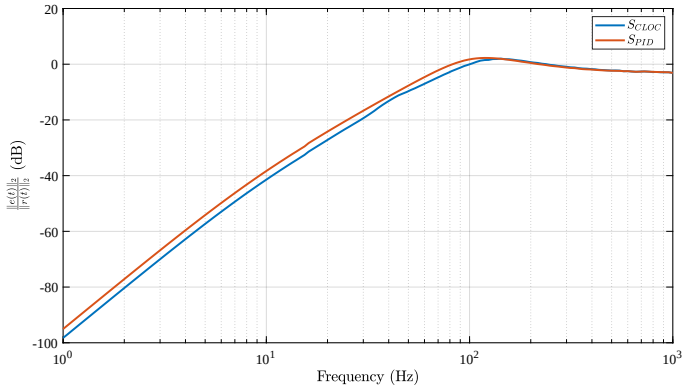

Figure 5.8: $\frac{\|e(t)\|_2}{\|r(t)\|_2}$ plotted for both controllers.

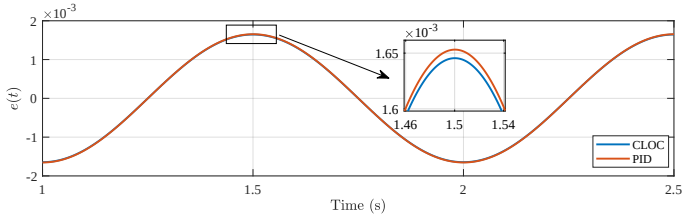

Figure 5.9: Sinusoidal tracking error of CLOC and PID for $r(t) = \sin(2\pi t)$.

the steady-state precision of the system. It can be concluded from the waterbed effect. Therefore, the band should be minimum only to stabilize the BLS.

As an illustrative example, two controllers will be compared, one with integer-order tamed differentiator, i.e., PID and one with complex-order tamed differentiator, i.e., CLOC. For cross-over frequency, $\omega_c = 100$ Hz is chosen, and following the rule of thumb presented in [2] for tuning PID,

$$\omega_i = \omega_c/10, \quad \omega_d = \omega_c/2.5, \quad \omega_t = 2.5\omega_c, \quad \beta = 0. \tag{5.17}$$

Following the steps for designing a CLOC, the following parameters has been tuned for CLOC

$$\omega_i = \omega_c/10, \quad \omega_d = \omega_c/1.5, \quad \omega_t = 1.5\omega_c, \quad \beta = 0.3. \tag{5.18}$$

For the approximation of complex-order tamed differentiator, following parameters have been tuned

$$\omega_l = 0.1^{0.5}\omega_c, \quad \omega_h = 10^{0.5}\omega_c, \quad \omega_r = \omega_l, \quad \omega_f = 10\omega_h,$$
$$N = M = 8, \quad \zeta = 3.314, \quad \eta = 7.714, \quad \gamma = 0. \tag{5.19}$$

The above parameters ensure that the positive slope of the phase occurs from half a decade before the cross-over frequency to half a decade after.

Fig. 5.5 shows the Bode diagram of the PID controller without plant and DF of CLOC. The figure clearly shows that using a complex-order tamed differentiator in CLOC, the same phase margin as PID is achieved with a lower positive gain slope around the omega, which resulted in higher gain at frequencies below bandwidth and lower gain at fre-

quencies higher than bandwidth compared to PID. Thus, better steady-state sinusoidal tracking and disturbance rejection and noise attenuation are expected according to the loop-shaping technique.
Open-loop frequency analysis of the two systems in Fig. 5.6. also reveals some helpful information. In addition to revealing the higher-order harmonic contents of the output of the CLOC system, it can be seen that at 12 Hz, where ψ crosses the zero line, the higher-order harmonics show a notch-like behaviour, and their magnitude will be zero. It also shows that the positive gain of ψ created a positive phase slope for CgLp. It should be noted that the discrepancy between the slope of ψ and the phase of CLOC at the beginning and end of $[\omega_l, \omega_h]$, is due to the fact that $[\omega_d, \omega_t]$ is smaller than $[\omega_l, \omega_h]$.
The step response of the CLOC and PID for bandwidth of 50 Hz, 100 Hz and 200 Hz has been obtained using the Simulink environment of Matlab and depicted in Fig. 5.7. It should be noted that the bandwidth change has been created only by changing k_p, and no other parameter has been changed. This figure reveals that CLOC shows a lower overshoot in all cases than PID even when two controllers have the same phase margin. It can be explained through the reset nature of the CLOC. As it is expected from Fig. 5.6, when the bandwidth changes from 100 Hz to 200 Hz, the phase margin of PID will be reduced and thus its overshoot will increase, while the phase margin of CLOC increases and thus its overshoot reduces. When bandwidth is changed to 50 Hz, both controllers lose phase margin and show an increase in overshoot; however, CLOC still shows a lower overshoot than PID even when its phase margin is lower than PID.
The sensitivity plot of the control system can be used to validate the improvement in steady-state performance. However, because reset control systems are nonlinear, therefore, sensitivity plots for them must be estimated; the sensitivity plot obtained using the DF approximation may not be accurate [23]. To calculate the sensitivity plot more precisely, a series of simulations were performed to track sinusoidal waves with different frequencies, and the $\frac{\|e(t)\|2}{\|r(t)\|2}$ was shown for both controllers in Fig. 5.8.
As expected, due to the higher open-loop gain at lower frequencies (see Fig. 5.6), CLOC shows a lower tracking error compared to PID and also a lower peak of sensitivity. Finally, to see the steady-state time-domain results, the sinusoidal tracking performance of the controllers for $r(t) = \sin(2\pi t)$ is depicted in Fig. 5.9.

5.6. CONCLUSIONS

This paper introduced a reset controller based on the structure of a CgLp with a shaped reset signal, which could approximate a complex-order transfer function. For this purpose, a shaping filter was designed for the reset signal, which could alter the DF of the reset controller to achieve the negative gain slope along with a positive phase slope. Furthermore, a tuning method was introduced to tune the gain slope and, more importantly, the phase slope. To illustrate the possible improvements of using such a controller, a comparison between CLOC and PID was made in the frequency and time domains. It was shown that CLOC could achieve the same phase margin as PID with a weaker linear tamed differentiator and showed a lower overshoot even with the same phase margin as PID. The weaker linear tamed differentiator also facilitated the CLOC to show higher gain in lower frequencies, thus showing a lower sinusoidal tracking error.
Implementing the proposed controller in practice in the presence of noise and distur-

bance for a more general plant may be a follow-up for this study.

BIBLIOGRAPHY

[1] K. J. Åström, "Limitations on control system performance", *European Journal of Control*, vol. 6, no. 1, pp. 2–20, 2000.

[2] R. M. Schmidt, G. Schitter, and A. Rankers, *The design of high performance mechatronics-: high-Tech functionality by multidisciplinary system integration*. Ios Press, 2020.

[3] J. Freudenberg, R. Middleton, and A. Stefanpoulou, "A survey of inherent design limitations", in *Proceedings of the 2000 American Control Conference. ACC (IEEE Cat. No. 00CH36334)*, IEEE, vol. 5, 2000, pp. 2987–3001.

[4] A. Oustaloup, F. Levron, B. Mathieu, and F. M. Nanot, "Frequency-band complex noninteger differentiator: Characterization and synthesis", *IEEE Transactions on Circuits and Systems I: Fundamental Theory and Applications*, vol. 47, no. 1, pp. 25–39, 2000.

[5] J. Sabatier, P. Lanusse, P. Melchior, and A. Oustaloup, "Fractional order differentiation and robust control design", *Intelligent systems, control and automation: science and engineering*, vol. 77, pp. 13–18, 2015.

[6] A. Oustaloup, *La commande CRONE: commande robuste d'ordre non entier*. Hermes, 1991.

[7] M. G. Moghadam, F. Padula, and L. Ntogramatzidis, "Tuning and performance assessment of complex fractional-order pi controllers", *IFAC-PapersOnLine*, vol. 51, no. 4, pp. 757–762, 2018.

[8] J. Clegg, "A nonlinear integrator for servomechanisms", *Transactions of the American Institute of Electrical Engineers, Part II: Applications and Industry*, vol. 77, no. 1, pp. 41–42, 1958.

[9] D. Valério, N. Saikumar, A. A. Dastjerdi, N. Karbasizadeh, and S. H. HosseinNia, "Reset control approximates complex order transfer functions", *Nonlinear Dynamics*, vol. 97, no. 4, pp. 2323–2337, 2019.

[10] N. Saikumar, D. Valério, and S. H. HosseinNia, "Complex order control for improved loop-shaping in precision positioning", *arXiv preprint arXiv:1907.09249*, 2019.

[11] A. Baños and A. Barreiro, *Reset control systems*. Springer Science & Business Media, 2011.

[12] I. Horowitz and P. Rosenbaum, "Non-linear design for cost of feedback reduction in systems with large parameter uncertainty", *International Journal of Control*, vol. 21, no. 6, pp. 977–1001, 1975.

[13] K. Krishnan and I. Horowitz, "Synthesis of a non-linear feedback system with significant plant-ignorance for prescribed system tolerances", *International Journal of Control*, vol. 19, no. 4, pp. 689–706, 1974.

[14] L. Hazeleger, M. Heertjes, and H. Nijmeijer, "Second-order reset elements for stage control design", in *2016 American Control Conference (ACC)*, IEEE, 2016, pp. 2643–2648.

[15] A. Baños and A. Vidal, "Definition and tuning of a PI+ CI reset controller", in *2007 European Control Conference (ECC)*, IEEE, 2007, pp. 4792–4798.

[16] O. Beker, C. Hollot, Y. Chait, and H. Han, "Fundamental properties of reset control systems", *Automatica*, vol. 40, no. 6, pp. 905–915, 2004.

[17] N. Saikumar, R. Sinha, and S. H. Hoseinnia, "'constant in gain lead in phase'element-application in precision motion control", *IEEE/ASME Transactions on Mechatronics*, 2019.

[18] N. Karbasizadeh, N. Saikumar, and S. Hossein Nia Kani, "Fractional-order single state reset element", English, *Nonlinear Dynamics*, vol. 104, no. 1, pp. 413–427, 2021, ISSN: 0924-090X. DOI: 10.1007/s11071-020-06138-9.

[19] N. Karbasizadeh, A. A. Dastjerdi, N. Saikumar, D. Valerio, and S. H. HosseinNia, *Benefiting from linear behaviour of a nonlinear reset-based element at certain frequencies*, 2020. arXiv: 2004.03529 [eess.SY].

[20] A. A. Dastjerdi and S. H. Hosseinnia, "A frequency-domain tuning method for a class of reset control systems", *IEEE Access*, vol. 9, pp. 40 950–40 962, 2021.

[21] Y. Guo, Y. Wang, and L. Xie, "Frequency-domain properties of reset systems with application in hard-disk-drive systems", *IEEE Transactions on Control Systems Technology*, vol. 17, no. 6, pp. 1446–1453, 2009.

[22] P. Nuij, O. Bosgra, and M. Steinbuch, "Higher-order sinusoidal input describing functions for the analysis of non-linear systems with harmonic responses", *Mechanical Systems and Signal Processing*, vol. 20, no. 8, pp. 1883–1904, 2006.

[23] N. Saikumar, K. Heinen, and S. H. HosseinNia, "Loop-shaping for reset control systems: A higher-order sinusoidal-input describing functions approach", *Control Engineering Practice*, vol. 111, p. 104 808, 2021.

[24] A. A. Dastjerdi, N. Saikumar, D. Valerio, and S. H. HosseinNia, *Closed-loop frequency analyses of reset systems*, 2020.

[25] Y. Guo, L. Xie, and Y. Wang, *Analysis and Design of Reset Control Systems*. Institution of Engineering and Technology, 2015, ISBN: 1849197032, 9781849197038.

[26] D. Nešić, L. Zaccarian, and A. R. Teel, "Stability properties of reset systems", *Automatica*, vol. 44, no. 8, pp. 2019–2026, 2008.

[27] A. A. Dastjerdi, A. Astolfi, and S. H. HosseinNia, *Frequency domain stability method for reset systems*, 2021. arXiv: 2009.00569 [eess.SY].

[28] I. Podlubny, *Fractional differential equations: an introduction to fractional derivatives, fractional differential equations, to methods of their solution and some of their applications*. Elsevier, 1998.

[29] S. G. Samko, A. A. Kilbas, and O. I. Marichev, *Fractional integrals and derivatives, translated from the 1987 russian original*, 1993.

[30] D. Valério and J. S. Da Costa, *An introduction to fractional control*. IET, 2013, vol. 91.

[31] N. Karbasizadeh, A. A. Dastjerdi, N. Saikumar, and S. H. HosseinNia, "Band-passing nonlinearity in reset elements", *IEEE Transactions on Control Systems Technology*, In press. [Online]. Available: https://arxiv.org/abs/2009.06091.

[32] M. S. Bahnamiri, N. Karbasizadeh, A. A. Dastjerdi, N. Saikumar, and S. H. HosseinNia, "Tuning of CgLp based reset controllers: Application in precision positioning systems", *IFAC-PapersOnLine*, vol. 53, no. 2, pp. 8997–9004, 2020. DOI: 10.1016/j.ifacol.2020.12.2017. [Online]. Available: https://doi.org/10.1016/j.ifacol.2020.12.2017.

[33] D. Valério and J. Sá da Costa, "Variable order fractional controllers", *Asian Journal of Control*, vol. 15, no. 3, pp. 648–657, 2013.

6

CONTINUOUS RESET

This paper addresses the main goal of using reset control in precision motion control systems, breaking the well-known "Waterbed effect". A new architecture for reset elements will be introduced which has a continuous output signal as opposed to conventional reset elements. A steady-state precision study is presented, showing that steady-state precision is preserved while the peak of sensitivity is reduced. The architecture is then used for a "Constant in Gain Lead in Phase" (CgLp) element and a numerical analysis of the transient response shows a significant improvement in the transient response. It is shown that by following the presented guideline for tuning, the settling time can be reduced and at the same time a no-overshoot step response can be achieved. A practical example is presented to verify the results and also to show that the proposed element can achieve a complex-order behaviour.

6.1. INTRODUCTION

Waterbed effect limits the performance of the linear control systems [1]. Almost every researcher in the field of control engineering has encountered this fundamental limitation. One can come up with different mathematical interpretations for it; however, most definitely, its practical effect is more important, especially for high-tech industrial applications such as precision motion control. One can interpret this effect by putting the transient and steady-state response of the system on two sides of this infamous waterbed, which implies that by improving one, you are sacrificing the other.

Reset control systems, first proposed by Clegg in [2], are proving themselves as alternatives to linear control systems, as they showed the potential to outperform linear control systems by breaking the waterbed effect limitation. Clegg proposed an integrator whose output will reset to zero whenever its input crosses zero. It was established that based

This chapter is published as:
N. Karbasizadeh, S. H. HosseinNia, Continuous reset element: Transient and steady-state analysis for precision motion systems, Control Engineering Practice, Volume 126, 2022, 105232, ISSN 0967-0661, https://doi.org/10.1016/j.conengprac.2022.105232.

on the Describing Function (DF) analysis, such an action will reduce the phase lag of the integrator by 52°. Although this already breaks the Bode's gain-phase relation for linear control systems, there are concerns while using Clegg's Integrator (CI) in practice, namely, the accuracy of DF approximation, limit-cycle, etc.
In order to address the drawbacks and exploit the benefits, the idea was later extended to more sophisticated elements such as the "First-Order Reset Element" [3], [4] and "Second-Order Reset Element" [5] or using Clegg's integrator in form of PI+CI [6] or resetting the state to a fraction of its current value, known as partial resetting [7]. Reset control has also recently been used to approximate complex-order filters [8], [9]. The advantage of using reset control over linear control has been shown in many studies, especially in precision motion control [7], [10]–[18]. However, these studies are mostly focused on solving one problem. For example, they either improve the transient [19] or steady-state response of the system while paying little or no attention to the other.
One of recent studies introduces a new reset element called "Constant-in-Gain, Lead-in-Phase" (CgLp) element, which is proposed based on the loop-shaping concept [9]. DF analysis of this element shows that it can provide broadband phase lead while maintaining constant gain. This element is used in the literature to replace some part of the differentiation action in PID controllers as it will help improve the precision of the system according to loop-shaping concept [9], [11], [13], [14].
In [11], [13], it is suggested that the DF analysis for the reset control systems can be inaccurate as it neglects the higher-order harmonics created in response of reset control systems. These studies also suggest that suppressing higher-order harmonics can improve the steady-state precision of the system.
One of the benefits of providing phase lead through CgLp is improving the transient response properties of the system, as it is shown that it reduces the overshoot and settling time of the system. However, the way to achieve this goal is not only through phase compensation around the cross-over frequency. It is shown in [20] that since reset control systems are nonlinear systems, the sequence of elements in the control loop affects the output of the system. It was shown that when the lead elements are placed before the reset element, it can improve the overshoot of the system. However, no systematic approach is proposed there to further improve the transient response. In [21], it is shown that by changing the resetting condition of the reset element to reset based on its input and its derivative, the overshoot limitation in linear control systems can be overcome. This limitation has also been broken using the same technique in another hybrid control system called "Hybrid Integrator Gain System" (HIGS) [22]. However, in these studies, the effect of such an action on steady-state performance of the system is not addressed.
Another important common property of all reset elements in the literature is the discontinuity of the output signal. This property is a cause for the presence of high-frequency content in the signals and subsequent practical problems [11]. Continuous-time implementation as opposed to discrete-time implementation of reset control and also soft resetting were introduced in the literature to mitigate this problem to some extent [23], [24]. However, this paper proposes an approach that can also be used in discrete time.
The main contribution of this paper is to propose a new architecture for the CgLp element which has a continuous output as opposed to conventional reset elements. This element drastically improves the transient response of systems without jeopardizing the

steady-state performance of the system by increasing higher-order harmonics. This paper shows that this architecture even reduces the higher-order harmonics by smoothing the reset jumps. Reset control systems are also known to have big jumps and peaks in their control input, which can be a limiting factor in practical applications due to saturation. The proposed architecture will also improve this drawback. A guideline for tuning the proposed architecture will also be provided.
The remainder of this paper is organized as follows. Section 6.2 presents the preliminaries of the study. The following section presents the continuous reset architecture. Section 6.4 will study the open-loop steady-state properties of the proposed architecture. The following two sections will numerically study the closed-loop transient and steady-state characteristics of the proposed controller. Section 6.7, will verify the results by presenting the results of an experiment on a precision positioning system system and, finally, the paper concludes along with some tips for ongoing works.

6.2. PRELIMINARIES

This section will discuss the preliminaries of this study.

6.2.1. DYNAMICS OF PRECISION MOTION SYSTEMS

The first stage in precise control of a mechatronic system is to determine the dynamics of motion. A friction-less moving mass is the most basic mechatronic system. Its motion dynamics are represented by a double integrator. A DC motor or a voice coil actuator-driven system are examples of such systems. In practice, the masses are usually constrained by springs, and there are always some amounts of damping present, which creates a mass-spring-damper dynamics. Such dynamics in the frequency domain has a constant spring line and a resonance peak in addition to the negative-sloped mass line. Most of the precision motion setups are well-designed systems that can be modeled as mass-spring-damper systems or a cascade of them [25]–[28]. Whether they are collocated or non-collocated systems, in practice, the cross-over frequency to control them is usually placed along the -2 slope mass line. Furthermore, the presence of integrator at lower frequencies makes the overall open-loop frequency domain characteristics of precision motion systems to closely resemble a mass system.
This paper consists of an analytical analysis on the steady-state properties of such systems and a numerical analysis of transient properties. Although analytical steady-state analysis will be carried out for general motion plants, for transient numerical analysis, for the sake of generality and simplicity, a mass plant will be assumed. However, in experimental results, it will be shown that the study holds for a mass-spring-damper system with higher frequency modes.

6.2.2. GENERAL RESET CONTROLLER

The general form of reset controllers used in this study is as following:

$$\sum_R := \begin{cases} \dot{x}_r(t) = A_r x_r(t) + B_r e(t), & \text{if } e(t) \neq 0 \\ x_r(t^+) = A_\rho x_r(t), & \text{if } e(t) = 0 \\ u(t) = C_r x_r(t) + D_r e(t) \end{cases} \tag{6.1}$$

where A_r, B_r, C_r, D_r denote the state space matrices of the Base Linear System (BLS) and the reset matrix is denoted by $A_\rho = \text{diag}(\gamma_1, ..., \gamma_n)$ which contains the reset coefficients for each state. $e(t)$ and $u(t)$ represent the input and output of the reset controller, respectively.
A special type of reset element which is of concern in this paper is the First-Order Reset Element (FORE). In the literature, this element is typically shown as $\frac{1}{s/\omega_r+1}$ with γ, where ω_r is the corner frequency, the arrow indicates the resetting action, and since the element has only one resetting state, $A_\rho = \gamma$.

6.2.3. H_β CONDITION

Among different criteria for stability of reset control systems [12], [29]–[33], despite of being conservative, H_β condition has gained attention because of simplicity and frequency domain applicability [7]. In [34], the H_β condition has been reformulated so that the frequency response functions of the controllers and the plant can be used directly. This method especially includes the case where the reset element is not the first element in the loop.

6

Theorem 6. *[34] Let us denote the frequency response functions of the open-loop BLS and the reset element by $O(j\omega)$ and $C_R(j\omega)$, respectively. And let the vector $\overrightarrow{\mathcal{N}}(\omega) \in \mathbb{R}^2$ be defined as $\overrightarrow{\mathcal{N}}(\omega) = [\ \mathcal{N}_X \quad \mathcal{N}_Y\ ]^T$ in which*

$$\begin{aligned} \mathcal{N}_X &= \Re\big(O(j\omega)\kappa(j\omega)\big), \\ \mathcal{N}_Y &= \Re\big(\kappa(j\omega)C_R(j\omega)\big), \end{aligned} \tag{6.2}$$

where $\kappa(j\omega) = 1 + O^*(j\omega)$, $O^*(j\omega)$ is the conjugate of $O(j\omega)$ and $\Re(.)$ stands for the real part of a complex number. Let

$$\theta_1 = \min_{\omega\in\mathbb{R}^+} \angle\overrightarrow{\mathcal{N}}(\omega) \text{ and } \theta_2 = \max_{\omega\in\mathbb{R}^+} \angle\overrightarrow{\mathcal{N}}(\omega). \tag{6.3}$$

Then the h_β condition for a reset control system is satisfied, and its response is Uniformly Bounded-Input Bounded-State (UBIBS) stable if

$$\Big(-\frac{\pi}{2} < \theta_1 < \pi\Big) \wedge \Big(-\frac{\pi}{2} < \theta_2 < \pi\Big) \wedge (\theta_2 - \theta_1 < \pi). \tag{6.4}$$

6.2.4. DESCRIBING FUNCTIONS

Describing function analysis is the known approach in the literature for approximation of frequency response of non-linear systems such as reset controllers [35]. However, the DF method only takes the first harmonic of Fourier series decomposition of the output into account and neglects the effects of the higher-order harmonics. This simplification can be significantly inaccurate under certain circumstances [13]. The "Higher-Order Sinusoidal Input Describing Function" (HOSIDF) method has been introduced in [36] to provide more accurate information on the frequency response of nonlinear systems by investigating higher-order harmonics of the Fourier series decomposition. In other words, in this method, the nonlinear element will be replaced by a virtual harmonic generator. This method was developed in [37] for reset elements defined by Eq. (6.1)

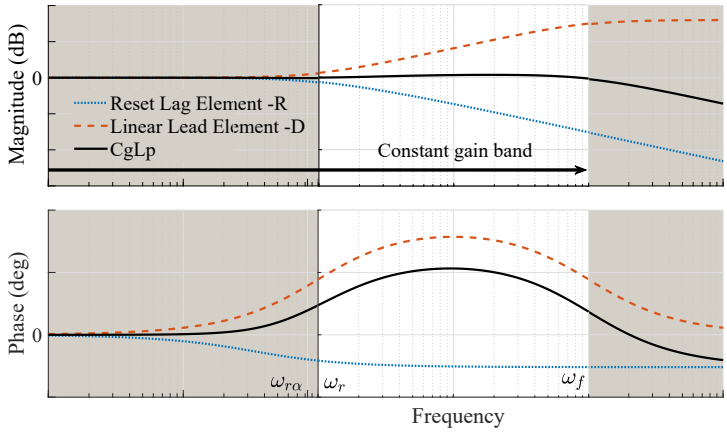

Figure 6.1: The concept of using combination of a reset lag and a linear lead element to form a CgLp element. The figure is from [9].

as follows:

$$
\begin{aligned}
H_n(\omega) &= \begin{cases} C_r(j\omega I - A_r)^{-1}(I + j\Theta(\omega))B_r + D_r, & n = 1 \\ C_r(j\omega n I - A_r)^{-1} j\Theta(\omega) B_r, & \text{odd } n > 2 \\ 0, & \text{even } n \geq 2 \end{cases} \\
\Theta(\omega) &= -\frac{2\omega^2}{\pi}\Delta(\omega)[\Gamma(\omega) - \Lambda^{-1}(\omega)] \\
\Lambda(\omega) &= \omega^2 I + {A_r}^2 \\
\Delta(\omega) &= I + e^{\frac{\pi}{\omega}A_r} \\
\Delta_\rho(\omega) &= I + A_\rho e^{\frac{\pi}{\omega}A_r} \\
\Gamma(\omega) &= \Delta_\rho^{-1}(\omega) A_\rho \Delta(\omega) \Lambda^{-1}(\omega)
\end{aligned}
\tag{6.5}
$$

where $H_n(\omega)$ is the n^{th} harmonic describing function for sinusoidal input with frequency ω.

6.2.5. CgLp

CgLp is a broadband phase compensation reset element which has a first harmonic constant gain behaviour while providing a phase lead [9]. This element consists of a reset lag element in series with a linear lead filter, namely $\sum_R$ and D, respectively. For FORE CgLp:

$$
\sum_R = \frac{1}{s/\omega_r + 1}, \qquad D(s) = \frac{s/\omega_{r\alpha} + 1}{s/\omega_f + 1} \tag{6.6}
$$

where $\omega_{r\alpha} = \alpha\omega_r$, α is a tuning parameter accounting for a shift in corner frequency of the filter due to resetting action, and $[\omega_r, \omega_f]$ is the frequency range where the CgLp will provide the required phase lead. The arrow indicates the resetting action as described in Eq. (6.1).

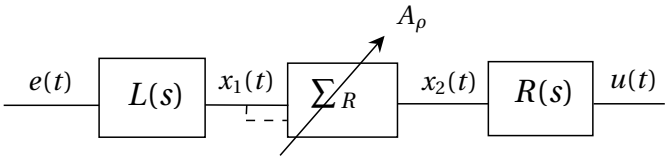

Figure 6.2: Proposed architecture for reset elements which includes a lead element, $L(s)$ before the reset element and ints inverse after the reset element. The proposed lead is $L(s) = \frac{s/\omega_l+1}{s/\omega_h+1}$ and $R(s) = \frac{1}{s/\omega_l+1}$.

CgLp provides the phase lead by using the reduced phase lag of reset lag element in combination with a corresponding lead element to create broadband phase lead. Ideally, the gain of the reset lag element should be canceled out by the gain of the corresponding linear lead element, which creates a constant gain behavior. The concept is depicted in Fig. 6.1.

6.3. PROPOSED ARCHITECTURE FOR CONTINUOUS RESET (CR) ELEMENTS

The new architecture which this paper proposes consists of adding a first-order lag element, $R(s)$, after the reset element and adding the inverse of it, which is basically a lead element, after the reset element. Fig. 6.2 shows the new architecture in which

$$L(s) = \frac{s/\omega_l + 1}{s/\omega_h + 1}, \quad R(s) = \frac{1}{s/\omega_l + 1}. \tag{6.7}$$

In the ideal case, $L(s) = R^{-1}(s)$, however, in order to make $L(s)$ proper and realizable, the presence of the denominator in $L(s)$ is necessary. However, assuming that ω_h is large enough, $R(s) \approx L^{-1}(s)$ in low frequencies. In the context of linear control systems, adding these two elements would almost have no effect on the output of the system at lower frequencies and would improve the noise attenuation behaviour at higher frequencies, provided the internal states were stable. However, in the context of nonlinear control systems, the output of the system will change significantly.
In this new architecture, the reset condition is changed from $e(t) = 0$ to $x_1(t) = 0$. Again considering that ω_h is large enough, the new resetting condition can be approximated as

$$x_1(t) = \dot{e}(t)/\omega_l + e(t) = 0. \tag{6.8}$$

The new reset element is reset based on a linear combination of $e(t)$ and $\dot{e}(t)$, where ω_l determines the weight of each. In closed loop, $e(t)$ and $\dot{e}(t)$ are the error and its differentiation.

Remark 9. *According to Theorem 6, a reset element in the CR architecture has the same stability properties as standing alone, as long as $O(s)$ stays the same, i.e., $R(s)$ and $L(s)$ cancel each other in the linear domain. In other words, the addition of $L(s)$ and $R(s)$ to the CR architecture does not affect the stability properties of the reset control system. However, for the architecture presented in this paper, the additional condition is $\omega_h \gg \omega_r$*

and $\omega_h \gg \omega_c$, where ω_c is the cross-over frequency.

Theorem 7. *The output of the proposed architecture is continuous as opposed to $\sum_R$ alone.*

Proof. If the reset instants are $\{t_k \mid k = 1,2,3,\cdots\}$, from Eq. (6.1) and Fig. 6.2, it can be seen that

$$\sum_R := \begin{cases} \dot{x}_r(t) = A_r x_r(t) + B_r x_1(t), & \text{if } t \neq t_k \\ x_r(t^+) = A_\rho x_r(t), & \text{if } t = t_k \\ x_2(t) = C_r x_r(t) + D_r x_1(t) \end{cases} \tag{6.9}$$

It is readily obvious that $x_2(t)$ is continuous on (t_{k-1}, t_k) and (t_k, t_{k+1}). However,

$$\lim_{t \to t_k^-} x_2(t) \neq \lim_{t \to t_k^+} x_2(t) \tag{6.10}$$

and thus it is discontinuous. Nevertheless, for $u(t)$ one can write

$$\underset{t_{k-1}<t\leq t_k}{u(t)} = \omega_l \left(e^{-\omega_l (t-t_{k-1})} u(t_{k-1}) + \int_{t_{k-1}}^{t} e^{-\omega_l (t-\tau)} x_2(\tau) d\tau \right). \tag{6.11}$$

It can be readily seen that

$$\lim_{t \to t_k^-} u(t) = \lim_{t \to t_k^+} u(t) = \omega_d \left(e^{-\omega_l (t_k - t_{k-1})} u(t_{k-1}) + \int_{t_{k-1}}^{t_k} e^{-\omega_l (t_k-\tau)} x_2(\tau) d\tau \right). \tag{6.12}$$

□

In addition to making the reset element output continuous, other motivations to use this architecture can be described in terms of steady-state and transient response of system, which will be discussed in details in following sections.

6.4. OPEN-LOOP STEADY-STATE PROPERTIES OF THE CR ARCHITECTURE

Frequency domain analysis is the popular approach for studying the steady-state response of a system. However, as mentioned earlier, because of the nonlinearity of reset elements, that is not directly possible. The DF and HOSIDF methods are two approaches to approximate a frequency response for a reset control systems, where DF can be regarded as a special case of HOSIDF in which only the first-order harmonic is studied. To illustrate how the HOSIDF approach can be used for the proposed CR architecture, one can refer to Fig. 6.3.

Proposition 1. *For $\omega_h = \infty$, the CR architecture has the same DF as the $\sum_R$ alone.*

Proof. Let the states in the CR architecture be denoted as shown in Fig. 6.2. For the purpose of DF and HOSIDF analysis, one should have $e(t) = \sin(\omega t)$. Obviously, the

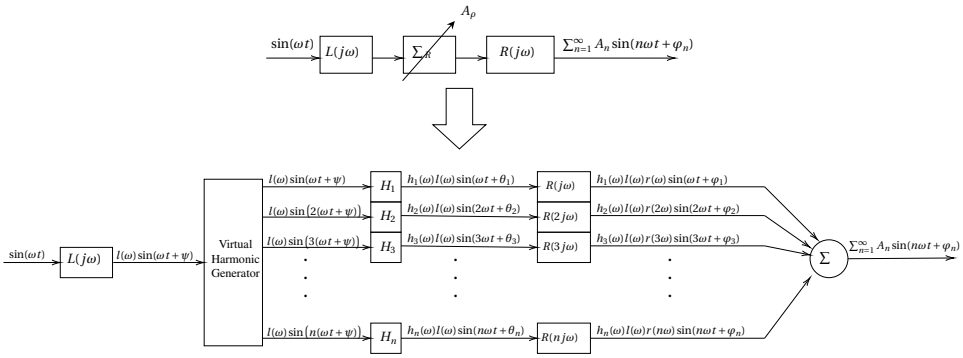

Figure 6.3: Representation of HOSIDF for open-loop analysis of the new architecture proposed. $l(\omega) = |L(j\omega)|$, $r(\omega) = |R(j\omega)|$ and $h_n(\omega) = |H_n(j\omega)|$, where $H_n(\omega)$ can be obtained from Eq. (6.5) for $\sum_R$.

steady-state response of $x_1(t)$ is:

$$x_1(t) = l(\omega)\sin(\omega t + \psi(\omega)) \tag{6.13}$$

where $l(\omega) = |L(j\omega)|$ and $\psi(\omega) = \angle L(j\omega)$. Taking $x_1(t)$ as the input to the reset element and according to Eq. (6.5),

$$x_{21}(t) = h_1(\omega)l(\omega)\sin(\omega t + \theta_1(\omega)) \tag{6.14}$$

where $x_{21}(t)$ stands for first harmonic of $x_2(t)$ and $h_1(\omega) = |H_1(j\omega)|$ and $\theta_1(\omega) = \psi(\omega) + \angle H_1(j\omega)$. And, lastly,

$$u_1(t) = h_1(\omega)l(\omega)r(\omega)\sin(\omega t + \varphi_1(\omega)) \tag{6.15}$$

where $u_1(t)$ stands for first harmonic of $u(t)$ and $r(t) = |R(j\omega)|$ and $\varphi_1(\omega) = \theta_1(\omega) + \angle R(j\omega)$. Since $R(j\omega) \approx L^{-1}(j\omega)$ for $\omega \ll \omega_h$, it can be seen that

$$|u_1(t)| = h_1(\omega), \tag{6.16}$$

$$\varphi_1(\omega) = \psi(\omega) + \angle H_1(j\omega) - \psi(\omega) = \angle H_1(j\omega). \tag{6.17}$$

□

Proposition 2. *The magnitude of higher-order harmonics for the CR architecture is reduced compared to the $\sum_R$ alone.*

Proof. Following the same reasoning as in Proposition 1, one has

$$u_n(t) = h_n(\omega)l(\omega)r(n\omega)\sin(n\omega t + \varphi_n(\omega)), \tag{6.18}$$

where $u_n(t)$ is the n^{th} harmonic of $u(t)$, $h_n(\omega) = |H_n(j\omega)|$ and $\varphi_n = \angle H_n(j\omega) + \angle L(j\omega) + \angle R(jn\omega)$. Since $r^{-1}(\omega) \approx l(\omega)$ for $\omega_h \gg \omega_l$, and since $l(\omega)$ is an increasing function

$$A_n(\omega) < h_n(\omega), \tag{6.19}$$

where $A_n(\omega)$ stands for $|u_n(t)|$. In other terms, for large enough ω_h,

$$A_n(\omega) \approx \sqrt{\frac{(\omega/\omega_l)^2 + 1}{(n\omega/\omega_l)^2 + 1}}\, h_n(\omega). \tag{6.20}$$

For $\omega \ll \omega_l$,

$$A_n(\omega) = h_n(\omega) \tag{6.21}$$

and for $\omega \gg \omega_l$,

$$A_n(\omega) = \frac{1}{n} h_n(\omega). \tag{6.22}$$

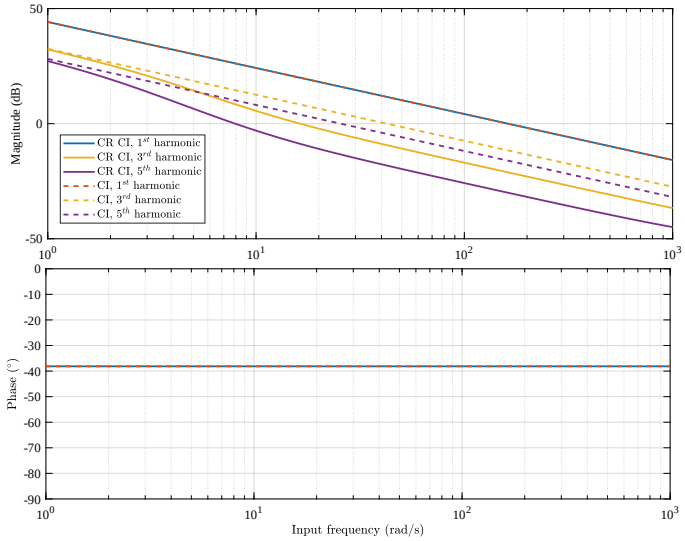

(a) HOSIDF of CI compared to CR CI. $\omega_l = 10$, $\omega_h = 1e4$ and $\gamma = 0$.

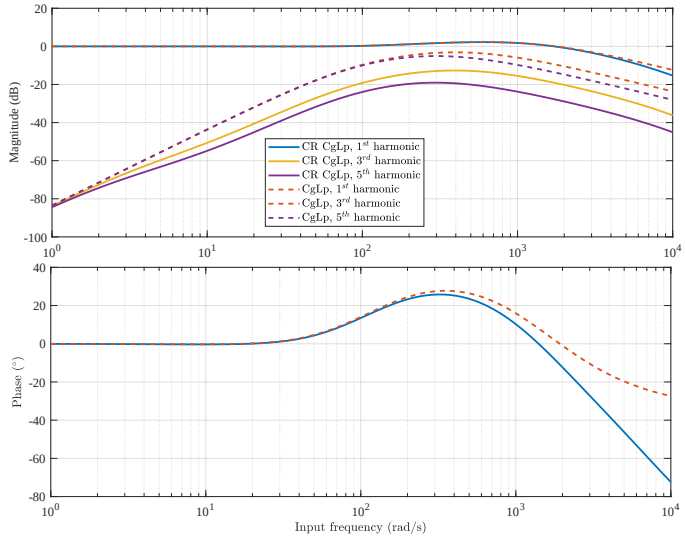

(b) HOSIDF of CgLp compared to CR CgLp. $\omega_l = 10$, $\omega_h = 1e4$, $\omega_r = 100$, $\omega_f = 1500$ and $\gamma = 0$.

Figure 6.4: HOSIDF of CI and CgLp compared to their CR architecture proposed in this paper. Frequencies are in rad/s.

□

Fig. 6.3 illustrates the harmonic generation for CR architecture.
Theorem 7 and Propositions 1 and 2 may seem somewhat trivial, however, they indicate very important features of the CR architecture in terms of steady-state performance. As mentioned earlier, the frequency domain analysis and design for reset control systems

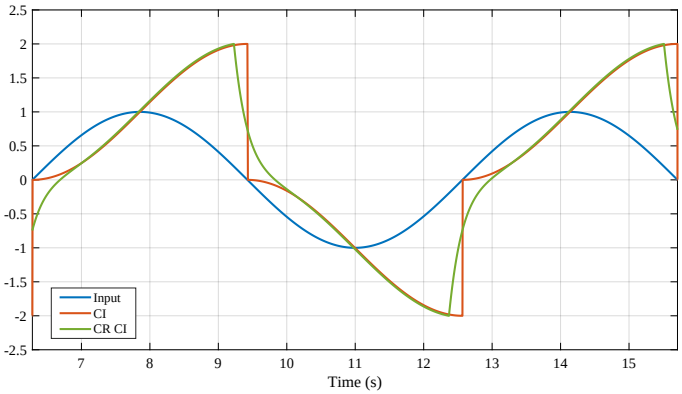

(a) Sinusoidal response of Clegg Integrator (CI) compared to CR CI. Input is $\sin(t)$.

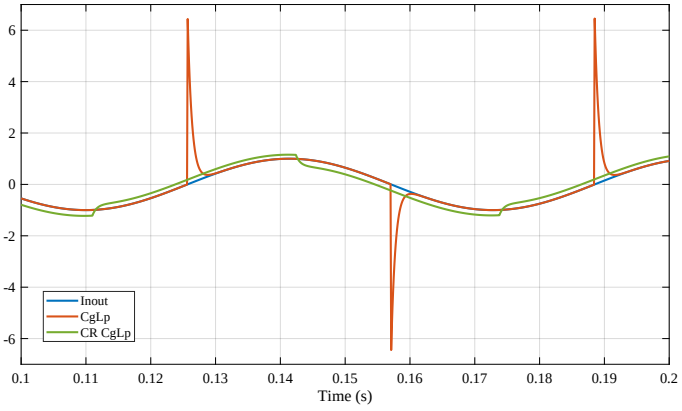

(b) Sinusoidal response of conventional CgLp compared to CR CgLp. The input is $\sin(100t)$.

Figure 6.5: Simulation results for sinusoidal response of CI and CgLp compared to their CR architecture proposed in this paper.

heavily depend on the accuracy of the DF approximation. The CR architecture maintains the DF characteristics of the reset elements and reduces the higher-order harmonics, which makes the DF approximation more accurate. It is shown in [11], [13] that it improves the performance of the systems in terms of steady-state precision.
Moreover, the discontinuity of the output signal in reset controllers creates practical problems such as amplifier or actuator saturation and excitation of higher frequency modes for complex plants. The CR architecture will solve these problems by reducing the known peaks in the controller output of the reset control systems.
In order to illustrate the effect of the CR architecture on HOSIDF of reset elements, the HOSIDF of a Clegg Integrator (CI) and a CR CI are compared in Fig. 6.4a, this figure shows that while the DF for these two elements are identical, a significant reduction in HOSIDF of CR CI with respect to CI occurs, this indicates that as we approach higher frequencies, the DF will become a more accurate approximation in CR CI. The same comparison is made for CgLp and CR CgLp in Fig. 6.4b. Both CgLps are designed to create a phase lead

of 15° at 100 rad/ s while maintaining constant gain. A significant reduction in the magnitude of higher-order harmonics is also clear here, which indicates that CR CgLp has a behaviour closer to the first-order harmonic, which is the ideal behavior for reset control systems.
In Fig. 6.5, the sinusoidal response of CI vs. CR CI at 1 rad/s and CgLp vs. CR CgLp at 100 rad/s are depicted. At both comparisons, it is clear that the output of CR architecture is continuous as opposed to reset elements in their conventional form, and the responses are much smoother, which shows the reduction of higher-order harmonics. Note that for the case of CgLp, the large peak in the response, which can cause the aforementioned practical issue, is removed in CR CgLp.
The superiority of CgLp control structures over other reset control strategies in precision motion control has been shown in many researches [9], [11], [14]. In the remainder of this paper, for the sake of conciseness, only the CR CgLp architecture will be studied. However, the same approach can be used for other reset control structures.
For the case of CR CgLp, the magnitude of higher-order harmonics for frequencies lower than ω_c (where it matters the most to the tracking and rejection of disturbances [11], [13]) is also affected by parameters other than ω_l. These parameters are ω_r and γ. However, unlike ω_l, these two parameters also affect the DF phase and consequently the amount of phase lead created by CR CgLp. This creates a trade-off between reduction of the magnitude of higher-order harmonics and maximum achievable Phase Advantage (PA) of CR CgLp. Fig. 6.6 illustrates the trade-off. CgLp will be logically designed to provide phase lead at cross-over frequency, i.e., ω_c. As ω_r approaches ω_c, the integral of 3^{rd} harmonic magnitude at frequencies below ω_c decreases significantly. The reduction of the integral value is an indication of the reduction in the magnitude of higher-order harmonics, in general. Furthermore, the peak of higher-order harmonics will also shift to higher frequencies when ω_r approaches higher frequencies. Thus, it seems logical to have this peak in frequencies where tracking and disturbance rejection performance is not a matter of concern, i.e., the frequencies after the bandwidth. When ω_r is in $[\omega_c, 1.5\omega_c]$, higher-order harmonics are very low and a PA of up to 35° is still achievable. This can be a general guideline for tuning ω_r in CR CgLp.

6.5. CLOSED-LOOP TRANSIENT RESPONSE PROPERTIES OF THE CR CGLP ARCHITECTURE

In the researches done on CgLp control systems in the literature, the only design parameter considered to change the transient response of systems is the phase margin. In the context of linear control systems, the phase margin is a determining parameter; however, that is not the case for the reset control system and especially for the CR architecture presented in this paper. Referring to Eq. (6.8), speaking in terms of the closed loop, in the CR architecture, the reset condition is not only based on the error signal, but a linear combination of error and its derivative. This will also change the transient response of the system [20], [22], [38]. In order to study the effect of the CR architecture parameters on the transient response of a closed-loop precision motion control system, a data-based approach has been used in this paper.
Fig. 6.7 shows the block diagram of the control loop. As shown in the figure, the reset

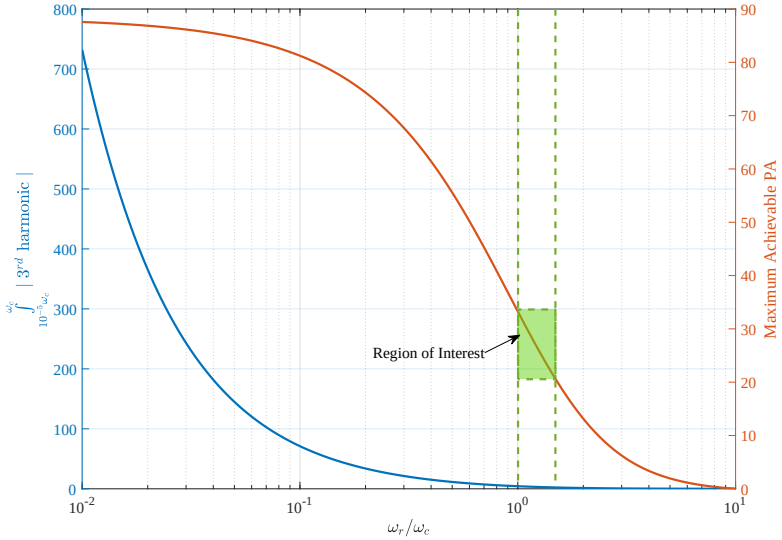

Figure 6.6: Integral of 3rd harmonic magnitude for frequencies below ω_c and the maximum achievable PA at ω_c vs. the ratio of ω_r to ω_c. $\gamma = -1$.

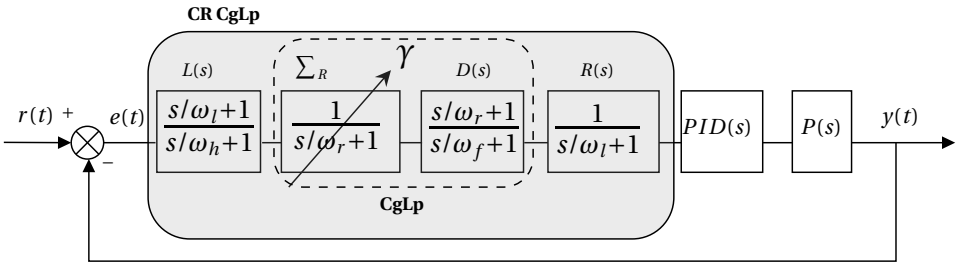

Figure 6.7: The control loop used for precision motion control using CR CgLp. $P(s)$ is the plant. $PID(s) = k_p\left(1+\omega_i/s\right)\left(\frac{s/\omega_d+1}{s/\omega_t+1}\right)$.

part of CgLp, i.e., $\sum_R$, is surrounded by $L(s)$ and $R(s)$ to create a CR CgLp.
Following the discussion in Section 6.2.1, the plant that is used for this data-based study is a mass system, i.e., $P(s) = 1/s^2$. In experimental validation, it will be shown that the analysis will also hold for mass-spring-damper systems.

The H_β condition for stability of the reset control systems necessarily requires the BLS to be stable. Thus, a PID controller is present in the loop. However, according to the loop-shaping technique, to ensure the maximum steady-state precision performance for the system, the differentiation part of the PID should be as weak as possible to only guarantee the stability of the BLS. Normally, such a tuning for the PID control system will perform poorly in terms of transient response in the absence of CR CgLp. Nevertheless, it will be shown that the presence of CR CgLp will significantly improve the transient response without affecting the maximally precise steady-state performance of the system. In this study, using a general rule of thumb, the PID is tuned so that the BLS has 5° phase

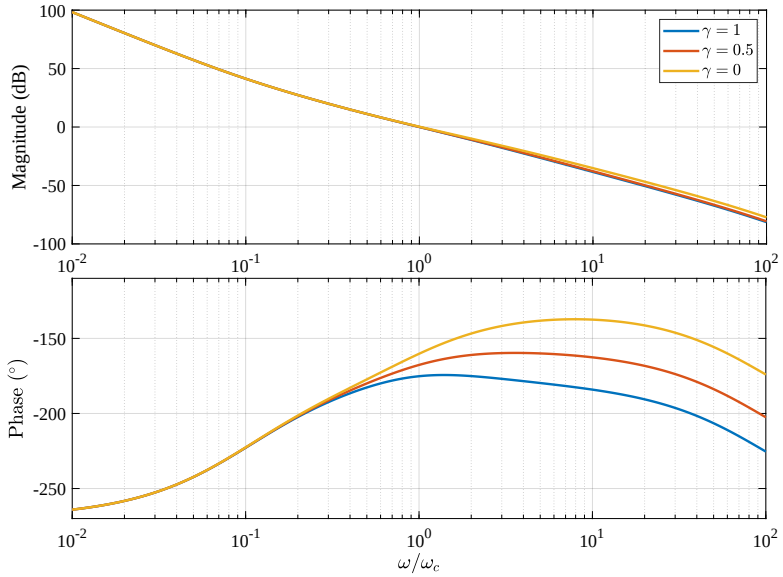

Figure 6.8: DF of the open loop system for different γ values versus the ration of ω/ω_c.

margin, which is enough to stabilize the BLS and since it has a weak differentiator, it does not jeopardize steady-state precision. The following equation shows the parameters chosen in this regard.

$$\omega_i = \omega_c/10, \quad \omega_d = \omega_c/1.2, \quad \omega_t = 1.2\omega_c \tag{6.23}$$

And consequently, k_p can be determined according to ω_c. According to the discussions in Section 6.4, without loss of generality, for this data-based study,

$$\omega_r = 1.2\omega_c. \tag{6.24}$$

This leaves the effect of γ and ω_l to be studied. Since ω_r and the PID parameters are fixed, the only parameter that affects the phase margin of the designed system is γ. It has to be noted that according to Proposition 1, CR architecture does not change the DF, thus ω_l does not have an effect on the phase margin. Fig. 6.8 shows the open-loop DF of the system under study and also the effect of γ on the phase margin. $\gamma = 1$ indicates the base linear system and as the value γ decreases, the phase margin will increase. At $\omega = \omega_c$, it can be seen that CR CgLp not only does not change the gain behaviour, but also creates a positive slope in phase, which resembles the complex-order controllers. In the following, the effect of phase margin and ω_l on overshoot and settling time of the closed-loop system will be shown.

6.5.1. OVERSHOOT

As mentioned before, it is expected that the variation of phase margin caused by variation of γ and the variation on ω_l create different transient responses for the closed-loop system. In order to do a data-based study, a unit step reference was given to the closed-loop system and the response was simulated using Simulink environment of Matlab. The

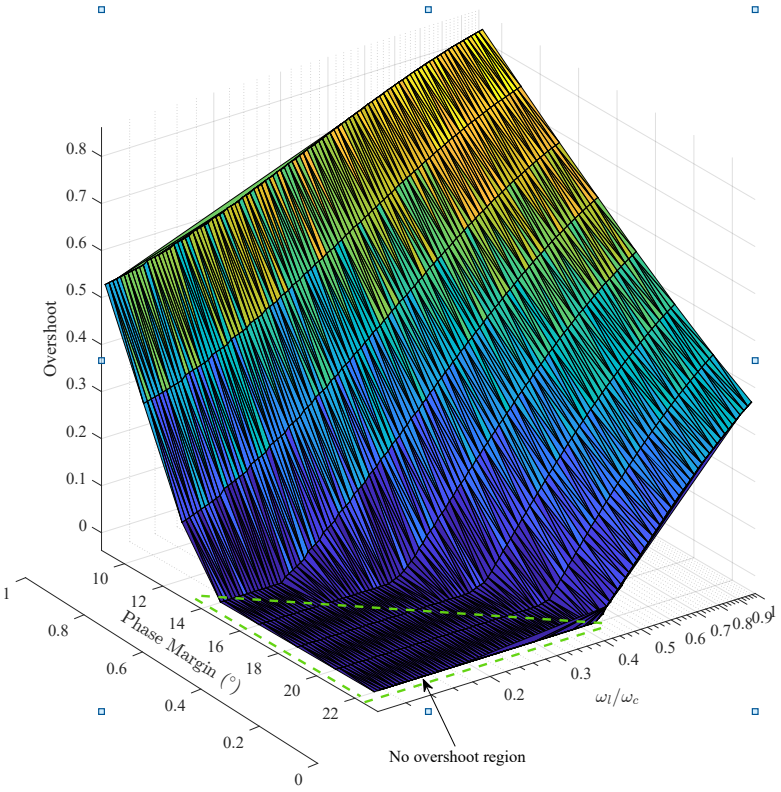

Figure 6.9: The overshoot of the system to a unit step for phase margin in range of [5,22] and $\omega_l/\omega_c \in [0.1,1]$. 5° of the phase margin is provided through the base linear system. The overshoot in the absence of the CR CgLp, i.e., BLS, is 0.962.

overshoot versus the variation of ω_l and phase margin is depicted in Fig. 6.9.
From Fig. 6.9, it can be concluded that, similarly to linear controllers, with increasing phase margin the overshoot decreases almost linearly. Furthermore, for a constant value of phase margin as ω_l decreases, the overshoot decreases, and for some configurations a non-overshoot performance is realizable. It should also be noted that as ω_l increases, it weakens the lead element $L(s)$ and therefore the system gradually tends to the performance of the conventional CgLp. The overshoot of the system in the absence of CR CgLp, i.e., BLS, is 96%.
In the range of Phase Margin (PM) $\in [10,30]$ and $\omega_l/\omega_c \in [0.1,1]$, the decrease in the overshoot (OS) is almost linear with respect to the decrease of $\log(\omega_l)$. A fitting operation reveals the following relation between the OS and PM and ω_l.

$$OS = 0.95\log\left(\frac{\omega_l}{\omega_c}\right) - 0.04PM + 1.25 \tag{6.25}$$

where PM is in degrees.
In order to better illustrate the effect of these two parameters on overshoot and in general transient response of the closed-loop system, one can refer to Fig. 6.10. For this

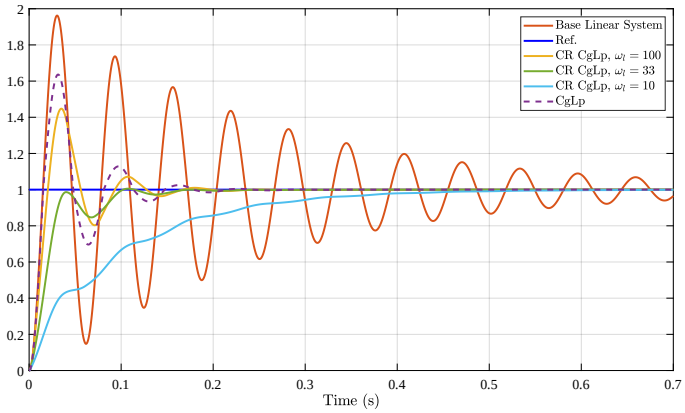

(a) Step response of closed-loop system for base linear system, CgLp and CR CgLp for various values of ω_l in rad/s. PM is fixed at 20° and $\omega_c = 100$ rad/s.

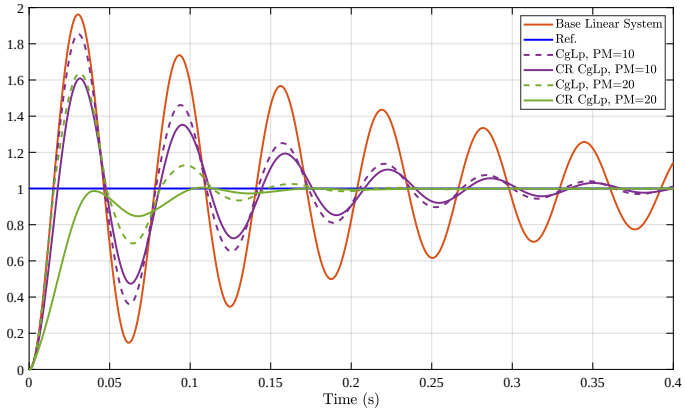

(b) Step response of closed-loop system for base linear system, CgLp and CR CgLp for various values of PM. $\omega_c = 33$ rad/s and $\omega_c = 100$ rad/s.

Figure 6.10: Closed-loop system step response for the base linear system, CgLp and CR CgLp for various values of PM and ω_l.

simulation $\omega_c = 100$ rad/s. Fig. 6.10a shows the reduction of overshoot by reduction of ω_l, the non-overshoot response is shown to be realizable. However, too much reduction of ω_l can result in long settling times, as is the case for $\omega_l = 10$ rad/s. Obviously, since CgLp does not contain ω_l, it has only one response.
Fig. 6.10b demonstrates the effect of PM on the step response of the system, while $\omega_l = 33$ rad/s, the presence of the CR architecture amplifies the reduction of overshoot caused by the increase of PM. It should be noted that various PM values are achieved by changing γ.
The study shows a significant improvement in the transient response of CR CgLp. It is worth mentioning that it will be shown later that this improvement in transient will not sacrifice the steady-state response.

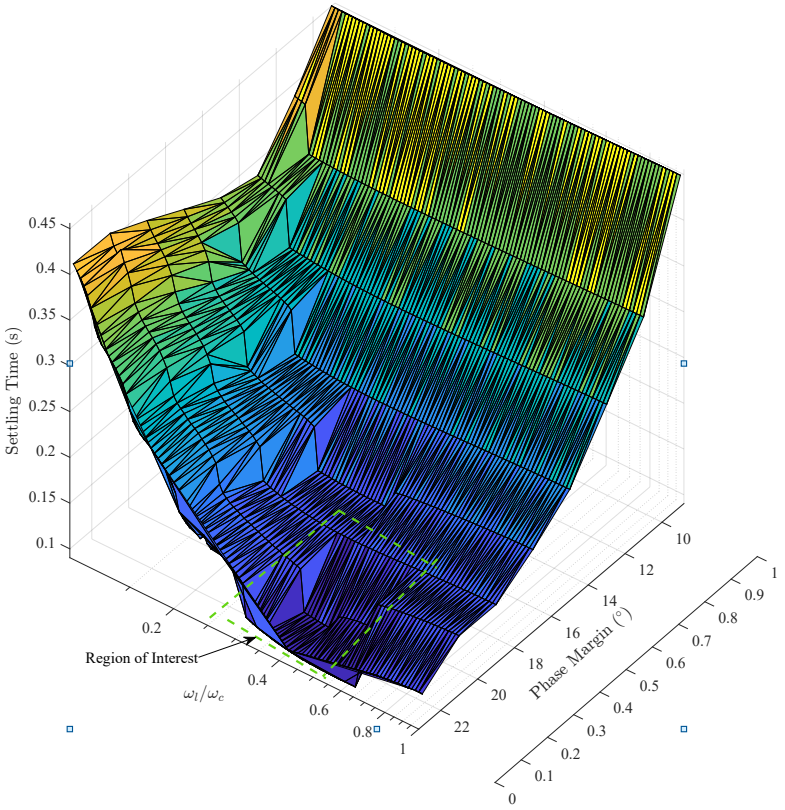

Figure 6.11: The settling time of the system for a unit step for phase margin in range of $[5,22]$ and $\omega_l/\omega_c \in [0.1,1]$. $\omega_c = 100$ rad/s. The settling time in the absence of the CR CgLp, i.e., BLS, is 0.945 s.

6.5.2. SETTLING TIME

According to Fig. 6.9 and 6.10a, reduction of ω_l generally decreases overshoot, it may have an adverse effect on settling time. In order to find a sweet spot where overshoot and settling time are improved simultaneously the same sweep as Fig. 6.9 has been done for settling time and depicted in Fig. 6.11. According to this figure, for a constant ω_l the settling time decreases with increase of PM as as like the case for linear controllers. However, there is no linear relation for ω_l/ω_c and settling time.
As a rule of thumb, $\omega_l/\omega_c \in [0.3,0.6]$ and PM larger than 20° show a favorable settling time. In this range, the settling time of the CR CgLp is shorter than that of CgLp and, referring to Fig. 6.9, non-overshoot performance can also be achieved. Thus, one can use this general rule of thumb as the tuning guideline of CR CgLp.

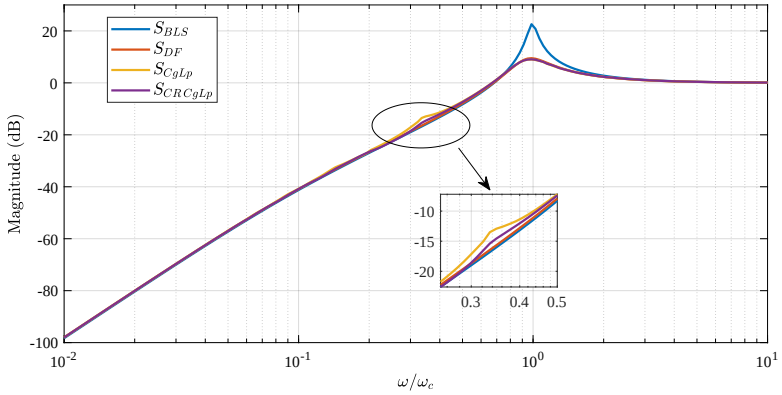

Figure 6.12: Sensitivity plot for BLS (S_{BLS}) along sensitivity for reset control systems calculated based on DF (S_{DF}), and sensitivity calculated based on infinity norm, i.e., $\frac{\|e(t)\|_2}{\|r(t)\|_2}$ for CgLp and CR CgLp (S_{CgLp} and $S_{\text{CR CgLp}}$).

6.6. CLOSED-LOOP STEADY-STATE PERFORMANCE OF THE CR CGLP ARCHITECTURE

As discussed earlier, the DF method can be used as an approximation for open-loop steady-state performance of reset control systems. The DF can also be used to find the sensitivity functions of closed-loop reset control systems using the linear relations between open-loop transfer functions and closed-loop sensitivity functions. While the resulted sensitivity plots show the ideal steady-state behaviour for the designed reset controllers, the presence of higher-order harmonics makes achieving it impossible. Thus, as discussed in Section 6.4, reducing higher-order harmonics brings the reset controller closer to the ideal behaviour.

It is shown that the CR architecture and its tuning guidelines can reduce the magnitude of higher-order harmonics. Thus, the actual closed-loop steady-state performance is expected to be very close to the approximation created by DF. To verify the latter, a comparison has been made. A series of simulations have been run to determine the actual values of the sensitivity functions for different frequencies. However, because of nonlinearity of the system, the output will not be sinusoidal. To approximate, the second norm of the signals has been used.

According to Fig. 6.12, the presence of either CgLp or CR CgLp reduces the peak of sensitivity significantly, which is logical because both of them increase the phase margin of the system. At the same time, because ω_r is tuned to reduce the higher-order harmonics, it was expected that sensitivity of CgLp and CR CgLp, namely, S_{CgLp} and $S_{\text{CR CgLp}}$, closely match the sensitivity of the BLS and the sensitivity approximated by DF, i.e., S_{BLS} and S_{DF}. However, the CR CgLp because of lower higher-order harmonics has a closer-to-ideal behaviour than CgLp. This analysis indicates that the significant improvement in the transient behaviour of the CR CgLp architecture not only has almost no negative effect on the steady-state behavior, but also positively affects it by reducing the peak of sensitivity.

Table 6.1: The rule of thumb tuning values for parameters of CR CgLp.

Parameter	ω_r	PM	ω_l	ω_h	ω_f
Value	$[\omega_c, 1.5\omega_c]$	$[15°, 25°]$	$[0.3\omega_c, 0.6\omega_c]$	$20\omega_c$	$20\omega_c$

To summarize the rule of thumb tuning guideline to CR CgLp elements the suggested values for different parameters are presented in Table 6.1.

The data-based analysis done in previous sections was for mass plants. However, the concepts and the procedure can be done for generalized for mass-spring-damper plants and the suggested rule of thumb tuning values roughly stands for every mass-spring-damper plant. To verify, in the next section, a practical example CR CgLp will be designed and tested for a precision motion setup which has a mass-spring-damper plant with high-frequency modes.

6.7. ILLUSTRATIVE PRACTICAL EXAMPLE

In order to validate the results of previous sections in precision motion control, an illustrative practical example is presented in this section. Comparison between different controllers such as PID, PID+CgLp and PID+CR CgLp is presented in this section. For the sake of conciseness, in the rest of the paper, PID+CgLp and PID+CR CgLp are shortly called, CgLp and CR CgLp controllers, respectively.

6.7.1. PLANT

The precision positioning stage "Spider" is depicted in Fig. 6.13 is a 3 degrees of freedom planar positioning stage which is used for validation. Since the reset controllers in this paper are defined for SISO systems, only actuator 1A is used to position the mass rigidly connected to it. An NI compactRIO system that is enhanced by an FPGA is used to implement the controllers at a sampling frequency of 10 kHz. A linear current source power amplifier is used to drive the voice coil actuator and a Mercury M2000 linear encoder, indicated as 4 in the Fig. 6.13 senses the position of the mass with a resolution of 100 nm. The stage FRF is identified and depicted in Fig. 6.14. The identification reveals that the plant shows a behaviour similar to that of a collocated double mass-spring-damper with additional parasitic dynamics at high frequencies. For better illustration of the control design, a mass-spring-damper transfer function has been fitted to the FRF data presented in Eq. (6.26).

$$P(s) = \frac{9836e^{-0.0001s}}{s^2 + 8.737s + 7376} \tag{6.26}$$

6.7.2. CONTROLLER DESIGN APPROACH

In order to compare the performance of PID and CR CgLp and show the superiority of the CR CgLp over PID in both steady-state and transient, four controllers were designed. PID controllers are tuned following the tuning rules presented in [26] and the reset con-

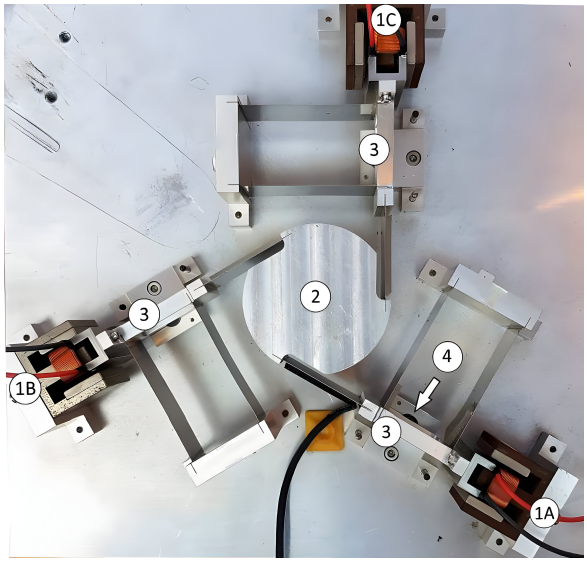

Figure 6.13: Three degrees of freedom planar precision positioning system called "Spider". Spider is actuated using three voice coil actuators indicated as 1A, 1B, and 1C. The actuators are directly connected to the masses indicated by 3. Each of these masses is solely connected to the base through two leaf flexures. The positions of these masses are sensed by linear encoders indicated by 4.

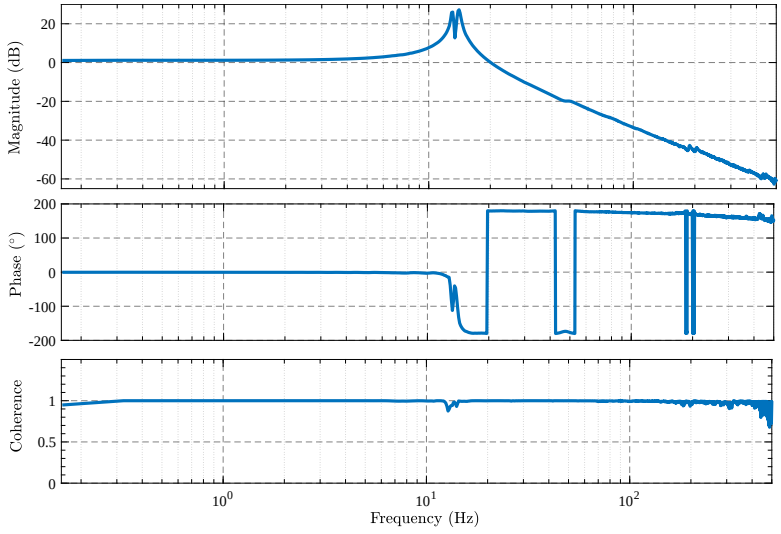

Figure 6.14: FRF identification of actuator 1A positioning the attached mass.

trollers are designed following the guidelines presented in the paper. The controller loop is already depicted in Fig. 6.7. However, due to the presence of noise in practice, a first-order low-pass filter, $\frac{1}{s/\omega_z+1}$, has been added to the loop. The parameters for the de-

Table 6.2: The parameters for designed controllers. $\omega_c = 400$ Hz.

Parameter	ω_i	ω_d	ω_t	ω_z	ω_r	ω_l	ω_h	ω_f
PID #1	$\omega_c/10$	$\omega_c/2.5$	$2.5\omega_c$	$5\omega_c$	N/A	N/A	N/A	N/A
PID #2	$\omega_c/10$	$\omega_c/5$	$5\omega_c$	$5\omega_c$	N/A	N/A	N/A	N/A
PID #1 + CgLp	$\omega_c/10$	$\omega_c/2.5$	$2.5\omega_c$	$5\omega_c$	ω_c	N/A	N/A	$20\omega_c$
PID #1 + CR CgLp	$\omega_c/10$	$\omega_c/2.5$	$2.5\omega_c$	$5\omega_c$	ω_c	$\omega_c/8$	$5\omega_c$	$20\omega_c$

signed controllers are presented in Table 6.2.

Since the input signal to $L(s)$ is $e(t)$, this element will amplify the noise present in $e(t)$ and thus creates excessive zero crossings and thus excessive reset actions [20]. To avoid this phenomenon, ω_h has chosen to be smaller than the rule-of-thumb guidelines provided in previous sections to better attenuate the high-frequency content of the signal. This change in ω_h increases the overshoot in step response, to compensate, ω_l has chosen to be smaller than rule-of-thumb guidelines.

PID #1 can also be considered the BLS for the CR CgLp *controller*, since the latter is simply PID #1 with CR CgLp *element* preceding it, as can be seen in Fig. 6.7. The practical study will show that adding the CR CgLp *element* to a linear PID controller will simultaneously improve the transient and steady state characteristics.

The open-loop HOSIDF analysis of the CR CgLp controller and the bode plot of the PID controllers are depicted in Fig. 6.15. Due to the choice of ω_r according to Fig. 6.6 and the architecture of CR CgLp, it can be seen that the magnitudes of higher-order harmonics for CR CgLp are at least 60 dB smaller than the first-order harmonic. Thus, the steady-state response of the system is expected to closely follow the amplitude of the first-order harmonic.

6.7.3. COMPARISON OF THE STEADY-STATE RESPONSE

For comparison of the precision of the controllers in terms of steady-state sinusoidal tracking the sensitivity plot of the controllers are depicted in Fig. 6.15. For this purpose, sinusoidal signals between 1 and 500 Hz have been input, as $r(t)$ and $\frac{\|e(t)\|_2}{\|r(t)\|_2}$ have been calculated and plotted for each sinusoidal.

In the range of $[1, 10]$ Hz, the sensitivity of all controllers appeared to be lower bounded by -60 dB; this effect is caused by the quantization and precision of the sensor. However, comparing PID #1 and CR CgLp in the range of $[10, 500]$ Hz reveals that the performance of CR CgLp closely matches PID #1 in lower frequencies and its peak of sensitivity is 1.5 dB lower. Thus, one can conclude that the steady-state performance of the linear controller is improved by introducing the proposed element. For the case of PID #2, the clear waterbed effect can be seen, i.e., by widening the differentiation band, at the cost of losing precision at lower frequencies, the peak of sensitivity is reduced. Unlike CR CgLp, where reduction of the peak of sensitivity is achieved without sacrificing the precision at lower frequencies. Although in the linear control context one would expect PID #2 to have a better transient response because of lower peak of sensitivity, in the next subsection, it will be shown that this does not hold true in nonlinear context and CR CgLp controller shows better transient response despite having a higher sensitivity peak.

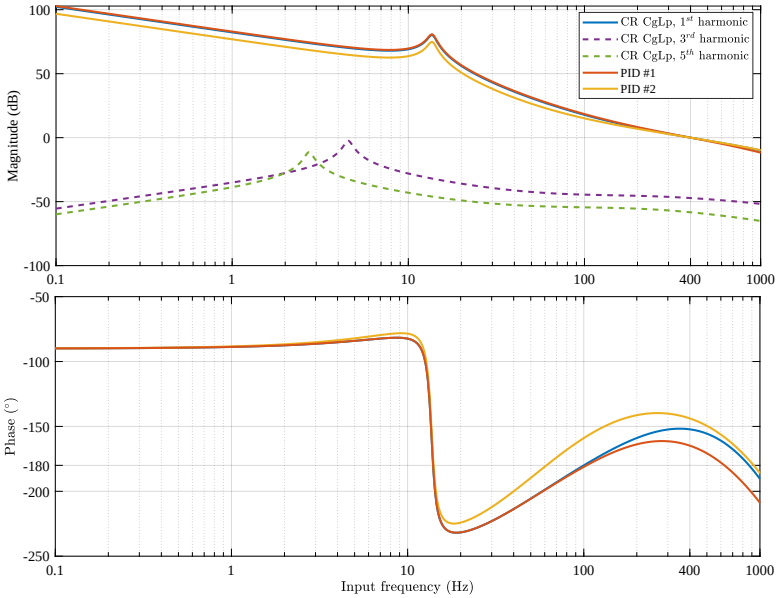

Figure 6.15: Open-loop HOSIDF analysis of the CR CgLp and Bode plot of PID controllers including the plant. PM for CR CgLp, PID #1 and PID #2 are respectively, 25°, 15° and 35°.

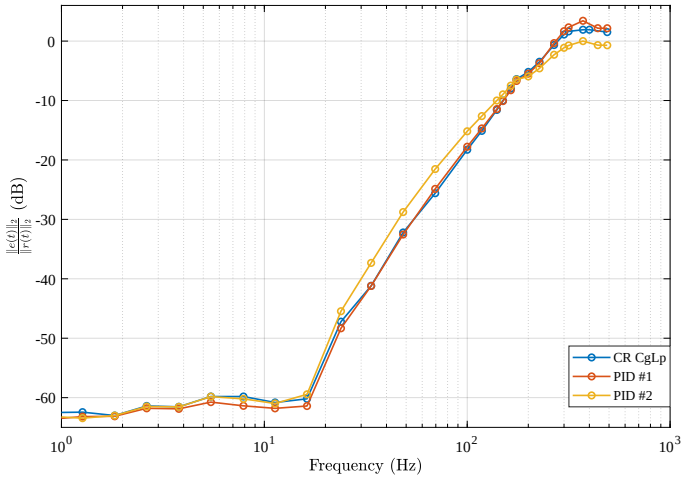

Figure 6.16: The closed-loop sensitivity of controllers for sinusoidal signals with frequencies in [1,500] Hz. Frequencies above 500 Hz are not recorded due to the actuator limitations. The sensitivity plot of CgLp closely matches that of CR CgLp, thus, it is not shown for the sake of clarity.

6.7.4. COMPARISON OF THE TRANSIENT RESPONSE

For comparison of the step responses of the controllers, a step input of 0.15μm height has been used. The responses of the controllers are depicted in Fig. 6.17. As can be seen, CR CgLp shows a non-overshoot performance, where PID #1 shows an overshoot of 38%.

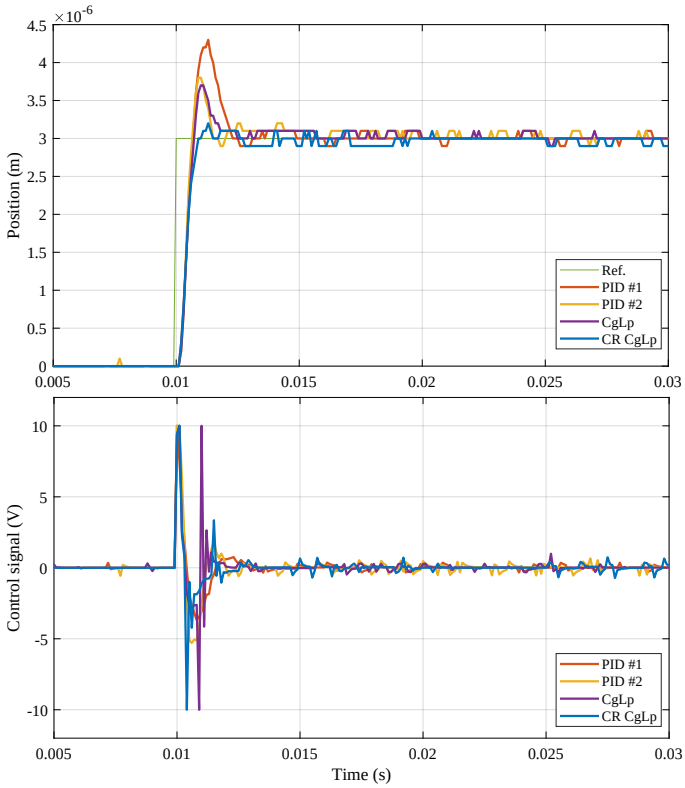

Figure 6.17: Step response and its corresponding control signal for the controllers introduced in Table 6.2. The overshoot for CR CgLp, PID #1, PID #2 and CgLp is respectively, 3%, 43%, 28%, 22% and the 96% settling times are, respectively, 11.6 ms, 12.2 ms, 14.4 ms and 11.8 ms.

It is noteworthy that according to Fig. 6.16, these two controllers have a matching sensitivity at lower frequencies. The settling time has also improved by 25%. This example clearly demonstrates that by adding CR CgLp *element* to an existing PID linear loop, one can achieve non-overshoot performance and a overall significantly improved transient response while maintaining steady-state precision.
The peak of sensitivity for both CgLp and CR CgLp controllers are the same, however, the overshoot of the CR CgLp is 28% lower than CgLp and that of CgLp is 10% lower than that of PID. This result validates that the transient performance of the reset controllers, especially the overshoot, is affected but not solely by PM and peak of sensitivity. The architecture and ω_l also play a role. The effect of ω_l will be further validated.
The reduction of overshoot for PID #2 compared to PID #1 was obvious due to the wider band of differentiation and thus reduced peak of sensitivity. However, despite the fact that its peak of sensitivity is lower than CR CgLp, the overshoot is still larger than that of CR CgLp. Meanwhile, steady-state precision has already been shown to be lower that CR CgLp. It has to be noted, because of the relatively high bandwidth which is chosen for the controllers, i.e., 400 Hz, and limitations of the actuator, control signal for the

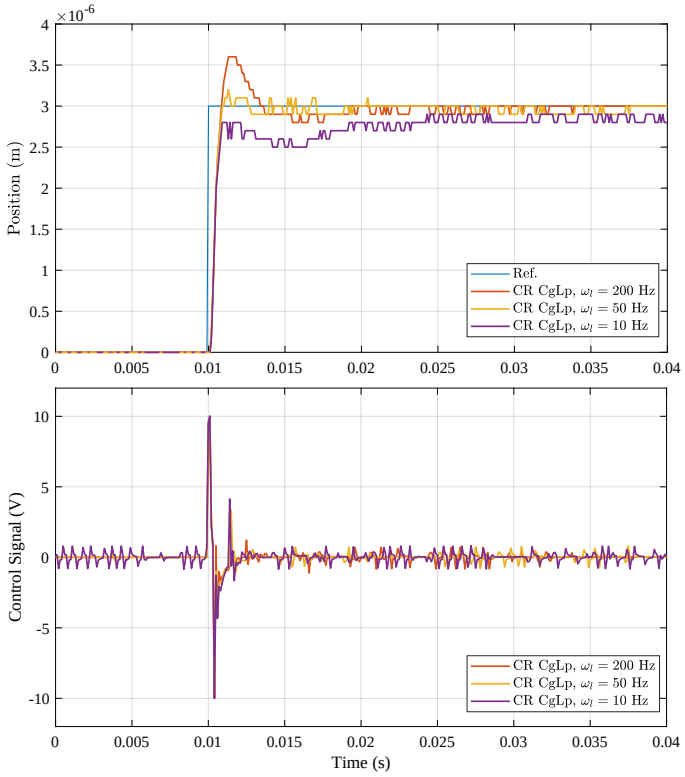

Figure 6.18: The effect of varying ω_l on transient response and its corresponding control signal of the CR CgLp.

controllers come close to saturation in only one sample of time. Nevertheless, it will be shown later that this is not the case for lower bandwidths, even for larger references.

6.7.5. THE EFFECT OF ω_l

In Fig. 6.17, $\omega_l = 50$ Hz. To validate the effect of ω_l on the transient response, the step response for different values of ω_l while maintaining the other parameters is depicted in Fig. 6.18. It can be clearly seen that the overshoot continues to decrease with a reduction of ω_l/ω_c. Furthermore, it can be also validated that settling time will increase when ω_l/ω_c drops below a certain threshold. This phenomenon may be due to the fact that too much reset and too soon resetting can jeopardize the effect of the integrator. It is noteworthy that according to Proposition 1, the value of ω_l does not have an effect on the DF and therefore on the steady-state tracking performance of the system.

6.7.6. COMPLEX-ORDER BEHAVIOUR

Another interesting behaviour of the CR CgLp controller is the ability to create a complex-order behaviour as depicted in Fig. 6.19. Two controllers have been designed for $\omega_c = 100$ Hz. In the case of a gain variation of 5 dB, ω_c will change to 150 Hz, in such a situation, the PID loses 3° of PM while CR CgLp will show a complex-order behaviour, mean-

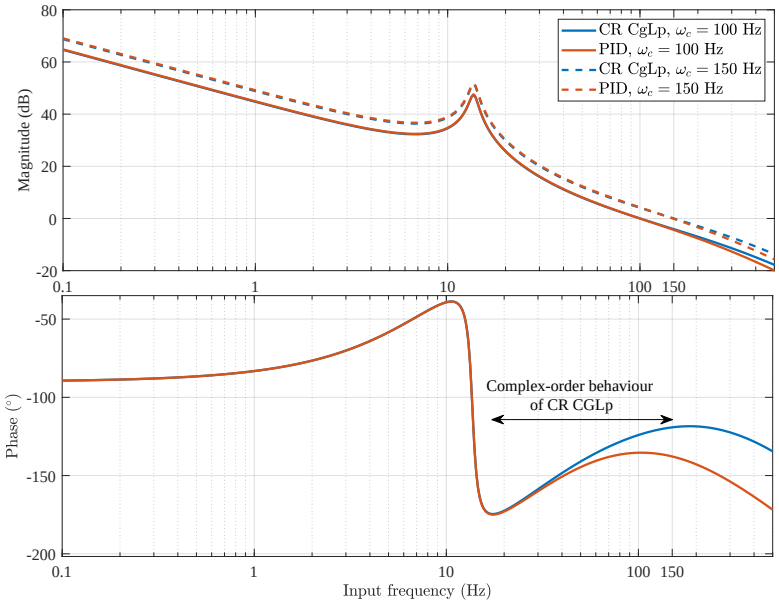

Figure 6.19: Bode diagram for a PID and DF diagram of a CR CgLp, showing the complex-order behaviour of CR CgLp. PM for CR CgLp at 100 Hz is 55° and for 150 Hz is 60°. PM for the PID at 100 Hz is 45° and for 150 Hz is 43°.

ing the phase increases while the gain decreases [8], and gain 5° more PM. Therefore, it is expected that the modulus margin for PID is expected to be decreased and for CR CgLp to be increased.
Furthermore, an increase in PID overshoot and a decrease in that of CR CgLp is expected. Validation of this expectation has been done in practice and the step responses are shown in Fig. 6.20. However, the increase in PM is not the only reason for decrease of overshoot in CR CgLp. Since ω_c increases and ω_l is kept constant, the ratio of ω_l/ω_c is subsequently reduced, which also helps reduce the overshoot.

6.8. CONCLUSION

A new architecture for reset elements, named “Continuous Reset Element” was presented in this paper. Such an architecture consists of having a linear lead and lag element, before and after a reset element. It was shown that such an architecture not only does not influence the DF gain and phase of the reset elements, but also reduces the magnitude of higher-order harmonics, which will positively affect the steady-state tracking precision of the reset controllers. Furthermore, it was shown that having a strictly proper lag element after the reset element will make the output of the reset element continuous as opposed to conventional reset elements.
Moreover, it was shown that such a CR architecture can also significantly improve the transient response of the reset control systems for mass-spring-damper plants without negatively affecting the steady-state performance– a break of the waterbed effect. To this

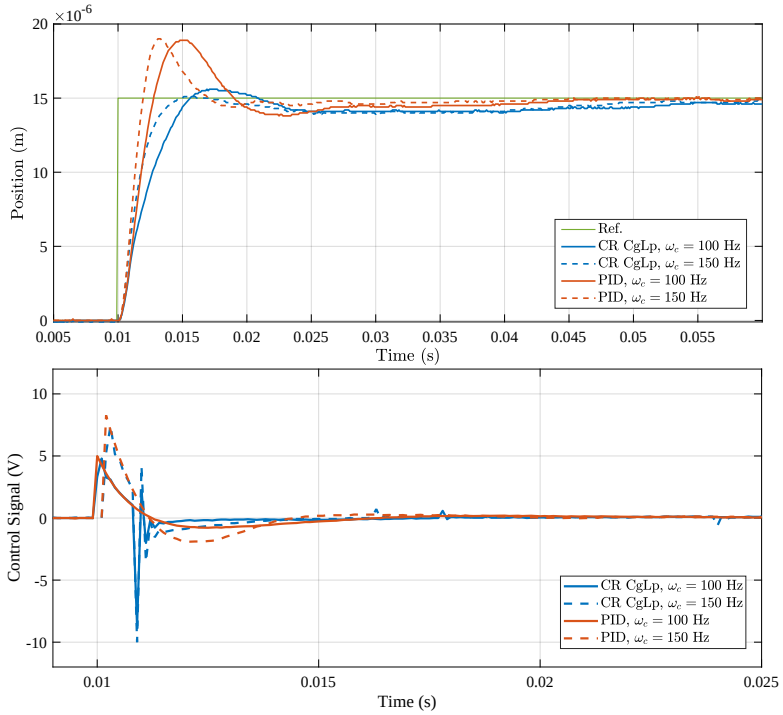

Figure 6.20: The step response and its corresponding control signal for the controllers shown in Fig. 6.19 for gain variation of 5 dB. PM for PID increases from 25% to 26% for increased ω_c, while PM for CR CgLp decreases from 4% to 0%.

end, a numerical study was done on a reset element called CgLp and a mass plant, and it was shown that by using the CR architecture, the settling time and overshoot of the CR CgLp control system can be improved together compared with the CgLp element itself and the BLS.

To further validate the achieved results, a practical example was introduced in which a precision motion setup was identified and four controllers were implemented and compared in terms of transient and steady-state performance. It was shown that for a mass-spring-damper plant the CR CgLp controller was able to achieve a no-overshoot performance and a reduced settling time while matching the steady-state performance of the PID BLS at lower frequencies and showing a reduced peak of sensitivity.

However, the presence of a lead element before a reset element can introduce excessive reset actions to the control because of noise. To avoid such a phenomenon, a low-pass filter or in general terms a shaping filter can be used to remove the high-frequency content of the signal. For which a more extensive research is required. The latter can be ongoing work of the proposed design.

BIBLIOGRAPHY

[1] H. W. Bode *et al.*, "Network analysis and feedback amplifier design", 1945.

[2] J. Clegg, "A nonlinear integrator for servomechanisms", *Transactions of the American Institute of Electrical Engineers, Part II: Applications and Industry*, vol. 77, no. 1, pp. 41–42, 1958.

[3] I. Horowitz and P. Rosenbaum, "Non-linear design for cost of feedback reduction in systems with large parameter uncertainty", *International Journal of Control*, vol. 21, no. 6, pp. 977–1001, 1975.

[4] K. Krishnan and I. Horowitz, "Synthesis of a non-linear feedback system with significant plant-ignorance for prescribed system tolerances", *International Journal of Control*, vol. 19, no. 4, pp. 689–706, 1974.

[5] L. Hazeleger, M. Heertjes, and H. Nijmeijer, "Second-order reset elements for stage control design", in *2016 American Control Conference (ACC)*, IEEE, 2016, pp. 2643–2648.

[6] A. Baños and A. Vidal, "Definition and tuning of a PI+ CI reset controller", in *2007 European Control Conference (ECC)*, IEEE, 2007, pp. 4792–4798.

[7] O. Beker, C. Hollot, Y. Chait, and H. Han, "Fundamental properties of reset control systems", *Automatica*, vol. 40, no. 6, pp. 905–915, 2004.

[8] D. Valério, N. Saikumar, A. A. Dastjerdi, N. Karbasizadeh, and S. H. HosseinNia, "Reset control approximates complex order transfer functions", *Nonlinear Dynamics*, vol. 97, no. 4, pp. 2323–2337, 2019.

[9] N. Saikumar, R. Sinha, and S. H. Hoseinnia, "'constant in gain lead in phase'element-application in precision motion control", *IEEE/ASME Transactions on Mechatronics*, 2019.

[10] A. Bisoffi, R. Beerens, W. Heemels, H. Nijmeijer, N. van de Wouw, and L. Zaccarian, "To stick or to slip: A reset PID control perspective on positioning systems with friction", *Annual Reviews in Control*, vol. 49, pp. 37–63, 2020, ISSN: 1367-5788. DOI: https://doi.org/10.1016/j.arcontrol.2020.04.010. [Online]. Available: https://www.sciencedirect.com/science/article/pii/S1367578820300201.

[11] N. Karbasizadeh, N. Saikumar, and S. Hossein Nia Kani, "Fractional-order single state reset element", English, *Nonlinear Dynamics*, vol. 104, no. 1, pp. 413–427, 2021, ISSN: 0924-090X. DOI: 10.1007/s11071-020-06138-9.

[12] A. Baños and A. Barreiro, *Reset control systems*. Springer Science & Business Media, 2011.

[13] N. Karbasizadeh, A. A. Dastjerdi, N. Saikumar, D. Valerio, and S. H. HosseinNia, *Benefiting from linear behaviour of a nonlinear reset-based element at certain frequencies*, 2020. arXiv: 2004.03529 [eess.SY].

[14] A. A. Dastjerdi and S. H. Hosseinnia, "A frequency-domain tuning method for a class of reset control systems", *IEEE Access*, vol. 9, pp. 40 950–40 962, 2021.

[15] D. Nesic, A. R. Teel, and L. Zaccarian, "Stability and performance of siso control systems with first-order reset elements", *IEEE Transactions on Automatic Control*, vol. 56, no. 11, pp. 2567–2582, 2011. DOI: 10.1109/TAC.2011.2114436.

[16] D. Wu, G. Guo, and Y. Wang, "Reset integral-derivative control for hdd servo systems", *IEEE Transactions on Control Systems Technology*, vol. 15, no. 1, pp. 161–167, 2006.

[17] Y. Zheng, Y. Chait, C. Hollot, M. Steinbuch, and M. Norg, "Experimental demonstration of reset control design", *Control Engineering Practice*, vol. 8, no. 2, pp. 113–120, 2000.

[18] Q. Chen, Y. Chait, and C. Hollot, "Analysis of reset control systems consisting of a fore and second-order loop", *J. Dyn. Sys., Meas., Control*, vol. 123, no. 2, pp. 279–283, 2001.

[19] Y. Guo, Y. Wang, L. Xie, H. Li, and W. Gui, "Optimal reset law design and its application to transient response improvement of hdd systems", *IEEE Transactions on Control Systems Technology*, vol. 19, no. 5, pp. 1160–1167, 2011. DOI: 10.1109/TCST.2010.2059027.

[20] C. Cai, A. A. Dastjerdi, N. Saikumar, and S. HosseinNia, "The optimal sequence for reset controllers", in *2020 European Control Conference (ECC)*, 2020, pp. 1826–1833. DOI: 10.23919/ECC51009.2020.9143690.

[21] G. Zhao, D. Nešić, Y. Tan, and C. Hua, "Overcoming overshoot performance limitations of linear systems with reset control", *Automatica*, vol. 101, pp. 27–35, 2019, ISSN: 0005-1098. DOI: https://doi.org/10.1016/j.automatica.2018.11.038. [Online]. Available: https://www.sciencedirect.com/science/article/pii/S0005109818305727.

[22] S. J. A. M. van den Eijnden, M. F. Heertjes, W. P. M. H. Heemels, and H. Nijmeijer, "Hybrid integrator-gain systems: A remedy for overshoot limitations in linear control?", *IEEE Control Systems Letters*, vol. 4, no. 4, pp. 1042–1047, 2020. DOI: 10.1109/LCSYS.2020.2998946.

[23] A. R. Teel, "Continuous-time implementation of reset control systems", *Trends in Nonlinear and Adaptive Control*, pp. 27–41, 2022.

[24] J. H. Le and A. R. Teel, "Passive soft-reset controllers for nonlinear systems", *arXiv preprint arXiv:2104.11414*, 2021.

[25] F. Boeren, T. Oomen, and M. Steinbuch, "Iterative motion feedforward tuning: A data-driven approach based on instrumental variable identification", *Control Engineering Practice*, vol. 37, pp. 11–19, 2015.

[26] R. M. Schmidt, G. Schitter, and A. Rankers, *The design of high performance mechatronics-: high-Tech functionality by multidisciplinary system integration*. Ios Press, 2020.

[27] S. van den Eijnden, M. Heertjes, and H. Nijmeijer, "Robust stability and nonlinear loop-shaping design for hybrid integrator-gain-based control systems", in *2019 American Control Conference (ACC)*, 2019, pp. 3063–3068. DOI: 10.23919/ACC.2019.8814888.

[28] D. J. Rijlaarsdam, V. Van Geffen, P. Nuij, J. Schoukens, and M. Steinbuch, "Frequency domain based feed forward tuning for friction compensation", *Proc. ASPE spring TM*, pp. 129–134, 2010.

[29] Y. Guo, L. Xie, and Y. Wang, *Analysis and Design of Reset Control Systems*. Institution of Engineering and Technology, 2015, ISBN: 1849197032, 9781849197038.

[30] S. Polenkova, J. W. Polderman, and R. Langerak, "Stability of reset systems", in *Proceedings of the 20th International Symposium on Mathematical Theory of Networks and Systems*, 2012, pp. 9–13.

[31] D. Nešić, L. Zaccarian, and A. R. Teel, "Stability properties of reset systems", *Automatica*, vol. 44, no. 8, pp. 2019–2026, 2008.

[32] P. Vettori, J. W. Polderman, and R. Langerak, "A geometric approach to stability of linear reset systems", in *21st International Symposium on Mathematical Theory of Networks and Systems, MTNS 2014*, University of Groningen, 2014, pp. 776–783.

[33] C. Prieur, I. Queinnec, S. Tarbouriech, and L. Zaccarian, "Analysis and synthesis of reset control systems", *Foundations and Trends in Systems and Control*, vol. 6, no. 2-3, pp. 117–338, 2018.

[34] A. A. Dastjerdi, A. Astolfi, and S. H. HosseinNia, *Frequency domain stability method for reset systems*, 2021. arXiv: 2009.00569 [eess.SY].

[35] Y. Guo, Y. Wang, and L. Xie, "Frequency-domain properties of reset systems with application in hard-disk-drive systems", *IEEE Transactions on Control Systems Technology*, vol. 17, no. 6, pp. 1446–1453, 2009.

[36] P. Nuij, O. Bosgra, and M. Steinbuch, "Higher-order sinusoidal input describing functions for the analysis of non-linear systems with harmonic responses", *Mechanical Systems and Signal Processing*, vol. 20, no. 8, pp. 1883–1904, 2006.

[37] N. Saikumar, K. Heinen, and S. H. HosseinNia, "Loop-shaping for reset control systems: A higher-order sinusoidal-input describing functions approach", *Control Engineering Practice*, vol. 111, p. 104 808, 2021.

[38] A. A. Dastjerdi and S. H. Hosseinnia, "A frequency-domain tuning method for a class of reset control systems", *IEEE Access*, vol. 9, pp. 40 950–40 962, 2021. DOI: 10.1109/ACCESS.2021.3064812.

7

STACKING INTEGRATORS IN RESET CONTROL SYSTEMS

According to the well-known loop-shaping control design approach, the steady-state precision of control systems can be improved by stacking integrators. However, due to the waterbed effect in linear control systems, such an action will worsen the transient response by increasing overshoot and creating wind-up problems. This paper presents a new architecture for rest control systems that can significantly decrease the overshoot and create a non-overshoot performance even in the presence of stacked integrators. The steady-state analysis of the proposed system will also show that the improved precision expected from stacked integrators can be achieved as well. A numerical simulation study is presented to verify the results and the tuning guide is presented.

7.1. INTRODUCTION

Increase the gain in lower frequencies as much as possible; this is one of the basic controller design criteria, particularly in precision motion control. The criterion comes from the well-known loop shaping technique for designing controllers in the frequency domain [1]. Such a design allows for reducing the steady-state error due to reference tracking and disturbances. One of the possible ways to increase the gain at lower frequencies is by stacking integrators. However, a well-known fundamental limitation of linear control systems precludes stacking too many integrators, the so-called "Waterbed Effect" [2]. One can interpret the waterbed effect for stacking integrators as excessive overshoot in the transient response. However, nonlinear control systems are not inherent to this limitations.

This chapter is published as:
N. Karbasizadeh and S. Hassan HosseinNia, "Stacking Integrators Without Sacrificing the Overshoot in Reset Control Systems," 2022 American Control Conference (ACC), Atlanta, GA, USA, 2022, pp. 893-899, doi: 10.23919/ACC53348.2022.9867231.

Reset control is one of the nonlinear control techniques which introduces a simple nonlinearity to control systems but allows the control system to overcome the linear control limitations. Reset controllers were first proposed by Clegg [3] in forms of a reset integrator that can improve the transient response of a control system. In order to address the drawbacks and exploit the benefits, the idea was later extended to more sophisticated elements such as "First-Order Reset Element" [4], [5] and "Second-Order Reset Element" [6] or using Clegg's integrator in form of PI+CI [7] or resetting the state to a fraction of its current value, known as partial resetting [8]. The reset control has also recently been used to approximate complex-order filters [9], [10]. The advantage of using reset control over linear control has been shown in many studies, especially in precision motion control [8], [11]–[20]. However, these studies are mainly focused on solving one problem. For example, they either improve transient or steady-state response of the system while paying little or no attention to the other.

One of recent studies introduces a new reset element called "Constant-in-Gain, Lead-in-Phase" (CgLp) element, which is proposed based on the loop-shaping concept [10]. Describing Function (DF) analysis of this element shows that it can provide a broadband phase lead while maintaining a constant gain. This element is used in the literature to replace some part of the differentiation action in PID controllers as it will help improve the precision of the system according to loop-shaping concept [10], [13], [16], [17].

In [13], [16], it is suggested that the DF analysis for the reset control systems can be inaccurate as it neglects the higher-order harmonics created in response of reset control systems. It is concluded that higher-order harmonics can adversely affect the steady-state precision of the system.

One of the benefits of providing phase lead through CgLp is improving the transient response properties of the system, as it is shown that it reduces the overshoot and settling time of the system. However, the way to achieve this goal is not only through phase compensation around the cross-over frequency. It is shown in [21] that since reset control systems are nonlinear systems, the sequence of elements in the control loop affects the output of the system. It was shown that when the lead elements are placed before the reset element, it can improve the overshoot of the system. However, no systematic approach is proposed there to further improve the transient response. In [22], it is shown that by changing the resetting condition of the reset element to reset based on its input and its derivative, the overshoot limitation in linear control systems can be overcome. This limitation has also been broken using the same technique in another hybrid control system called "Hybrid Integrator Gain System" (HIGS) [23]. However, in these studies, the effect of such an action on steady-state performance of the system is not addressed.

The main contribution of this paper is to propose a new architecture for the CgLp element which can benefit from increased steady-state precision due to stacked integrators while compensating for the increased overshoot and even eliminating the overshoot. This paper shows that this architecture will not even increase the maximum of control input and thus is less prone to wind-up problems. A guideline for tuning the proposed architecture is also provided.

The remainder of this paper is organized as follows.

Section 7.2 introduces the preliminaries of the research. Section 7.3 presents the proposed reset control architecture and its properties. Section 7.4 will introduce the sug-

gested control loop design and Section 7.5 will present a numerical study on the closed-loop transient response of the proposed control system and provides the tuning guideline. Section 7.6 presents the closed-loop steady-state performance analysis of the proposed control system. Finally, the paper closes with conclusion and ongoing work tips.

7.2. PRELIMINARIES

This section will discuss the preliminaries of this study.

7.2.1. GENERAL RESET CONTROLLER

The general form of reset controllers used in this study is as following:

$$\sum_R := \begin{cases} \dot{x}_r(t) = A_r x_r(t) + B_r e(t), & \text{if } e(t) \neq 0 \\ x_r(t^+) = A_\rho x_r(t), & \text{if } e(t) = 0 \\ u(t) = C_r x_r(t) + D_r e(t) \end{cases} \tag{7.1}$$

where A_r, B_r, C_r, D_r denote the state space matrices of the base linear system (BLS), and the reset matrix is denoted by $A_\rho = \text{diag}(\gamma_1, ..., \gamma_n)$ which contains the reset coefficients for each state. $e(t)$ and $u(t)$ represent the input and output of the reset controller, respectively.

7.2.2. H_β CONDITION

The quadratic stability of the closed loop reset system when the base linear system is stable can be examined by the following condition [8], [24].

Theorem 8. *There exist a constant $\beta \in \Re^{n_r \times 1}$ and a positive definite matrix $P_\rho \in \Re^{n_r \times n_r}$, such that the restricted Lyapunov equation*

$$P > 0, \quad A_{cl}^T P + P A_{cl} < 0 \tag{7.2}$$

$$B_0^T P = C_0 \tag{7.3}$$

has a solution for P, where C_0 and B_0 are defined by

$$C_0 = \begin{bmatrix} \beta C_p & 0_{n_r \times n_{nr}} & P_\rho \end{bmatrix}, \qquad B_0 = \begin{bmatrix} 0_{n_p \times n_r} \\ 0_{n_{nr} \times n_r} \\ I_{n_r} \end{bmatrix}. \tag{7.4}$$

and

$$A_\rho^T P_\rho A_\rho - P_\rho \leq 0 \tag{7.5}$$

where A_{cl} is the closed-loop A-matrix including an LTI plant dynamics. n_r is the number of states that are reset and n_{nr} is the number of non-resetting states, and n_p is the number of states for the plant. A_p, B_p, C_p, D_p are the state space matrices of the plant.

In [25], the H_β condition is extended to systems where the reset element is not the first element in the loop, in other words, the input to the reset element is a shaped error signal. The stability analysis of elements presented in this paper can be done using theories in [25].

7.2.3. DESCRIBING FUNCTIONS

Describing function analysis is the known approach in the literature for approximation of frequency response of non-linear systems such as reset controllers[26]. However, the

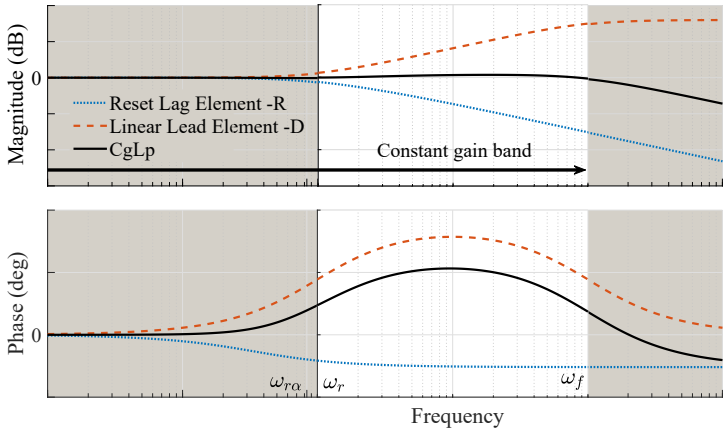

Figure 7.1: The concept of using combination of a reset lag and a linear lead element to form a CgLp element. The figure is from [10].

DF method only takes the first harmonic of Fourier series decomposition of the output into account and neglects the effects of the higher-order harmonics. This simplification can be significantly inaccurate under certain circumstances [16], [27]. The "Higher-Order Sinusoidal Input Describing Function" (HOSIDF) method has been introduced in[28] to provide more accurate information about the frequency response of nonlinear systems by investigating higher-order harmonics of the Fourier series decomposition. In other words, in this method, the nonlinear element will be replaced by a virtual harmonic generator. This method was developed in[29], [30] for reset elements defined by Eq. (7.1) as follows:

$$
\begin{aligned}
H_n(\omega) &= \begin{cases} C_r(j\omega I - A_r)^{-1}(I + j\Theta(\omega))B_r + D_r, & n = 1 \\ C_r(j\omega n I - A_r)^{-1} j\Theta(\omega) B_r, & \text{odd } n > 2 \\ 0, & \text{even } n \geq 2 \end{cases} \\
\Theta(\omega) &= -\frac{2\omega^2}{\pi}\Delta(\omega)[\Gamma(\omega) - \Lambda^{-1}(\omega)] \\
\Lambda(\omega) &= \omega^2 I + {A_r}^2 \\
\Delta(\omega) &= I + e^{\frac{\pi}{\omega}A_r} \\
\Delta_\rho(\omega) &= I + A_\rho e^{\frac{\pi}{\omega}A_r} \\
\Gamma(\omega) &= \Delta_\rho^{-1}(\omega) A_\rho \Delta(\omega) \Lambda^{-1}(\omega)
\end{aligned}
\tag{7.6}
$$

where $H_n(\omega)$ is the n^{th} harmonic describing function for sinusoidal input with frequency ω.

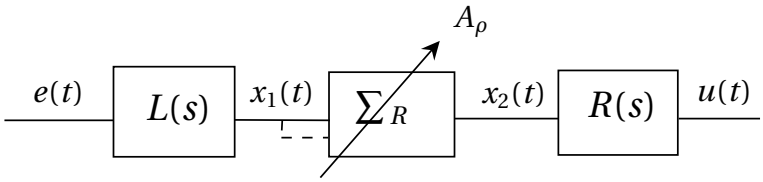

Figure 7.2: Proposed architecture for reset elements which includes a lead element, $L(s)$ before the reset element and ints inverse after the reset element. The proposed lead is $L(s) = \frac{s/\omega_l+1}{s/\omega_h+1}$ and $R(s) = \frac{1}{s/\omega_l+1}$.

7.2.4. CGLP

CgLp is a broadband phase compensation reset element which has a first harmonic constant gain behaviour while providing a phase lead [10]. This element consists in a reset lag element in series with a linear lead filter, namely $\sum_R$ and D. For FORE CgLp:

$$\sum_{FORE} = \frac{1}{s/\omega_r + 1}, \qquad D(s) = \frac{s/\omega_{r\alpha} + 1}{s/\omega_f + 1} \tag{7.7}$$

where $\omega_{r\alpha} = \alpha\omega_r$, α is a tuning parameter accounting for a shift in corner frequency of the filter due to resetting action, and $[\omega_r, \omega_f]$ is the frequency range where the CgLp will provide the required phase lead. The arrow indicates the resetting action as described in Eq. (7.1), i.e., the state matrix of the element is multiplied by A_ρ when the reset condition is met.

CgLp provides the phase lead by using the reduced phase lag of reset lag element in combination with a corresponding lead element to create broadband phase lead. Ideally, the gain of the reset lag element should be canceled out by the gain of the corresponding linear lead element, which creates a constant gain behavior. The concept is depicted in Fig. 7.1.

7.3. PROPOSED ARCHITECTURE FOR CONTINUOUS RESET (CR) ELEMENTS

The new architecture which this paper proposes consists of adding a first-order lead element, $L(s)$, before the reset element and adding the inverse of it, which is basically a lag element, after the reset element. Fig. 7.2 depicts the new architecture in which

$$L(s) = \frac{s/\omega_l + 1}{s/\omega_h + 1}, \quad R(s) = \frac{1}{s/\omega_l + 1}. \tag{7.8}$$

The presence of the denumerator in $L(s)$ is to make transfer function proper. If ω_h is large enough, $R(s) \approx L^{-1}(s)$ in low frequencies. In the context of linear control systems, adding these two elements would almost have no effect on the output of the system, provided the internal states are stable. However, in the context of nonlinear control systems, the output of the system will change significantly.

In this new architecture, the reset condition is changed from $e(t) = 0$ to $x_1(t) = 0$. Considering that ω_h is large enough, the new resetting condition can be approximated as

$$x_1(t) = \dot{e}(t)/\omega_l + e(t) = 0. \tag{7.9}$$

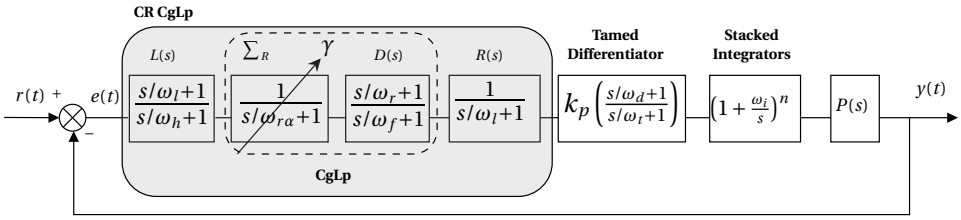

Figure 7.3: Proposed control loop for motion control with stacked integrators and CR CgLp.

The new reset element is reset based on a linear combination of $e(t)$ and $\dot{e}(t)$, where ω_l determines the weight of each. Apparently, in the closed loop, $e(t)$ and $\dot{e}(t)$ can be translated as error and its differentiation.

Remark 10. *Following the stability criteria presented in [25] for reset elements with shaped error signal, a reset element in CR architecture has the same stability properties as the reset element standing alone. In other words, the addition of $L(s)$ and $R(s)$ to the CR architecture does not affect the stability properties of the reset element.*

The output of the proposed architecture is continuous as opposed to $\sum_R$ alone. The reason for the continuity of the output of this element is the existence of the lag element after the reset element, which makes the discontinuous output of the reset element continuous.

A known property of conventional reset elements is the existence of high peaks in the control input signal, which can result in actuator or amplifier saturation. However, the continuity of the output of the CR element significantly reduces such peaks, and consequently saturation problems.

7.4. PROPOSED CONTROL LOOP ARCHITECTURE

The proposed closed-loop block diagram for having stacked integrators along with a CR CgLp to compensate the transient overshoot is presented in Fig. 7.3. In order to avoid amplifying the frequencies higher than the bandwidth, the differentiator has been tamed [1]. In the tamed differentiator,

$$\omega_d = \omega_c / a, \quad \omega_t = a\omega_c \tag{7.10}$$

where ω_c is the cross-over frequency of the system. This tuning allows the maximum phase lead of the diffrentiator to be achieved at ω_c. The stacked integrators, following the rule of thumb presented in [1] has a corner frequency of

$$\omega_i = \omega_c / 10. \tag{7.11}$$

Such a tuning results in loss of about 5° of Phase Margin (PM) for each stacked integrator. Thus, one can expect an increase in overshoot and settling time as n increases. On the other hand, as n increases, the steady-state precision of the system is expected to increase.

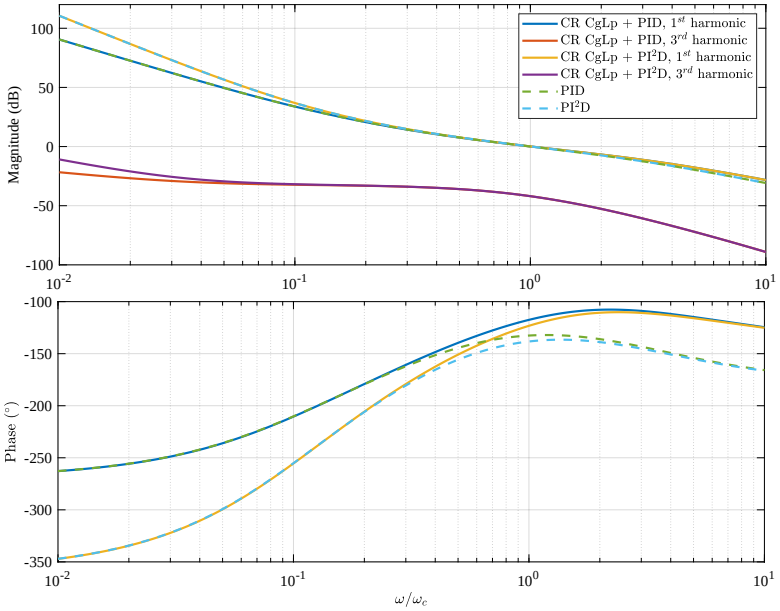

Figure 7.4: DF and HOSIDF analysis of CR CgLp+PI^{n}D compared to PI^{n}D. For the sake of clarity, only $n = 1,2$ is shown. As a rule of thumb $a = 3$.

Remark 11. *For large enough ω_h, i.e, $\omega_h \approx \infty$, the CR architecture has the same DF as the $\sum_R$ alone.*

7

It is worth mentioning that the CgLp element has a constant gain and since according to Remark 11, CR architecture will not change the gain and phase behaviour of CgLp, the overall control loop will have a DF gain and phase matching to that of PI^{n}D. Thus, the control design in open-loop can be done in frequency domain.
According to the guidelines presented in [10], [13], [17] for the tuning of the CgLp elements, the following values can be proposed for the CgLp parameters:

$$\omega_r = \omega_c, \quad \gamma = 0, \quad \alpha = 1.1, \quad \omega_f = 20\omega_c. \tag{7.12}$$

The open-loop DF and HOSDF analysis of control loop presented in Fig. 7.3 for $n = 1,2$, tuned according to (7.10), (7.11) and (7.12) is depicted in Fig. 7.4. Furthermore, in order to observe the effect of CR CgLp, the open-loop Bode plot for the controller in the absence of CR CgLp is also depicted in the same plot.
Without loss of generality, the plant is assumed to be a mass with $P(s) = 1/s^2$. As a rule of thumb for Fig. 7.4, $a = 3$ for the tamed differentiator. As expected and revealed in Fig. 7.4, the gain of DF for CgLp+PI^{n}D matches PI^{n}D, however, a phase lead has been provided. For an added differentiator, both controllers lose around 5° of PM. This trend continues as more integrators are stacked, but is not shown in the plot for the sake of clarity.

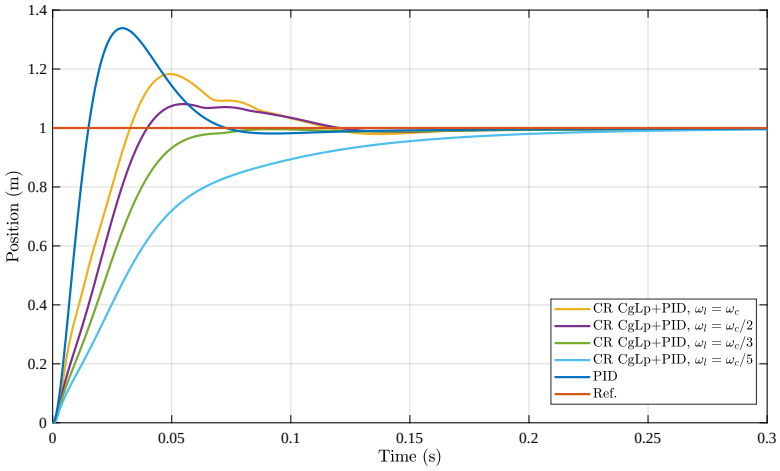

Figure 7.5: Step response of PID and CR CgLp+PID for different values of ω_l.

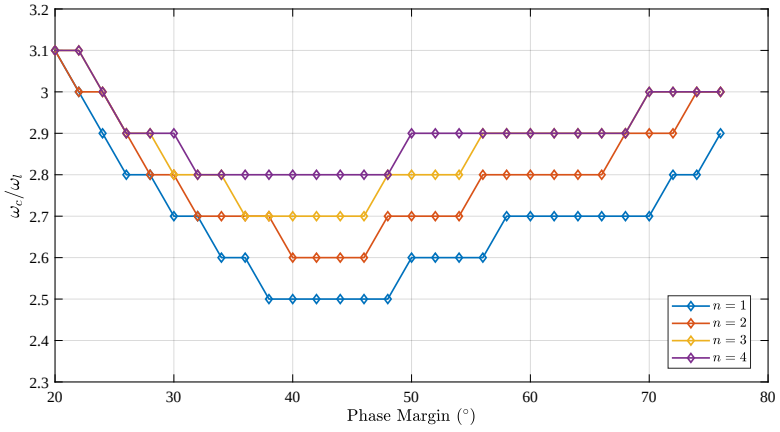

Figure 7.6: The maximum ratio of ω_c/ω_l to achieve a no-overshoot performance for different values of PM and for $n = 1,...,4$. Note that 15° of PM is provided by CR CgLp.

7.5. CLOSED-LOOP TRANSIENT RESPONSE

Because of the phase lead provided by CR CgLp, it is expected that CgLp+PI^{n}D show a lower overshoot as compared to PI^{n}D. Although this expectation holds, for reset control systems, PM is not the only parameter affecting the transient response. In CR CgLp controllers, ω_l also significantly affects the transient response, as discussed in (7.9), the reset condition in closed loop changes.

The effect of presence of CR CgLp and variation ω_l on the step response of the CR CgLp+PID control system has been simulated in Simulink environment of Matlab and presented Fig. 7.5. Without loss of generality, ω_c has been chosen to be 100 rad/s.
Fig. 7.5 reveals that not only does the phase lead provided by CgLp improve the transient

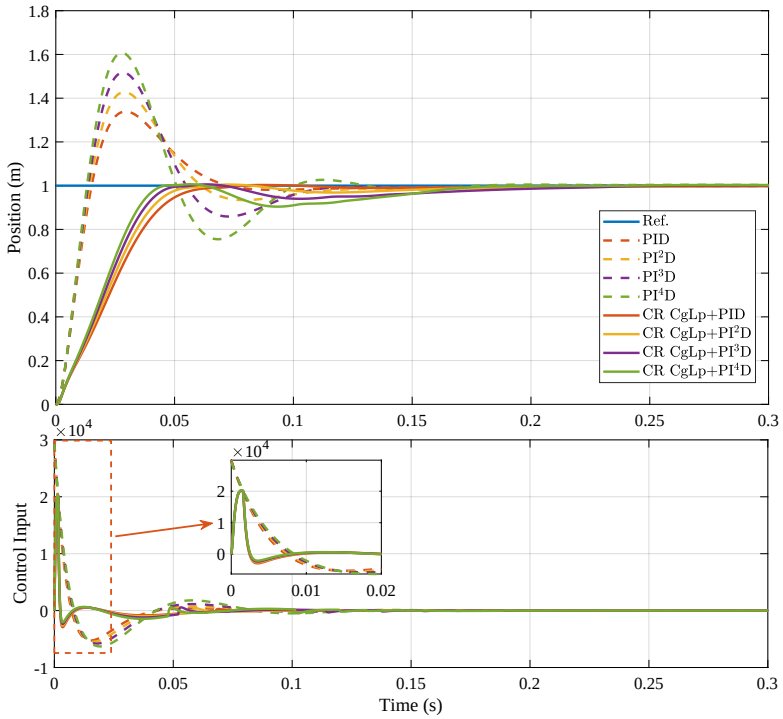

Figure 7.7: Step response of CR CgLp+PI^{n}D and PI^{n}D for $n = 1,...,4$. $\omega_c = 100$ rad/s and $a = 3$. The PM for PI^{n}D is $45-5(n-1)$ and for CR CgLp+PI^{n}D is $60-5(n-1)$ degrees. For CR CgLp+PI^{n}D, $\omega_c/\omega_l = 3$.

7

by reducing the overshoot, but also increasing the ratio of ω_c/ω_l also reduces the overshoot. It is worth mentioning that changing ω_c/ω_l, neither affects the gain behaviour of DF nor its phase.

Fig. 7.5 also shows that by increasing ω_c/ω_l, one can achieve a non-overshoot performance, while this performance is not achievable by PID no matter how wide the differentiation range is. However, too much increase of ω_c/ω_l can result in a longer settling time. To find the combinations of PM and ω_c/ω_l that can result in non-overshoot performance for $n = 1,...,4$, a series of simulations has been carried out, and the result is presented in Fig. 7.6. Note that 15° of PM is provided by CR CgLp.

Fig. 7.6 suggests that even for 4 stacked integrators a non-overshoot performance is achievable. However, for a certain PM, stacking integrators require a higher ration of ω_c/ω_l to achieve non-overshoot. As a rule of thumb, one can suggest $\omega_c/\omega_l = 3$ for PM larger than 25°.

Fig. 7.7 shows that the step response of CR CgLp+PI^{n}D and PI^{n}D for $n = 1,...,4$ for a constant differentiation band, i.e., a. Figure reveals that while stacking integrators will increase overshoot for linear controllers, CR CgLp+PI^{n}D, maintains a no-overshoot performance. The control input plot also shows another interesting properties of CR CgLp+PI^{n}D. Although 4 integrators are stacked for CR CgLp+PI^{4}D, the maximum of its control input

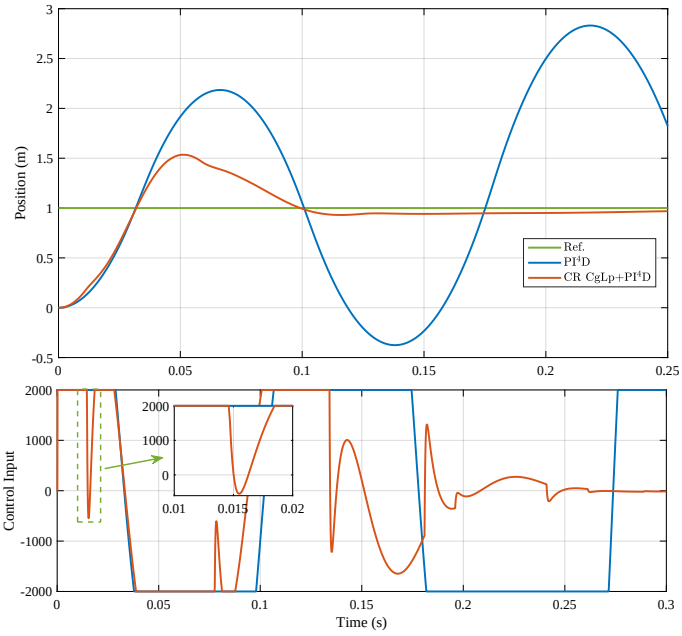

Figure 7.8: Step response of CR CgLp+PI^{4}D and PI^{4}D. The controllers are the same as in Fig. 7.7 and the control input signal is saturated at 2000 level.

Table 7.1: The approximate saturation level which makes the controllers presented in Fig. 7.7 unstable. Data are obtained by numerical analysis with Simulink.

	$n=1$	$n=2$	$n=3$	$n=4$
PI^{n}D	320	750	1300	2100
CR CgLp+PI^{n}D	300	700	1200	1900

is lower than that of PID. This indicates that actuator and amplifier saturation problems, despite stacked integrators, will not happen for the architecture presented in this paper. Furthermore, the wind-up phenomenon is one of the known problems discouraging the usage of multiple integrators in linear domain. In order to study the robustness of CR CgLp+PI^{n}D and comparison with PI^{n}D, a saturation block was implemented in the simulations to replicate actuator saturation. The results for $n=4$ which is the one with the most vulnerability to wind-up is presented in Fig. 7.8, other controllers are not shown for the sake of clarity. Moreover, the approximate saturation limit which makes each of the controllers unstable is presented in Table 7.1. Figure 7.8 reveals that although the transient response has worsened due to saturation, the resetting action prevented the wind-up to create unsuitability for CR CgLp+PI^{4}D at this saturation level. Fig. 7.8 also shows that the continuity of the control input signal is preserved in the presence of saturation.

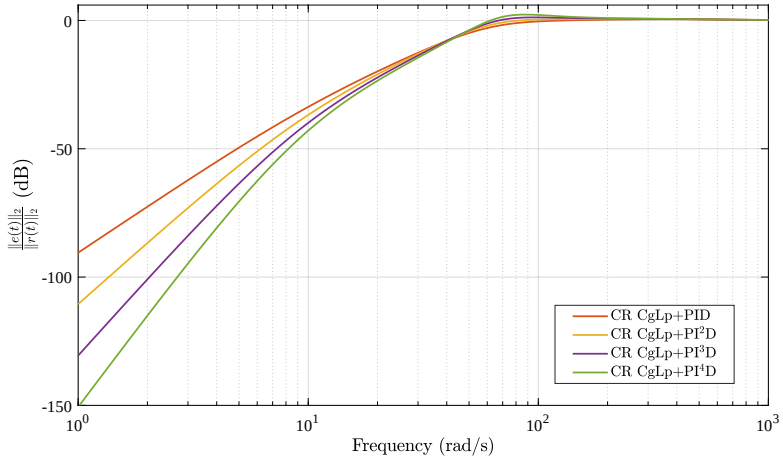

Figure 7.9: $\frac{\|e(t)\|_2}{\|r(t)\|_2}$ plotted for CR CgLp+PI^{n}D. The plots closely match to the sensitivity plots calculated based on DF analysis.

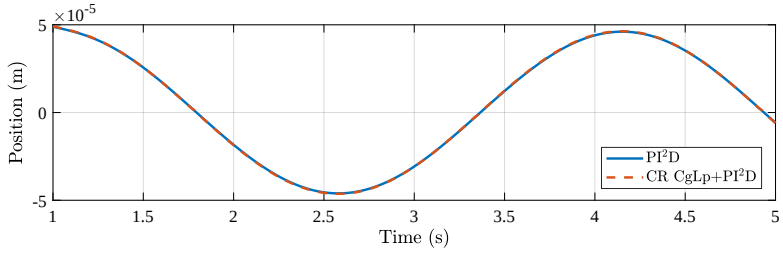

(a) Steady-state error of the PI^{2}D and CR CgLp+PI^{2}D for a sinusoidal input of $\sin(2t)$.

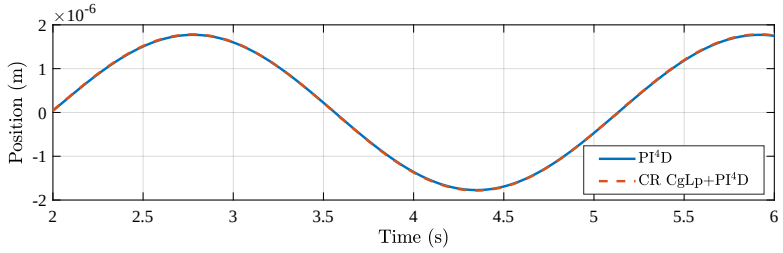

(b) Steady-state error of the PI^{4}D and CR CgLp+PI^{4}D for a sinusoidal input of $\sin(2t)$. Both plots completely match each other and are on top of each other.

Figure 7.10: Steady-state error of the PI^{n}D and CR CgLp+PI^{n}D for $n = 2, 4$ to a sinusoidal input of $\sin(2t)$.

7.6. CLOSED-LOOP STEADY-STATE PERFORMANCE

The main motivation for stacking integrators is to increase the gain at lower frequencies and consequently decrease the error due to sinusoidal tracking and disturbance resection of the control system. In order to verify the improvement in steady-state performance, one may refer to the sensitivity plot of the control system. However, since reset

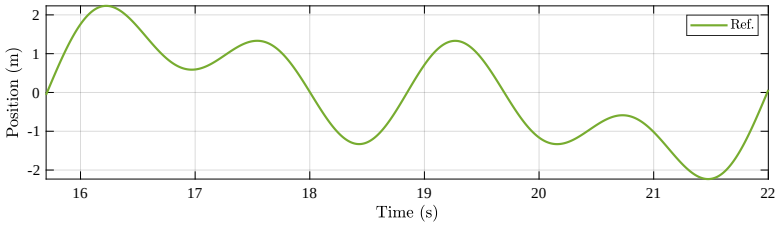

(a) Multi-sinusoidal reference for tracking comparison of the controllers. $r(t) = \sin(t) + \sin(2t) + \sin(4t)$.

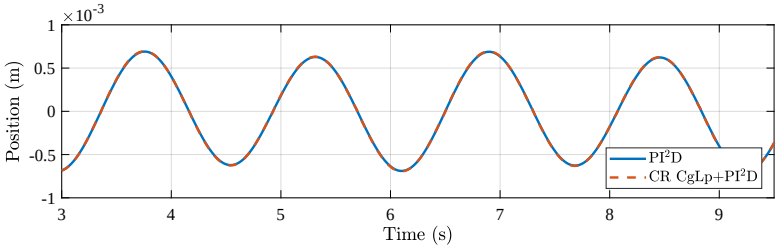

(b) Steady-state error of the PI^2D and CR CgLp+PI^2D for a multi-sinusoidal input of Fig. 7.11a.

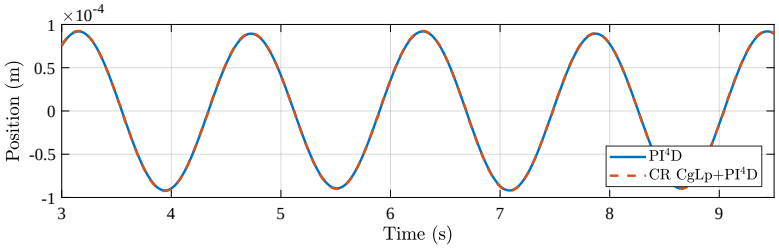

(c) Steady-state error of the PI^4D and CR CgLp+PI^4D for a multi-sinusoidal input of Fig. 7.11a.

Figure 7.11: Steady-state tracking performance comparison of the PI^nD and CR CgLp+PI^nD for $n = 2, 4$ for multi-sinusoidal input.

control systems are nonlinear and sensitivity plot should be approximated for them, one may find sensitivity plot calculated based on DF approximation not accurate [29]. In order to more accurately calculate the sensitivity plot, a series of simulations had been carried out for tracking of sinusoidal waves with different frequencies and the $\frac{\|e(t)\|_2}{\|r(t)\|_2}$ has been plotted for CR CgLp+PI^nD controllers in Fig. 7.7. The results are plotted in Fig. 7.9. The simulation results closely match the sensitivity plots calculated based on DF analysis. Thus, the sensitivity results are not plotted for the sake of clarity. Fig. 7.9 reveals that the stacked integrators are perfectly reducing the gain at lower frequencies as it would be expected for linear control systems. Thus, the stacked integrators are expected to improve the steady-state precision in terms of tracking and disturbance rejection.
To better illustrate the steady-state performance of the CR CgLp+PI^nD controllers, the steady-state error of controllers to sinusoidal input of $\sin(2t)$ is simulated and depicted in Fig. 7.10. The results show that the stacked integrators are performing as expected. Furthermore, the tracking performance of CR CgLp+PI^nD controllers for a multi-sinusoidal

input,

$$r(t) = \sin(t) + \sin(2t) + \sin(4t) \tag{7.13}$$

has been compared to that of PI^{n}D and the steady-state error is depicted in Fig. 7.11. The comparison verifies that for multi-sinusoidal input as well as sinusoidal ones, the stacked integrators for CR CgLp+PI^{n}D, performs as expected.

7.7. CONCLUSIONS

This paper presented a new architecture for a known reset element, called CgLp. The new architecture adds a linear lead element before and a linear lag element after the reset element. The reset law was shown to change due to this change. Furthermore, it was shown that this change significantly improves the transient response of the control system by especially decreasing overshoot. It was shown that the main limitation on linear control systems for stacking multiple investigators, i.e., excessive overshoot, can be solved by adding the proposed reset element to the existing linear control loop. A numerical study was done to show the effect of tuning parameters on the transient performance of the proposed reset element in controlling a mass plant and it was shown that even for 4 stacked integrators, a no-overshoot performance can be achieved. Moreover, it was shown that the maximum of control input signal for the new architecture is lower than the linear controllers for a similar step input and the new architecture is more robust to instability which may arise from wind-up phenomenon. The steady-state performance analysis of the proposed control system showed that the main objective of the stacked integrators, i.e., the reduction of the sensitivity function gain at lower frequencies, is achieved even with the presence of the proposed reset element.
Practical implementation of the proposed reset element in the presence of noise and for more general motion plants such as mass-spring-damper systems is the ongoing work of this research.

BIBLIOGRAPHY

[1] R. M. Schmidt, G. Schitter, and A. Rankers, *The design of high performance mechatronics-: high-Tech functionality by multidisciplinary system integration*. Ios Press, 2020.

[2] H. W. Bode *et al.*, "Network analysis and feedback amplifier design", 1945.

[3] J. Clegg, "A nonlinear integrator for servomechanisms", *Transactions of the American Institute of Electrical Engineers, Part II: Applications and Industry*, vol. 77, no. 1, pp. 41–42, 1958.

[4] I. Horowitz and P. Rosenbaum, "Non-linear design for cost of feedback reduction in systems with large parameter uncertainty", *International Journal of Control*, vol. 21, no. 6, pp. 977–1001, 1975.

[5] K. Krishnan and I. Horowitz, "Synthesis of a non-linear feedback system with significant plant-ignorance for prescribed system tolerances", *International Journal of Control*, vol. 19, no. 4, pp. 689–706, 1974.

[6] L. Hazeleger, M. Heertjes, and H. Nijmeijer, "Second-order reset elements for stage control design", in *2016 American Control Conference (ACC)*, IEEE, 2016, pp. 2643–2648.

[7] A. Baños and A. Vidal, "Definition and tuning of a PI+ CI reset controller", in *2007 European Control Conference (ECC)*, IEEE, 2007, pp. 4792–4798.

[8] O. Beker, C. Hollot, Y. Chait, and H. Han, "Fundamental properties of reset control systems", *Automatica*, vol. 40, no. 6, pp. 905–915, 2004.

[9] D. Valério, N. Saikumar, A. A. Dastjerdi, N. Karbasizadeh, and S. H. HosseinNia, "Reset control approximates complex order transfer functions", *Nonlinear Dynamics*, vol. 97, no. 4, pp. 2323–2337, 2019.

[10] N. Saikumar, R. Sinha, and S. H. Hoseinnia, "'constant in gain lead in phase'element-application in precision motion control", *IEEE/ASME Transactions on Mechatronics*, 2019.

[11] A. Bisoffi, R. Beerens, W. Heemels, H. Nijmeijer, N. van de Wouw, and L. Zaccarian, "To stick or to slip: A reset PID control perspective on positioning systems with friction", *Annual Reviews in Control*, vol. 49, pp. 37–63, 2020, ISSN: 1367-5788. DOI: https://doi.org/10.1016/j.arcontrol.2020.04.010. [Online]. Available: https://www.sciencedirect.com/science/article/pii/S1367578820300201.

[12] Q. Chen, Y. Chait, and C. Hollot, "Analysis of reset control systems consisting of a fore and second-order loop", *J. Dyn. Sys., Meas., Control*, vol. 123, no. 2, pp. 279–283, 2001.

[13] N. Karbasizadeh, N. Saikumar, and S. Hossein Nia Kani, "Fractional-order single state reset element", English, *Nonlinear Dynamics*, vol. 104, no. 1, pp. 413–427, 2021, ISSN: 0924-090X. DOI: 10.1007/s11071-020-06138-9.

[14] N. Karbasizadeh and S. H. HosseinNia, *Continuous reset element*, 2021. DOI: 10.48550/ARXIV.2110.12801. [Online]. Available: https://arxiv.org/abs/2110.12801.

[15] A. Baños and A. Barreiro, *Reset control systems*. Springer Science & Business Media, 2011.

[16] N. Karbasizadeh, A. A. Dastjerdi, N. Saikumar, D. Valerio, and S. H. HosseinNia, *Benefiting from linear behaviour of a nonlinear reset-based element at certain frequencies*, 2020. arXiv: 2004.03529 [eess.SY].

[17] A. A. Dastjerdi and S. H. Hosseinnia, "A frequency-domain tuning method for a class of reset control systems", *IEEE Access*, vol. 9, pp. 40 950–40 962, 2021.

[18] D. Wu, G. Guo, and Y. Wang, "Reset integral-derivative control for hdd servo systems", *IEEE Transactions on Control Systems Technology*, vol. 15, no. 1, pp. 161–167, 2006.

[19] Y. Zheng, Y. Chait, C. Hollot, M. Steinbuch, and M. Norg, "Experimental demonstration of reset control design", *Control Engineering Practice*, vol. 8, no. 2, pp. 113–120, 2000.

[20] L. Chen, N. Saikumar, and S. H. HosseinNia, "Development of robust fractional-order reset control", *IEEE Transactions on Control Systems Technology*, vol. 28, no. 4, pp. 1404–1417, 2020. DOI: 10.1109/TCST.2019.2913534.

[21] C. Cai, A. A. Dastjerdi, N. Saikumar, and S. HosseinNia, "The optimal sequence for reset controllers", in *2020 European Control Conference (ECC)*, 2020, pp. 1826–1833. DOI: 10.23919/ECC51009.2020.9143690.

[22] G. Zhao, D. Nešić, Y. Tan, and C. Hua, "Overcoming overshoot performance limitations of linear systems with reset control", *Automatica*, vol. 101, pp. 27–35, 2019, ISSN: 0005-1098. DOI: https://doi.org/10.1016/j.automatica.2018.11.038. [Online]. Available: https://www.sciencedirect.com/science/article/pii/S0005109818305727.

[23] S. J. A. M. van den Eijnden, M. F. Heertjes, W. P. M. H. Heemels, and H. Nijmeijer, "Hybrid integrator-gain systems: A remedy for overshoot limitations in linear control?", *IEEE Control Systems Letters*, vol. 4, no. 4, pp. 1042–1047, 2020. DOI: 10.1109/LCSYS.2020.2998946.

[24] Y. Guo, L. Xie, and Y. Wang, *Analysis and Design of Reset Control Systems*. Institution of Engineering and Technology, 2015, ISBN: 1849197032, 9781849197038.

[25] A. A. Dastjerdi, A. Astolfi, and S. H. HosseinNia, "A frequency-domain stability method for reset systems", in *2020 59th IEEE Conference on Decision and Control (CDC)*, IEEE, 2020, pp. 5785–5791.

[26] Y. Guo, Y. Wang, and L. Xie, "Frequency-domain properties of reset systems with application in hard-disk-drive systems", *IEEE Transactions on Control Systems Technology*, vol. 17, no. 6, pp. 1446–1453, 2009.

[27] N. Karbasizadeh, A. A. Dastjerdi, N. Saikumar, and S. H. HosseinNia, *Band-passing nonlinearity in reset elements*, 2020. DOI: 10.48550/ARXIV.2009.06091. [Online]. Available: https://arxiv.org/abs/2009.06091.

[28] P. Nuij, O. Bosgra, and M. Steinbuch, "Higher-order sinusoidal input describing functions for the analysis of non-linear systems with harmonic responses", *Mechanical Systems and Signal Processing*, vol. 20, no. 8, pp. 1883–1904, 2006.

[29] N. Saikumar, K. Heinen, and S. H. HosseinNia, "Loop-shaping for reset control systems: A higher-order sinusoidal-input describing functions approach", *Control Engineering Practice*, vol. 111, p. 104 808, 2021.

[30] A. A. Dastjerdi, N. Saikumar, D. Valerio, and S. H. HosseinNia, *Closed-loop frequency analyses of reset systems*, 2020.

8

DAMPING ANALYSIS OF TRANSIENT RESPONSE IN RESET CONTROL SYSTEMS

The high-tech industry continuously pushes the boundaries of controller performance to achieve faster and more precise machines. Currently, linear control is the standard in the industry. These controllers suffer from the waterbed effect and Bode's phase/gain relation, which impose inherent limitations on the precision and robustness of the system. Reset control is a popular strategy to get around these limitations and improve performance. The damping in reset control systems is not only determined by the phase margin of the system but is also dependent on the exact sequence of controller elements. Currently, finding the optimal controller sequence is done through the simulation of the step response. However, this fails to provide insight into the underlying cause of the additional damping achieved by specific controller configurations. This paper proposes an analytical approach to analyze the damping of transient response reset control systems. Analytical analysis provides a better understanding of sequence-dependent damping and assists in controller design. First, the analytical expressions of the step response and the states of the system are derived, which are used to define the energy of the system. The step response and energy equations are used to characterize the damping in a reset control system. To show the value of the proposed method, the damping in a reset control system is assessed as an illustrative example. It is found that when a lead is in front of a reset element, the reset controller can provide more damping because it reduces the oscillatory content in the step response.

The contents of this chapter is under preparation for submission. The first author is Mees Vanderbroeck. The author of this dissertation has contributed to the idea generation and supervision.

8.1. INTRODUCTION

The high-tech industry constantly pushes the boundaries of controller performance to achieve faster and more precise machines. PID control is the current standard for controlling precision motion systems. With the use of loop-shaping and feed-forward techniques, high bandwidth, robust, and high precision control can be achieved. However, linear control suffers from the waterbed effect and Bode's phase/gain relationship [1], [2]. These limit the level of robustness and precision achieved within linear control. By breaking Bode's phase/gain relationship and omitting the waterbed effect, higher bandwidth and precision can be achieved. Nonlinear control can offer an opportunity to satisfy the increasing demands of the industry on controller performance [3]–[6].

Reset control is a nonlinear control technique popularised due to its compatibility with PID control and loop-shaping techniques. Reset control involves resetting one or more states of a controller when a reset condition is satisfied. The first reset control element was a reset integrator introduced by Clegg [7]. This reset element could significantly reduce the phase lag of the linear integrator. Since then, many other reset elements have been introduced and implemented [8]–[13]. In general, reset elements can reduce the phase lag of a control system compared to its linear counterpart without compromising other aspects of the controller. In the literature, it is shown that reset control can significantly improve controller performance in the frequency domain and steady-state response [14]–[20].

The advantages of reset controllers can also be seen in improved transient performance with reduction and prevention of overshoot [8], [18], [19]. In linear control of motion systems, a reduction in overshoot can be attributed to an increase in phase margin. However, research has shown that the sequence of control elements can change the overshoot of a reset control system (RCS) [21] or HIGS [22], regardless of the phase margin. In [21] and [11], it is shown that placing a lead before a reset element can reduce overshoot compared to when the lead is after the reset element. Currently, the step response is simulated to find the optimal controller configuration for transient performance. However, this fails to provide insight into the underlying cause of the extra damping achieved by specific control element sequences. Suppose that the damping of the step response could be analyzed analytically, independently of the phase margin. In that case, the origin of the additional damping could be better understood and used to improve the design of reset controllers to improve transient performance.

The contribution of this paper is to develop an analytical approach to analyze the damping of the transient response in reset control systems. This approach relies on deriving an analytical expression of the step response and the system's states. With these expressions, the dependence of damping on the controller sequence can be determined. To show the merits of the damping analysis, the step response of a reset controller is analyzed for different sequence of controller as an illustrative example. The remainder of the paper will be structured as follows. In Section 8.2, background knowledge of reset control is provided. Section 8.3 contains the analytical derivation of the step response, its derivatives, and the states of a general reset control system. The damping analysis methods of base linear stable reset control systems are proposed in Section 8.4. Section 8.5 provides an illustrative example of the proposed methods. Lastly, conclusions and

future work are discussed in section 8.6.

8.2. PRELIMINARIES

8.2.1. DEFINITION GENERAL RESET CONTROLLER

Reset control systems can be written as 8.1.

$$\Sigma_R := \begin{cases} \dot{x}_r = A_r x_r(t) + B_r e(t), & \text{if} \quad e(t) \neq 0 \\ x_r(t^+) = A_\rho x_r(t), & \text{if} \quad e(t) = 0 \\ u(t) = C_r x_r(t) + D_r e(t) \end{cases} \tag{8.1}$$

The matrices A_r, B_r, C_r, D_r describe the state-space representation of the Base Linear System (BLS) of the reset system. The BLS is equivalent to the reset system without a resetting action. The matrix A_ρ determines the amount of reset for each state when the reset condition is met. $x_r(t)$, $e(t)$, and $u(t)$ describe the reset states of the controller, the input of the controller and the output of the controller, respectively.

8.2.2. RELEVANT RESET ELEMENTS

CLEGG INTEGRATOR

The Clegg Integrator (CI) was the first reset element introduced in [7]. Based on describing function analysis, a reduction of 52° phase lag can be achieved by applying the reset to a linear integrator. The state-space representation of a CI can be written in the form 8.1, where:

$$A_r = 0, B_r = 1, C_r = 1, D_r = 0, A_\rho = 0 \tag{8.2}$$

(GENERALIZED) FIRST/SECOND ORDER RESET ELEMENT

As an extension of the CI, the First-Order Reset Element (FORE) was introduced in [8]. FORE is a first-order low-pass filter with a resetting action. It provides more design freedom than the CI by changing the filter's corner frequency ω_r. The conventional FORE in [8] fully resets when the reset condition is met. The generalized FORE (GFORE), introduced in [23], also allows for a partial reset of the FORE. The amount of reset is defined as γ. Note that the actual corner frequency of the reset filter is different from ω_r. The actual corner frequency shifts for different values of γ. The frequency shift can be taken into account using $\omega_{r\alpha_s} = \omega_r/\alpha_s$ instead. Here, α_s is a correction factor whose value depends on the amount of reset according to [10]. The state-space representation of GFORE can be written to the form in 8.1, where:

$$A_r = -\omega_r, B_r = \omega_r, C_r = 1, D_r = 0, A_\rho = \gamma \tag{8.3}$$

The reset equivalent of a second-order low-pass filter is called the Second-Order Reset Element (SORE) and was introduced in [9]. The additional control parameter β_r can be used to change the damping of the element. The generalized SORE (GSORE) also allows partial reset determined by γ_1 and γ_2. Both parameters individually determine the amount of reset of each separate controller state. A state-space representation of GSORE can be written in the form in 8.1, where:

$$A_r = \begin{bmatrix} 0 & 1 \\ -\omega_r^2 & -2\beta_r\omega_r \end{bmatrix}, B_r = \begin{bmatrix} 0 \\ \omega_r^2 \end{bmatrix}, \\ C_r = \begin{bmatrix} 1 & 0 \end{bmatrix}, D_r = [0], A_\rho = \begin{bmatrix} \gamma_1 & 0 \\ 0 & \gamma_2 \end{bmatrix} \tag{8.4}$$

In contrast to linear control, the exact state-space representation of a reset system does influence the output of the system in nonlinear control [24]. In other words, the output depends on the exact configuration of the control elements because the superposition principle does not apply [25]. The correct state-space representation should be used to describe the actual reset control system.

Both GFORE and GSORE can be described in transfer function form:

$$GFORE(s) = \frac{1}{s/\omega_r + 1} \quad \gamma \tag{8.5}$$

$$GSORE(s) = \frac{1}{(s/\omega_r)^2 + (2s\beta_r/\omega_r) + 1} \quad \gamma_1, \gamma_2 \tag{8.6}$$

The arrow crossing the equation shows that the element is a reset element with γ_1 and γ_2 defining the amount of reset of each state.

CONSTANT IN GAIN LEAD IN PHASE

The Constant in gain Lead in phase (CgLp) element was introduced in [10]. The element can create a phase lead while the gain remains constant by using the difference in phase shift of a linear and a reset element.

A CgLp element combines a reset lag filter $R(s)$ with a linear lead filter $L(s)$ of equal order. The reset lag filter can be a GFORE or GSORE. These filters can be described in transfer function form:

$$R(s) = \frac{1}{s/\omega_{r\alpha_s} + 1} \quad \gamma \quad \text{or} \quad \frac{1}{(s/\omega_{r\alpha_s})^2 + (2s\beta_r/\omega_{r\alpha_s}) + 1} \quad \gamma \tag{8.7}$$

and

$$L(s) = \frac{s/\omega_r + 1}{s/\omega_f + 1} \quad \text{or} \quad \frac{(s/\omega_r)^2 + (2s\beta_r/\omega_r) + 1}{(s/\omega_f)^2 + (2s/\omega_f) + 1} \tag{8.8}$$

ω_r and ω_f are the corner frequency and the termination frequency of the lead filter, respectively. $\omega_{r\alpha_s} = \omega_r/\alpha_s$ is the corner frequency correction of the reset element to match the corner frequency ω_r of the lead filter. For frequencies between ω_r and ω_f, the CgLp provides a phase lead with a unity gain, as seen in Figure 8.1. The state-space matrices of a CgLp element consisting of a GFORE are as follows:

$$A_r = \begin{bmatrix} -\omega_{r\alpha_s} & 0 \\ -\omega_f & \omega_f \end{bmatrix}, B_r = \begin{bmatrix} \omega_{r\alpha_s} \\ 0 \end{bmatrix}, \\ C_r = \begin{bmatrix} \frac{\omega_f}{\omega_r} & (1 - \frac{\omega_f}{\omega_r}) \end{bmatrix}, D_r = [0], A_\rho = \begin{bmatrix} \gamma & 0 \\ 0 & 1 \end{bmatrix} \tag{8.9}$$

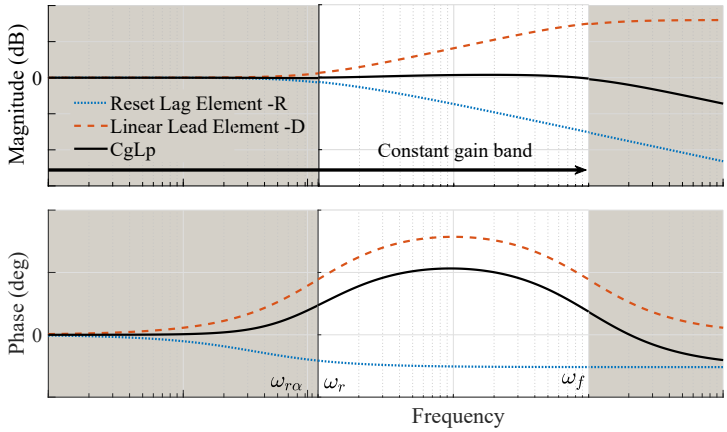

Figure 8.1: First-order describing function of a CgLp element [10].

Note that this state-space representation describes a CgLp where the lead element is after the reset element. The state-space realization should be changed when the order is switched.

8.2.3. DESCRIBING FUNCTIONS

Loop shaping techniques are the industry standard for tuning controllers. This technique is based on the frequency response of the system. Unfortunately, the frequency response of a nonlinear system cannot be captured entirely by a single frequency domain function. The frequency response function of nonlinear systems can be approximated with the Describing Function (DF) [26]. The DF is used primarily in the design of reset control systems. However, this approximation only considers the first harmonic of the Fourier series. Therefore, only considering the DF may be an inaccurate approximation of the frequency domain response of a nonlinear system. To consider the effect of higher-order harmonics, the Higher-Order Sinusoidal Input Describing Functions (HOSIDFs) of the nonlinear system introduced in [23] can be calculated. The HOSIDFs of a reset element described in 8.1 can be found using 8.10 introduced in [27].

$$G_n(j\omega) = \begin{cases} C_r(j\omega I - A_r)^{-1}(I + j\Theta_\rho(\omega))B_r + D_r & n = 1 \\ C_r(nj\omega I - A_r)^{-1}(I + j\Theta_\rho(\omega))B_r & \text{odd } n \geq 2 \\ 0 & \text{even } n \geq 2 \end{cases} \tag{8.10}$$

where,

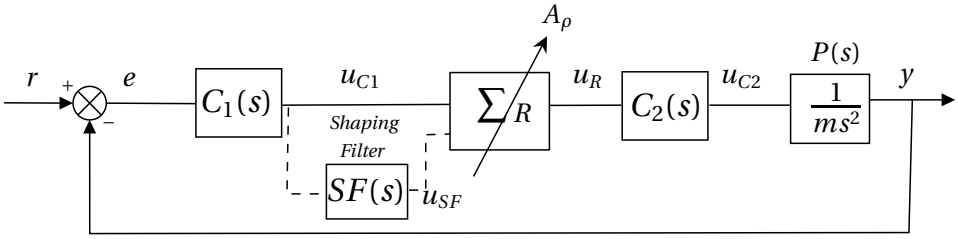

Figure 8.2: General SISO reset control system with a mass plant.

$$
\begin{aligned}
\Theta_\rho(\omega) &= \frac{2\omega^2}{\pi}\Delta(\omega)(\Gamma(\omega)-\Lambda^{-1}) \\
\Gamma(\omega) &= \Delta_\rho(\omega)^{-1}A_\rho\Delta(\omega)\Lambda(\omega)^{-1} \\
\Delta_\rho(\omega) &= I + A_\rho e^{\frac{A_r\pi}{\omega}} \\
\Delta(\omega) &= I + e^{\frac{A_r\pi}{\omega}} \\
\Lambda(\omega) &= \omega^2 I + A_r
\end{aligned}
\tag{8.11}
$$

In general, the loop-shaping of reset control systems is based on the first-order DF. Furthermore, the system is tuned to reduce the magnitude of the HOSIDFs to make the approximation of the frequency response by the DF as representative as possible.

8

8.3. ANALYTICAL DERIVATION STEP RESPONSE OF RESET CONTROL SYSTEM WITH MASS PLANTS

Consider the general Single-Input Single-Output (SISO) reset control system with a mass plant $P(s) = \frac{1}{ms^2}$ in Figure 8.2. The closed-loop system consists of two linear controllers $C_1(s)$ and $C_2(s)$. These are placed before and after the reset control element Σ_R. The output of the shaping filter $SF(s)$, defines the reset condition of Σ_R.

The system can mathematically be described by the system of equations in 8.12-8.21. Here $\{A_{c_1}, B_{c_1}, C_{c_1}, D_{c_1}\}$ and $\{A_{c_2p}, B_{c_2p}, C_{c_2p}\}$ are the minimal realizations of $C_1(s)$ and $C_2(s)P(s)$ respectively. Likewise, $\{A_r, B_r, C_r, D_r, A_\rho\}$ is the minimal realization of the reset element Σ_R as shown in 8.1. $x_{c_1} \in \mathbb{R}^{n_1}$, $x_r \in \mathbb{R}^{n_r}$, and $x_{c_2p} \in \mathbb{R}^{n_2}$ are the states of the first linear controller, the reset element, and the linear elements after the reset block. A_ρ is the reset matrix of the reset element. Finally, $\{A_{sf}, B_{sf}, C_{sf}, D_{sf}\}$ is the minimal realization of the shaping filter with the state $x_{sf} \in \mathbb{R}^{n_{sf}}$. In this analysis, only physical systems are considered. Therefore, it can be assumed that the system is strictly proper, and the output $y(t)$ depends only on states $x_{c_2p}(t)$.

$$
\begin{cases}
\dot{x}_{c_1}(t) &= A_{c_1} x_{c_1}(t) + B_{c_1} e(t) & (8.12)\\
u_{c_1}(t) &= C_{c_1} x_{c_1}(t) + D_{c_1} e(t) & (8.13)\\
\dot{x}_{sf}(t) &= A_{sf} x_{sf}(t) + B_{sf} u_{c_1}(t) & (8.14)\\
u_{sf}(t) &= C_{sf} x_{sf}(t) + D_{sf} u_{c_1}(t) & (8.15)\\
\dot{x}_r(t) &= A_r x_r(t) + B_r u_{c_1}(t), \quad u_{sf}(t) \neq 0 & (8.16)\\
x_r(t^+) &= A_\rho x_r(t), \qquad\qquad u_{sf}(t) = 0 & (8.17)\\
u_r(t) &= C_r x_r(t) + D_r u_{c_1}(t) & (8.18)\\
\dot{x}_{c_2p}(t) &= A_{c_2p} x_{c_2p}(t) + B_{c_2p} u_r(t) & (8.19)\\
y(t) &= C_{c_2p} x_{c_2p}(t) & (8.20)\\
e(t) &= r(t) - y(t) & (8.21)
\end{cases}
$$

The closed-loop state-space representation of the complete system can be written as follows:

$$
\begin{cases}
\dot{x}(t) = A_{cl} x(t) + B_{cl} r(t), & \text{if} \quad u_{sf}(t) \neq 0\\
x(t^+) = \hat{A}_\rho x(t), & \text{if} \quad u_{sf}(t) = 0\\
y(t) = C_{cl} x(t)\\
u_{sf}(t) = C_{rline} x(t) + D_{rline} r(t)
\end{cases}
\tag{8.22}
$$

where

$$
\begin{aligned}
x(t) &= \begin{bmatrix} x_r \\ x_{c_1} \\ x_{sf} \\ x_{c_2p} \end{bmatrix}, x(t) \in \mathbb{R}^n\\
A_{cl} &= \mathbb{R}^{n \times n}, B_{cl} = \mathbb{R}^n\\
C_{cl} &= \begin{bmatrix} 0^{n-n_2} & C_{c_2p} \end{bmatrix},\\
\hat{A}_\rho &= \begin{bmatrix} A_\rho & 0 \\ 0 & I^{(n-n_r)\times(n-n_r)} \end{bmatrix}\\
C_{rline} &= \begin{bmatrix} 0^{n_r} \\ D_{sf} C_{c_1} \\ C_{sf} \\ -D_{sf} D_{c_1} C_{c_2p} \end{bmatrix}^T,\\
D_{rline} &= D_{sf} D_{c_1}
\end{aligned}
\tag{8.23}
$$

The entries of A_{cl} and B_{cl} depend on the state-space matrices of the individual control elements. The expressions of the entries of A_{cl} and B_{cl} can be found in Appendix A.

8.3.1. ENERGY AND POWER OF MASS PLANT

In motion control systems, damping can be defined as the dissipation of the energy of the plant. As a result, the oscillations are suppressed, and the response is slowed. The energy of the system in Figure 8.2 depends only on the kinetic energy of the plant since it controls a single mass plant.

$$E(t) = \frac{1}{2} m \dot{y}(t)^2 \tag{8.24}$$

The only way the plant's energy can change is when the controller applies power to the plant since no other forces are considered. The power delivered by the controller can be described by:

$$P(t) = \frac{d}{dt} E(t) = m \ddot{y}(t) \dot{y}(t) \tag{8.25}$$

When the controller applies negative power to the plant, the sign of the acceleration and the velocity terms have to be opposite. In short, the controller provides damping to the system when the power is negative. Therefore, the damping of a mass plant system can be analyzed by looking at the acceleration and velocity response. When the acceleration and velocity response could be described analytically, the damping would also be described analytically.

8.3.2. ANALYTICAL DERIVATION OF SOLUTION OF RCS WITH MASS PLANTS

In this section, the analytical expressions of the step response and its derivatives are derived for the reset control system in Figure 8.2. It needs to be proven that the system can be transformed into a zero-input/unforced system when the reference is constant to find the expressions. Then the solution of the step response of the reset control system can be found by considering the homogeneous solution of the base linear system to multiple linked initial value problems. The initial state of the new initial value problem after any reset is the last state just before the reset, which has been reset. Furthermore, by decomposing the system matrix A_{cl}, the step response can be written as a linear combination of sine, cosine, and exponential terms, which depend on the eigenvalues and eigenvectors of the system matrix. Finally, the step response expression can be differentiated to retrieve an expression for the velocity and acceleration response.

This paper considers the damping of the transient response of reset control systems. Therefore, a step input is considered the system's input for the remainder of this paper. This section provides an analytical solution to the step response of the reset control system. The solution can then be used to analyze the damping of the step response.

First, let the set I of all reset instances be defined by 8.26.

$$I = \{t_i | u_{sf}(t_i) = 0, t_i = \langle t_{i-1}, t_{i+1} \rangle, i = 0, 1, 2, ...\} \tag{8.26}$$

Furthermore, consider $t_0 = 0$ as the step instance of the reference. During and after the step instance, the reference will be constant $r(t) = r_0, t \geq t_0$. t_0 is also the starting point of the analysis. Since only physical systems with a mass plant are considered, we can assume the following:

Assumption 1. *$C_2 P(s)$ contains at least one integrator.*

This assumption leads to the following lemma, as introduced in [28].

Lemma 2. *Consider the response of the closed-loop RCS in 8.22 for a constant reference input $r(t) = r_0$. Suppose Assumption 1 holds. Then there exists a $x_{c_2 p0} \in \mathbb{R}^{n_2}$ for which $A_{c_2 p} x_{c_2 p0} = 0$, and $C_{c_2 p} x_{c_2 p0} = r_0$.*

Proof. If $C_2P(s)$ contains an internal model of $r(t) = r_0$ there exists a $x_{c_2p0} \in \mathbb{R}^{n_2}$ for which $A_{c_2p}x_{c_2p0} = 0$, and $C_{c_2p}x_{c_2p0} = r_0$. Therefore, such an x_{c_2p0} exists when $C_2P(s)$ contains at least one integrator since $\mathcal{L}\{r_0\} = \frac{r_0}{s}$. □ □

Now, define system 8.27, which is a zero-input version of system 8.22. In this system, the step height r_0 is only found in the system output $y(t)$.

$$\begin{cases} \dot{\hat{x}} = A_{cl}\hat{x}(t), & \text{if} \quad u_{sf}(t) \neq 0 \\ \hat{x}(t^+) = \hat{A}_\rho \hat{x}(t), & \text{if} \quad u_{sf}(t) = 0 \\ y(t) = C_{cl}\hat{x}(t) + r_0 \\ u_{sf}(t) = C_{rline}\hat{x}(t) \end{cases} \tag{8.27}$$

Then the existence of x_{c_2p0} can be used to prove Lemma 3.

Lemma 3. *Suppose Assumption 1 holds. Consider a constant reference $r(t) = r_0$. The system 8.22 and 8.27 are equivalent under the state transformation $\hat{x}(t) = x(t) - x_0$, where $x_0 = \left[0^{n-n_2} x_{c_2p0}\right]^T$.*

Proof. First, substitute the state transformation back into system 8.27:

$$\begin{cases} \dot{x} - \dot{x}_0 = A_{cl}x(t) - A_{cl}x_0, & \text{if } u_{sf}(t) \neq 0 \\ x(t^+) - x_0 = \hat{A}_\rho x(t) - \hat{A}_\rho x_0, & \text{if } u_{sf}(t) = 0 \\ y(t) = C_{cl}x(t) - C_{cl}x_0 + r_0 \\ u_{sf}(t) = C_{rline}x(t) - C_{rline}x_0 \end{cases} \tag{8.28}$$

Now use the fact that $\dot{x}_0 = 0$, $\hat{A}_\rho x_0 = x_0$, the expressions of the elements of $A_{cl}, B_{cl}, C_{cl}, C_{rline}$, and D_{rline} which can be found in 8.23 and Appendix A. Lastly, use $A_{c_2p}x_{c_2p0} = 0$ and $C_{c_2p}x_{c_2p0} = r_0$ from Lemma 2, to find that 8.27 is equivalent to 8.22. □ □

A more detailed proof can be found in the Appendix B.

Remark 12. *Since $C_2P(s)$ contains at least one integrator, the transformation state x_0 can be written as follows:*

$$x_{c_2p0} = \begin{bmatrix} 0^{n-n_2} & d_1 & d_2 & \cdots & d_{n_2-1} & 1 \end{bmatrix}^T r_0 \tag{8.29}$$

Coefficients d_j for $j = 1, 2, \cdots, n_2 - 1$ correspond to the denominator coefficients in the form of $C_2P(s)$ in 8.30.

$$C_2P(s) = \frac{c_{n_2-1}s^{n_2-1} + \cdots + c_1 s + c_0}{s^{n_2} + d_{n_2-1}s^{n_2-1} + \cdots + d_1 s} \tag{8.30}$$

Remark 13. *From 8.27 and 8.26 it can be concluded that between the reset instances t_i and t_{i+1} the system behaves like the BLS:*

$$\dot{\hat{x}}(t) = A_{cl}\hat{x}(t), \qquad t \in \langle t_i, t_{i+1}] \tag{8.31}$$

Theorem 9. *Consider the RCS in 8.22 and its transformed equivalent in 8.27. Suppose Assumption 1 holds and $r(t) = r_0$. Then the system response can be expressed as:*

$$\hat{x}(t) = e^{A_{cl}(t-t_i)}\hat{x}(t_i) = \Phi(t - t_i)\hat{x}(t_i), \qquad t \in \langle t_i, t_{i+1}] \tag{8.32}$$

Here, $\Phi(t)$ is called the state-transition matrix.

Proof. Lemma 3 shows that the original system in 8.22 is equivalent to the zero-input system shown in 8.27. The solution of the base linear version of the zero-input system is:

$$\hat{x} = e^{A_{cl}t}\hat{x}(0) \tag{8.33}$$

8

Following Remark 13, the system behaves like the BLS when $t \notin I$. Therefore, the response between two reset instances will be a linear initial value problem, where the states at the last reset instance are the initial states, as expressed in 8.32. □ □

Assumption 2. *A_{cl} is diagonalizable with n distinct eigenvalues.*

Lemma 4. *Suppose Assumption 2 holds. Then the response of the RCS depends on the eigenvalues and eigenvectors, the reset instances, and the states in those resets. The entries of the transition matrix are:*

$$\Phi_{kl}(t-t_i) = \sum_{j=1}^{n} a_{kj} b_{jl} e^{\lambda_j (t-t_i)} \tag{8.34}$$

in which $a_{kj} = V_{kj}$, $b_{jl} = (V^{-1})_{jl}$, $\lambda_j = \Lambda_{jj}$. Here V contains the eigenvectors and Λ the eigenvalues of A_{cl}.

Proof. If A_{cl} is diagonalizable, it can be decomposed into $A_{cl} = V\Lambda V^{-1}$. Therefore, the transition matrix can be expressed as $\Phi(t-t_i) = Ve^{A_{cl}(t-t_i)}V^{-1}$. This leads to the expression in 8.34. Combining 8.32 and 8.34 shows the dependence on the eigenvalues and eigenvectors of A_{cl}, the reset instances, and the states in the reset instances. □ □

Lemma 5. *Consider Assumption 2 to hold. Furthermore, consider λ_h and λ_m to be a complex conjugate pair of eigenvalues of A_{cl}, such that $\lambda_h = \overline{\lambda_m}$. Then,*

$$a_{kh} b_{hl} = \overline{a_{km} b_{ml}} = \sigma_{kl,h} + \tau_{kl,h} i \tag{8.35}$$

In which, $\sigma kl, h$ is the real part of $a_{kh}b_{hl}$ and $a_{km}b_{ml}$. Moreover, $\tau_{kl,h}$ is the imaginary part of $a_{kh}b_{hl}$ and $\overline{a_{km}b_{ml}}$.

Proof. System matrix A_{cl} can be written as $A_{cl} = V\Lambda V^{-1}$ since it is assumed to be diagonalizable in Assumption 2. A_{cl} is considered to be real in 8.23. Therefore, all imaginary terms should cancel each other for A_{cl} to be real:

$$\Im(\sum_{j=1}^{n} a_{kj} b_{jl} \lambda_j) = 0 \tag{8.36}$$

Then, 8.35 needs to hold if λ_h and λ_m are a complex conjugate pair of eigenvalues. Hence, the claim is proven. □ □

Lemma 6. *Consider the RCS in 8.27 for a constant step reference r_0. Suppose Assumptions 1 and 2 hold. Then the states of the RCS can be described by:*

$$\hat{x}_k(t) = \sum_{l=1}^{n} \Phi_{kl}(t-t_i)\hat{x}_l(t_i), \qquad t \in \langle t_i, t_{i+1}]$$

Where, the expression of state-transition matrix entry Φ_{kl} is:

$$\begin{aligned} \Phi_{kl}(t-t_i) = \sum_{j=1}^{n_{pair}} & 2e^{\alpha_j (t-t_i)} [\sigma_{kl,j} \cos(\beta_j (t-t_i)) \\ & - \tau_{kl,j} \sin(\beta_j (t-t_i))] \\ & + \sum_{q=n_{imag}+1}^{n} a_{kq} b_{ql} e^{\lambda_q (t-t_i)} \end{aligned} \tag{8.38}$$

In which, $\lambda_{2j-1} = \overline{\lambda_{2j}} = \alpha_j + \beta_j i$, $a_{n(2j-1)}b_{(2j-1)l} = \overline{a_{n(2j)}b_{(2j)l}} = \sigma_{nl,j} + \tau_{nl,j}i$, and $\Im(\lambda_q) = 0$. Finally, n_{pair} is the number of complex conjugate pairs of eigenvalues of A_{cl} such that $n_{imag} = 2n_{pair}$ and $n_{real} = n - 2n_{pair}$.

Proof. The eigenvalues of the closed-loop system matrix A_{cl} can be real or part of a complex conjugate pair of eigenvalues. Consider the complex conjugate pair of eigenvalues λ_h and λ_m, $\lambda_h = \overline{\lambda_m} = \alpha + \beta i$. Then the terms in 8.34 that are linked to this pair of eigenvalues can be expressed by 8.39 when Lemma 5 is applied.

$$\begin{aligned} &a_{kh}b_{hl}e^{\lambda_h(t-t_i)} + a_{km}b_{ml}e^{\lambda_m(t-t_i)} \\ &\quad = \sigma_{kl,h}e^{\alpha(t-t_i)}(e^{\beta(t-t_i)i} + e^{-\beta(t-t_i)i}) \\ &\quad + \tau_{kl,h}e^{\alpha(t-t_i)}(e^{\beta(t-t_i)i} - e^{-\beta(t-t_i)i}) \end{aligned} \tag{8.39}$$

Now Euler's formula is used to rewrite 8.39 to:

$$\begin{aligned} &a_{kh}b_{hl}e^{\lambda_h(t-t_i)} + a_{km}b_{ml}e^{\lambda_m(t-t_i)} \\ &\quad = 2\sigma_{kl,h}e^{\alpha(t-t_i)}\cos(\beta(t-t_i)) \\ &\quad - 2\tau_{kl,h}e^{\alpha(t-t_i)}\sin(\beta(t-t_i)) \end{aligned} \tag{8.40}$$

The substitution of 8.40 into 8.34 for every complex conjugate pair of eigenvalues results in 8.38. Therefore, the states of the RCS 8.27 can be described by 8.37. □ □

Without loss of generality, the following assumption can be made:

Assumption 3. *The state-space representation of $C_2P(s)$ is in observable canonical form such that $C_{cl} = \begin{bmatrix} 0^{n-1} & 1 \end{bmatrix}$.*

Theorem 10. *Consider the RCS in 8.27 for a constant step reference r_0. Suppose Assumptions 1-3 hold. Then the step response of the system is defined as:*

$$y(t) = r_0 + \sum_{l=1}^{n} \Phi_{nl}(t-t_i)\hat{x}_l(t_i), \qquad t \in \langle t_i, t_{i+1}] \tag{8.41}$$

The Φ_{nl} is the last row of the state-transition matrix.

Proof. Since Assumption 3 holds, the step response will be the sum of the step height r_0 and the value of the state $\hat{x}_n(t)$. Using Lemma 6 to rewrite $\hat{x}_n(t)$ gives 8.41. □ □

Corollary 1. *Consider the RCS in 8.27 for a constant step reference r_0. Suppose Assumptions 1-3 hold. Then the velocity response of the system is defined as:*

$$\dot{y}(t) = \sum_{l=1}^{n} \dot{\Phi}_{nl}(t-t_i)\hat{x}_l(t_i), \qquad t \in \langle t_i, t_{i+1}] \tag{8.42}$$

Where the time derivative of the state-transition matrix entry $\dot{\Phi}_{nl}$ is:

$$\begin{aligned} \dot{\Phi}_{nl}(t-t_i) = &\sum_{j=1}^{n_{pair}} 2e^{\alpha_j(t-t_i)} \\ &\big[(\alpha_j\sigma_{nl,j} - \beta_j\tau_{nl,j})\cos(\beta_j(t-t_i)) \\ &- (\beta_j\sigma_{nl,j} + \alpha_j\tau_{nl,j})\sin(\beta_j(t-t_i))\big] \\ &+ \sum_{q=n_{imag}+1}^{n} \lambda_q a_{nq} b_{ql} e^{\lambda_q(t-t_i)} \end{aligned} \tag{8.43}$$

Proof. The derivative of the entries of the state transition matrix can be split into cosine,

sine, and exponential terms. The derivative of the cosine terms is:

$$\begin{aligned}\frac{d}{dt}\left(2\sigma_{nl,j}e^{\alpha_j(t-t_i)}\cos\left(\beta_j(t-t_i)\right)\right) = \\ 2\sigma_{nl,j}\alpha_j e^{\alpha_j(t-t_i)}\cos\left(\beta_j(t-t_i)\right) \\ -2\sigma_{nl,j}\beta_j e^{\alpha_j(t-t_i)}\sin\left(\beta_j(t-t_i)\right)\end{aligned} \tag{8.44}$$

Similarly, the derivative of the sine terms is:

$$\begin{aligned}\frac{d}{dt}\left(-2\tau_{nl,j}e^{\alpha_j(t-t_i)}\sin\left(\beta_j(t-t_i)\right)\right) = \\ -2\tau_{nl,j}\alpha_j e^{\alpha_j(t-t_i)}\sin\left(\beta_j(t-t_i)\right) \\ -2\tau_{nl,j}\beta_j e^{\alpha_j(t-t_i)}\cos\left(\beta_j(t-t_i)\right)\end{aligned} \tag{8.45}$$

Finally, the derivative of the terms corresponding to the real eigenvalues:

$$\frac{d}{dt}\left(a_{nq}b_{ql}e^{\lambda_q(t-t_i)}\right) = \lambda_q a_{nq}b_{ql}e^{\lambda_q(t-t_i)} \tag{8.46}$$

Combining the sinusoidal and exponential terms in 8.44-8.46 yields the derivative of the state-transition entries in 8.43. □ □

Corollary 2. *Consider the RCS in 8.27 with a constant step reference r_0. Suppose Assumptions 1-3 hold. Then the acceleration response of the system is defined as:*

$$\ddot{y}(t) = \sum_{l=1}^{n}\ddot{\Phi}_{nl}(t-t_i)\hat{x}_l(t_i), \qquad t\in\langle t_i, t_{i+1}] \tag{8.47}$$

Where the second time derivative of the state transition matrix entry $\ddot{\Phi}_{nl}$ is:

$$\begin{aligned}\ddot{\Phi}_{nl}(t-t_i) = \sum_{j=1}^{n_{pair}} 2e^{\alpha_j(t-t_i)} \\ \left[(\alpha_j^2\sigma_{nl,j} - 2\alpha_j\beta_j\tau_{nl,j} - \beta_j^2\sigma_{nl,j})\cos(\beta_j(t-t_i))\right. \\ \left. -(\alpha_j^2\tau_{nl,j} + 2\alpha_j\beta_j\sigma_{nl,j} - \beta_j^2\tau_{nl,j})\sin(\beta_j(t-t_i))\right] \\ + \sum_{q=n_{imag}+1}^{n}\lambda_q^2 a_{nq}b_{ql}e^{\lambda_q(t-t_i)}\end{aligned} \tag{8.48}$$

Proof. The second derivative of the state-transition matrix entries can again be split into cosine, sine, and exponential terms, similar to the proof of Corollary 1. The derivative of the cosine terms in the entry of the velocity state-transition matrix is:

$$\begin{aligned}\frac{d}{dt}\left(2(\alpha_j\sigma_{nl,j} - \beta_j\tau_{nl,j})e^{\alpha_j(t-t_i)}\cos(\beta_j(t-t_i))\right) = \\ 2\alpha_j(\alpha_j\sigma_{nl,j} - \beta_j\tau_{nl,j})e^{\alpha_j(t-t_i)}\cos(\beta_j(t-t_i)) \\ -2\beta_j(\alpha_j\sigma_{nl,j} - \beta_j\tau_{nl,j})e^{\alpha_j(t-t_i)}\sin(\beta_j(t-t_i))\end{aligned} \tag{8.49}$$

Similarly, the derivative of the sine terms is:

$$\begin{aligned}\frac{d}{dt}\left(-2(\beta_j\sigma_{nl,j} + \alpha_j\tau_{nl,j})e^{\alpha_j(t-t_i)}\sin(\beta_j(t-t_i))\right) = \\ -2\alpha_j(\beta_j\sigma_{nl,j} + \alpha_j\tau_{nl,j})e^{\alpha_j(t-t_i)}\sin(\beta_j(t-t_i)) \\ -2\beta_j(\beta_j\sigma_{nl,j} + \alpha_j\tau_{nl,j})e^{\alpha_j(t-t_i)}\cos(\beta_j(t-t_i))\end{aligned} \tag{8.50}$$

Finally, the derivative of the terms corresponding to the real eigenvalues:

$$\frac{d}{dt}\left(\lambda_q a_{nq}b_{ql}e^{\lambda_q(t-t_i)}\right) = \lambda_q^2 a_{nq}b_{ql}e^{\lambda_q(t-t_i)} \tag{8.51}$$

Combining the sinusoidal and exponential terms in 8.49-8.51 yields the second derivative of the state-transition entries in 8.48. □ □

Now, 8.42 and 8.47 can be used to express the energy and power of the plant analytically. The energy and power expressions can be used to analyze the damping in the step response for all reset control systems described by Figure 8.2 as long as Assumptions 1-3 are valid. Moreover, the analytical expression of the step response itself can be used to see the effect of different controllers on the damping of the response.

8.4. DAMPING ANALYSIS OF RESET CONTROL SYSTEMS WITH STABLE BLS

In this section, the analytical expressions introduced in Section 8.3 are used to analyze the damping of the base-linear-stable reset control systems in Figure 8.2. For the BLS to be stable, the eigenvalues of the system matrix A_{cl} in 8.23 are all required to have a negative real part. Therefore, $\alpha_j < 0$ and $\lambda_{Rh} < 0$ for all positive integers j and h in 8.52.

$$\lambda = \begin{bmatrix} \alpha_1 + \beta_1 i \\ \alpha_1 - \beta_1 i \\ \vdots \\ \alpha_{n_{pair}} + \beta_{n_{pair}} i \\ \alpha_{n_{pair}} - \beta_{n_{pair}} i \\ \lambda_{R1} \\ \vdots \\ \lambda_{Rn_{real}} \end{bmatrix} \tag{8.52}$$

Note that λ_{Rh} is the $q = h + n_{imag}$-th eigenvalue of the system. Theorem 10 can be used to express the step response of the RCS analytically in 8.53. Note that the coefficients $c_{y_{I(2k-1)}}$ and $c_{y_{I(2k)}}$ correspond to the complex conjugate eigenvalue pairs, and c_{y_R} corresponds to the real eigenvalues, respectively. Consider an exponential term to be faster than another when its corresponding eigenvalues are more negative.

$$\begin{aligned} y(t) = & r_0 + \sum_{k=1}^{n_{pair}} c_{y_{I(2k-1)}}(t_i) e^{\alpha_k (t-t_i)} \cos(\beta_k (t-t_i)) \\ & + c_{y_{I(2k)}}(t_i) e^{\alpha_k (t-t_i)} \sin(\beta_k (t-t_i)) \\ & + \sum_{h=1}^{n_{real}} c_{y_{Rh}}(t_i) e^{\lambda_{Rh}(t-t_i)}, \qquad t \in \langle t_i, t_{i+1}] \end{aligned} \tag{8.53}$$

Here, the coefficients c_{y_I} and c_{y_R} are defined by:

$$c_{y_{I(2k-1)}}(t_i) = \sum_{l=1}^{n} 2\sigma_{nl,k} \hat{x}_l(t_i) \tag{8.54}$$

$$c_{y_{I(2k)}}(t_i) = \sum_{l=1}^{n} -2\tau_{nl,k} \hat{x}_l(t_i) \tag{8.55}$$

$$c_{y_{Rh}}(t_i) = \sum_{l=1}^{n} a_{n(h+n_{imag})} b_{(h+n_{imag})l} \hat{x}_l(t_i) \tag{8.56}$$

The sine and cosine terms of each complex pair of eigenvalues in 8.53 can be combined into a single (shifted) sine term:

$$\begin{aligned} y(t) =& r_0 + \sum_{k=1}^{n_{pair}} c_{y_{I(2k-1)(2k)}}(t_i) e^{\alpha_k (t-t_i)} \\ & \sin\left(\beta_k (t-t_i) + \psi_{y(2k-1)(2k)}(t_i)\right) \\ & + \sum_{h=1}^{n_{real}} c_{y_{Rh}}(t_i) e^{\lambda_{Rh}(t-t_i)}, \qquad t \in \langle t_i, t_{i+1}] \\ =& r_0 + y_{osci}(t) + y_{base}(t), \qquad t \in \langle t_i, t_{i+1}] \end{aligned} \tag{8.57}$$

In which, $c_{y_{I(2k-1)(2k)}}(t_i) = \sqrt{c_{y_{I(2k-1)}}(t_i)^2 + c_{y_{I(2k)}}(t_i)^2}$ and $\psi_{(2k-1)(2k)}(t_i) = \frac{c_{y_{I(2k-1)}}(t_i)}{c_{y_{I(2k)}}(t_i)}$.

In short, the step response consists of a baseline response $y_{base}(t)$, which is a sum of exponentials belonging to the real eigenvalues that decay to zero over time. The oscillatory term $y_{osci}(t)$ adds an oscillation with decreasing amplitude to the baseline response and is linked to the complex pairs of eigenvalues. Over time, the total response will tend to $y(t) = r_0$ since both the oscillatory and baseline response will asymptotically go to zero. The more negative the eigenvalue, the faster the exponential term will decay. The longer the time after the last reset, the more dominant the slower exponents will be. Moreover, the coefficients control the magnitude of the oscillatory and exponential terms. The values of the coefficients only change during the reset instances. The way the coefficients change during resets depends on $\sigma_{nl,k}$, $\tau_{nl,k}$, $a_{n(h+n_{imag})} b_{(h+n_{imag})l}$, and the state values at reset.

Similarly, the velocity and acceleration response can be written in the same form as 8.57. The velocity response and its coefficients are defined by:

$$\begin{aligned} \dot{y}(t) =& \sum_{k=1}^{n_{pair}} c_{\dot{y}_{I(2k-1)(2k)}}(t_i) e^{\alpha_k (t-t_i)} \\ & \sin\left(\beta_k (t-t_i) + \psi_{\dot{y}(2k-1)(2k)}(t_i)\right) \\ & + \sum_{h=1}^{n_{real}} c_{\dot{y}_{Rh}}(t_i) e^{\lambda_{Rh}(t-t_i)}, \qquad t \in \langle t_i, t_{i+1}] \\ =& \dot{y}_{osci}(t) + \dot{y}_{base}(t) \end{aligned} \tag{8.58}$$

In which,

$$c_{\dot{y}_{I(2k-1)(2k)}}(t_i) = \sqrt{\alpha_j^2 + \beta_j^2}\, c_{y_{I(2k-1)(2k)}}(t_i) \tag{8.59}$$

$$\psi_{\dot{y}_{I(2k-1)(2k)}}(t_i) = \psi_{y_{I(2k-1)(2k)}}(t_i) + \tan^{-1}\left(\frac{\beta_j}{\alpha_j}\right) \tag{8.60}$$

$$c_{\dot{y}_{Rh}}(t_i) = \lambda_{Rh} c_{y_{Rh}}(t_i) \tag{8.61}$$

The acceleration response and its coefficients are described by:

$$\begin{aligned}\ddot{y}(t) = &\sum_{k=1}^{n_{pair}} c_{\ddot{y}_{I(2k-1)(2k)}}(t_i) e^{\alpha_k (t-t_i)} \\ &\sin\left(\beta_k (t-t_i) + \psi_{\ddot{y}(2k-1)(2k)}(t_i)\right) \\ &+ \sum_{h=1}^{n_{real}} c_{\ddot{y}_{Rh}}(t_i) e^{\lambda_{Rh}(t-t_i)}, \qquad t \in \langle t_i, t_{i+1}] \\ &= \ddot{y}_{osci}(t) + \ddot{y}_{base}(t)\end{aligned} \tag{8.62}$$

In which,

$$c_{\ddot{y}_{I(2k-1)(2k)}}(t_i) = (\alpha_j^2 + \beta_j^2) c_{y_{I(2k-1)(2k)}}(t_i) \tag{8.63}$$

$$\psi_{\ddot{y}_{I(2k-1)(2k)}}(t_i) = \psi_{y_{I(2k-1)(2k)}}(t_i) + 2\tan^{-1}\left(\frac{\beta_j}{\alpha_j}\right) \tag{8.64}$$

$$c_{\ddot{y}_{Rh}}(t_i) = \lambda_{Rh}^2 c_{y_{Rh}}(t_i) \tag{8.65}$$

The velocity and acceleration response coefficients depend on the step response coefficients that belong to the same eigenvalue. However, these coefficients are scaled differently depending on the related eigenvalue.

The coefficients defined above characterize the step, velocity, and acceleration response. By looking at the evolution of the coefficients over time, the path of the step response and the plant energy can be approximated by only taking the dominant exponential terms into account. The dominant exponential terms are the exponents whose coefficients are significantly larger in magnitude than the coefficients of the other exponents. In the following sections, two approaches are introduced to analyze the damping of reset systems with mass plants. First, the coefficients of the step response itself are used to analyze the damping. Subsequently, the power and energy expressions are used to develop an approach to determine the damping of the system. Both lead to a similar analysis, but achieve it with a slightly different method.

8.4.1. DAMPING ANALYSIS: STEP RESPONSE

The damping of the step response can be analyzed directly from the analytic expression of the step response. The damping of a system is higher when the overshoot is reduced, and the response reaches the reference slower. By increasing the magnitude of the decay rate α_k and decreasing the magnitude of $c_{y_{I(2k-1)(2k)}}(t_i)$ in 8.57, the damping can be increased as the magnitude of the oscillatory components is reduced. Moreover, the coefficients $c_{y_{Rh}}(t_i)$ in 8.57 determine the time it takes for the baseline response to vanish. When the slower exponential terms (smallest $|\lambda_{Rh}|$) are dominant and have negative coefficients, the baseline response will slowly decay and drop below zero. The slower the dominant exponential terms, the more damped the step response will be because the system has more time to reduce the oscillations before overshoot occurs. Note that the amount that the coefficients can change between resets is bounded by the change of the plant location, since the plant location in 8.53 at reset is defined by 8.66. Therefore, a dominant exponential term will always be accompanied by another dominant exponential term whose coefficient is of the opposite sign.

$$y(t_i) = r_0 + \sum_{k=1}^{n_{pair}} c_{y_{I(2k-1)}}(t_i) + \sum_{h=1}^{n_{real}} c_{y_{Rh}}(t_i) \tag{8.66}$$

The damping of the step response can be assessed by looking at the evolution of the coefficients. The following steps can be used as a guide to analyze the damping of the reset control system.

1. Calculate the eigenvalues and eigenvectors of the system matrix A_{cl}.
2. Calculate the values of the coefficients $c_{y_{I(2k-1)(2k)}}(t_i)$ and $c_{y_{Rh}}(t_i)$ for the reset instances t_i. Here $h = 1, 2, ..., n_{real}$
3. Identify the dominant exponential terms based on the magnitude of the coefficients.
4. For the significant oscillatory coefficients: the faster the coefficient is reduced to zero, the faster the oscillations are removed from the response. The slower oscillatory terms should be reduced faster to achieve a damped response since their effect is the most persistent.
5. For the baseline coefficients: consider only the dominant baseline terms. If the coefficient of the slowest dominant exponential term is negative, the response will be better damped and will not likely overshoot. By contrast, if the coefficient of the slowest exponential term is positive, the response will be less damped. Moreover, the slower the most dominant term, the more the system is damped.

Note that the coefficients are only changed during the reset instances. With a shaping filter, the reset instances could be designed so that the coefficients are updated beneficially. Moreover, the evolution of the coefficients depends on the eigenvectors of the matrix of the system. These determine the weights of the states in the calculation of the coefficients 8.54-8.56. By changing the values of the controller parameter or the configuration, the eigenvectors could be designed to favor a particular state in calculating the step response coefficient. Lastly, states can be designed to favorably influence the coefficients by changing parameter values and controller configuration.

8.4.2. DAMPING ANALYSIS: ENERGY AND POWER

As mentioned in Section 8.3.1, the controller dampens the system when it applies negative power to the plant. In general, the controller should apply sufficient negative power to the system to dissipate all energy exactly when it reaches the reference point to prevent overshoot.

For the controller to apply negative power, the acceleration and velocity terms in 8.25 should have the opposite sign. Therefore, a negative acceleration is required to remove the initial kinetic energy needed to move the plant toward the reference point in the step response.

In 8.62-8.65, the acceleration response and its coefficients are defined. The coefficient of the oscillatory terms should be reduced when damping is required. Otherwise, the power will eventually become positive and add energy to the system. Due to the

exponential decay of the baseline response, the coefficients of the slowest dominant exponential terms should be negative to prevent the power from becoming positive. The dominant exponential terms are those whose coefficients have a significant magnitude compared to the other coefficients. In contrast to the step response, the acceleration response is not necessarily continuous. Therefore, the acceleration (and power) can change instantaneously during reset. Consequently, the coefficients change with it according to 8.67. Therefore, the coefficient sum should be the opposite sign of the velocity for the controller to apply damping after the reset.

$$\begin{aligned}\ddot{y}(t_i) = &\sum_{k=1}^{n_{pair}} c_{\ddot{y}_{I(2k-1)(2k)}}(t_i)\sin\left(\psi_{\ddot{y}_{I(2k-1)(2k)}}(t_i)\right) \\ &+ \sum_{h=1}^{n_{real}} c_{\ddot{y}_{Rh}}(t_i)\end{aligned} \tag{8.67}$$

Note that $c_{\ddot{y}_{I(2k-1)(2k)}}$ and $c_{\ddot{y}_{Rh}}$ are scaled versions of $c_{y_{I(2k-1)(2k)}}$ and $c_{y_{Rh}}$. The coefficients are scaled by the square of the corresponding eigenvalues 8.63, 8.65. The acceleration coefficients of fast exponential terms will become more dominant than the step coefficients since they are scaled more.

Looking at the coefficients $c_{\ddot{y}}$, one can analyze the damping of the reset controller. The following steps can be used as a guideline to analyze the damping of the step response in a reset control system:

1. Calculate the eigenvalues and eigenvectors of the system matrix A_{cl}.
2. Calculate the values of the coefficients $c_{\ddot{y}_{I(2k-1)(2k)}}(t_i)$ and $c_{\ddot{y}_{Rh}}(t_i)$ for the reset instances t_i.
3. Identify the dominant exponential terms based on the magnitude of the coefficients.
4. For the significant oscillatory coefficients: the faster the coefficients are reduced, the faster the oscillations are removed from the response. The presence of oscillations in power will lead to the addition of energy at some point, which causes a loss of damping.
5. For the baseline coefficients: consider only the dominant baseline terms. If the sum of the coefficients in 8.67 is negative, the controller will dissipate energy directly after reset. Then the damping will be applied longer if the coefficient of the slowest dominant exponential term is negative. Therefore, the response will be more damped and less likely to overshoot. On the contrary, if the coefficient of the slowest exponential term is positive, the energy will increase again, which decreases the damping. Finally, the slower the most dominant exponential term, the longer the controller provides damping if the coefficient is negative.

Note that the coefficients $c_{\ddot{y}}$ could be designed similarly to the coefficients c_y as they are proportional to each other. However, the exact value of the eigenvalues is relevant for tuning $c_{\ddot{y}}$ since the coefficients of the faster exponential terms will be scaled more.

In short, one can use the step response and power expressions to analyze the damping in a reset control system with stable BLS controlling a mass plant.

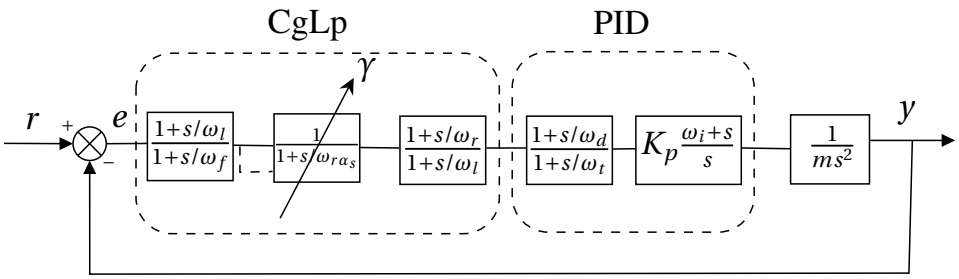

Figure 8.3: Diagram of CgLp-PID controlling a mass plant.

8.5. ILLUSTRATIVE EXAMPLE: DAMPING ANALYSIS OF CGLP-PID

To illustrate the use of the damping analyses introduced in Section 8.4, consider the CgLp-PID controlling a mass plant in Figure 8.3. [11] and [21] have shown the dependency of the step response on the sequence of control elements. Moreover, both [11], and [21] show that in a CgLp element, it could be beneficial to use a Lead-Reset configuration compared to a Reset-Lead configuration. The Lead-Reset sequence can provide more damping to the system and reduce overshoot for the same phase margin. The CgLp-PID damping analysis provides insight into the additional damping attained by the Lead-Reset configuration.

The lead element of a conventional CgLp (see Section 8.2) is divided into two separate lead elements in Figure 8.3. By changing the value of ω_l, the lead strength can be changed before and after the reset block. The lead after the reset element will vanish when ω_l is close to ω_r, which results in a Lead-Reset configuration. Similarly, the lead before the reset element will disappear when ω_l approaches ω_f, resulting in a Reset-Lead configuration. Therefore, ω_l can control the lead placement in the CgLp element. In this example, the damping of the step response is analyzed for different values of ω_l. Since the first-order DF is independent of ω_l, all changes in damping can be attributed to lead placement because the phase margin will be equal for all controllers.

The controller is tuned such that the BLS is stable and has a small phase margin of 5° at a bandwidth frequency of $f_c = 100Hz$. Full reset ($\gamma = 0$) is chosen for simplicity. The correction factor α_s is taken to be 1.62 according to [10]. The CgLp element is tuned to provide phase lead over an extensive frequency range, such that the effect of the location of the lead element is significant when sweeping ω_l over this range. Through the broadband phase lead provided by the CgLp, the phase margin of the RCS is 55°. Therefore, the RCS is expected to provide more damping than the BLS. The controller and system parameters are listed in Table 8.1.

Consider the states of the system to be defined as follows:

$$\hat{x}(t) = \begin{bmatrix} \hat{x}_r & \hat{x}_{L1} & \hat{x}_{L2} & \hat{x}_D & \hat{x}_{PIplant} \end{bmatrix}^T \tag{8.68}$$

Here, $\hat{x}_r$ is the state of the reset element. $\hat{x}_{L1}$, $\hat{x}_{L2}$, and $\hat{x}_D$ are the states of the lead elements before the reset element, after the reset element, and in the PID. The combined

Table 8.1: Control and system parameters of CgLp-PID with a mass plant.

Symbol	Description	Value
ω_c	Bandwidth frequency	100 Hz
ω_r	Corner frequency of lead filter in CgLp	$\omega_c/6$
ω_f	Taming frequency of lead filter in CgLp	$10\omega_c$
α_s	Correction factor reset element	1.62
$\omega_{r\alpha_s}$	Corner frequency of reset element	ω_r/α_s
ω_i	Corner frequency of lag filter in PID	$\omega_c/10$
ω_d	Corner frequency of lead filter in PID	$\omega_c/1.5$
ω_t	Taming frequency of lead filter in PID	$1.5\omega_c$
K_p	Proportional gain in PID	1432
m	Mass of mass plant	5e-3 kg
r_0	Step amplitude	1 μm
ω_l	Lead location parameter	$[\omega_r, \omega_f]$

PI controller and mass plant states are $\hat{x}_{PIplant}$. Then the system can be described by 8.69-8.72.

$$A_{cl} = \begin{bmatrix} -\omega_{r\alpha_s} & \omega_{r\alpha_s} & 0 & 0 & 0 & 0 & -\omega_{r\alpha_s}\frac{\omega_f}{\omega_l} \\ 0 & -\omega_f & 0 & 0 & 0 & 0 & -\omega_f(1-\frac{\omega_f}{\omega_l}) \\ \omega_l(1-\frac{\omega_l}{\omega_r}) & 0 & -\omega_l & 0 & 0 & 0 & 0 \\ \frac{\omega_l\omega_t}{\omega_r}(1-\frac{\omega_t}{\omega_d}) & 0 & \omega_t(1-\frac{\omega_t}{\omega_d}) & -\omega_t & 0 & 0 & 0 \\ \frac{\omega_l\omega_t}{\omega_r\omega_d}\frac{K_p\omega_i}{m} & 0 & \frac{\omega_t}{\omega_d}\frac{K_p\omega_i}{m} & \frac{K_p\omega_i}{m} & 0 & 0 & 0 \\ \frac{\omega_l\omega_t}{\omega_r\omega_d}\frac{K_p}{m} & 0 & \frac{\omega_t}{\omega_d}\frac{K_p}{m} & \frac{K_p}{m} & 1 & 0 & 0 \\ 0 & 0 & 0 & 0 & 0 & 1 & 0 \end{bmatrix} \tag{8.69}$$

$$C_{cl} = \begin{bmatrix} 0 & 0 & 0 & 0 & 0 & 0 & 1 \end{bmatrix} \tag{8.70}$$

$$C_{rline} = \begin{bmatrix} 0 & 1 & 0 & 0 & 0 & 0 & -\frac{\omega_f}{\omega_l} \end{bmatrix} \tag{8.71}$$

$$\hat{A}_\rho = \begin{bmatrix} \gamma & 0 \\ 0 & I^{6\times 6} \end{bmatrix} \tag{8.72}$$

The eigenvalues of the system matrix of the CgLp-PID are given by 8.73. Note that the first six eigenvalues are independent of the location of the lead filter in the CgLp. As intended, all eigenvalues have a negative real part, making the BLS stable.

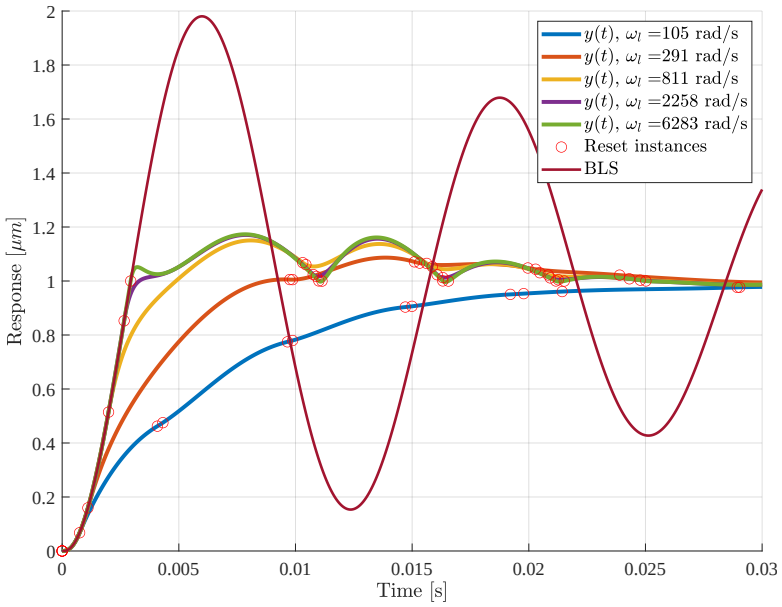

Figure 8.4: Step response of CgLp-PID with mass plant for different ω_l values.

$$\lambda = \begin{bmatrix} -29.8 + 492.4 \\ -29.8 - 492.4 \\ -6350.1 \\ -719.1 \\ -98.8 \\ -62.8 \\ -\omega_l \end{bmatrix} \tag{8.73}$$

Using 8.41, the step response can be determined analytically for different lead location parameter values ω_l. Assume that the systems are entirely at rest when $t = 0$. The initial state of the system will then be $x(0) = \hat{\begin{bmatrix} 0^{6\times 1} \\ -r_0 \end{bmatrix}}$. The step responses of the different controllers are shown in Figure 8.4. The percentage overshoot of the CgLp-PID compared to the BLS as a function of ω_l can be seen in Figure 8.5. The reset implementation decreases the system's overshoot through the extra phase margin. Additionally, the overshoot is decreased further when more lead is placed before the reset element, like in [11] and [21]. In a small frequency range ($\omega_l \in [\omega_r, 135]$), the overshoot is prevented entirely. The following sections analyze how the system provides more damping for lower ω_l values.

8.5.1. DAMPING ANALYSIS: STEP RESPONSE

In this section, the step response damping analysis from Section 8.4 is used to see how the placement of the lead changes the damping of the step response. The step response

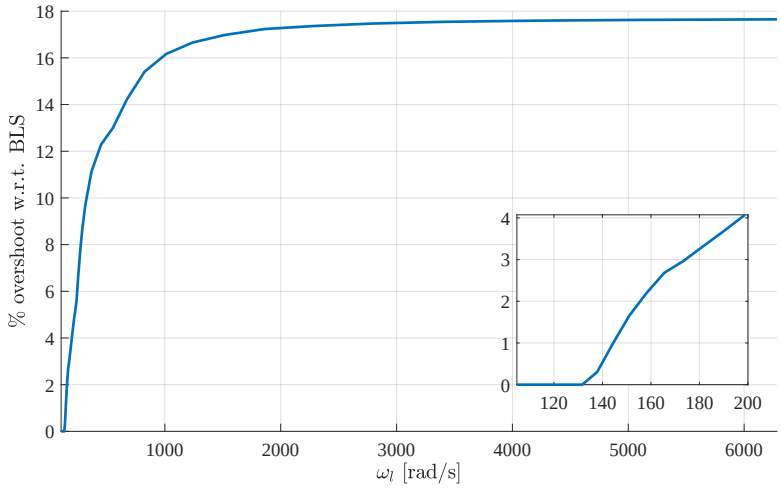

Figure 8.5: Percentage overshoot in step response of CgLp-PID compared to BLS for different ω_l values.

of the CgLp-PID consists of one oscillatory term and five baseline exponential terms 8.74-8.76.

$$y(t) = r_0 + y_{osci}(t) + y_{base}(t), \qquad t \in \langle t_i, t_{i+1}]$$ (8.74)

In which,

$$\begin{aligned} y_{osci}(t) &= c_{y_{I12}}(t_i) e^{-29.8(t-t_i)} \\ &\quad \sin(492.4(t-t_i) + \psi_{y_{I12}}(t_i)), \qquad t \in \langle t_i, t_{i+1}] \end{aligned}$$ (8.75)

$$\begin{aligned} y_{base}(t) &= c_{y_{R1}}(t_i) e^{-6350.1(t-t_i)} \\ &\quad + c_{y_{R2}}(t_i) e^{-719.1(t-t_i)} + c_{y_{R3}}(t_i) e^{-98.8(t-t_i)} \\ &\quad + c_{y_{R4}}(t_i) e^{-62.8(t-t_i)} + c_{y_{R5}}(t_i) e^{-\omega_l(t-t_i)}, \\ &\quad t \in \langle t_i, t_{i+1}] \end{aligned}$$ (8.76)

Firstly, the coefficient $c_{y_{I12}}$ and the decay rate α determine the amplitude of the oscillatory content. Note that the magnitude of α is low compared to the other eigenvalues. Therefore, the reduction of $c_{y_{I12}}$ will be vital for reducing the amplitude of the oscillations before it leads to overshoot. In Figure 8.6 it can be seen that the coefficient is reduced more and earlier in the response when more lead is present before the reset element. The earlier reduction can partially be attributed to the earlier reset of these systems. However, the oscillatory term is also reduced more in controllers with lower ω_l when the first reset happens simultaneously. In Figure 8.7, all systems have the same t_1. Here, the reduction of the oscillation coefficient is still greater for lower ω_l. In short, the more lead is placed before the reset element, the more and faster the oscillatory content of the step response is damped.

Secondly, the coefficients c_{y_R} determine which exponential terms are relevant for the baseline response. From Figure 8.8, it can be concluded that $c_{y_{R2}}$, $c_{y_{R3}}$, and $c_{y_{R5}}$ are

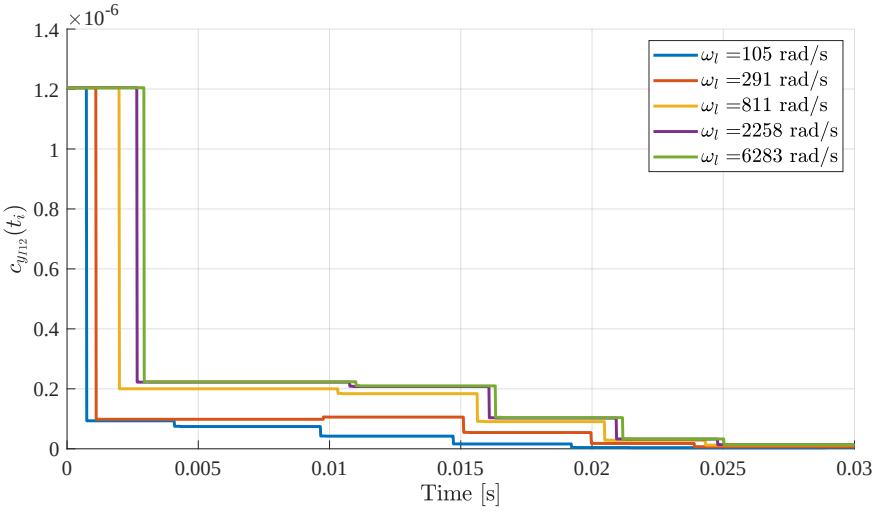

Figure 8.6: Oscillatory coefficient evolution for different ω_l.

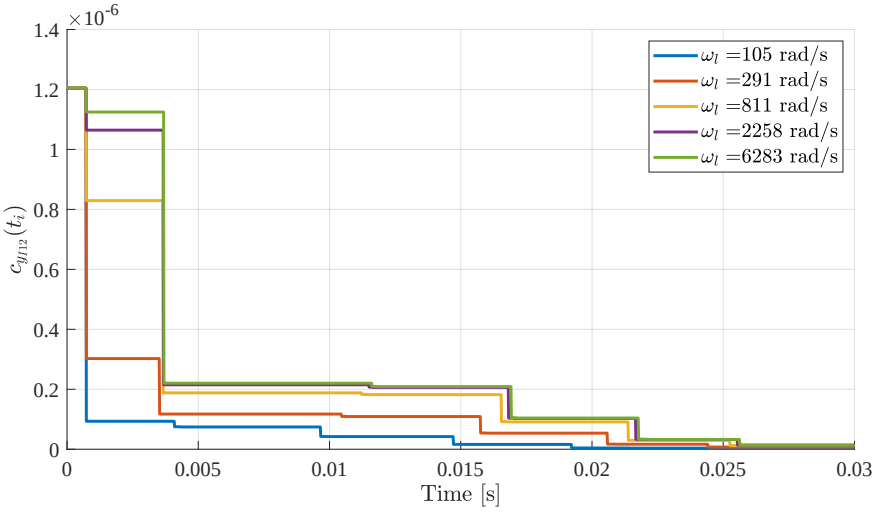

Figure 8.7: Oscillatory coefficient evolution for different ω_l when t_1 is fixed.

the dominant exponential terms to approximate the baseline response. The exponential term with coefficient $c_{y_{R1}}$ becomes significant when $\omega_l = 6283$ rad/s. However, its effect on the step response will be little since the corresponding eigenvalue λ_{R1} is large compared to the other dominant exponents. Therefore, in this analysis, the exponential term with coefficient $c_{y_{R1}}$ will be neglected. Generally, the more lead is placed after the reset element, the more dominant the faster exponents will be. Faster dominant exponential terms cause the baseline response to become faster, which limits the time the oscillatory coefficient has to be decreased. Therefore, overshoot is more likely and severe when

Table 8.2: Error of approximation of step response by using the oscillatory terms, and baseline terms corresponding to λ_{R2}, λ_{R3}, and λ_{R5}. Frequencies are in rad/s and errors are in μm.

Lead placement	$\omega_l = 105$	$\omega_l = 291$	$\omega_l = 811$	$\omega_l = 2258$	$\omega_l = 6283$
$\tilde{e}_{RMS}$	0.0014	0.0010	0.0009	0.0009	0.0066
$\max(\lvert\tilde{e}(t)\rvert)$	0.0114	0.0114	0.0114	0.0114	0.1060

more lead is after the reset element. Note that ω_l determines the decay rate of the exponential corresponding to λ_{R5}. Therefore, the baseline response of the coefficients in Figure 8.8d will be faster than in Figure 8.8c.

The step response of each system can be approximated by $\tilde{y}(t) = y_{osci}(t) + \tilde{y}_{base}(t)$. Here, $\tilde{y}_{base}(t)$ is composed of the dominant exponents in 8.77. The composition of the approximated step response can be seen in Figure 8.9. In short, from the analysis of the step response coefficients can be concluded that the step response is less damped, the more lead is after the reset element. The oscillation coefficient has been reduced less when the baseline response approaches zero, and a faster baseline response is caused by the faster exponential terms being more dominant when ω_l increases. Maximal and root mean square (RMS) error values $\tilde{e}(t)$ are given in Table 8.2 to show the accuracy of the approximation. Here, the approximation error is given by $\tilde{e}(t) = y(t) - \tilde{y}(t)$.

$$\begin{aligned}\tilde{y}_{base}(t) = c_{y_{R2}}(t_i)e^{-719.1(t-t_i)} + c_{y_{R3}}(t_i)e^{-98.8(t-t_i)} \\ + c_{y_{R5}}(t_i)e^{-\omega_l(t-t_i)}, \qquad t \in \langle t_i, t_{i+1}]\end{aligned} \tag{8.77}$$

It can be concluded that the dominant exponential terms can approximate the step response of this system well, since the RMS error value does not exceed 1% of the step height. Note that the maximum error for the system where $\omega_l = \omega_f$ is more significant than in the other systems because the baseline exponential term with coefficient $c_{y_{R1}}$ is not considered in the approximation. Since this baseline term decays quickly, it only leads to significant errors during resets, as seen in Figure 8.10. However, the approximation can still be used to analyze the damping of the system, since the RMS error is less than 1%.

8.5.2. DAMPING ANALYSIS: ENERGY AND POWER

In this section, the energy and power damping analysis method introduced in Section 8.4 is used to analyze how the placement of the lead changes the damping of the step response. For the system to be adequately damped, all plant energy should be dissipated when the reference is reached, as mentioned in Section 8.4.2. The plant will overshoot when there is not enough energy dissipated, which is mathematically defined in 8.78. Here, $t_{E=0}$ is when all the energy of the plant at the first reset $E(t_1)$ is dissipated. $t_{y=r_0}$ is the instance where the output crosses the reference for the first time. To prevent overshoot $t_{E=0}$ should be equal to $t_{y=r_0}$.

$$E(t_1) - \int_{t_1}^{t_{E=0}} P(t)\,dt = 0 \tag{8.78}$$

The reset instances are determined by the output of the first lead filter, since no shap-

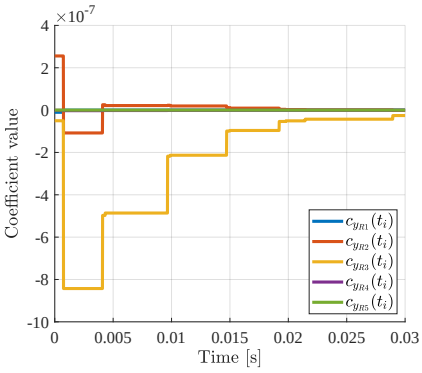

(a) $\omega_l = 105$ rad/s.

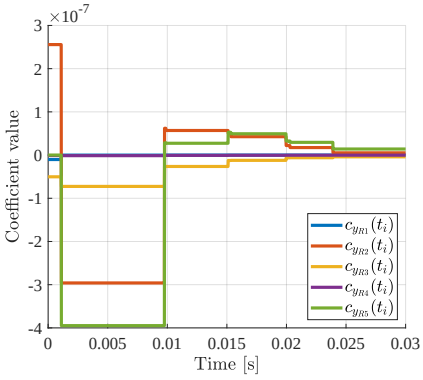

(b) $\omega_l = 291$ rad/s.

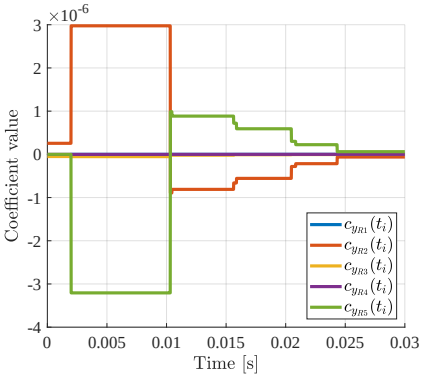

(c) $\omega_l = 811$ rad/s.

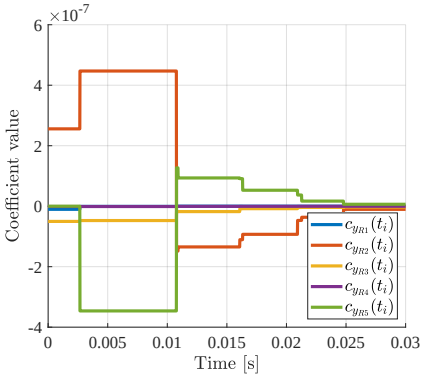

(d) $\omega_l = 2258$ rad/s.

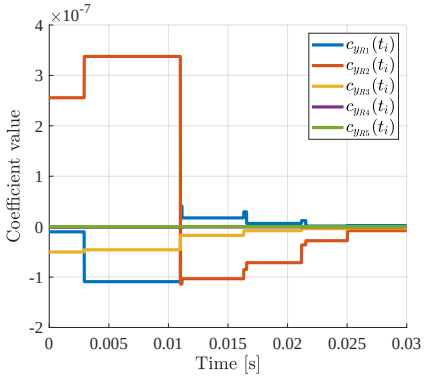

(e) $\omega_l = 6283$ rad/s.

Figure 8.8: Baseline coefficients for different ω_l values.

ing filter is applied. Earlier resets could be advantageous in limiting the plant energy in the first reset instance. When $\omega_l = \omega_f$ the resets will occur when $y(t_i) = r_0$. The late reset will inherently result in overshoot, since the system contains a slowly decaying os-

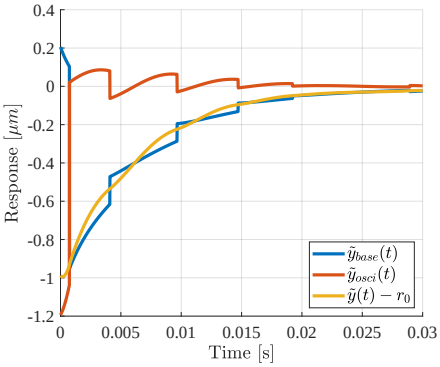

(a) $\omega_l = 105$ rad/s.

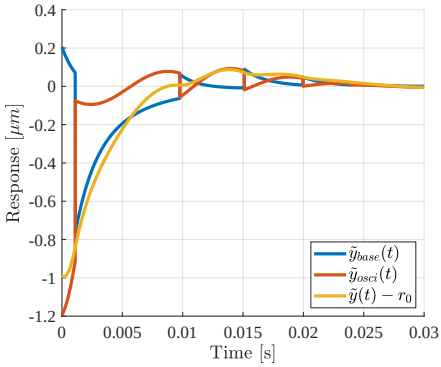

(b) $\omega_l = 291$ rad/s.

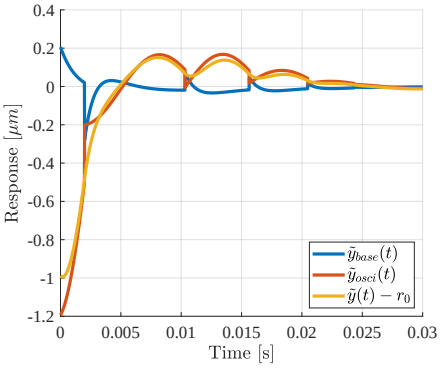

(c) $\omega_l = 811$ rad/s.

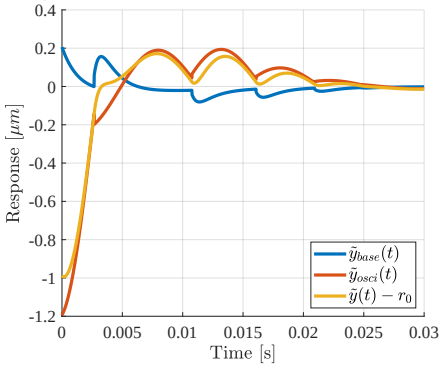

(d) $\omega_l = 2258$ rad/s.

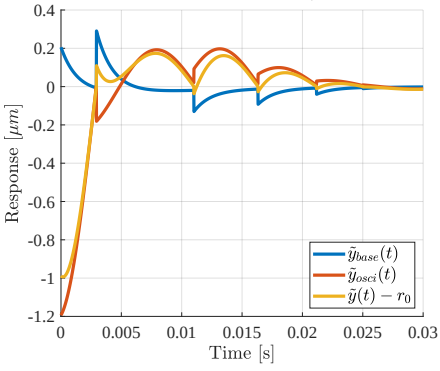

(e) $\omega_l = 6283$ rad/s.

Figure 8.9: Approximation of the step response $\tilde{y}(t)$ as the sum of the oscillatory term $\tilde{y}_{osci}(t)$ and the dominant baseline terms $\tilde{y}_{base}(t)$.

cillatory term. Therefore, implementing a shaping filter could be beneficial to reset the controller earlier when ω_l is close to ω_f. When more leads are in front of the reset element, earlier resets are expected, as the reset instances by approximation depend on the linear combination of the output and velocity response when $\omega_f \gg \omega_l$ [11]. Therefore, a

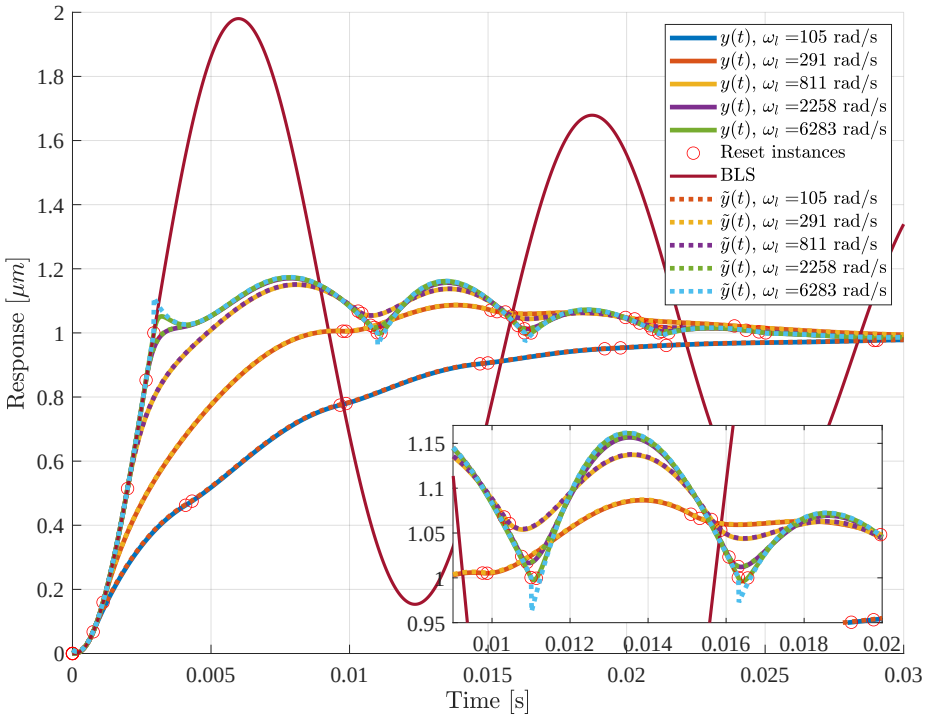

Figure 8.10: Approximation of the step response and the step response of CgLp-PID with mass plant system for different ω_l.

lower ω_l could be advantageous in limiting the amount of plant energy in the first reset instance when no shaping filter is present.

In line with Section 8.4.2, the acceleration coefficients $c_{\ddot{y}}$ are determined to analyze the dissipation of the energy of the controllers. The acceleration response of the CgLp-PID consists of one oscillatory term and five exponential baseline terms 8.79-8.81.

$$\ddot{y}(t) = r_0 + \ddot{y}_{osci}(t) + \ddot{y}_{base}(t), \qquad t \in \langle t_i, t_{i+1}] \tag{8.79}$$

In which,

$$\begin{aligned} \ddot{y}_{osci}(t) &= c_{\ddot{y}_{I12}}(t_i) e^{-29.8(t-t_i)} \\ &\quad \sin(492.4(t-t_i) + \psi_{\ddot{y}_{I12}}(t_i)), \qquad t \in \langle t_i, t_{i+1}] \end{aligned} \tag{8.80}$$

$$\begin{aligned} \ddot{y}_{base}(t) &= c_{\ddot{y}_{R1}}(t_i) e^{-6350.1(t-t_i)} \\ &\quad + c_{\ddot{y}_{R2}}(t_i) e^{-719.1(t-t_i)} + c_{\ddot{y}_{R3}}(t_i) e^{-98.8(t-t_i)} \\ &\quad + c_{\ddot{y}_{R4}}(t_i) e^{-62.8(t-t_i)} + c_{\ddot{y}_{R5}}(t_i) e^{-\omega_l(t-t_i)}, \\ &\quad t \in \langle t_i, t_{i+1}] \end{aligned} \tag{8.81}$$

Firstly, the sum of the coefficients in 8.67 determines the acceleration after reset. The sum of the different controllers is provided in Figure 8.11. The more lead there is after

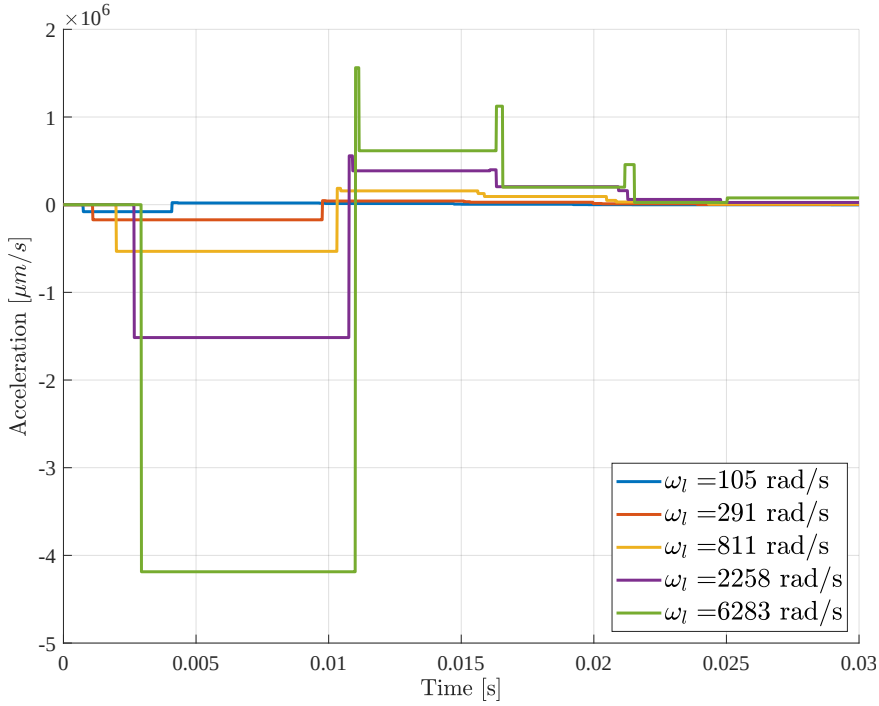

Figure 8.11: Acceleration after last reset for different ω_l.

the reset element, the more acceleration changes during reset. In the first reset, all controllers provide negative acceleration. Therefore, the controller immediately provides more damping during the first reset when ω_l is greater.

Moreover, the coefficient $c_{\ddot{y}_{I12}}$ determines the amplitude of the oscillations of the control power. The evolution of $c_{\ddot{y}_{I12}}$ for different ω_l can be seen in Figure 8.12. The more lead there is before the reset element, the more the oscillations are reduced. Note that the faster oscillation reduction can be partially attributed to the earlier reset for lower ω_l. However, the oscillations are also reduced less when the first reset is equal for all systems, as shown in Figure 8.7 in the previous section. In general, when more lead is after the reset element, oscillations in the power expression could cause the energy to increase again and cause overshoot.

Finally, the coefficients $c_{\ddot{y}_R}(t_i)$ determine the baseline acceleration response. The coefficients for the different lead placements can be seen in Figure 8.13. The significant coefficients for the acceleration response are $c_{\ddot{y}_{R1}}$, $c_{\ddot{y}_{R2}}$, and $c_{\ddot{y}_{R5}}$. Note that $c_{\ddot{y}_{R5}}$ is only significant when ω_l is large and represents a fast exponential term. The more lead is present before the reset element, the more dominant the faster exponential terms will become, suggesting a fast decay of power. Therefore, the higher ω_l, the faster the damping vanishes.

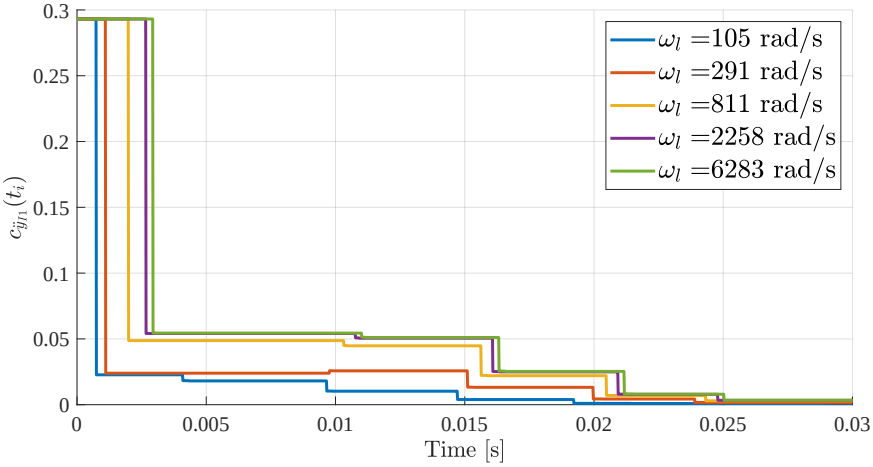

Figure 8.12: Oscillatory coefficient value for different ω_l.

In short, the damping of the CgLp-PID controller is expected to increase immediately after the first reset for a higher ω_l. However, the higher ω_l, the faster the baseline acceleration and power decay. Therefore, the lead after reset provides high but short damping. In contrast, lead before reset provides low but sustained damping. Moreover, more significant acceleration oscillations can cause overshoot due to the power becoming positive. Combined with the earlier reset, the step response will be damped more when ω_l.

The energy and power of the plant for different ω_l can be seen in Figure 8.14 and 8.15, which validates the conclusion of the coefficient analysis. Especially the late first reset and the oscillations in power cause the overshoot of the step response. Enough energy is dissipated only when ω_l is sufficiently low 8.78.

Both step response and energy analysis show that the oscillatory content is reduced the more lead is located before the reset element. The decrease in oscillations can be attributed to the reduction of higher-order harmonics in the open-loop frequency response of the system shown in Figure 8.16. The third and fifth harmonics are reduced in magnitude at the oscillation frequency $\beta = 492$ rad/s for lower values of ω_l, reducing the amplitude of the oscillations more at that frequency. In general, higher-order harmonics should be reduced at oscillation frequencies in the response (given by the imaginary part β of the complex eigenvalues) for the response to be more damped.

In short, the step response and energy analysis show that the system is more damped when more lead is located before the reset element, similar to what was found in [11], [21]. Therefore, the use of a lead-reset configuration in a CgLp-PID controller with a mass plant is beneficial in reducing and preventing overshoot. At the same time, the settling time remains approximately constant, as seen in Figure 8.4. Note that the rise

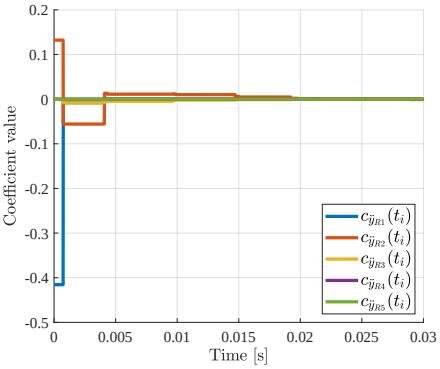

(a) $\omega_l = 105$ rad/s.

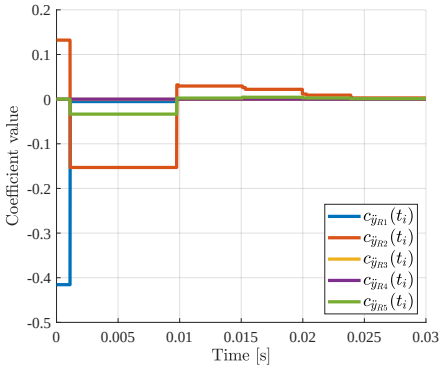

(b) $\omega_l = 291$ rad/s.

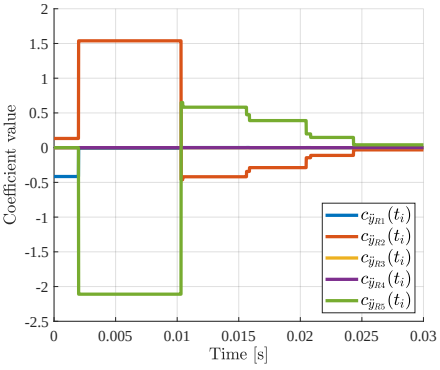

(c) $\omega_l = 811$ rad/s.

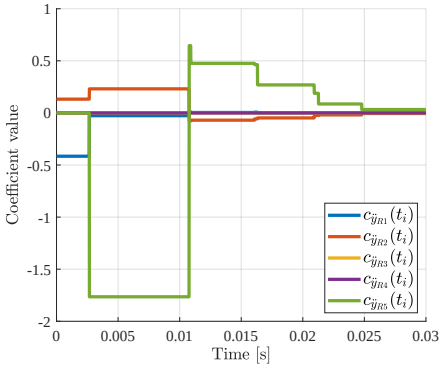

(d) $\omega_l = 2258$ rad/s.

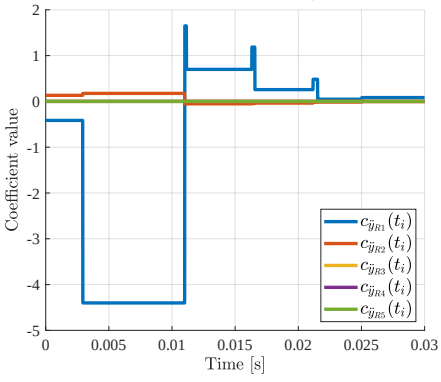

(e) $\omega_l = 6283$ rad/s.

Figure 8.13: Approximation of the step response $y(t)$ as the sum of the oscillatory term $y_{osci}(t)$ and the dominant baseline terms $y_{base}(t)$.

time will increase when more lead is placed before the reset. When a maximum rise time is required, placing more lead after the reset element could be beneficial.

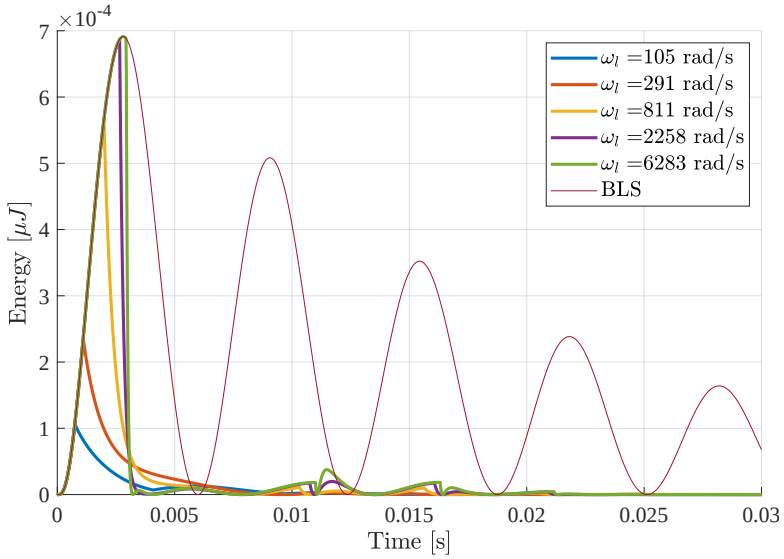

Figure 8.14: Plant energy of CgLp-PID with mass plant for different ω_l.

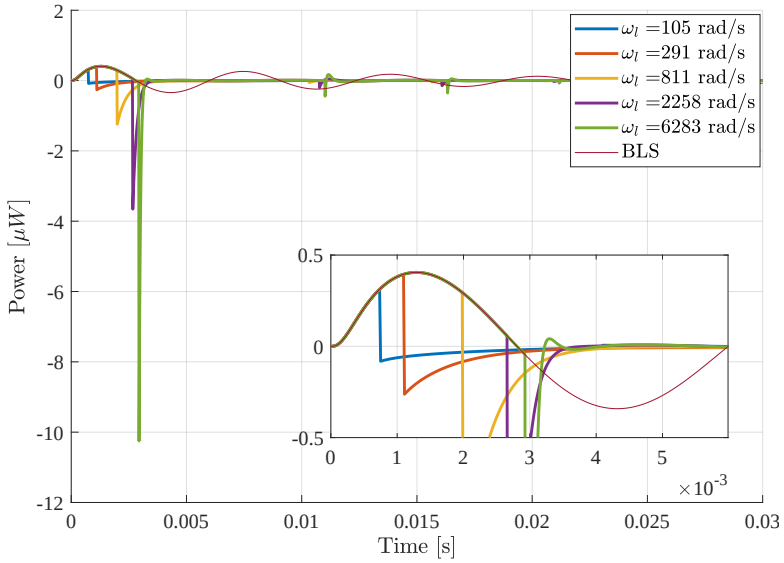

Figure 8.15: Controller power of CgLp-PID with mass plant for different ω_l.

8.6. CONCLUSIONS AND FUTURE WORK

The response of a reset control system depends on the exact controller configuration. Dependence on the controller sequence changes the damping of the response without influencing the first-order frequency response. Therefore, the amount of damping in

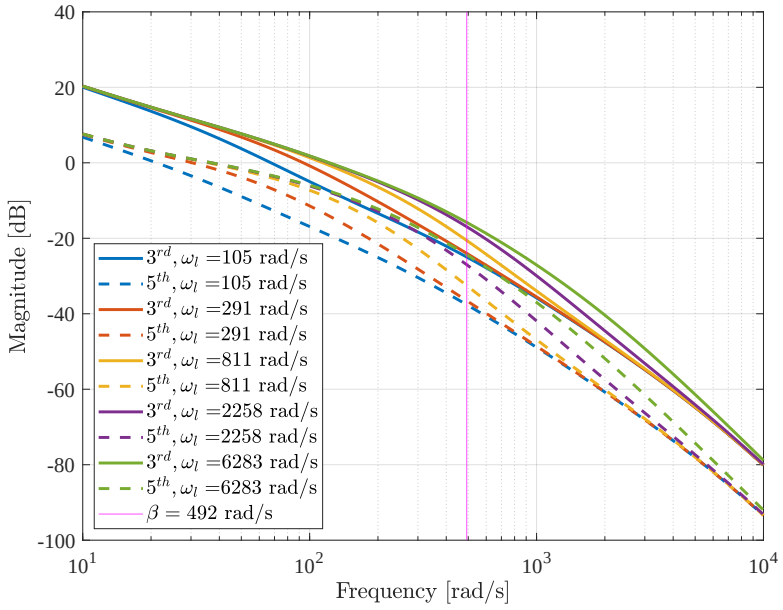

Figure 8.16: HOSIDFs of open-loop CgLp-PID with mass plant system for different ω_l.

a reset control system cannot be captured only with respect to the phase margin. Currently, the step response is calculated numerically to see the effect of different sequences of controller elements on the transient response. However, this does not provide insight into the underlying cause of the additional damping. This paper proposes an analytical approach to analyze the damping of the transient response of reset control systems that control a mass plant. The approach provides a method to explore how different controller configurations with the same control elements change the damping of the step response.

First, the step response and its derivatives are derived for reset control systems with mass plants. Analytical expressions are used to analyze the damping of the step response in reset control systems with stable base linear systems. By reducing the oscillatory terms and making the slower exponential terms more dominant, the damping of the step response can be increased. Additionally, analyzing the controller's energy dissipation can provide insight into the damping of the step response. By delivering sustained negative power, energy can be dissipated such that overshoot is prevented. Similar to the step response, oscillations should be reduced for the response to be damped.

To show the value of the proposed methods, the damping in a CgLp-PID controlling a mass plant is analyzed. It was shown that the damping of the step response could be increased by placing the CgLp lead element before the reset element, reducing oscillations faster and making slower exponential terms more dominant. The oscillation is reduced more, since the magnitude of the higher-order harmonics is lower at the oscillation frequency.

To use the proposed damping analysis methods, the base linear system should contain at least one integrator. When mass-spring-damper plants are considered, the analytical derivation should be altered or an additional integrator should be added. Moreover, the proposed energy analysis assumes the plant to be a single mass. More work is needed to extend this method to accommodate more complex plants.

Furthermore, this paper only provides insight into the underlying mechanics of damping in reset control systems. The CgLp-PID example shows that the reduction of higher-order harmonics at the response oscillation frequency increases the damping. More work is needed on how to design higher-order harmonics to enhance transient performance. The tuning of the reset instances, eigenvalues, and eigenvectors of the system should be considered when developing novel tuning guidelines.

Furthermore, more work is needed to gain insight into the dependence of damping on high-order harmonics. The added damping through the reduction of higher-order harmonics holds for the CgLp-PID example. A more rigid theory is to be formulated, which would offer the possibility of formulating new tuning guidelines for transient performance in reset control.

Finally, analytical expressions could provide a way to develop a novel way to define the stability of a reset control system. Stability could be guaranteed if a specific system decreases the overall energy of the system during reset instances. This would be especially interesting if stable reset systems with unstable BLS could be included since these are excluded when the H_β condition is used to assess stability properties [18].

BIBLIOGRAPHY

[1] R. Schmidt, G. Schitter, A. Rankers, and J. van Eijk, *The design of high performance mechatronics: high-tech functionality by multidisciplinary system integration*, 2nd revised. Netherlands: IOS Press, 2014, ISBN: 978-1-61499-367-4. DOI: 10.3233/978-1-61499-368-1-i.

[2] A. Baños and A. Barreiro, *Reset Control Systems*. London: Springer London, 2012, ISBN: 978-1-4471-2216-6. DOI: 10.1007/978-1-4471-2250-0.

[3] S.-K. Kuo, X. Shan, and C.-H. Menq, "Large travel ultra precision xy-/spl theta/motion control of a magnetic-suspension stage", *IEEE/ASME transactions on mechatronics*, vol. 8, no. 3, pp. 334–341, 2003.

[4] S.-K. Kuo and C.-H. Menq, "Modeling and control of a six-axis precision motion control stage", *IEEE/ASME transactions on Mechatronics*, vol. 10, no. 1, pp. 50–59, 2005.

[5] S. Mittal and C.-H. Menq, "Precision motion control of a magnetic suspension actuator using a robust nonlinear compensation scheme", *IEEE/ASME Transactions on Mechatronics*, vol. 2, no. 4, pp. 268–280, 1997.

[6] X. Shan, S.-K. Kuo, J. Zhang, and C.-H. Menq, "Ultra precision motion control of a multiple degrees of freedom magnetic suspension stage", *IEEE/ASME Transactions on mechatronics*, vol. 7, no. 1, pp. 67–78, 2002.

[7] J. C. Clegg, "A nonlinear integrator for servomechanisms", *Transactions of the American Institute of Electrical Engineers, Part II: Applications and Industry*, vol. 77, pp. 41–42, 1 Jul. 1958, ISSN: 0097-2185. DOI: 10.1109/tai.1958.6367399.

[8] I. Horowitz and P. Rosenbaum, "Non-linear design for cost of feedback reduction in systems with large parameter uncertainty", *International Journal of Control*, vol. 21, no. 6, pp. 977–1001, 1975, ISSN: 13665820. DOI: 10.1080/00207177508922051.

[9] L. Hazeleger, M. Heertjes, and H. Nijmeijer, "Second-order reset elements for stage control design", in *Proceedings of the American Control Conference*, vol. 2016-July, Institute of Electrical and Electronics Engineers Inc., Jul. 2016, pp. 2643–2648, ISBN: 9781467386821. DOI: 10.1109/ACC.2016.7525315.

[10] N. Saikumar, R. K. Sinha, and S. Hassan Hosseinnia, "'Constant in Gain Lead in Phase' Element-Application in Precision Motion Control", *IEEE/ASME Transactions on Mechatronics*, vol. 24, no. 3, pp. 1176–1185, Jun. 2019, ISSN: 1941014X. DOI: 10.1109/TMECH.2019.2909082.

[11] N. Karbasizadeh and S. H. HosseinNia, "Continuous reset element: Transient and steady-state analysis for precision motion systems", *Control Engineering Practice*, vol. 126, p. 105 232, 2022, ISSN: 0967-0661. DOI: https://doi.org/10.1016/j.conengprac.2022.105232. [Online]. Available: https://www.sciencedirect.com/science/article/pii/S096706612200106X.

[12] N. Karbasizadeh, N. Saikumar, and S. H. HosseinNia, "Fractional-order single state reset element", *Nonlinear Dynamics*, 2021, ISSN: 1573269X. DOI: 10.1007/s11071-020-06138-9.

[13] D. Valério, N. Saikumar, A. A. Dastjerdi, N. Karbasizadeh, and S. H. HosseinNia, "Reset control approximates complex order transfer functions", *Nonlinear Dynamics*, vol. 97, no. 4, pp. 2323–2337, Sep. 2019, ISSN: 1573269X. DOI: 10.1007/s11071-019-05130-2.

[14] Q. Chen, Y. Chait, and C. Hollot, "Analysis of reset control systems consisting of a fore and second-order loop", *J. Dyn. Sys., Meas., Control*, vol. 123, no. 2, pp. 279–283, 2001.

[15] O. Beker, C. Hollot, Q. Chen, and Y. Chait, "Stability of a reset control system under constant inputs", in *Proceedings of the 1999 American Control Conference (Cat. No. 99CH36251)*, IEEE, vol. 5, 1999, pp. 3044–3045.

[16] Y. Zheng, Y. Chait, C. Hollot, M. Steinbuch, and M. Norg, "Experimental demonstration of reset control design", *Control Engineering Practice*, vol. 8, no. 2, pp. 113–120, 2000.

[17] S. H. HosseinNia, I. Tejado, and B. M. Vinagre, "Fractional-order reset control: Application to a servomotor", *Mechatronics*, vol. 23, no. 7, pp. 781–788, 2013.

[18] O. Beker, C. V. Hollot, Y. Chait, and H. Han, "Fundamental properties of reset control systems", *Automatica*, vol. 40, pp. 905–915, 6 2004, ISSN: 00051098. DOI: 10.1016/j.automatica.2004.01.004.

[19] O. Beker, C. Hollot, and Y. Chait, "Plant with integrator: An example of reset control overcoming limitations of linear feedback", *IEEE Transactions on Automatic Control*, vol. 46, no. 11, pp. 1797–1799, 2001. DOI: 10.1109/9.964694.

[20] D. Wu, G. Guo, and Y. Wang, "Reset integral-derivative control for hdd servo systems", *IEEE Transactions on Control Systems Technology*, vol. 15, no. 1, pp. 161–167, 2006.

[21] C. Cai, A. A. Dastjerdi, N. Saikumar, and S. H. HosseinNia, "The optimal sequence for reset controllers", in *2020 European Control Conference (ECC)*, IEEE, 2020, pp. 1826–1833.

[22] S. Van den Eijnden, M. F. Heertjes, W. Heemels, and H. Nijmeijer, "Hybrid integrator-gain systems: A remedy for overshoot limitations in linear control?", *IEEE Control Systems Letters*, vol. 4, no. 4, pp. 1042–1047, 2020.

[23] P. W. Nuij, O. H. Bosgra, and M. Steinbuch, "Higher-order sinusoidal input describing functions for the analysis of non-linear systems with harmonic responses", *Mechanical Systems and Signal Processing*, vol. 20, no. 8, pp. 1883–1904, Nov. 2006, ISSN: 08883270. DOI: 10.1016/j.ymssp.2005.04.006.

[24] N. Karbasizadeh, A. A. Dastjerdi, N. Saikumar, D. Valerio, and S. H. HosseinNia, "Benefiting from Linear Behaviour of a Nonlinear Reset-based Element at Certain Frequencies", Apr. 2020. DOI: 10.1109/ANZCC50923.2020.9318363. [Online]. Available: http://arxiv.org/abs/2004.03529%20http://dx.doi.org/10.1109/ANZCC50923.2020.9318363.

[25] Q. Chen, *Reset control systems: Stability, performance and application*. University of Massachusetts Amherst, 2000.

[26] Y. Guo, L. Xie, and Y. Wang, *Analysis and Design of Reset Control Systems*. Institution of Engineering and Technology, 2015, ISBN: 1849197032.

[27] N. Saikumar, K. Heinen, and S. H. HosseinNia, "Loop-shaping for reset control systems: A higher-order sinusoidal-input describing functions approach", *Control Engineering Practice*, vol. 111, Jun. 2021, ISSN: 09670661. DOI: 10.1016/j.conengprac.2021.104808.

[28] Q. Chen, C. V. Hollot, Y. Chait, and O. Beker, "On reset control systems with second-order plants", in *Proceedings of the American Control Conference*, vol. 1, IEEE, 2000, pp. 205–209. DOI: 10.1109/acc.2000.878828.

A

MATRIX ENTRIES SYSTEM MATRIX RCS SYSTEM

The entries of the system matrices A_{cl} and B_{cl} can be derived for the general RCS in Figure 8.2 from 8.12-8.21.

$$A_{cl} = \begin{bmatrix} A_{cl11} & A_{cl12} & A_{cl13} & A_{cl14} \\ A_{cl21} & A_{cl22} & A_{cl23} & A_{cl24} \\ A_{cl31} & A_{cl32} & A_{cl33} & A_{cl34} \\ A_{cl41} & A_{cl42} & A_{cl43} & A_{cl44} \end{bmatrix}, \qquad B_{cl} = \begin{bmatrix} B_{cl1} \\ B_{cl2} \\ B_{cl3} \\ B_{cl4} \end{bmatrix} \tag{A.1}$$

where,

$$\begin{aligned} A_{cl11} &= A_r, & A_{cl12} &= B_r C_{c_1}, & A_{cl13} &= 0^{n_r \times n_{sf}}, & A_{cl14} &= -D_{c_1} B_r C_{c_2 p} \\ A_{cl21} &= 0^{n_1 \times n_r}, & A_{cl22} &= A_{c_1}, & A_{cl23} &= 0^{n_1 \times n_{sf}}, & A_{cl24} &= -B_{c_1} C_{c_2 p} \\ A_{cl31} &= 0^{n_{sf} \times n_r}, & A_{cl32} &= B_{sf} C_{c_1}, & A_{cl33} &= A_{sf}, & A_{cl34} &= -D_{c_1} B_{sf} C_{c_2 p} \\ A_{cl41} &= B_{c_2 p} C_r, & A_{cl42} &= D_r B_{c_2 p} C_{c_1}, & A_{cl43} &= 0^{n_2 \times n_{sf}}, & A_{cl44} &= A_{c_2 p} - D_{c_1} D_r B_{c_2 p} C_{c_2 p} \\ B_{cl1} &= D_{c_1} B_r, & B_{cl2} &= B_{c_1}, & B_{cl3} &= D_{c_1} B_{sf}, & B_{cl4} &= D_{c_1} D_r B_{c_2 p} \end{aligned} \tag{A.2}$$

B

PROOF TRANSFORM EQUALITY

In this appendix the proof of Lemma 3 is showed with intermediate steps

The Lemma states that systems 8.22 and 8.27 are equivalent under state transformation $\hat{x}(t) = x(t) - x_0$ when considering a constant reference for a system where $C_2P(s)$ contains at least 1 integrator.

Here, $x_0 = \begin{bmatrix} 0^{n-n_2} & x_{c_2p0} \end{bmatrix}^T$. Substituting the state transformation in the transformed system gives:

$$\begin{cases} \dot{x} - \dot{x}_0 = A_{cl}x(t) - A_{cl}x_0, & \text{if } u_{sf}(t) \neq 0 \quad \text{(B.1)} \\ x(t^+) - x_0 = \hat{A}_\rho x(t) - \hat{A}_\rho x_0, & \text{if } u_{sf}(t) = 0 \quad \text{(B.2)} \\ y(t) = C_{cl}x(t) - C_{cl}x_0 + r_0 & \quad \text{(B.3)} \\ u_{sf}(t) = C_{rline}x(t) - C_{rline}x_0 & \quad \text{(B.4)} \end{cases}$$

We rewrite each equation separately to find the system in 8.22.

Equation B.1 For the first equation, use the fact that $\dot{x}_0 = 0$ and that the expressions of the entries of A_{cl} are provided in Appendix A. Furthermore, use the equations in Lemma 2. Then we can rewrite the first equation of system 8.22 to:

$$\begin{aligned} \dot{x} &= A_{cl}x - A_{cl}x_0 \\ &= A_{cl}x + \begin{bmatrix} D_{c_1}B_rC_{c_2p} \\ B_{c_1}C_{c_2p} \\ D_{c_1}B_{sf}C_{c_2p} \\ -A_{c_2p} + D_{c_1}D_rB_{c_2p}C_{c_2p} \end{bmatrix} x_{c_2p0} \\ &= A_{cl}x + \begin{bmatrix} D_{c_1}B_r \\ B_{c_1} \\ D_{c_1}B_{sf} \\ D_{c_1}D_rB_{c_2p} \end{bmatrix} r_0 \end{aligned} \quad \text{(B.5)}$$

From Appendix A, the expression of B_{cl} can be retrieved:

$$B_{cl} = \begin{bmatrix} D_{c_1} B_r \\ B_{c_1} \\ D_{c_1} B_{sf} \\ D_{c_1} D_r B_{c_2 p} \end{bmatrix} \tag{B.6}$$

Therefore the first equation of systems 8.22 and 8.27 are equivalent.

Equation B.2 For equation B.2 it is straightforward, that $\hat{A}_\rho x_0 = 0$. Therefore, the second equation of systems 8.22 and 8.27 are equivalent.

Equation B.2 For the third equation, use the expression of C_{cl} in 8.23 and the equations in Lemma 2, to find that:

$$\begin{aligned} y(t) &= C_{cl} x(t) - C_{cl} x_0 + r_0 \\ &= C_{cl} x(t) - C_{c_2 p} x_{c_2 p 0} + r_0 \\ &= C_{cl} x(t) \end{aligned} \tag{B.7}$$

Therefore, the third equation of systems 8.22 and 8.27 are equivalent.

Equation B.4 For the fourth equation, use the expression of C_{rline} and D_{rline} in 8.23, and the equations in Lemma 2, to find that:

$$\begin{aligned} u_{sf}(t) &= C_{rline} x(t) - C_{rline} x_0 \\ &= C_{rline} x(t) + D_{sf} D_{c_1} C_{c_2 p} x_{c_2 p 0} \\ &= C_{rline} x(t) + D_{rline} r_0 \end{aligned} \tag{B.8}$$

Therefore, all the equations of systems 8.22 and 8.27 are equivalent. This proves that systems 8.22 and 8.27 are equivalent under state transformation $\hat{x}(t) = x(t) - x_0$.

9

IMPROVING THE NOISE ROBUSTNESS OF CONTINUOUS RESET CONTROL SYSTEMS

Reset control is able to achieve better performance than linear control. However, the lack of robustness to measurement noise prevents recently designed reset elements from being implementable in industry. The measurement noise present in the reset line creates excessive resets, which degrade the performance of the transient and steady-state reset controller. This paper presents a new control loop architecture that improves the robustness to the measurement noise of reset controllers. The proposed architecture consists of a separate feedback line for the reset condition, which is filtered by an observer. It is shown both theoretically and practically that the new architecture significantly improved performance compared to conventional reset controllers. The transient and steady-state performance of a CR CgLp-PID controller, including measurement noise, is improved, while preserving the robustness to parameter uncertainty. Stability conditions for the closed-loop based on the H_β-condition are given and simulation results are verified on an experimental setup.

9.1. INTRODUCTION

The high-tech sector is continuously improving the performance of its positioning systems. Currently, almost all control schemes are linear PID controllers with one or two additional linear filters. However, the desired performance exceeds the performance that can be reached by linear control. More specifically, Bode's integral theorem limits these controllers, as it creates a trade-off between disturbance rejection and noise attenuation on the one hand and robustness and transient response on the other. This concept is also known as the waterbed effect [1]. This trade-off is inherent for linear controllers;

The contents of this chapter is under preparation for submission. The second author is Tiis van der Werf. The author of this dissertation has contributed as the first author and to the supervision.

however, nonlinear control has the potential to remove this limitation. Consequently, nonlinear control can improve upon classical PID control.

Reset control has been studied as a nonlinear control method and can be utilized to further improve controller performance without large compromises [2]–[7]. For example, reset control can reduce overshoot and settling time, while also improving disturbance rejection [8]. To improve tracking, steady-state precision and bandwidth frequency, the 'Constant-in-Gain Lead-in-Phase' (CgLp) element can be added to linear controllers for an extra phase without the compromise of an increase in gain [9], [10]. Recently, the CgLp element was further improved in overshoot and settling time performance when used in a Continuous Reset (CR) structure [11]. In addition, this structure also provides a continuous controller output, which is more feasible for an actuator.

Some disadvantages of reset control and specifically CR structure remain unsolved, one of them being the robustness to measurement noise [11]. The measurement noise present in the reset line, i.e., the signal whose zero crossings determine the reset instants, can create unwanted excessive reset instants, which leads to performance deterioration. The lead filter used before the reset element in CR amplifies the high-frequency spectrum in the reset signal and worsens the problem [12].

Frequency filters such as Low-Pass Filters (LPF) have been suggested as a noise filter for reset control by using them on the reset line [11], [12]. Although the high-frequency noise is successfully reduced, the gain of the describing function (DF) and the phase of the system are negatively influenced. The regularization of the reset condition, which is initially used for preventing zenoness [13] can also be used to reduce the effect of noise on the measurement signal [14]. However, it was shown that sinusoidal tracking was only improved for a certain frequency band, leading to the investigation of observers, as they may have less influence on the DF and are not restricted in the frequency domain [15].

Disturbance and state observers have been widely used in industry to filter noisy measurements and improve system performance [16]–[18]. State observers have been used in combination with hybrid systems [19] and reset control in specific [20] to estimate hidden states. In addition, they can also be used to filter measurement noise. Since the high-tech industry requires high bandwidth frequencies for their motion stages, filters that depend on heavy, real-time calculations are not applicable. The static Kalman filter is a less complicated filter that does not require real-time parameter evaluations, so it remains a possible solution for high-tech systems.

This paper proposes a new control loop architecture that includes a separate feedback line for the calculation of the reset condition. A static Kalman filter is used on this separate feedback line to filter out the measurement noise. The aim is to improve the robustness of the reset control elements to measurement noise and to reduce excessive resets. An analysis of the transient and steady-state performance of the control loop is done in simulations and experiments.

The remainder of this paper is structured as follows. In Section 9.2 the preliminaries of the study are given. After this, the effect of measurement noise on reset control is shown in Section 9.3. The proposed loop architecture and its stability conditions are presented in Section 9.4 and an analysis on the closed-loop transient performance of the proposed architecture is done in Section 9.6.3. The closed-loop steady-state perfor-

mance is analyzed in section 9.6.4, and a practical example on a motion stage can be found in section 9.7. Finally, the conclusion of this paper is given in Section 9.8.

9.2. PRELIMINARIES

This section provides the preliminaries of the study.

9.2.1. RESET CONTROL

Reset control is a nonlinear form of control that most commonly relies on a zero-crossing reset law. A general state space form is written down in (9.1) as a Single Input Single Output (SISO) system. It behaves as a linear system for non-zero input $e(t)$. When the input crosses zero, the state is 'reset' by means of the A_ρ matrix. Generally, this matrix has a diagonal shape: $A_\rho = \text{diag}(\gamma_1, \gamma_2, ..., \gamma_n)$, with $\gamma_n \in [-1, 1]$. A reset time instance $t_k > 0$ is defined by $e(t_k) = 0$.

$$\sum_R : \begin{cases} \dot{x}_r(t) = A_r x_r(t) + B_r e(t) & \text{if } e(t) \neq 0, \\ x_r(t^+) = A_\rho x_r(t) & \text{if } e(t) = 0, \\ u_r(t) = C_r x_r(t) + D_r e(t). \end{cases} \tag{9.1}$$

The A_r, B_r, C_r, D_r matrices form the Base Linear System (BLS) of the reset control system and $e(t)$ and $u_r(t)$ are the input and output of the reset element, respectively.

9.2.2. DESCRIBING FUNCTION

nonlinear systems cannot be cast into a linear frequency domain function, which causes design difficulties as an approximation has to be made. A quasi-linearization method, called the sinusoidal input Describing Function (DF) is used to approximate the behaviour of nonlinear systems [21]. This allows industry to keep using loop-shaping method in frequency domain for the design of the nonlinear controllers. However, the DF method only takes into account the first-order harmonic of the Fourier series and neglects higher-order harmonics. Approximation using only the first order can be significantly inaccurate [22]. The Higher Order Sinusoidal Input Describing Function (HOSIDF) is used to calculate the higher-order harmonics of the output signal of nonlinear controllers. The HOSIDF method for reset elements defined by (9.1) was introduced by [23], [24] as:

$$H_n(\omega) = \begin{cases} C_r(j\omega I - A_r)^{-1}(I + j\Theta(\omega))B_r + D_r, & n = 1 \\ C_r(jn\omega I - A_r)^{-1} j\Theta(\omega) B_r, & \text{odd } n > 2 \\ 0, & \text{even } n \geq 2 \end{cases} \tag{9.2}$$

with,

$$\begin{aligned} \Theta(\omega) &= \frac{-2\omega^2}{\pi}\Delta(\omega)(\Gamma(\omega) - \Lambda^{-1}(\omega)) \\ \Lambda(\omega) &= \omega^2 I + A_r^2 \\ \Delta(\omega) &= I + e^{\frac{\pi}{\omega}A_r} \\ \Delta_r(\omega) &= I + A_\rho e^{\frac{\pi}{\omega}A_r} \\ \Gamma(\omega) &= \Delta_r^{-1}(\omega) A_\rho \Delta(\omega) \Lambda^{-1}(\omega) \end{aligned} \tag{9.3}$$

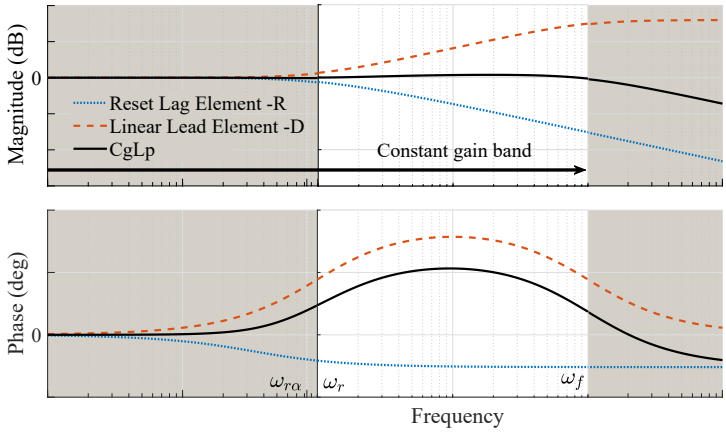

Figure 9.1: The concept of using combination of a reset lag and a linear lead element to form a CgLp element. The figure is from [9].

where $H_n(\omega)$ is the n^{th} harmonic describing function.

9.2.3. RESET ELEMENTS

Varying forms of reset elements can be described by the SISO system in (9.1). Reset control is originating from the resetting Clegg Integrator (CI) that was presented in [25]. The main advantage of adding the reset action is the increase in phase from $-90°$ to $-38°$, with almost no increase in gain. This property is mainly used to increase the phase margin of a system. Later, the Clegg integrator was combined with linear elements to form a PI+CI structure, which uses a CI and a PI in parallel where the ratio between the two can be tuned [26]. The First-Order Reset Element (FORE) was introduced in [27] and additionally the Second-Order Reset Element (SORE) was first presented in [3]. These elements behave like a first- and second-order LPF, respectively, and provide the same phase advantage as the Clegg integrator in a range of frequencies.

In [9] the FORE and SORE were combined with a linear (tamed) lead filter to form the CgLp structure. It achieves a broadband phase lead while keeping the gain constant, which is visualized by the bode plot in Fig. 9.1. The CgLp element has a constant gain in the frequency range $100-3000$ rad/s, while a phase lead of $15°$ is created. This would not be possible for linear control, as this behaviour does not adhere to Bode's gain-phase relationship. The general reset structure in (9.1) can be used to make a FORE-based CgLp if the matrices are chosen as in (9.4).

$$\begin{aligned} A_r &= \begin{bmatrix} -\omega_{r\alpha} & 0 \\ \omega_f & \omega_f \end{bmatrix}, B_r = \begin{bmatrix} \omega_{r\alpha} \\ 0 \end{bmatrix}, \\ C_r &= \begin{bmatrix} \frac{\omega_f}{\omega_r} & (1-\frac{\omega_f}{\omega_r}) \end{bmatrix}, D_r = [0], A_\rho = \begin{bmatrix} \gamma & 0 \\ 0 & 1 \end{bmatrix} \end{aligned} \tag{9.4}$$

Where $\omega_{r\alpha}$ is pole of the lag element, ω_r and ω_f are the zero and pole of the tamed lead element respectively. The CgLp element is used to partly replace the D action of the PID controller. For example, in [10] it is shown that the D action of the PID controller can be

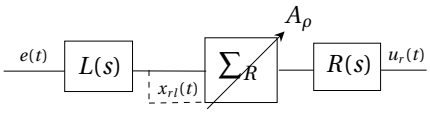

Figure 9.2: Block scheme of the CR structure [11]. Arrow indicates reset action.

minimal to ensure stability of the BLS, and that the major phase lead can be provided by the CgLp element to ensure the best performance.

9.2.4. CONTINUOUS RESET ARCHITECTURE

The previously mentioned reset elements all have a discontinuous output signal which creates practical problems when inputted to an actuator. Therefore, a different control architecture called “Continuous Reset" (CR) for reset elements was introduced to create a continuous output signal this architecture reduces the higher-order harmonics significantly while maintaining the favorable first-order harmonic [11]. Furthermore, the architecture significantly improves the transient response in terms of overshoot and settling time.

The CR structure consists of a lead filter, reset element, and a lag filter in series as shown by Fig. 9.2. The lead and lag filters presented in [11] are defined by (9.5).

$$L(s) = \frac{s/\omega_l + 1}{s/\omega_h + 1}, \quad R(s) = \frac{1}{s/\omega_l + 1} \tag{9.5}$$

If ω_h is chosen to be relatively large enough with respect to the bandwidth frequency, the CR lead and lag filters cancel each other and almost do not influence the DF of the controller. With the same assumption, one can approximate the reset law by

$$x_{rl}(t) = \dot{e}(t)/\omega_l + e(t) = 0. \tag{9.6}$$

It has been shown that the magnitude of higher-order harmonics is reduced by putting a reset element inside the CR structure. As a result, the first-order DF will be a better approximation of the actual controller and the result of the loop-shaping procedure is closer to ideal [11].

9.2.5. OBSERVER-BASED FILTERS

State estimators were introduced as a method to reconstruct hidden states of a process [28]–[30]. A state space system is used to estimate the process states and can also be used to filter out noise. Luenberger observer and a static Kalman filter are among the most known types which are very similar with slight difference in calculation of the gain. Such filters will be used further in this paper.

9.2.6. PSEUDO-SENSITIVITY

For linear systems, the sensitivity is defined by (9.7).

$$S = \frac{1}{1 + C(s)P(s)} \tag{9.7}$$

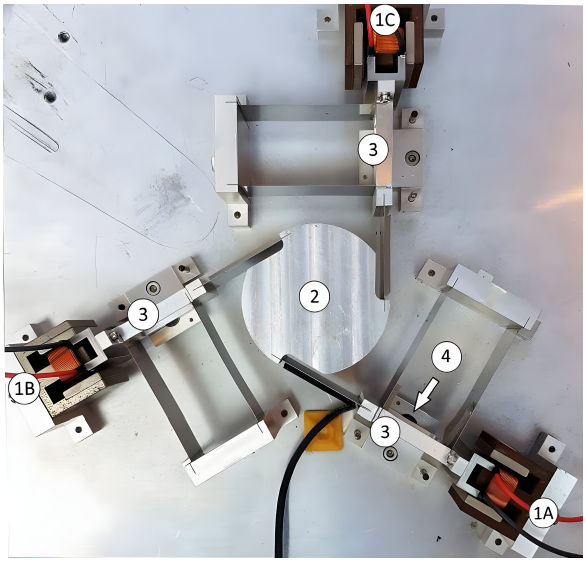

Figure 9.3: Three degrees of freedom planar precision positioning system called "Spider". Spider is actuated using three voice coil actuators indicated as 1A, 1B and 1C. The actuators are directly connected to masses indicated by 3. Each of these masses are solely connected to the base through two leaf flexures. The position of these masses are being sensed by linear encoders indicated by 4.

However, this does not hold for nonlinear controllers and a new definition is needed. In [24], the pseudo-sensitivity is defined as below.

$$|S_\infty(j\omega)| = \frac{\max\limits_{t>t_{ss}}|e(t)|}{|r(t)|} \tag{9.8}$$

where $r(t) = \sin(\omega t)$ and $e(t)$ are the reference and error, respectively. And t_{ss} is the first reset instant after steady state.

9

9.2.7. PLANT

The main application of this paper is precision motion control and most of the precision motion setups can be simplified and modeled as Mass-Spring-Damper (MSD) systems [11]. This paper will use precision positioning stage called "Spider" for numerical and practical study. Sipder is depicted in Fig. 9.3 is a 3 degrees of freedom planar positioning stage. Only the actuator 1A is used in this paper's SISO investigation to position the mass rigidly attached to it. The controllers are implemented at a sampling frequency of 10kHz using an NI compactRIO system with FPGA as the main controller. The voice coil actuator is driven by a linear current source power amplifier, and a Mercury M2000 linear encoder, shown as 4 in the Fig. 9.3 detects the mass's position with a resolution of 100 nm. The stage's FRF is recognized and displayed in Fig. 9.4. The identification reveals that the plant behaves similarly to a collocated double mass-spring-damper at high frequencies, with additional parasitic dynamics. The mass-spring-damper transfer

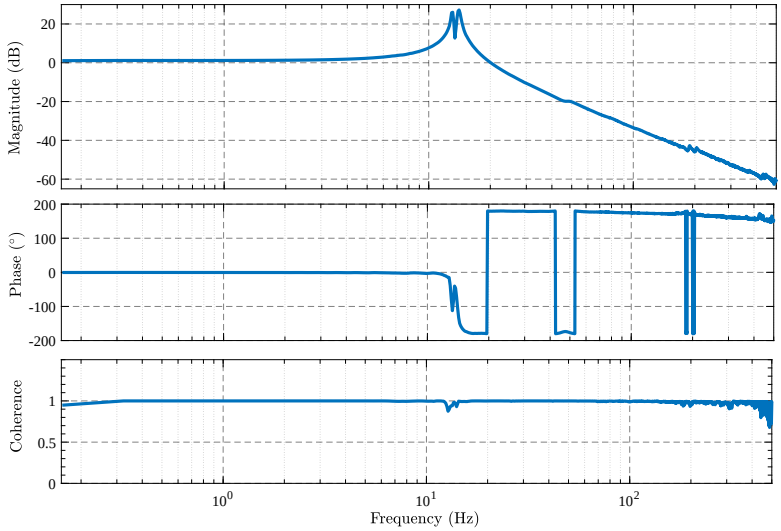

Figure 9.4: FRF identification of actuator 1A positioning the attached mass.

function which has been fitted to the FRF data shown in Eq. (9.9).

$$P(s) = \frac{8569e^{-0.0001s}}{s^2 + 5.329s + 7760} \tag{9.9}$$

9.3. EFFECT OF NOISE ON RESET CONTROL

Performance degradation due to measurement noise has been reported for various control loops. For linear control, it mostly degrades the steady-state positioning and tracking since the accuracy is only limited by the noise level, i.e., the accuracy cannot be increased beyond the signal to noise ratio (SNR). For reset control, the zero-crossing detection is affected by the noise as well, which introduces extra degradation of the performance.

When measurement noise is considered to be additive and white, similar results are observed when the reset instances t_k are altered. Moreover, the noise not only creates different but also extra, excessive zero crossings in the measurement signal. A sinusoidal error signal $e(t) = A\sin(\omega t)$ has two zero crossings per period at $t_k = \frac{\pi k}{\omega}$, $k = [1,2,3,...]$. One readily concludes that more zero crossings per period are found in the same signal with additive white noise $e(t) = A\sin(\omega t) + d(t)$, with $d(t) \approx N(0,R)$. Furthermore, excessive resets especially occur when the original signal is small relative to the noise variance and the original reset instants are not necessarily zero crossings anymore. Figure 9.5 shows the excessive resets for CR CgLp-PID and CgLp-PID controllers when a reference of 10 Hz is given. For the control loops without noise, periodic resets are seen. For the loops with noise, the reset condition is excessively activated. The difference between CR CgLp-PID and CgLp-PID can also be observed. The extra lead filter in the CR structure is amplifying high frequency content of the signal, causing even more resets than the CgLp-PID controller.

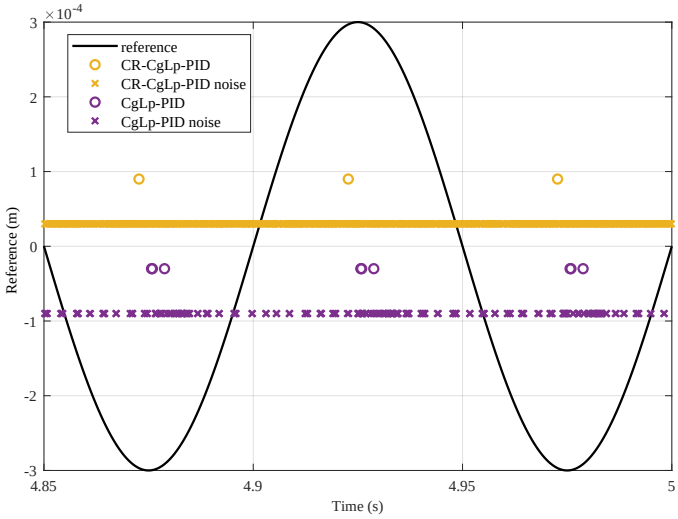

Figure 9.5: Reset instances of two controllers with and without white noise, $P_n = 2e^{-12}$ W, $\omega_{ref} = 10$ Hz.

An illustration of the effects of these excessive resets on the tracking performance is given in the pseudo-sensitivity plot in Fig. 9.6, in which a mass-spring-damper plant is controlled by a PID, a CgLp-PID, and a CR CgLp-PID controller. All three controllers were tuned to have the same phase margin of 40° at bandwidth frequency of 150 Hz. Additive white noise with $P_n = 2e^{-12}$ W and a reference amplitude of $A_{ref} = 300$ μm are used. Figure 9.6 shows that the response of the linear controller converges to the SNR of −46.5 dB for low frequencies. Note that the nonlinear controllers have an even higher minimum at low frequencies and therefore their performance is degraded more than that of linear controller.

A similar conclusion is drawn when the transient performance is analyzed. Figure 9.7 shows the step response for the same control loops with and without white noise. The step response of the PID controller is not affected by the noise, whereas both reset controllers perform worse when fed with noisy measurements. The CR CgLp-PID controller shows a large overshoot which decays very slow, making the controller unsuitable for practical implementations.

A couple of mitigations for these problems were proposed in literature. For quantization noise specifically, a time regularization has been proposed to avoid zenoness in reset control, which in fact caps the number of resets per a defined period of time [31]. Using an LPF to filter x_{rl}, general high-frequency noise can be removed [11], [12]. These mitigations were able to reduce the amount of excessive resets, but their main disadvantage is the phase increase in the DF of the Open Loop (OL). This conflicts with one of the main purposes of using reset controllers which was adding phase margin. To demonstrate the effect of using an LPF to filter x_{rl}, one can refer to [32] to find the equations for first- and higher-order harmonics. In case a transfer function, namely $F(s)$, is used on

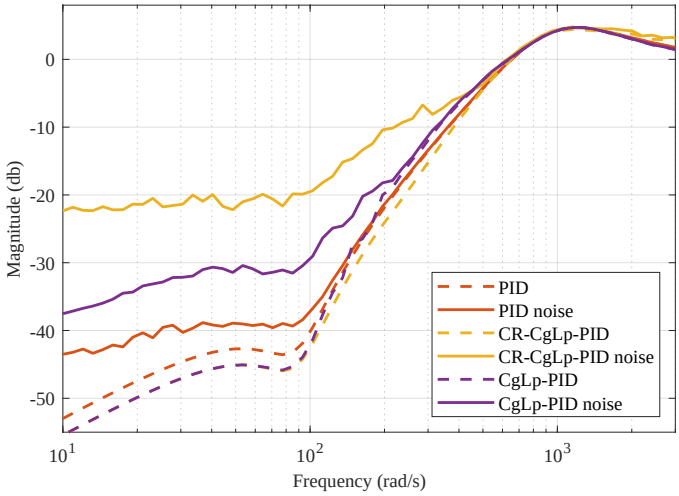

Figure 9.6: Pseudo-sensitivity of linear and nonlinear controllers with and without white noise, $P_n = 2e^{-12}$ W, $A_{ref} = 300\ \mu$m

the reset line, as shown in Fig. 9.8, the HOSIDF equations will change to [33]

$$
\begin{aligned}
G_{\varphi n}(\omega) &= \begin{cases} C_r(A_r - j\omega I)^{-1}\Theta_\varphi(\omega) \\ \qquad + C_r(j\omega I - A_r)^{-1}B_r + D_r, & n = 1 \\ C_r(A_r - j\omega n I)^{-1}\Theta_\varphi(\omega), & \text{odd } n > 2 \\ 0 & \text{even } n \geq 2 \end{cases} \\
\Theta_\varphi(\omega) &= \frac{-2j\omega e^{j\varphi}}{\pi}\Omega(\omega)\left(\omega I\cos(\varphi) - A_r\sin(\varphi)\right)\Lambda^{-1}(\omega)B_r, \\
\Omega(\omega) &= \Delta(\omega) - \Delta(\omega)\Delta_r^{-1}(\omega)A_\rho\Delta(\omega)
\end{aligned}
\tag{9.10}
$$

where $\varphi = \angle F(j\omega)$. In order to visualize the effects of having a LPF as $F(s)$, one can refer to Fig. 9.9. It is obvious that presence of a LPF as a shaping filter reduces the phase advantage of the reset element. As corner frequency of LPF is reduced the drop in phase advantage increases.

9

9.4. PROPOSED CONTROL LOOP ARCHITECTURE

As discussed in previous section, the main drawback of CR architecture originates from amplification of high-frequency content of x_{rl} signal which creates unwanted and excessive reset instants which in turn deteriorates the performance. In order to mitigate this problem, this paper proposes and studies two changes to the control loop which either can be used alone or in combination with each other to tackle the problem based on the noise level in different applications.

The first approach is to change the structure of $L(s)$ and $R(s)$. In the original CR architecture they are respectively first order lead and lag elements and the effect of the shifting their corner frequency on the performance of the system has been studied [11].

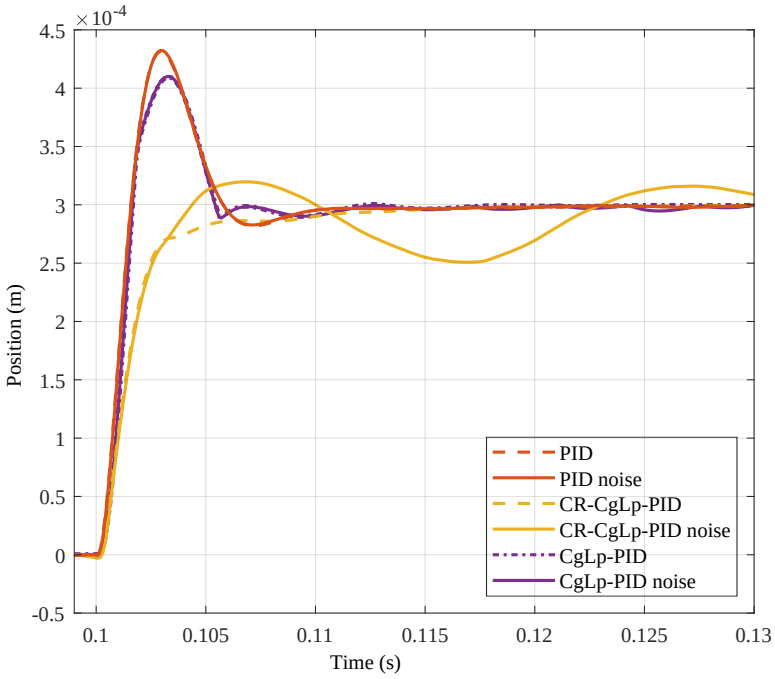

Figure 9.7: Step response of linear and nonlinear controllers with and without white noise, $P_n = 2e^{-12}$ W

It was there shown that by shifting the corner frequency of $L(s)$ to the left, overshoot reduces. However, from some point on, reducing the corner frequency would not decrease overshoot any further. From the studies in [11], one may conclude that the phase lead created by the lead element changes the reset instants which in turn reduces the overshoot. Nevertheless, such phase can be created by higher-order lead elements with less amplification of high-frequency content of the noisy reset signal. Figure 9.10 shows the concept.

The second approach is to use other filtering methods on x_{rl} which can effectively reduce the amount of noise without creating considerable phase lag. One of the well-known methods is to use observer-based filters such as Luenberger observer or static Kalman filter. In the literature, one of the main drawbacks for using such observers is the inaccuracy of the model used in the observer. However, in this study, such observers are used only to filter out the noise on x_{rl} and the main signal in the loop remains unaffected. It will shown that because only zero-crossings matter for x_{rl}, the effect of model-inaccuracy will be significantly lower.

Figure 9.11 shows the the overall proposed closed-loop architectures which includes both of the proposed changes. In this loop, The first-order lead and lag elements in CR architecture, namely, $L(s)$ and $R(s)$ are replaced with lead and lag elements of order $\lambda \in \mathbb{R}^+$. Furthermore, a separate feedback signal filtered by a static Kalman filter is used to recreate the reset signal, i.e., $x_{rl}(t)$. Based on the level of noise in the system, one may choose to either use this recreated reset signal or simply use an LPF. The following

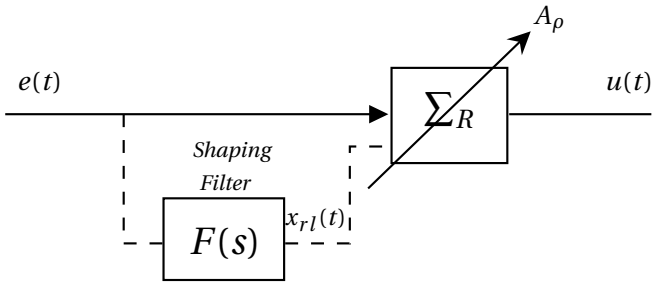

Figure 9.8: A reset element with shaped reset signal. The resetting action is determined by $x_{rl}(t)$ which is not equal to $e(t)$, i.e., the resetting condition is $x_{rl}(t) = 0$.

sections will study the proposed changes in more detail.

9.5. INCREASING THE ORDER OF $L(s)$ AND $R(s)$

This section proposes increasing the order of the lead and lag element used in CR architecture, namely, $L(s)$ and $R(s)$ to achieve phase lead required to improve the transient response with less amplification of higher frequencies. As shown in Fig. 9.10, having a maximum amplification, i.e., M_{max}, as a design parameter, one can achieve higher phase lead, i.e., P_{max} with higher-order lead element. In this paper, without loss of generality, $\lambda = 2$ will be studied as an example since it shows the significant enough improvement in practice.

9.5.1. SECOND-ORDER $L(s)$ AND $R(s)$

Having $\lambda = 2$, P_{max} is not only affected by ω_h/ω_l, but also by the damping factor of the second-order polynomials. Then one has

$$L(s) = R^{-1}(s) = \frac{\frac{s^2}{\omega_l^2} + \frac{2\zeta s}{\omega_l} + 1}{\frac{s^2}{\omega_h^2} + \frac{2\zeta s}{\omega_h} + 1}, \tag{9.11}$$

and thus obviously

$$M_{max} = \frac{\lim\limits_{\omega\to\infty} \left|L(j\omega)\right|}{\lim\limits_{\omega\to 0} \left|L(j\omega)\right|} = \frac{\omega_h^2}{\omega_l^2} \tag{9.12}$$

$$P_{max} = \angle L\left(j\omega_m\right) = \tan^{-1}\left(\frac{4\zeta\left(M_{max}^{1/4} - M_{max}^{-1/4}\right)}{2 - M_{max}^{1/2} - M_{max}^{-1/2} + 4\zeta^2}\right) \tag{9.13}$$

where $\omega_m = \sqrt{\omega_l\omega_h}$.

The main motivation in proposing this new change is to reduce ω_h/ω_l which will result in reduction of M_{max}. One may decrease ζ to compensate the effect of reduction of ω_h/ω_l on P_{max}. Nevertheless, both reduction of ω_h/ω_l and ζ result in narrower phase lead which makes the system less robust to gain variations.

Reduction of ω_h/ω_l will also become contrary to [11] where ω_h where suggested to be relatively large. Thus, the proposed modification prescribes some new investigations.

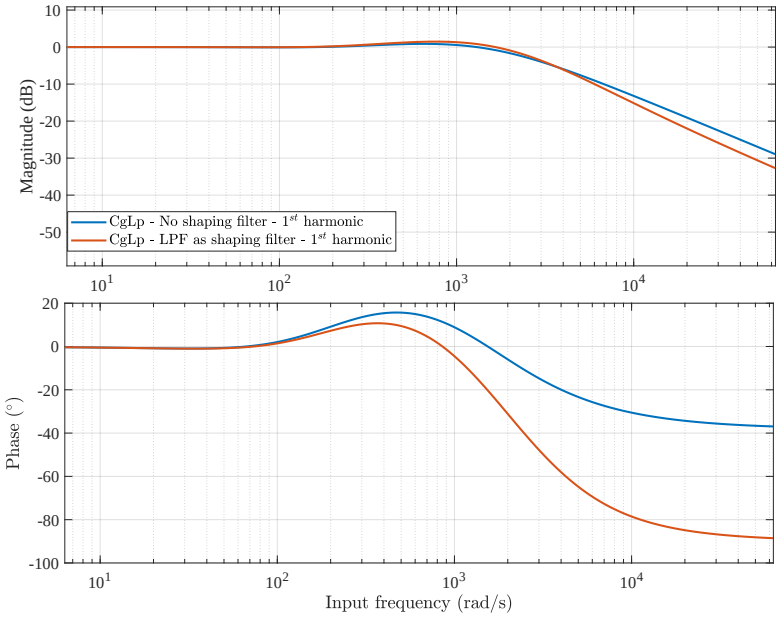

Figure 9.9: First-order harmonic comparison of a CgLp without shaping filter and one with $1/(s/\omega_{CO}+1)$ as shaping filter where $\omega_{CO} = 400$ Hz. For both CgLps, $\omega_r = 33$ Hz, $\omega_f = 240$ Hz, $\omega_{r\alpha} = 0.93\omega_r$ and $\gamma = 0$.

In the previous study, since ω_h was relatively large, only a sweep on ω_l was carried on numerically to see the effect on transient response of the system. However in new structure for $L(s)$, a study is needed to show the relation of P_{max} with transient response. For this purpose a numerical study by means of simulations is done. The simulations is done using Simulink environment of Matlab. In order to solely see the effect of change of parameters, the simulations has been done in the absence of noise. Thus, the control loop showed in Fig. 9.11 is used without any filtering of x_{rl}, i.e., no LPF nor observer-based filter is present. According to the guidelines presented in [11] and (9.11), the following is chosen for the design of the controller based on cross-over frequency, ω_c, of 150 Hz.

$$\sum_R = \frac{1}{s/\omega_{r\alpha}+1}\left(\frac{s/\omega_r+1}{s/\omega_f+1}\right)^{\gamma}, \tag{9.14}$$

$$C(s) = k_p\left(\frac{s/\omega_i+1}{s}\right)\left(\frac{s/\omega_d+1}{s/\omega_t+1}\right) \tag{9.15}$$

where

$$\omega_i = \omega_c/10, \quad \omega_d = \omega_c/a, \quad \omega_t = a\omega_c,$$
$$\omega_r = 1.2\omega_c, \quad \omega_f = 20\omega_r, \quad \omega_{r\alpha} = 1.2\omega_r,$$
$$\gamma = 0.$$

Since the nonlinearity of the system is desired around the bandwidth region [22], in this study $\omega_m = \omega_c$. Furthermore, without loss of generality by choosing $M_{max} = 15$ dB one will have $\omega_h/\omega_l = 2.37$. For the numerical study, a sweep is done on ζ and step response

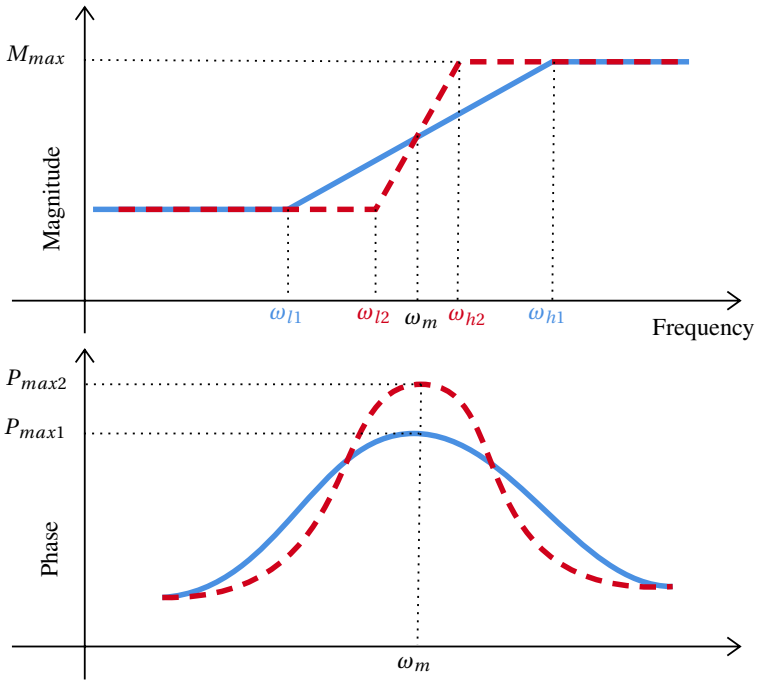

Figure 9.10: The concept of using higher-order lead element in CR CgLp to have less amplification of high-frequency content of noisy reset signal.

of the system is recorded. According to [11], since $R(s) = L^{-1}(s)$, the DF of the system will not change by the sweep, however the higher-order harmonics change. Figure 9.12 shows the open-loop Bode diagram of the BLS and HOSIDF of the overall reset control system for a CgLp-PID, a CR CgLp-PID with first-order $L(s)$ and $R(s)$ and two cases of second-order ones with $\zeta = 0.75$ and $\zeta = 2$. The last two correspond respectively to $P_{max} = 61°$ and $P_{max} = 25°$. The plant is introduced by (9.9) and $a = 1.5$ to stabilize the BLS and to satisfy $\omega_c = 150$ Hz, $k_p = 58$. The first-order harmonic of both cases are identical but as ζ changes the higher-order harmonics change slightly in middle-rage frequencies. The figure also shows that CR CgLp-PID with second-order $L(s)$ and $R(s)$ have higher-order harmonics comparable to original version of CR CgLp-PID with first-order filters. For CR CgLp-PID with first-order filters corner frequencies are set to satisfy $M_{max} = 15$ dB, that are $\omega_l = 63$ Hz and $\omega_h = 355$ Hz. Figure 9.13 shows the step response of the systems with various ζ. It is evident that decreasing ζ which results in increasing P_{max} decrease overshoot and settling time. It can be also seen in controller output signal that reset instants happens sooner when decreasing ζ. It is also revealed that with increasing P_{max}, lower overshoot can be achieved when compared to CR CgLp-PID with first-order $L(s)$ and $R(s)$.

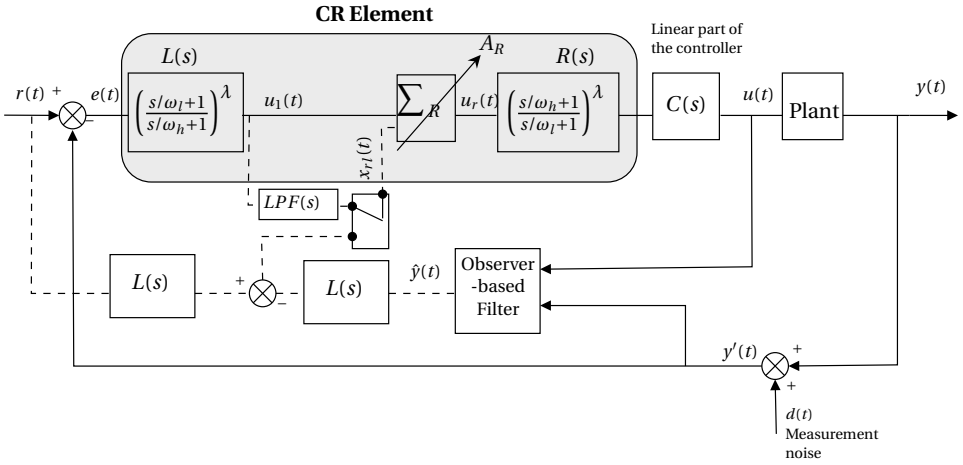

Figure 9.11: The concept of using higher-order lead element in CR CgLp to have less amplification of high-frequency content of noisy reset signal. $LPF(s) = 1/(s/\omega_{CO}+1)$.

9.5.2. VARIATION OF MSD PLANT

In order to verify if the trend shown in Fig. 9.13 holds for varied other MSD plants, a series of simulations is performed. To show the effect of variation of frequency and magnitude of resonance peak the transfer function of the plant is altered as follows

$$P(s) = \frac{8569e^{-0.0001s}}{s^2 + 5.329s + k_s} \tag{9.16}$$

where $k_s \in [1\ 1e4]$. The change in stiffness makes sure that the frequency and magnitude of the resonance peak of the plant is changed. However, for each k_s, k_p is changed to keep the bandwidth constant and thus other parameters of the controller has not been changed. Results show that the variation of plant while bandwidth and phase margin are constant has almost no effect on the overshoot and settling time.

The mitigating effect of increasing the order of $L(s)$ and $R(s)$ on noise problem of CR architecture, which is the main objective, will be also shown in a further section in an practical experiment.

9

9.6. OBSERVER-BASED FILTER

In this approach to reduce the effect of noise in CR structure, a separated feedback line is used for the reset signal of the CR CgLp-PID controller. This separate reset feedback line is filtered by an observer to reduce the amount of excessive resets by filtering the noise out of the measurement signal as shown in Fig. 9.11.

In this new loop architecture, the reset condition has changed from (9.6) to (9.17).

$$x_{rl}(t) = \dot{\hat{e}}(t)/\omega_l + \hat{e}(t) = 0 \tag{9.17}$$

where $\hat{e}(t) = r(t) - \hat{y}(t)$. The main motivation for this change is that the observer output $\hat{y}(t)$ is less deteriorated by the measurement noise than the plant output $y(t)$. While the reset feedback line is filtered by the observer, the general feedback line is kept intact. Noise is therefore still influencing the error that is fed to the controller. If the observer is

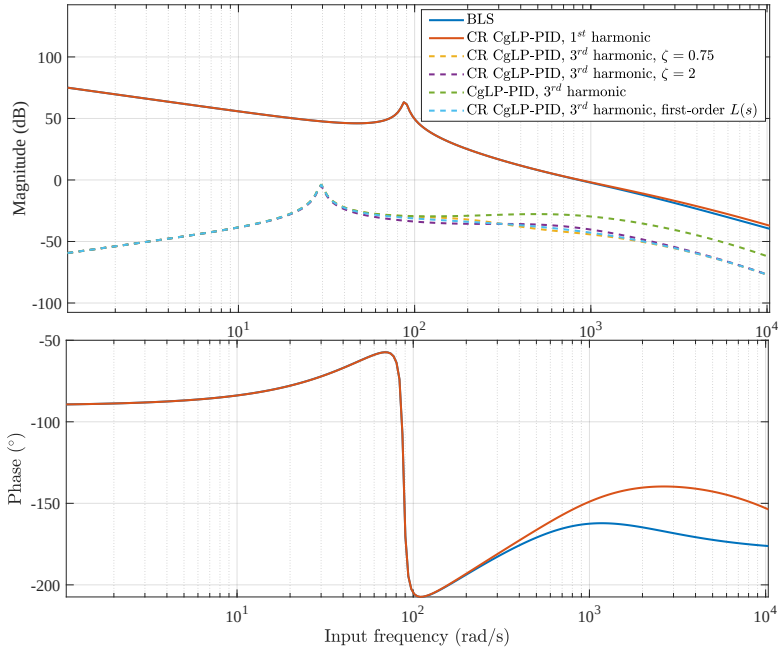

Figure 9.12: The open-loop Bode for BLS and HOSIDF of the overall reset control system for CgLp, CR CgLp with first-order $L(s)$ and $R(s)$ and second-order ones with $\zeta = 0.75$ and $\zeta = 2$. The last two correspond respectively to $P_{max} = 61°$ and $P_{max} = 25°$. First harmonic of all cases are identical.

also placed on the general feedback line, noise could be completely filtered out in theory. However, the dependence of the observer on the correctness of the state space matrices is critical. Wrong estimation of the parameters causes performance issues in that configuration. On the reset feedback line, only the zero-crossings are used to calculate the control output. It will be shown later that the proposed configuration is more robust to model inaccuracies.

9

9.6.1. STABILITY OF THE PROPOSED CONTROL LOOP

In this section stability conditions are given for the proposed control loop. The stability of reset control systems has been investigated thoroughly in literature [10], [24], [34]–[36]. Previous work is exploited to prove the stability for the proposed system. Consider the proposed architecture from Fig. 9.11 when it is switched to observer-based filter mode and let it be separated in a linear and a reset part. The reset part can be described by (9.18), with inputs $u_1(t), x_{rl}(t)$ and output $u_r(t)$.

$$\sum_R := \begin{cases} \dot{x}_r(t) = A_r x_r(t) + B_r u_1(t) & \text{if } x_{rl}(t) \neq 0, \\ x_r(t^+) = A_\rho x_r(t) & \text{if } x_{rl}(t) = 0, \\ u_r(t) = C_r x_r(t) + D_r u_1(t). \end{cases} \tag{9.18}$$

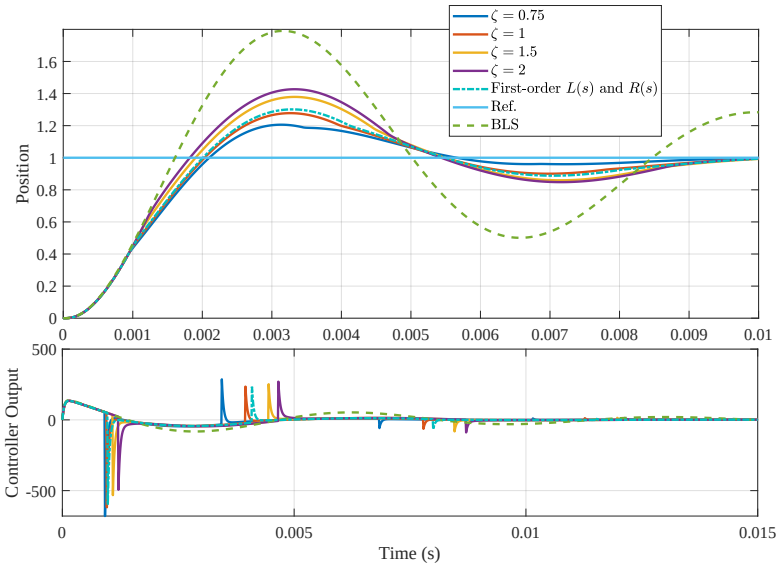

Figure 9.13: The step response for BLS and CR CgLp-PID, showing the effect of varying ζ on transient response.

The linear system is described by (9.19) with input u_r and $w(t) = \begin{bmatrix} r(t) & d(t) \end{bmatrix}$, and output y, x_{rl}, u_1 [24].

$$(\mathscr{L}): \begin{cases} \dot{\eta}(t) = A\eta(t) + B_u u_r(t) + B w(t) \\ y(t) = C\eta(t) \\ x_{rl}(t) = C_{rl}\eta(t) + D_{url} u_r(t) + D_{rl} w(t) \\ u_1(t) = C_1\eta(t) + D_{u1} u_r(t) + D_1 w(t) \end{cases} \tag{9.19}$$

In which η is containing the controller, plant, and observer states. Both systems can be combined to retrieve the closed-loop state space representation of the overall system that can be written as (9.20).

$$\begin{cases} \dot{x}(t) = \bar{A}x(t) + \bar{B}w(t) & \text{if } x_{rl}(t) \neq 0, \\ x(t^+) = \bar{A}_\rho x(t) & \text{if } x_{rl}(t) = 0, \\ y(t) = \bar{C}x(t) & \\ x_{rl}(t) = \bar{C}_{rl}x(t) + \bar{D}_{rl}w(t) & \end{cases} \tag{9.20}$$

where $x(t) = \begin{bmatrix} x_r(t)^T & \eta(t)^T \end{bmatrix}^T$, $\bar{A} = \begin{bmatrix} A_r + B_r D_{u1} C_r & B_r C_1 \\ B_u C_r & A \end{bmatrix}$, $\bar{B} = \begin{bmatrix} B_r D_1 \\ B_u D_1 \end{bmatrix}$, $\bar{C} = \begin{bmatrix} 0 & C \end{bmatrix}$, $\bar{C}_{rl} = \begin{bmatrix} 0_{1\times n_r} & C_{rl} \end{bmatrix}$, $\bar{D}_{rl} = D_{rl}$, $\bar{A}_\rho = \begin{bmatrix} A_\rho & 0 \\ 0 & I \end{bmatrix}$, and including that $D_p = D_r = D_{ue} = \mathbf{0}$.

When studying the stability of the unforced system by assuming $w(t) = 0$, it is concluded that $\hat{y} = y' = y$ if the observer matrices are matching the plant. If they differ from the actual plant state-space matrices, the well-posedness property of the reset instances are preserved if the observer is stable, implicating that all eigenvalues of the state transition matrix of the observer $(A_L - LC_L)$ are located in the left half plane.

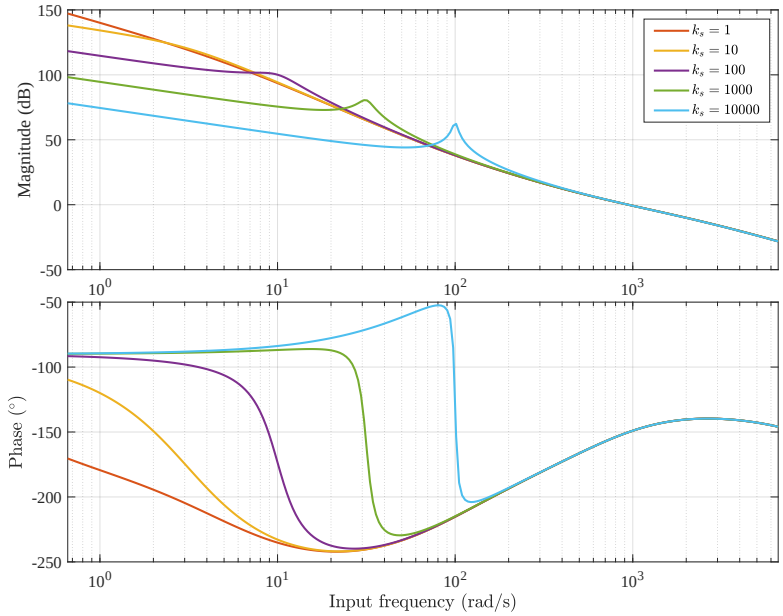

(a) Open-loop DF of the systems with plants with $k_s \in [1\ 1e4]$.

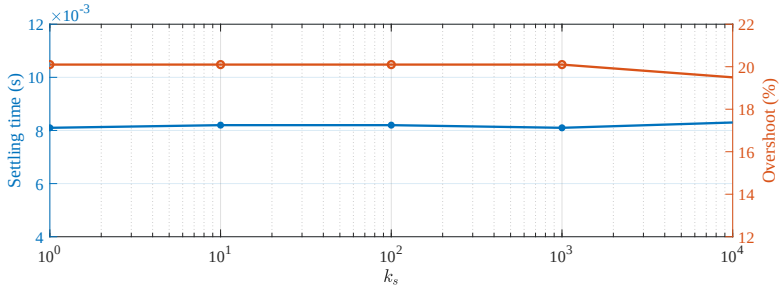

(b) Step response overshoot and settling time for systems with plants with $k_s \in [1\ 1e4]$.

Figure 9.14: Results of studying overshoot and settling time when the k_s of the plant is varying and bandwidth and phase margin are kept constant.

9

Hence, the quadratic stability can be guaranteed if the H_β condition is satisfied for the system without observer [24]. The H_β-condition can be used to prove that the zero equilibrium of the reset control system with $r(t) = w(t) = 0$ is quadratically stable [24], [35], [37]. The H_β-condition is briefly recalled in Theorem 1.

Theorem 11. *The unforced reset control system* (9.20) *is quadratically stable if and only if there exist* $\beta \in \mathbb{R}^{n_r \times 1}$ *and* $\rho = \rho^T > 0$, $\rho \in \mathbb{R}^{n_r \times n_r}$, *such that*

$$H_\beta(s) = C_0(sI - \bar{A})^{-1}B_0 \tag{9.21}$$

is strictly positive real (SPR), the set $(\bar{A}, B_0)$ *and* $\bar{A}, C_0$ *are controllable and observable re-*

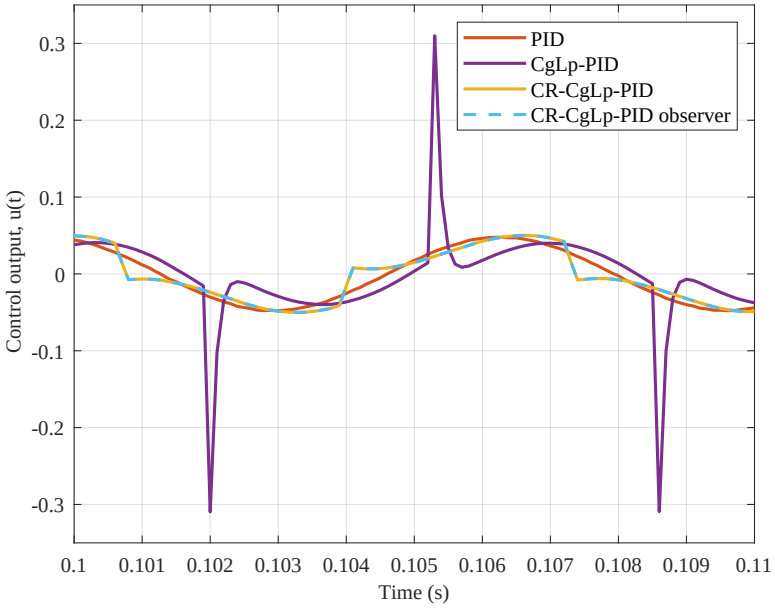

Figure 9.15: Control output of PID, CgLp-PID, CR CgLp-PID, and the proposed control loop to a sinusoidal reference, with $r(t) = 3e^{-4}\sin 942t$

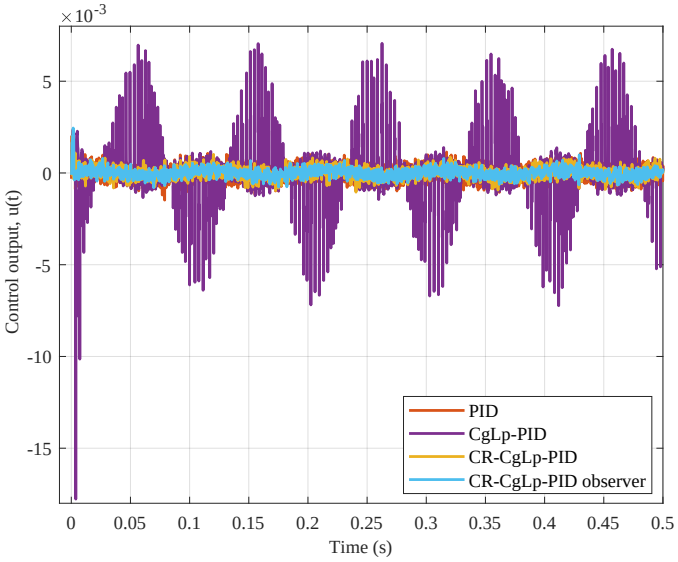

Figure 9.16: Control output of PID, CgLp-PID, CR CgLp-PID, and the proposed control loop to a sinusoidal reference, with $r(t) = 3e^{-4}\sin 63t$

spectively, with

$$C_0 = \begin{bmatrix} \rho & \beta C_{rl} \end{bmatrix}, B_0 = \begin{bmatrix} I_{n_r \times n_r} \\ 0_{n_p \times n_r} \end{bmatrix}, \rho = \rho^T > 0, \rho \in \mathbb{R}^{n_r \times n_r} \tag{9.22}$$

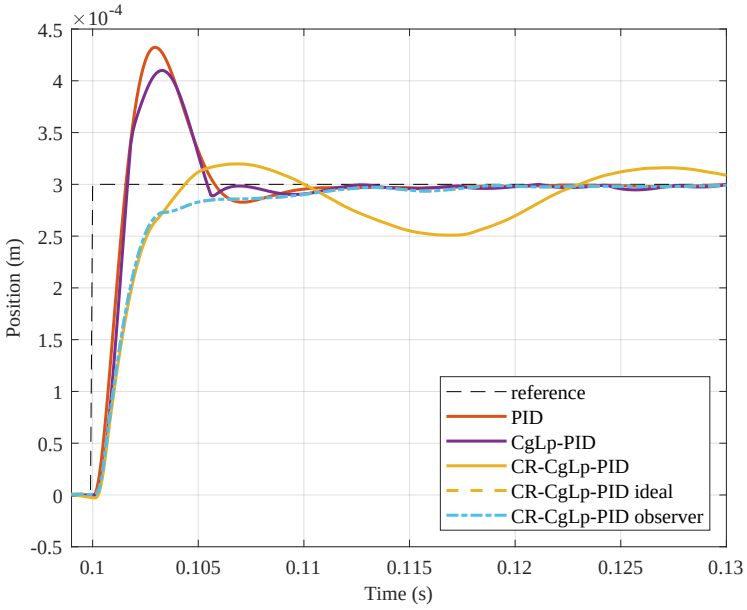

Figure 9.17: Step response of the proposed control loop with and without using an observer, white additive measurement noise with $P_n = 2e^{-12}$ W

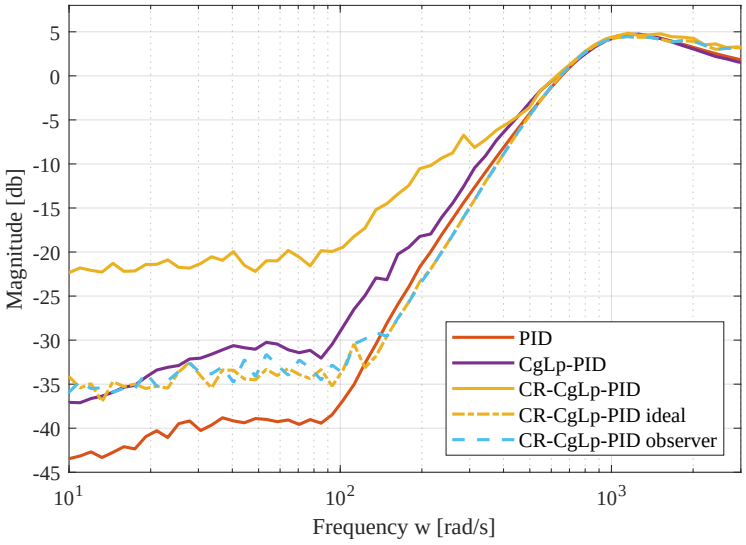

Figure 9.18: Pseudo-sensitivity of the proposed control loop with and without using an observer, white additive noise with $SNR = 46.5$ dB

and

$$A_\rho^T \rho A_\rho - \rho < 0. \tag{9.23}$$

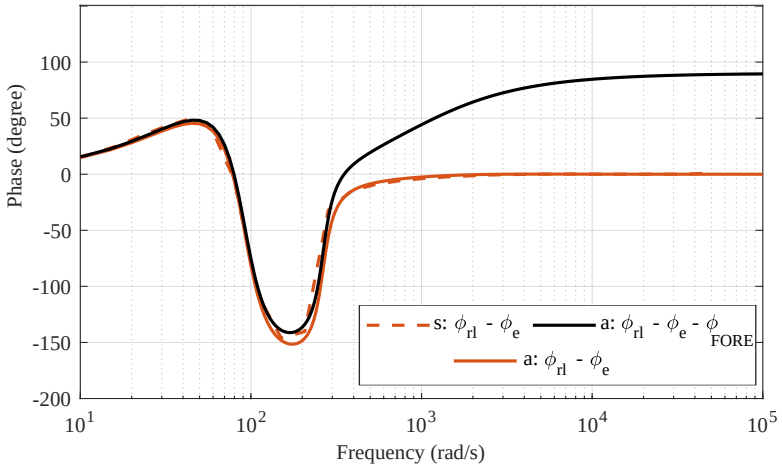

Figure 9.19: Phase shift in the error signals of the proposed control loop with model inaccuracy of $\omega_n = 1.05\omega_n$. Simulation results are denoted by *s*, analytical results denoted by *a*. $\phi_e = \angle E(j\omega), \phi_r l = \angle X_{rl}(j\omega), \phi_r l = \angle H_{1,FORE}(\omega)$.

Definition 1. *The reset control system (9.20) is uniformly bounded-input bounded-state (UBIBS) stable if for each $\sigma > 0$, there exists $\mu > 0$ such that for each initial condition x_0 and each bounded input $w(t)$, the solution $x(t, x_0, w)$ continues over $\mathbb{R}^+$ and*

$$\|x_0\| < \sigma, \quad \|w\|_\infty < \sigma \Rightarrow \|x(t, x_0, w)\| < \mu$$

for all $t \geq 0$.

Theorem 12. *For the system (9.20), when $w(t) \neq 0$, the system is UBIBS stable on the condition that the unforced system is quadratically stable and the H_β condition is satisfied.*

Proof. A similar approach as the proof of Lemma 2 in [38] can be used. A new system is defined as:

$$z(t) = x(t) - x_l(t), \tag{9.24}$$

in which $x_l(t) = \begin{bmatrix} x_{\rho l}^T(t) & \eta^T(t) \end{bmatrix}^T$ denotes the base linear system. The dynamics of $z(t)$ satisfy:

$$\begin{cases} \dot{z}(t) = \bar{A} z(t), & x_{rl} \neq 0 \\ z(t^+) = \bar{A}_\rho x(t) - x_l(t) & x_{rl} = 0 \\ x_{rl}(t) = \bar{C}_{rl} x(t) + \bar{D}_{rl} w(t). \end{cases} \tag{9.25}$$

Where $z(t) = \begin{bmatrix} z_{\bar{\rho}}^T(t) & z_\rho^T(t) \end{bmatrix}^T$. Here $z_{\bar{\rho}}(t)$ and $z_\rho(t)$ denote the states that are not reset and the states that are reset, respectively. Similar to [35], for UBIBS stability it is sufficient to show that $\|z_{\bar{\rho}}(t)\| + \|z_\rho(t)\|$ is bounded. Now the quadratic Lyapunov function $V(t) = z^T(t) P z(t)$ can be considered and used to conclude that $\|z_{\bar{\rho}}(t)\| + \|z_\rho(t)\|$ is bounded. Since H_β condition is satisfied one can find a $P = P^T$ such that

$$P = \begin{bmatrix} P_1 & (\beta C_{rl})^T \\ \beta C_{rl} & \rho \end{bmatrix} \tag{9.26}$$

with $P_1 > 0$. By using the KYP Lemma and the same procedure used in [35], it yields

$$V(t) \leq e^{\epsilon(t-t_i)} V(t_i^+), \quad t \in (t_i, t_{i+1}], \epsilon > 0. \tag{9.27}$$

Therefore one can consider the Lyapunov function at reset instance and then write

$$V(t) = z_{\tilde{\rho}}^T(t) P_1 z_{\tilde{\rho}}(t) + 2 z_{\rho}^T(t) \beta C_{rl} z_{\tilde{\rho}}(t) + z_{\rho}^T(t) \rho z_{\rho}(t) \tag{9.28}$$

Evaluating at $t = t_i^+$ we derive

$$\begin{aligned} V\left(t_i^+\right) = V(t_i) + x_r^T(t_i) \left(A_\rho^T \rho A_\rho - \rho\right) x_r(t_i) \\ + 2\left(A_\rho^T - I\right) x_r^T(t_i) \beta C_{rl} z_{\tilde{\rho}}(t_i) - 2 x_r^T(t_i) A_\rho^T \rho x_{\rho l}(t_i) \end{aligned} \tag{9.29}$$

Now, let the maximum eigenvalue of $A_\rho^T \rho A_\rho - \rho$ be λ_{max} and note that $\lambda_{max} < 0$ since $A_\rho^T \rho A_\rho - \rho < 0$. Now one can write

$$\begin{aligned} V\left(t_i^+\right) \leq & V(t_i) - |\lambda_{\max}| x_r^T(t_i) x_r(t_i) z_{\tilde{\rho}}(t_i) \\ & + 2\left(A_\rho^T - I\right) x_r^T(t_i) \beta C_{rl} - 2 x_r^T(t_i) A_\rho^T \rho x_{\rho l}(t_i) \Rightarrow \\ V\left(t_i^+\right) \leq & V(t_i) + 2\|x_r(t_i)\| \left(\left\| A_\rho^T - I \right\| \left\| \beta C_{rl} z_{\tilde{\rho}}(t_i) \right\| \right. \\ & \left. + \left\| A_\rho \rho x_{\rho l}(t_i) \right\| \right) \end{aligned} \tag{9.30}$$

Since the BLS is stable, one concludes that $\|x_{\rho l}(t_i)\|$ is bounded. Next it is shown that the term $\|\beta C_{rl} z_{\tilde{\rho}}(t_i)\|$ is bounded by recalling the reset condition at reset instance $x_{rl}(t_i^+) = \bar{C}_{rl} x(t_i^+) + \bar{D}_{rl} w(t_i^+) = 0$. Since the reset condition is not a function of the resetting states

$$-D_{rl} w(t_i^+) = C_{rl} x_{\tilde{\rho}}(t_i^+) = C_{rl} z_{\tilde{\rho}}(t_i^+) + C_{rl} x_{\tilde{\rho} l}(t_i^+). \tag{9.31}$$

Thus,

$$\|C_{rl} z_{\tilde{\rho}}(t_i^+)\| \leq \|D_{rl} w(t)_i^+\| + \|C_{rl} x_{\tilde{\rho} l}(t_i^+)\|. \tag{9.32}$$

Since the input $w(t)$ is bounded by definition, and again $\|x_{\tilde{\rho} l}(t)\|$ is bounded because the BLS is stable, we conclude that $\|C_e z_{\tilde{\rho}}(t)\|$ is bounded as well. The rest of the proof including the boundedness of $\|x_\rho(t)\|$ is already done in [38]. □

Since the stability conditions are derived, the rest of the paper focuses on the performance of the proposed control loop.

9.6.2. CONTROLLER OUTPUT

For the sake of comparison with respect to conventional CgLp, CR CgLp and PID controllers, a numerical simulation in Simulink is performed. Fig. 9.16 shows the controller output $u(t)$ for a sinusoidal reference of $r(t) = 3e^{-4}\sin(10\pi t)$. White noise with $P_n = 2e^{-12}$ W is added to the measurement, $y' = y + d(t)$, and observer gain are calculated using Ricatii equations based on this noise power. It should be noted that in this simulation $L(s)$ and $R(s)$ are first order filters.

It can clearly be seen that the power output of the CR-based structures is much less than the CgLp only. Furthermore, the proposed architecture also improves upon the conventional CR CgLp-PID and PID loops. The new architecture with observer has a RMS value of $2.3e^{-4}$ whereas the CR CgLp-PID and PID controllers output a signal with RMS $2.8e^{-4}$ and $3.6e^{-4}$, respectively. It is mainly because of omission of excessive resets created by noise.

Figure 9.15 shows the control signal when a reference of $r(t) = 3e^{-4}\sin(150\pi t)$ is given to the system. At this bandwidth frequency, where the higher-order harmonics are their

maximum amplitude, it is seen that the sharp peaks in the control output are removed when using a CR structure. The output of the CR structure is much smoother than the CgLp controller. The proposed control loop therefore has lower higher-order harmonics than the CgLp-PID controlled loop. It was also previously shown in [11]. In addition, the observer-based control loop shows the same response as the conventional CR CgLp-PID controlled loop.

9.6.3. CLOSED-LOOP TRANSIENT PERFORMANCE

In this section the closed-loop transient performance is analyzed by numerical simulations.

Consider the closed-loop system as shown in Fig. 9.11, including white additive sensor noise $d(t)$ with noise power $P_n = 2e^{-12}$ W. The proposed control loop is compared with a standard PID controller and a CgLp-PID controller which are tuned for the same bandwidth frequency of 150 Hz and phase margin of 40°. The observer is implemented is a static Kalman filter for which the gains are calculated using Ricatii equation.
The step response of the control loops can be seen in Fig. 9.17. For comparison, an ideal case is added in which no noise is added to the reset feedback line. The observer-based control loop removes the large overshoot and oscillations that were caused by the measurement noise. Besides this, the settling time is decreased drastically with respect to the other controllers. There is almost no difference between the ideal case and the proposed control loop, which implicates that the observer is correctly filtering the measurement signal.

9.6.4. CLOSED-LOOP STEADY-STATE PERFORMANCE

In this section, the closed-loop steady-state performance is analyzed by numerical simulations.

Considering the same loops with the same added noise, a sinusoidal reference with amplitude $A_{ref} = 300\ \mu$m, was used to generate the pseudo-sensitivity plot in Fig. 9.18. At lower frequencies where the error to noise ratio is lower, the pseudo-sensitivity was approximately below bounded by −23 dB for CR CgLp-PID. This is reduced when using the observed-based filtering of the reset line to −36 dB. Again the proposed control loop is also compared to a control loop in which the reset feedback line is not deteriorated by noise. It can be seen that by using the observer a similar performance can be obtained as the ideal case.

9.6.5. OBSERVER MODEL INACCURACY

The previous simulations shows the possible improvements of the transient performance, but it remains an ideal case since the state space matrices of the observer are exactly matching the plant process. Therefore, a non-ideal case is considered in which the state space matrices of the observer and the actual plant process are intentionally mismatched. The observer is only acting on the signal that determines the reset instants (reset line) and not the main signal of the control loop and reset instants are determined by zero-crossings of the reset line. It means that any gain inaccuracy in the model will have no impact on performance of the control loop as it does not change the zero-crossings. However, phase inaccuracy does have an impact which will be investigated in this sec-

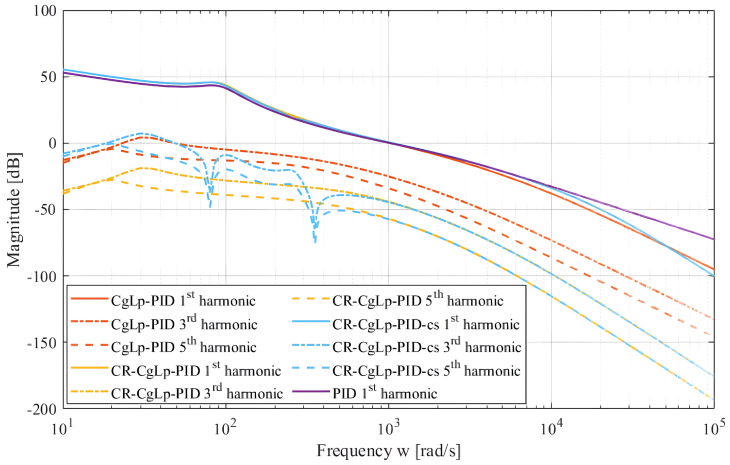

Figure 9.20: Open-loop bode plot of the proposed control loop with higher-order harmonics, and with approximated shaping filter

tion. This investigation is done through simulation for transient response and for the steady-state analysis and analytical approximation approach is presented.
to the CR CgLp-PID controller in ideal case.

In order to integrate the effect of the phase inaccuracy of the observer in the sensitivity analytically, a new open loop is calculated using shifted reset instants. With this method, the DF of the open loop can be calculated using the HOSIDF methods in (9.10).

The phase inaccuracy can be approximated by the phase difference of the error and the reset line in the observer-based control loop as described by (9.33).

$$\Delta\phi = \phi_{x_{rl}} - \phi_e \tag{9.33}$$

Both phases can be calculated with respect to the input $r(t)$ by means of the transfer functions (9.34) and (9.35). In these transfer functions, the reset system (9.18) is approximated by its BLS and the noise is assumed to be zero.

$$e(t) = r(t) - y(t) = \left(1 - \frac{Y(s)}{R(s)}\right) r(t) \tag{9.34}$$

$$x_{rl}(t) = r(t) - \hat{y}(t) = \left(1 - \frac{\hat{Y}(s)}{U(s)} P(s)^{-1} \frac{Y(s)}{R(s)}\right) r(t) \tag{9.35}$$

Fig. 9.19 shows the phases of the two error signals and their difference for 5% shift in resonance frequency. Simulation results are also included. Using this phase shift, an open-loop HOSIDF is calculated for this model inaccuracy.

An increase in higher-order harmonics is caused by the observer with model inaccuracy, as can be seen in Fig. 9.20. The notches in the higher-order harmonics can be explained by analyzing the difference between $\Delta\phi$ and the phase of the reset element. This is visualized by the black line in Fig. 9.19. The notches are created when the reset instances coincide with the zero-crossings of the state, and as a result the state is reset from zero to zero. This happens if the phase difference between the FORE element and the shaping filter is equal to an integer multiple of π. In those cases, the system behaves

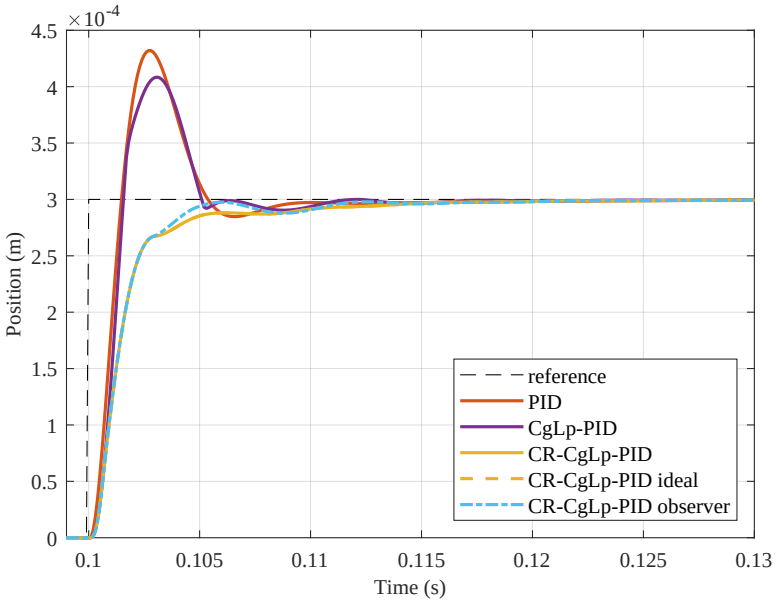

Figure 9.21: Step response of the proposed control loop with and without using an observer, in which $\omega_n = 1.05\omega_n$

entirely linear as the resets do not affect the output and the higher-order harmonics are therefore zero [22]. For the same inaccuracy in resonance frequency is applied to study the its effect on transient response. No noise is added to the simulations to clearly isolate the effects of the model mismatch. It can be seen in Fig. 9.21 that the step response of the observer-based system shows a slight increase in overshoot due to the model mismatch, but the performance remains very similar with respect

9.7. EXPERIMENTAL EXAMPLE

An experiment is designed and performed to verify and study the previous discussions in the paper in practice. In this experiment the same plant as described in 9.2.7 is being controlled with 4 different controllers, namely

1. PID
2. CR CgLp-PID with first order $L(s)$ and $R(s)$ with an LPF on the reset line (CRLPF1)
3. CR CgLp-PID with second order $L(s)$ and $R(s)$ with an LPF on the reset line (CRLPF2)
4. CR CgLp-PID with second order $L(s)$ and $R(s)$ with an observer-based filter on the reset line (CRob)

All the controllers are designed for a cross-over frequency of $\omega_c = 150$ Hz and a phase margin of 40°. The parameters for the controllers and the Bode plot for the PID and HOSIDF for nonlinear controllers are presented in Table 9.1 and Fig 9.22.

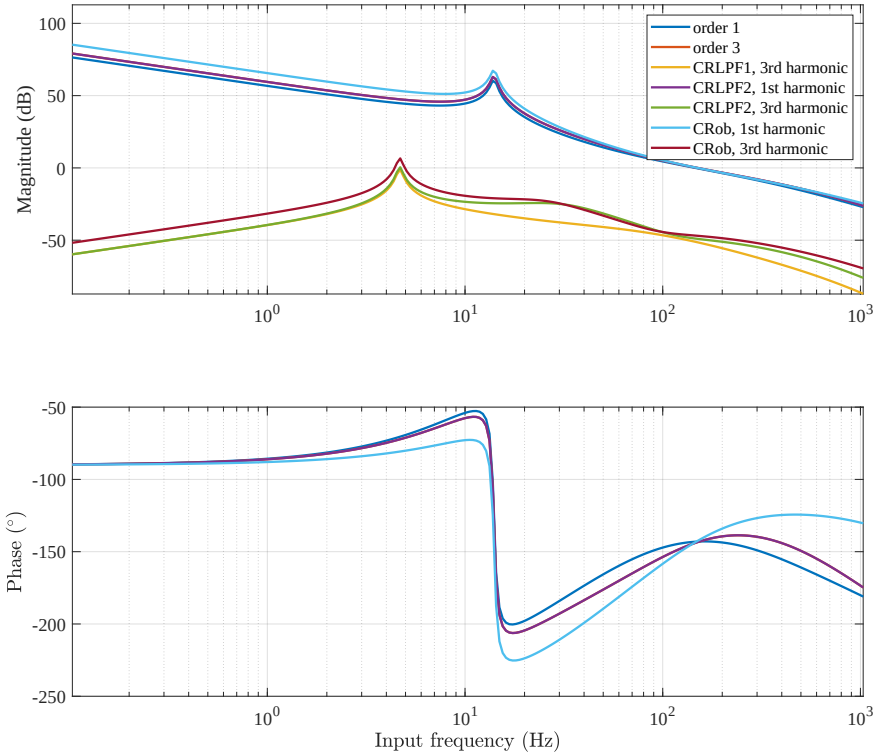

Figure 9.22: Open-loop Bode plot and HOSIDF of the designed controllers for the experiment.

Table 9.1: The parameters of designed controllers for experiments. ω_c = 150 Hz. γ for all nonlinear controllers is -0.3.

Parameter	ω_i	ω_d	ω_t	ω_{CO}	ω_r	ω_l	ω_h	ω_f	λ	ζ
PID	$\omega_c/10$	$\omega_c/2.5$	$2.5\omega_c$	N/A	N/A	N/A	N/A	N/A	N/A	N/A
CRLPF1	$\omega_c/10$	$\omega_c/1.5$	$1.5\omega_c$	$5\omega_c$	ω_c	$\omega_c/7$	$7\omega_c$	$20\omega_c$	1	N/A
CRLPF2	$\omega_c/10$	$\omega_c/1.5$	$1.5\omega_c$	$5\omega_c$	ω_c	$\omega_c/2$	$2\omega_c$	$20\omega_c$	2	0.5
CRob	$\omega_c/5$	$\omega_c/1.5$	$1.5\omega_c$	N/A	ω_c	$\omega_c/2$	$2\omega_c$	$20\omega_c$	2	0.5

As shown and discussed in Fig. 9.9, because of the presence of LPF on the reset line for CRLPF1 and CRLPF2, the phase margin for these controllers decreases. Since observer-based controller (CRob) does not suffer from this phase loss and in order to have a fair comparison between controllers in terms of phase margin, CRob is designed to have a stronger integrator.

The response of the controllers for a step of 30 μm and their corresponding controller output is depicted in Fig. 9.23. All of the controllers show improved step response compared to convectional CR CgLp with the level of noise present. Although all are comparable in terms of transient response, their steady-state performance is different which is

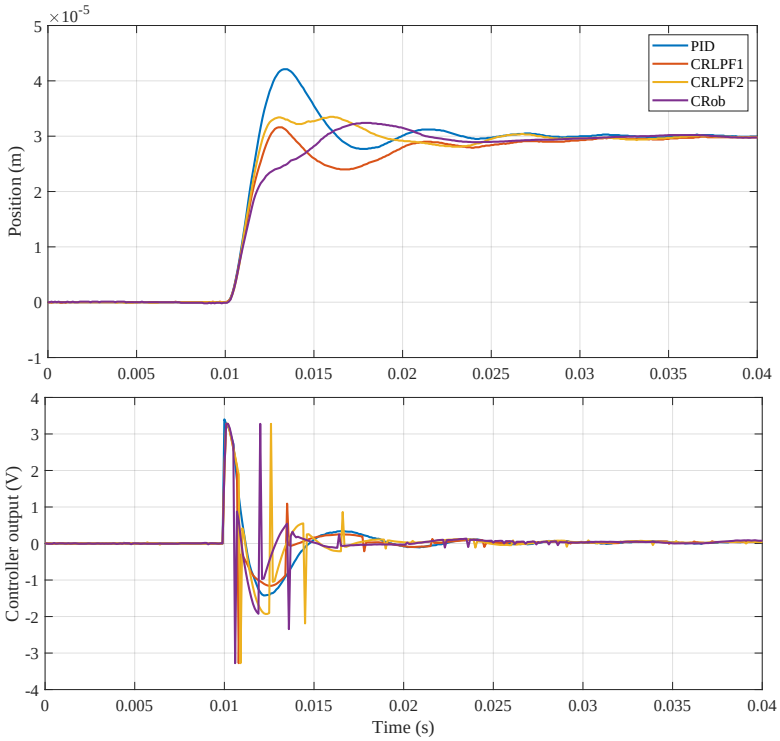

Figure 9.23: Step response and controller output of the controllers.

shown in what follows.

Figure 9.24 shows $\frac{\|e(t)\|_\infty}{\|r(t)\|_\infty}$ and $\frac{\|e(t)\|_2}{\|r(t)\|_2}$ for $t > t_{ss}$ for the response of the systems to sinusoidal input. The conventional controller (CRLPF1), is seemed to be below-bounded at lower frequencies which happens because of excessive resets happening especially at lower frequencies where the ratio between tracking error and noise drops. However, using second-order $L(s)$ and $R(s)$, there is less amplification of high frequency content of the signal, which in turn results in less excessive resets and lower sensitivity. A further improvement can be seen for observer-based CR CgLp controller because of better filtering of the noise from the reset signal.
It is noteworthy that, the dynamics of the plant definitely differs from the model used in the observer. However, still a better a performance than other controllers could be achieved.

9.8. CONCLUSION

While the required accuracy demands in industry keep increasing, the linear PID controller performance is limited by the waterbed effect. Reset control can break this waterbed effect by using for example the CR CgLp-PID controller architecture. Despite improvements, the CR based controller shows minimal robustness to noise. The high

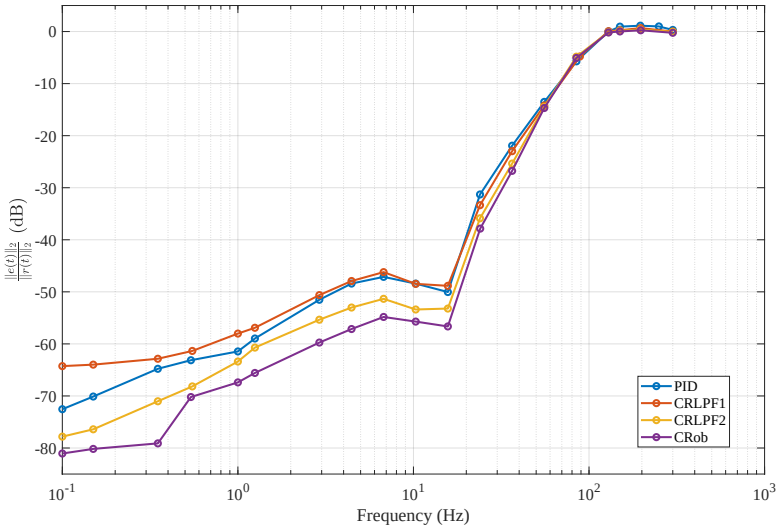

(a) Pseudo-sensitivity of the controllers based on RMS $e(t)$, $t > t_{ss}$.

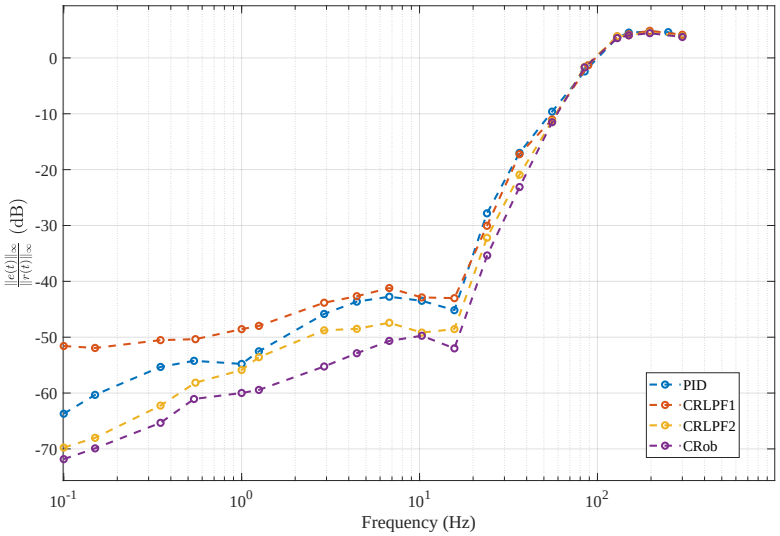

(b) Pseudo-sensitivity of the controllers based on max $e(t)$, $t > t_{ss}$.

Figure 9.24: Experimental results obtained from pseudo-sensitivity analysis of the response of the controllers for sinusoidal input.

frequency content of noise present in the reset line causes unwanted excessive resets which degrade the overall performance of the reset controller.

This paper proposed an observer based solution that does not harm the phase of the DF, contrary to prior solutions that were suggested in literature. The presented solution consists of a separate feedback line for the reset condition that is filtered by an observer. Stability conditions based on the H_β-condition of derived in previous work was altered

to apply to the new control loop architecture with the observer.

Transient and steady-state tracking were analysed in numerical simulations, in which the proposed control loop was compared with conventional linear and reset control. The proposed architecture showed a decrease in overshoot and lower settling time with respect to the conventional CR controller architecture when measurement noise was included. In addition, the pseudo-sensitivity was reduced by 13 dB at low frequencies without compromising the phase margin of the system. Analytical work and simulations showed normal robustness to parameter uncertainty in the observer. The RMS of the control output during low frequency tracking was decreased by 15% with respect to the conventional CR-structure.

By using an observer to filter out measurement noise on the reset feedback line, the transient and steady-state performance of CR CgLp in sub-optimal environments was improved. Therefore this paper provides a solution that brings reset control closer to implementation in the high-tech industry.

BIBLIOGRAPHY

[1] R. Schmidt, G. Schitter, A. Rankers, and J. van Eijk, *The design of high performance mechatronics: high-tech functionality by multidisciplinary system integration*, 2nd revised. Netherlands: IOS Press, 2014, ISBN: 978-1-61499-367-4. DOI: 10.3233/978-1-61499-368-1-i.

[2] O. Beker, C. Hollot, and Y. Chait, "Plant with integrator: An example of reset control overcoming limitations of linear feedback", *IEEE Transactions on Automatic Control*, vol. 46, no. 11, pp. 1797–1799, 2001. DOI: 10.1109/9.964694.

[3] H. N. L.Hazeleger M. Heertjes, "Second-order reset elements for stage control design", *Proceedings of the American Control Conference*, vol. 2016-July, pp. 2643–2648, Jul. 2016, ISSN: 07431619. DOI: 10.1109/ACC.2016.7525315.

[4] S. van den Eijnden, M. Heertjes, and H. Nijmeijer, "Robust stability and nonlinear loop-shaping design for hybrid integrator-gain-based control systems", in *2019 American Control Conference (ACC)*, 2019, pp. 3063–3068. DOI: 10.23919/ACC.2019.8814888.

[5] S. J. A. M. van den Eijnden, M. F. Heertjes, W. P. M. H. Heemels, and H. Nijmeijer, "Hybrid integrator-gain systems: A remedy for overshoot limitations in linear control?", *IEEE Control Systems Letters*, vol. 4, no. 4, pp. 1042–1047, 2020. DOI: 10.1109/LCSYS.2020.2998946.

[6] L. Hazeleger, M. Heertjes, and H. Nijmeijer, "Second-order reset elements for stage control design", in *2016 American Control Conference (ACC)*, IEEE, 2016, pp. 2643–2648.

[7] A. R. Teel, "Continuous-time implementation of reset control systems", *Trends in Nonlinear and Adaptive Control*, pp. 27–41, 2022.

[8] Y. W. D. Wu G. Guo, "Reset integral-derivative control for hdd servo systems", *IEEE Transactions on Control Systems Technology*, vol. 15, pp. 161–167, 1 Jan. 2007, ISSN: 10636536. DOI: 10.1109/TCST.2006.883230.

[9] N. Saikumar, R. K. Sinha, and S. H. HosseinNia, "'Constant in Gain Lead in Phase' element-application in precision motion control", *IEEE/ASME Transactions on Mechatronics*, vol. 24, pp. 1176–1185, 3 Jun. 2019, ISSN: 1941014X. DOI: 10.1109/TMECH.2019.2909082.

[10] A. A. Dastjerdi, N. Saikumar, and S. H. HosseinNia, "Tuning of a class of reset elements using pseudo-sensitivities", in *European Control Conference (ECC)*, 2021, pp. 1187–1192. DOI: 10.23919/ECC54610.2021.9654942.

[11] N. Karbasizadeh and S. H. HosseinNia, "Continuous reset element: Transient and steady-state analysis for precision motion systems", *Control Engineering Practice*, vol. 126, p. 105 232, Sep. 2022, ISSN: 0967-0661. DOI: 10.1016/J.CONENGPRAC.2022.105232.

[12] C. Cai, A. A. Dastjerdi, N. Saikumar, and S. HosseinNia, "The optimal sequence for reset controllers", *European Control Conference (ECC)*, 2020.

[13] D. Nešić, L. Zaccarian, and A. Teel, "Stability properties of reset systems", *IFAC Proceedings volumes*, vol. 38, no. 1, pp. 67–72, 2005.

[14] B. Kieft, S. H. HosseinNia, and N. Saikumar, "Time regularization as a solution to mitigate quantization induced performance degradation", in *2021 European Control Conference (ECC)*, 2021, pp. 2458–2464. DOI: 10.23919/ECC54610.2021.9655182.

[15] S. Shaik, J. Popat, and T. K. Kumar, "Kalman filter based phase delay reduction technique", *2016 International Conference on Recent Trends in Information Technology, ICRTIT*, pp. 1–5, Sep. 2016. DOI: 10.1109/ICRTIT.2016.7569549.

[16] R. Miklosovic, A. Radke, and Z. Gao, "Discrete implementation and generalization of the extended state observer", *Proceedings of the American Control Conference*, vol. 2006, pp. 2209–2214, 2006, ISSN: 07431619. DOI: 10.1109/acc.2006.1656547.

[17] D. Yoo, S. S. Yau, and Z. Gao, "Optimal fast tracking observer bandwidth of the linear extended state observer", *International Journal of Control*, vol. 80, pp. 102–111, 1 Jan. 2007, ISSN: 00207179. DOI: 10.1080/00207170600936555.

[18] Y.-D. Yoon, E. Jung, A. Yoo, and S.-K. Sul, "Dual observers for the disturbance rejection of a motion control system", *IEEE Industry Applications Annual Meeting*, 2007.

[19] F. Fichera, C. Prieur, S. Tarbouriech, and L. Zaccarian, "Using luenberger observers and dwell-time logic for feedback hybrid loops in continuous-time control systems", *International Journal of Robust and Nonlinear Control*, vol. 23, no. 10, pp. 1065–1086, 2013. DOI: https://doi.org/10.1002/rnc.2922. eprint: https://onlinelibrary.wiley.com/doi/pdf/10.1002/rnc.2922. [Online]. Available: https://onlinelibrary.wiley.com/doi/abs/10.1002/rnc.2922.

[20] H. Li, C. Du, and Y. Wang, "Optimal reset control for a dual-stage actuator system in hdds", *IEEE/ASME Transactions on Mechatronics*, vol. 16, pp. 480–488, 3 Jun. 2011, ISSN: 10834435. DOI: 10.1109/TMECH.2011.2123104.

[21] Y. Guo, W. Gui, C. Yang, and L. Xie, "Stability analysis and design of reset control systems with discrete-time triggering conditions", *Automatica*, vol. 48, pp. 528–535, 3 2012, ISSN: 00051098. DOI: 10.1016/j.automatica.2011.12.001. [Online]. Available: http://dx.doi.org/10.1016/j.automatica.2011.12.001.

[22] N. Karbasizadeh, A. A. Dastjerdi, N. Saikumar, and S. H. HosseinNia, "Band-passing nonlinearity in reset elements", *IEEE Transactions on Control Systems Technology*, vol. 31, no. 1, pp. 333–343, 2023. DOI: 10.1109/TCST.2022.3178043.

[23] N. Saikumar, K. Heinen, and S. H. HosseinNia, "Loop-shaping for reset control systems", *Control Engineering Practice*, vol. 111, p. 104 808, Jun. 2021, ISSN: 09670661. DOI: 10.1016/j.conengprac.2021.104808.

[24] A. A. Dastjerdi, A. Astolfi, N. Saikumar, N. Karbasizadeh, D. Valerio, and S. H. HosseinNia, "Closed-loop frequency analysis of reset control systems", *IEEE transactions on automatic control*, in press.

[25] J. C. Clegg, "A nonlinear integrator for servomechanisms", *Transactions of the American Institute of Electrical Engineers, Part II: Applications and Industry*, vol. 77, pp. 41–42, 1 Jul. 1958, ISSN: 0097-2185. DOI: 10.1109/tai.1958.6367399.

[26] A. Baños and A. Vidal, "Design of reset control systems: The pi plus ci compensator", *Journal of Dynamic Systems Measurement and Control*, vol. 134, pp. 051003/1–11, Jun. 2012. DOI: 10.1115/1.4004773.

[27] I. Horowitz and P. Rosenbaum, "Non-linear design for cost of feedback reduction in systems with large parameter uncertainty", *International Journal of Control*, vol. 21, pp. 977–1001, 6 1975, ISSN: 13665820. DOI: 10.1080/00207177508922051.

[28] R. E. Kalman, "A new approach to linear filtering and prediction problems", *ASME - Journal of Basic Engineering*, vol. 82, pp. 35–45, D 1960.

[29] D. G. Luenberger, "Observing the state of a linear system", *IEEE Transactions on Military Electronics*, vol. 8, pp. 74–80, 2 1964, ISSN: 05361559. DOI: 10.1109/TME.1964.4323124.

[30] J. Farrell, *4 State Estimation*. Academic press, 2005.

[31] D. Nešić, L. Zaccarian, and A. R. Teel, "Stability properties of reset systems", *Automatica*, vol. 44, no. 8, pp. 2019–2026, 2008.

[32] N. Karbasizadeh and S. H. HosseinNia, "Complex-order reset control system", in *2022 IEEE/ASME International Conference on Advanced Intelligent Mechatronics (AIM)*, 2022, pp. 427–433. DOI: 10.1109/AIM52237.2022.9863350.

[33] N. Karbasizadeh, A. A. Dastjerdi, N. Saikumar, and S. H. HosseinNia, "Band-passing nonlinearity in reset elements", *IEEE Transactions on Control Systems Technology*, In press. [Online]. Available: https://arxiv.org/abs/2009.06091.

[34] H. Hu, Y. Zheng, Y. Chait, and C. Hollot, "On the zero-input stability of control systems with clegg integrators", *Proceedings of the 1997 American Control Conference (Cat. No.97CH36041)*, vol. 1, 408–410 vol.1, 1997. DOI: 10.1109/ACC.1997.611829.

[35] O. Beker, C. V. Hollot, Y. Chait, and H. Han, "Fundamental properties of reset control systems", *Automatica*, vol. 40, pp. 905–915, 6 2004, ISSN: 00051098. DOI: 10.1016/j.automatica.2004.01.004.

[36] A. Baños, J. Carrasco, and A. Barreiro, "Reset times-dependent stability of reset control systems", *IEEE Transactions on Automatic Control*, vol. 56, pp. 217–223, 1 Jan. 2011, ISSN: 00189286. DOI: 10.1109/TAC.2010.2088892.

[37] Y. Guo, L. Xie, and Y. Wang, *Analysis and Design of Reset Control Systems*. Institution of Engineering and Technology, Nov. 2015, ISBN: 9781849197038. DOI: 10.1049/PBCE094E.

[38] A. A. Dastjerdi, A. Astolfi, and S. H. HosseinNia, *Frequency domain stability method for reset systems*, 2021. arXiv: 2009.00569 [eess.SY].

10

Practical Implementation of a Reset Controller to Improve Performance of an Industrial Motion Stage

In this work the Proportional Clegg Integrator (PCI), a resetting PI element, is studied with the aim of improving the performance of an industrial motion stage currently controlled by a linear controller. A novel parallel Continuous Reset (CR) architecture, based on the PI, is presented, along with frequency-based tuning guidelines, similar to Linear Time-Invariant (LTI) loopshaping techniques. Open-loop Higher-Order Sinusoidal Input Describing Functions (HOSIDFs) and pseudo-sensitivities computed through analytically-derived approximate closed-loop HOSIDFs, were effectively applied to predict steady-state performance. Experimental results, obtained on a wire bonding machine, confirmed that resonance-induced vibrations of the machine's base frame can be suppressed more effectively by adopting a PCI-PID controller compared to the currently used linear controller. The novel structure not only reduces unwanted excitation of higher-order harmonics of the base frame resonance, like the series CR architecture recently introduced in literature, but also avoids amplification of noise when implemented in practice. With the novel parallel structure, a significant (32%) decrease in the root mean square of the error could be achieved in steady-state when compared to the linear controller currently used and the series CR reset structure.

This chapter is conditionally accepted for publication in the journal of IEEE Transactions on Control Systems Technology as:
D. Caporale, L. F. van Eijk*, N. Karbasizadeh*, S. Beer, D. Kostic, and S. H. HosseinNia, "Practical Implementation of a Reset Controller to Improve Performance of an Industrial Motion Stage"
* These authors contributed equally to the paper.
The author of this dissertation has contributed to idea generation and supervision.

10.1. INTRODUCTION

Linear Time-Invariant (LTI) control is indisputably the most popular choice for motion control strategies, with the overwhelming majority of industry relying on it [1]. The success of LTI control can be attributed to the simplicity it offers regarding the controller design process. It allows for the use of classical control theory, which offers frequency domain tools to predict steady-state performance, as well as determine stability and robustness of feedback systems. All of this can be done solely on the basis of a non-parametric plant model, that is, a frequency response function (FRF). These tools are often used in industry to shape the open- and closed-loop transfer functions to obtain the desired controller characteristics, which is often referred to as loopshaping [2]. Nevertheless, LTI control suffers from inherent limitations, such as the 'waterbed effect' [3] and 'Bode's gain-phase relationship' [4]. Therefore, employing such controllers creates a trade-off between e.g., rise time, tracking precision, noise suppression, and robustness. Improving one characteristic requires to worsen at least one of the other characteristics as a consequence. For this reason, for the last few decades nonlinear control has been given great consideration in the literature. To the best of the authors' knowledge, it has been analytically proven for three nonlinear control elements that they can overcome certain inherent limitations of LTI control, which are the hybrid integrator-gain system (HIGS) [5], reset control [6], and variable control control (VGC) [7]. Nevertheless, adoption in industry is still scarce [1]. One of the main contributing factors is that for most techniques, it is not possible to get a reliable indication on the steady-state performance of the system in the frequency domain, thus preventing the use of loopshaping techniques [8]. In VGC, the gain of the controller is dependent on the input amplitude, allowing to have a steeper magnitude-slope in the open-loop FRF at low and high frequencies, respectively, due to the difference in amplitude between low and high frequency disturbances/noise. This allows to better suppress low-frequent disturbances and high-frequent noise [9]. However, since the frequency response of such a filter is dependent also on the amplitude of the input [10], it is not suitable for systems whose reference is unknown a priori, thus for many industrial applications. This issue does not occur for HIGS and reset control, since their nonlinearity is not amplitude dependent. Among the two, reset control offers better frequency-based steady-state performance prediction methods, including closed-loop methods [10], [11], which are lacking for HIGS-based systems [12]. Numerous other (more popular) nonlinear control techniques exist, such as adaptive sliding mode control [13]. However, it is unclear for these techniques how to intuitively design a controller that outperforms a well-designed LTI controller in an industrial setting, solely based on a non-parametric model of the plant, e.g. using frequency-domain analysis tools. With this work, the authors hope to get one step closer towards this goal for reset control in specific.

The reset control appeared for the first time in the literature more than 60 years ago [14]. However, only four decades later the field has been given enough attention to be considered a potentially reliable alternative to linear control [15]. Recent literature demonstrated that steady-state performance prediction based on frequency domain and stability analysis methods exists for some particular reset control structures [11]. This makes it possible to design and analyze these particular nonlinear controllers in a similar way as linear controllers, while overcoming the inherent limitations of their linear

counterparts. However, a considerable part of literature works focus on the 'Constant in gain-Lead in phase' (CgLp) element [16]–[18]. Nevertheless, this element is more complex to tune, and simplicity is of high importance in industry.

A different structure, known as the Proportional Clegg Integrator (PCI) allows a larger low frequency open-loop gain compared to an equivalent LTI Proportional Integrator (PI) system, for the same phase margin, based on a Sinusoidal Input Describing Function (SIDF) analysis. This leads to improved disturbance suppression when paired with an LTI PID, thus potentially improving the tracking performance of the system. Although having a structure simpler than that of the CgLp element, the PCI has been studied in literature for such purpose only once. In [19], a PCI-PID system was compared to a PI-PID system for reference tracking, with the former one not being able to outperform its linear counterpart. However, since then new steady-state performance analysis tools have been developed. Additionally, it was recently demonstrated that the performance of a reset element can be potentially further improved when used in a Continuous Reset (CR) architecture, capable of reducing the nonlinearity of the reset element over a broad frequency band [20].

The aim of this paper is to study the viability of a PCI-PID controller, within the CR framework, to increase the performance of an industrial motion stage. It is demonstrated that while the CR architecture presented in [20] achieves good results in simulations, when applied in practice, a detrimental issue arises: measurement noise is amplified, leading to poor performance. Therefore, a novel parallel CR structure is implemented to ensure low-frequency disturbance suppression of the PCI and to reduce the broad-band nonlinearities of the CR element. State-of-the-art frequency domain analysis tools are used to analyze controllers. The findings are experimentally validated on the motion stage of an industrial wire bonder, a machine that creates interconnections between chips and their packaging.

The next section (Section 10.2) includes the necessary background theory in terms of reset control. In the subsequent section (Section 10.3) the PCI-PID structure will be introduced. The advantages and drawbacks of the series CR architecture are also presented. A novel parallel CR structure is presented in Section 10.4, along with tuning guidelines. In Section 10.5, a discrete-time implementation of the reset controller is proposed. This implementation is utilized in Section 10.6, where experimental results on a wirebonding machine are discussed. Finally, conclusions and suggestions for future work are given in Section 10.7.

10.2. PRELIMINARIES

10.2.1. DEFINITION OF RESET ELEMENT

In this paper the definition from [11], given as

$$\mathscr{R} = \begin{cases} \dot{x}_r(t) = A_r x_r(t) + B_r e_r(t), & \text{if } \big(x_r(t), e_r(t)\big) \notin \mathscr{M} \\ x_r^+(t) = A_\rho x_r(t), & \text{if } \big(x_r(t), e_r(t)\big) \in \mathscr{M} \\ u_r(t) = C_r x_r(t) + D_r e_r(t), \end{cases} \tag{10.1}$$

is used to describe a Single-Input Single-Output (SISO) reset system $\mathscr{R}$. The first and last lines of (10.1) describe a standard LTI system in state-space, where $A_r \in \mathbb{R}^{n_r \times n_r}$, $B_r \in \mathbb{R}^{n_r \times 1}$, $C_r \in \mathbb{R}^{1 \times n_r}$ and $D_r \in \mathbb{R}$ are the Base Linear System (BLS) matrices, $x_r(t) \in \mathbb{R}^{n_r \times 1}$

is the reset element's state vector with $n_r \in \mathbb{N}$ number of states, $e_r(t) \in \mathbb{R}$ is its input, $u_r(t) \in \mathbb{R}$ is its output and $t \in \mathbb{R}^+$ indicates time. For the sake of brevity, the dependency on t will be omitted henceforward. The LTI system description holds true whenever (x_r, e_r) is not part of the reset surface $\mathscr{M}$. However, if (x_r, e_r) is part of $\mathscr{M}$, the after-reset state at the reset time instant $x_r^+ = \lim_{y \to t+0} x_r(y)$ is determined by the reset matrix $A_\rho = \text{diag}(\gamma_1, \ldots, \gamma_{n_r})$, with $|\gamma_i| \leq 1 \; \forall i \in \mathbb{N}$. If $A_\rho = I^{n_r \times n_r}$, resets do not affect the system, which thus behaves like its BLS, defined as

$$R(s) = C_r(sI - A_r)^{-1}B_r + D_r, \tag{10.2}$$

with $s \in \mathbb{C}$ being the Laplace variable.

In this work, we define the reset surface as

$$\mathscr{M} := \{e_r = 0 \wedge (I - A_\rho)x_r \neq 0\}. \tag{10.3}$$

Namely, for this reset condition a prediction method has been developed in [10], which can fully accurately describe the open-loop steady-state performance using higher-order SIDFs (HOSIDFs), based solely on an FRF of the plant. Furthermore, this method has been extended to also provide an approximation of the closed-loop steady-state performance [10], which we will exploit later in this work (more detail in Section 10.2.3). Another popular reset condition is the one where resets occur when the input and output have opposite sign [21]. However, no similar HOSIDF-method is available for this condition. To the best of the author's knowledge, open-loop performance prediction based on HOSIDFs has been investigated for one other reset condition, which initiates resets based on a time-dependent trigger signal [22]. However, no closed-loop performance prediction method based on HOSIDFs has been developed for this type of reset condition.

10.2.2. CONTROL SYSTEM ARCHITECTURE

In [11] the closed-loop reset system architecture depicted in Fig. 10.1 was presented. C_1 and C_2 are SISO LTI filters, G is the plant, $r \in \mathbb{R}$ is the reference, $u \in \mathbb{R}$ is defined as the controller output, $d \in \mathbb{R}$ is the disturbance, $n \in \mathbb{R}$ is the sensor noise, $y \in \mathbb{R}$ is the true output, $y^* = y + n$ is the measured output, $e = r - y^*$ is the error and $v = u + d$ is the plant input.

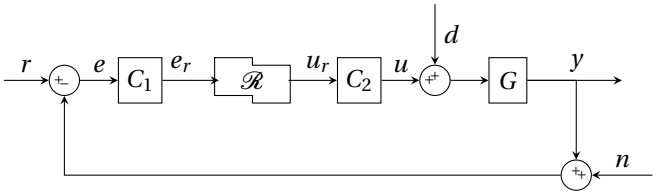

Figure 10.1: Reset control feedback system architecture (adapted from [11]).

10.2.3. PREDICTIVE PERFORMANCE

The steady-state input-output relationship of an LTI system can be easily calculated based on its transfer function or FRF. As an example, consider the SISO LTI system C_1

subject to a sinusoidal input

$$e(t) = \hat{e}\sin(\omega t + \varphi_e), \tag{10.4}$$

with input frequency $\omega \in \mathbb{R}^+$, amplitude $\hat{e} \in \mathbb{R}^+$, and phase $\varphi_e \in \mathbb{R}$. Then, its steady-state output signal is given by

$$e_r(t) = |C_1(j\omega)|\hat{e}\sin\big(\omega t + \varphi_e + \angle C_1(j\omega)\big), \tag{10.5}$$

where $C_1(j\omega)$ is the FRF of the respective LTI system. For reset controllers as in (10.1), the output signal is generally not a pure sinusoid when subject to a sinusoidal input

$$e_r(t) = \hat{e}_r \sin(\omega t + \varphi_{e_r}), \tag{10.6}$$

with input amplitude $\hat{e}_r \in \mathbb{R}^+$ and phase $\varphi_{e_r} \in \mathbb{R}$. However, since the output is periodic with the same period as the input signal [23], the output can be described by the Fourier series [24]

$$u_r(t) = \sum_{n=1}^{\infty} |H_n(\omega)|\hat{e}_r \sin\big(n(\omega t + \varphi_{e_r}) + \angle H_n(\omega)\big), \tag{10.7}$$

where H_1 is called the SIDF and all H_n with $n > 1$ are referred to as the Higher-Order SIDFs (HOSIDFs), $n \in \mathbb{N}$. A quasi-linear approximation of a reset controller, equivalent to a Bode plot of an LTI system, can be created by means of the SIDF [25]. However, (10.7) shows that reset control systems suffer from the effect of harmonic generation. This denotes that the output signal, given an input sinusoid of a certain frequency, consists of not only the excitation frequency but also higher-order harmonics at multiples of the excitation frequency [26]. The HOSIDFs introduced in [24], provide information on the generation of higher-order harmonics. The HOSIDFs for reset controller $\mathscr{R}$ with the reset condition as in (10.3), can be analytically computed using [10, Theorem 3.1] (see also [27]), which is repeated for convenience in Theorem 13.

Theorem 13. *[10, Theorem 3.1] For a reset controller $\mathscr{R}$ as in (10.1) with reset condition (10.3), the HOSIDFs are given by*

$$H_n(\omega) = \begin{cases} C_r(j\omega I - A_r)^{-1}\big(I + j\Theta_D(\omega)\big)B_r + D_r, & \text{for} \quad n = 1, \\ C_r(j\omega n I - A_r)^{-1} j\Theta_D(\omega) B_r, & \text{for odd} \quad n \geq 2, \\ 0, & \text{for even} \quad n \geq 2, \end{cases} \tag{10.8}$$

with $j := \sqrt{-1}$ and

$$\Lambda(\omega) = \omega^2 I + A_r^2,$$
$$\Delta(\omega) = I + e^{\frac{\pi}{\omega}A_r},$$
$$\Delta_r(\omega) = I + A_\rho e^{\frac{\pi}{\omega}A_r},$$
$$\Gamma_r(\omega) = \Delta_r^{-1}(\omega) A_\rho \Delta(\omega) \Lambda^{-1}(\omega),$$
$$\Theta_D(\omega) = \frac{-2\omega^2}{\pi}\Delta(\omega)[\Gamma_r(\omega) - \Lambda^{-1}(\omega)].$$

The HOSIDFs can be easily augmented in case LTI systems are present in series before or after the reset controller, as depicted in Fig. 10.1. The resulting open-loop steady-state output signal given an input sinusoid (10.4) can be computed as an infinite sum of sinusoids

$$\begin{aligned} u(t) \quad &= \sum_{n=1}^{\infty} |C_1(j\omega)||H_n(\omega)||C_2(nj\omega)|\hat{e}\sin\big(n(\omega t+\varphi_e) \\ &\quad + n\angle C_1(j\omega) + \angle H_n(\omega) + \angle C_2(nj\omega)\big). \end{aligned} \tag{10.9}$$

The effectiveness of loopshaping in case of LTI systems comes from the fact that it is possible to easily relate the open-loop and the closed-loop through the sensitivity equations. In [10] it was, however, shown that even when having a low magnitude, HOSIDFs are usually not negligible in closed-loop and simply utilizing the SIDF provides a highly inaccurate approximation of the closed-loop FRF. In [28, Definition 5] the so-called pseudo-sensitivity $S_\infty(\omega)$ was proposed, with magnitude defined as

$$|S_\infty(\omega)| = \frac{\max\limits_{0<t<2\pi/\omega} e_{ss}(\omega,t)}{r_0}, \tag{10.10}$$

where $e_{ss}(\omega,t)$ is the steady-state error of the closed-loop reset system excited by a reference input $r(t) = r_0\sin(\omega t)$, with $r_0 \in \mathbb{R}^+$. It allows to combine the information on closed-loop higher order harmonics into an analogue of a sensitivity function for reset systems, thus helpful for loopshaping. Although the principle of superposition does not hold, it was established that even for non-sinusoidal inputs, the pseudo-sensitivity functions can provide a reliable quantitative steady-state performance prediction to effectively design reset controllers [29]. An analytical method, capable of relating open- and closed-loop HOSIDFs, with a non-parametric plant model (FRF) given some assumptions, was established in [10] and is given in Theorem 14.

Theorem 14. *[10] Given a closed-loop reset system with input $r = \sin(\omega t)$, the steady-state error is given by*

$$e_{ss}(t) = \sum_{n=1}^{\infty} |S_n(j\omega)|\sin\big(n\omega t + \angle S_n(j\omega)\big), \tag{10.11}$$

with

$$S_n(j\omega) = \begin{cases} S_1(j\omega), & \text{for} \quad n=1, \\ -\dfrac{L_n(j\omega)}{1+L_{BLS}(nj\omega)}\left(|S_1(j\omega)|\,e^{jn\angle S_1(j\omega)}\right), & \\ & \text{for odd} \quad n\geq 2, \\ 0, & \text{for even} \quad n\geq 2, \end{cases} \tag{10.12}$$

and

$$S_1(j\omega) = \frac{1}{1+L_1(j\omega)},$$
$$L_n(j\omega) = G(jn\omega)C_2(jn\omega)H_n(\omega)C_1(j\omega)e^{j(n-1)\angle C_1(j\omega)},$$

as long as the following assumptions hold true:

1. *The system is input-to-state convergent,*
2. *The resets are a result of only the first harmonic of e_r.*

The first assumption, on input-to-state convergence, holds when the reset system satisfies the H_β-condition [28]. The second assumption allows the signal e_r to be non-sinusoidal, as long as the zero crossings of the first harmonic and the actual signal coincide. When the controller is designed such that the higher-order harmonics of e_r are kept small compared to the first harmonic, it shows to be a useful assumption. Namely, the accuracy of closed-loop steady-state performance prediction can be improved compared to the SIDF method, as shown in [10].

Remark 14. *In Theorem 14, the effect of measurement noise is not considered, although it can potentially have an effect on the reset instants. In this work, we assume that the effect of measurement noise on error e is negligible. However, this does not necessarily mean that the measurement noise is negligible in the signal e_r, which is further discussed in Section 10.3.*

10.2.4. PRACTICAL ASPECTS WHEN TUNING WITH HOSIDFS

HOSIDFs are the prevailing method to perform steady-state performance prediction for reset systems in the frequency-domain. Nevertheless, some aspects must be taken into account when using them. First, in this work, the control design is done in such a manner that the magnitudes of all higher order harmonics are low compared to the first harmonic, such that they do not have a major impact on the response. Namely, in that case the closed-loop steady-state performance can be accurately predicted using Theorem 14. If the higher-order harmonics are not small, it is unclear what the steady-state performance of the system looks like. Furthermore, given that the first harmonic is dominant, the SIDF can still be a useful aid in the control design procedure.

Theorem 13 allows to compute open-loop HOSIDFs only for reset controllers with continuous dynamics for the base-linear system. In the case of a discrete implementation of the base-linear dynamics, it will thus be assumed that the sampling frequency is high enough to ensure that the change in HOSIDFs caused by discretization is negligible in the frequency range of interest.

As shown in (10.11), the greater the number of HOSIDFs that are accounted for in the sum, the more accurate the result. However, as for the open-loop method, when using a plant FRF, which is the common practical industry standard, information on the n^{th} HOSIDF can only be provided for frequencies $\omega \leq \omega_{max}/n$, where $\omega_{max} \in \mathbb{R}^+$ is the largest frequency for which FRF data is available. This makes the accuracy of the method frequency dependent: the higher the frequency, the fewer HOSIDFs can be taken into account, and hence the more inaccurate the result. Nevertheless, this still provides more information and thus a more accurate solution than solely using the SIDF to compute the closed-loop HOSIDFs. In fact, the method was utilized in [10] for the design of the controller for a precision positioning stage.

A pseudo-sensitivity can be viewed as a 'worst-case scenario' closed-loop sensitivity in terms of steady-state performance, as only information on the maximum amplitude is regarded. This conservative approach ensures that the reset controller does not excessively amplify signals of certain frequencies in closed loop. A constraint on the peak of the pseudo-sensitivity is not equivalent for robustness, but it prevents large amplification of the reference profile.

10.3. PCI-PID

A PCI is a resetting integrator with corner frequency $\omega_r \in \mathbb{R}^+$. The state-space matrices are given by

$$A_r = 0,\ B_r = \omega_r,\ C_r = 1,\ D_r = 1,\ A_\rho = \gamma. \tag{10.13}$$

Non-linearity affects mostly the low frequencies in the range $\omega < \omega_r$, where resetting leads to a smaller phase lag compared to a linear integrator and a constant positive magnitude offset. Nevertheless, contrary to a PI, a PCI cannot be utilized to suppress steady-state errors. This is due to the fact that resetting causes the stored energy of the integral action, required to avoid a steady-state error, to be eliminated, introducing a limit cycle behaviour [30]. Therefore, instead of replacing the 'PI-part' of the linear PID controller with a PCI element, the PCI element can be utilized in addition to the existing linear PID.

It is common for industrial motion stages to be controlled with cutting-edge feedforward controllers which are capable of tracking a predetermined reference. Feedback control is then mostly needed to increase tracking precision by suppressing disturbances or to compensate for the dynamics not modeled in the feedforward controller. For improved tracking precision, it is necessary to increase the open-loop gain at low frequencies. Due to Bode's gain-phase relationship, this affects the phase margin of the system, and thus its stability and robustness. With reset control this limitation can be overcome, allowing a larger low-frequency open-loop gain compared to an LTI system for the same phase margin, according to the SIDF. However, it should be noted that a PCI also introduces phase lag, be it in a reduced extent compared to a PI. Therefore, a system controlled by a PCI-PID controller has an increased magnitude peak in the pseudo-sensitivity compared to the same system controlled solely by the same PID controller. This must be accounted for by assuring that the PCI is used with a LTI controller with a high phase margin. A PCI-PID is then constructed by selecting $C_1 = 1$, $\mathscr{R}$ as a PCI and C_2 as an LTI PID controller, defined as

$$C_{PID}(s) = \underbrace{k_P}_{\text{P}}\ \underbrace{\left(1+\frac{\omega_I}{s}\right)}_{\text{I}}\underbrace{\left(\left(1+\frac{s}{\omega_D}\right)\Big/\left(1+\frac{s}{\omega_T}\right)\right)}_{\text{D}}, \tag{10.14}$$

with $k_P \in \mathbb{R}$ and $\omega_I, \omega_D, \omega_T \in \mathbb{R}^+$ in rad/s.

As a PCI only has two parameters, ω_r and γ, its tuning is relatively straightforward. With increasing ω_r, the magnitude and phase behaviour of the SIDF and HOSIDFs can be shifted to the right. This will lead to a higher gain at frequencies lower than the bandwidth, but also to a larger magnitude for the HOSIDFs and a lower phase margin. A similar effect is given by γ. Decreasing γ leads to a smaller phase lag and slightly greater gain at the cost of larger magnitude for the HOSIDFs. As depicted in Fig. 10.2, it is thus possible to achieve the same phase margin for different combinations of γ and ω_r. It should be noted that usually for $n > 3$, the magnitude of the n^{th} HOSIDF of a PCI has a similar shape as that of the 3^{rd} HOSIDF but with a lower gain, as portrayed in Fig. 10.3. For this reason, it is usually only necessary to analyse the 3^{rd} HOSIDF in order to comprehend the behaviour of all HOSIDFs [10].

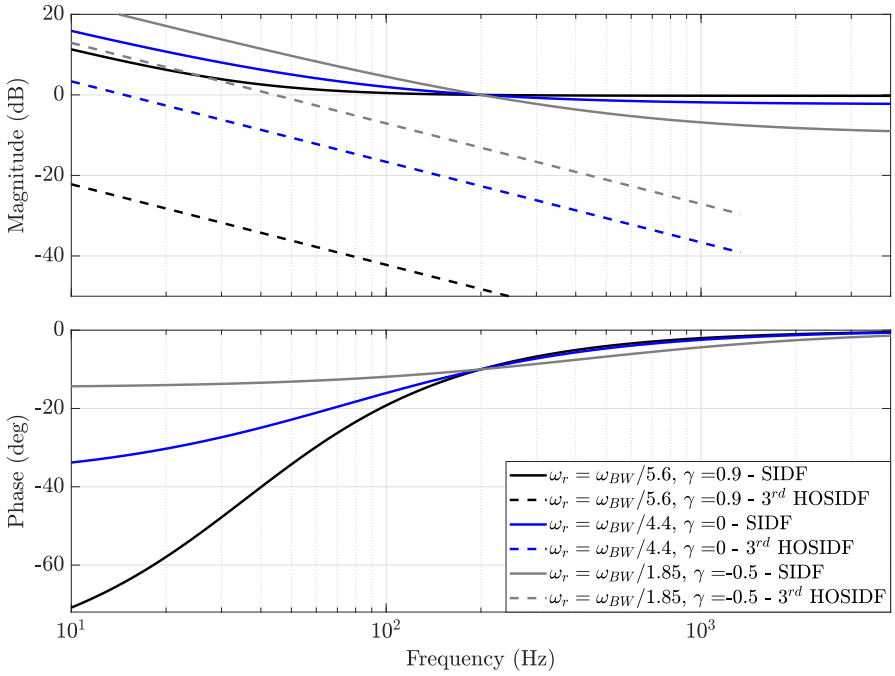

Figure 10.2: Magnitude and phase characteristics of the SIDF and 3$^{\text{rd}}$ harmonic of three PCI elements with different combinations of ω_r and γ resulting in a phase lag of 10° at 200 Hz. The gain was adjusted to keep the crossover frequency ω_{BW} at 200 Hz.

10.3.1. Lowering HOSIDFs

The trade-off between HOSIDFs and low frequency gain poses a constraint on the tuning of a PCI element. Therefore, it would be beneficial to lower the HOSIDFs without affecting the SIDF. This can be achieved by using the CR architecture developed in [20]. The principle can be explained by (10.9). The magnitude of the n^{th} HOSIDF is directly proportional to $|C_1(j\omega)|$ and $|C_2(jn\omega)|$. Therefore, to minimize the HOSIDFs, a lead element should be placed in C_1 and a lag element in C_2. Furthermore, an n_l^{th} order lead filter F_l can be defined as

$$F_l(s) = \left(\frac{\frac{s}{\omega_d}+1}{\frac{s}{\omega_t}+1}\right)^{n_l}, \quad \omega_d < \omega_t, \tag{10.15}$$

with ω_d, $\omega_t \in \mathbb{R}^+$ in rad/s and $n_l \in \mathbb{N}$. When keeping the PID in C_2, but also adding F_l and F_l^{-1} to C_1 and C_2, respectively, it is possible to tune the magnitude of HOSIDFs and their active region, without affecting the SIDF. Furthermore, when stability is assessed by means of the H_β-condition [31], filters F_l and F_l^{-1} have no influence on the analysis. To determine the range in which HOSIDFs have the most significant effect, and which HOSIDF has the greatest effect, the power spectral density of the error signal when utilizing a PCI-PID without CR can be analyzed. In case feedforward control is employed, most of the power is usually caused by either external disturbances

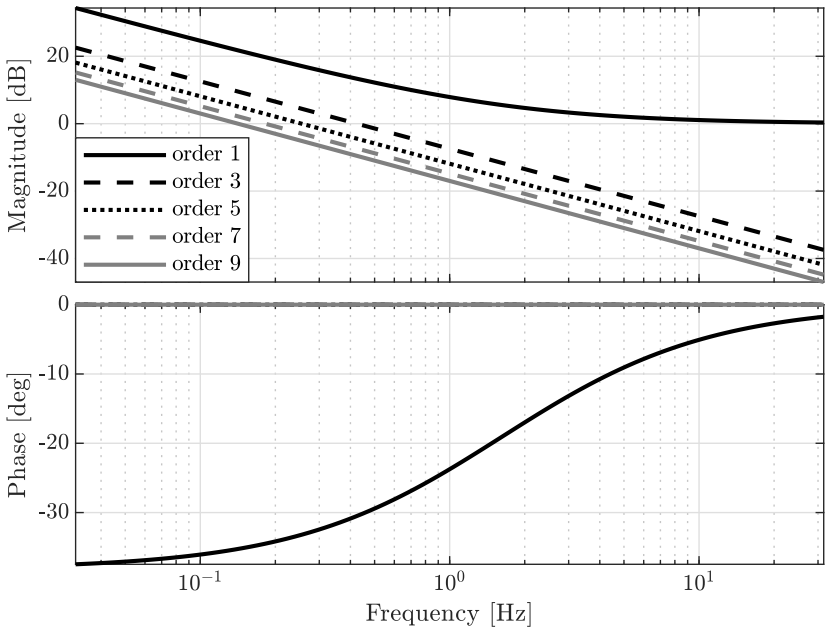

Figure 10.3: Magnitude and phase characteristics of the odd-order HOSIDFs of a PCI as in (10.1), (10.3), (10.13), with $\omega_r = 2\pi$ and $\gamma = 0$.

or resonances not modeled in the feedforward. If a disturbance/resonance is present at frequency ω_{dis}, the n^{th} HOSIDF will show the undesired excitation of higher-order harmonics at frequency $n\omega_{dis}$. By choosing $\omega_d = \omega_{dis}$ and $\omega_t = n\omega_{dis}$, the relative suppression of the n^{th} HOSIDF at $\omega = \omega_{dis}$ caused by adding CR elements can be defined as $H_\varsigma(\omega_{dis}, n) = |F_l(j\omega_{dis})||F_l^{-1}(jn\omega_{dis})|$. The order of the lead filter n_l can then be increased such that the amount of suppression also increases by a factor $n_l H_\varsigma(\omega_{dis}, n)$.

10.3.2. EFFECT OF NOISE

In [20] it was demonstrated that having C_1 as a first-order lead filter results in the reset instants being affected not only by e, but also by $\dot{e}$. The change in reset instants will affect steady-state performance in case noise is present in the system. To compute the open-loop SIDF and HOSIDFs, it is assumed that the input is a sinusoid, which allows to predetermine the reset instants t_k. When there is noise in the system, the reset instants could differ. The higher the power of the noise, the higher the chance of one of these undesired resets. A lead element such as F_l increases the magnitude of the high-frequency content of the output signal. The power of the noise present in the error signal e at ω is therefore increased with increasing $H_\varsigma(\omega_{dis}, n)$ hence causing the SIDF and HOSIDFs more unreliable.

Next, the effect of noise on the CR architecture will be visualized through an example. A PCI-PID was tuned for a plant resembling a highly damped non-collocated double

mass-spring-damper system

$$G_1(s) = \frac{ds+k}{m_1 m_2 s^4 + d(m_1+m_2)s^3 + k(m_1+m_2)s^2}, \tag{10.16}$$

with parameter values given in Table 10.1. The parameter values of the respective LTI PID controller PID_1 and of the PCI are also given in the table. The open-loop block diagram is shown in Fig. 10.4. PID_1 was tuned so that the LTI part of the open loop system has $\approx 40°$ phase margin at $\omega_{BW} = 200$ Hz, allowing the PCI to have $10°$ phase lag at 200 Hz for the open loop SIDF phase margin to be $30°$. Two different F_l & F_l^{-1} pairs were tuned allowing two CR architectures to be used, CR_1 and CR_2 respectively, with the values of the corresponding parameters also given in Table 10.1. Both F_l & F_l^{-1} pairs have the same ω_d and ω_t, while $n_l = 1$ for CR_1, $n_l = 2$ for CR_2, and both pairs are tuned assuming a disturbance $d = \sin(\omega_{dis} t)$, where $\omega_{dis} = 50$ Hz, is acting on the system. Thus, through the tuning it is assured that $H_\varsigma(\omega_{dis}, 3) < 0$ dB. In fact for CR_1, $H_\varsigma(\omega_{dis}, 3) = -6.02$ dB and for CR_2, $H_\varsigma(\omega_{dis}, 3) = -12.04$ dB. The resulting open-loop FRFs are visualized in Fig. 10.5. It can be appreciated how the HOSIDFs are lowered with increasing $H_\varsigma(\omega_{dis}, n)$, whereas the SIDF remains unchanged. The magnitude plots of the pseudo-sensitivities, computed using Theorem 14 after discretising all LTI parts of the system at 8 kHz using Tustin's approximation, are given in Fig. 10.6. As expected, a decrease in $H_\varsigma(\omega_{dis}, n)$ at low frequencies corresponds to a lower magnitude of the pseudo-sensitivity. Hence, better disturbance suppression can be achieved, caused by the suppression of the HOSIDFs.

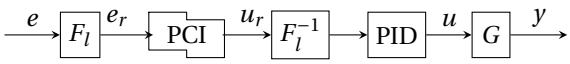

Figure 10.4: Series CR PCI-PID block diagram.

Table 10.1: Parameter values of G_1, PID_1, PCI, and F_l, used for CR_1 and CR_2.

G_1	m_1	m_2	k	d
	100	100	1.97×10^9	4.6×10^4
PID_1	k_P	ω_I	ω_D	ω_T
	8.204×10^7	20 Hz	76.92 Hz	520 Hz
PCI	ω_r	γ		
	60 Hz	0		
CR_1	ω_d	ω_t	n_l	
	50 Hz	50×3 Hz	1	
CR_2	ω_d	ω_t	n_l	
	50 Hz	50×3 Hz	2	

A Simulink simulation was then performed with inputs $r(t) = 0$, $n(t) = 0$, and $d(t) = \sin(\omega_{dis} t)$, where $\omega_{dis} = 50$ Hz. The resulting closed-loop errors are given in Fig. 10.7. The Cumulative Power Spectral Density (CPSD) of the PCI-PID system without CR shows that the power spectrum has peaks at odd multiples of ω_{dis}, such as 150 Hz and 250 Hz. These power peaks are the peaks of the third and the fifth harmonics resulting from the

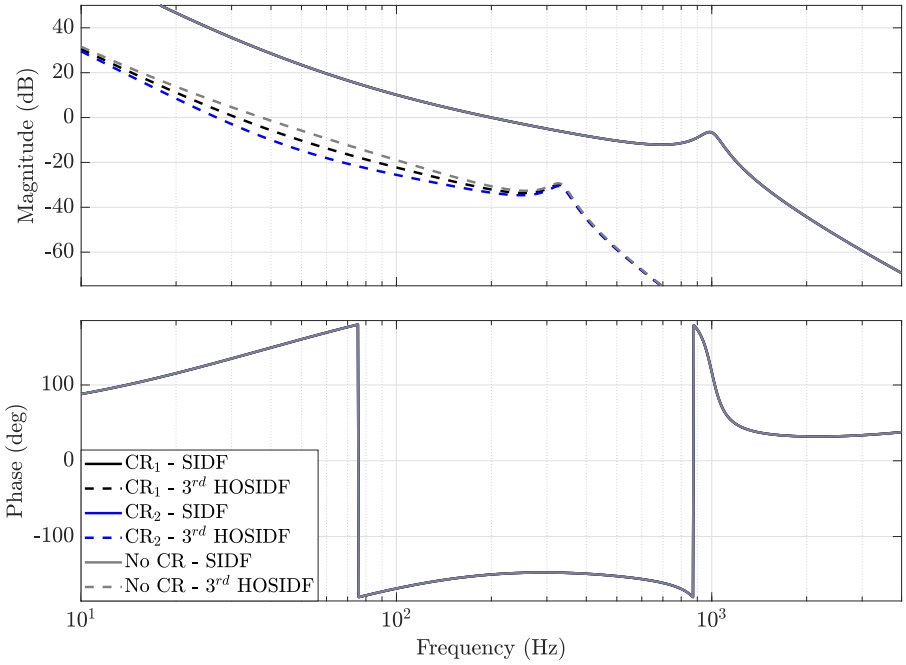

Figure 10.5: Magnitude and phase characteristics of the SIDF and 3rd harmonic of the open-loop system with G_1 as the plant, PID_1 as the PID controller, PCI as $\mathscr{R}$ and without CR architecture, with CR_1 or CR_2 respectively. All SIDFs are identical and therefore plotted on top of each other.

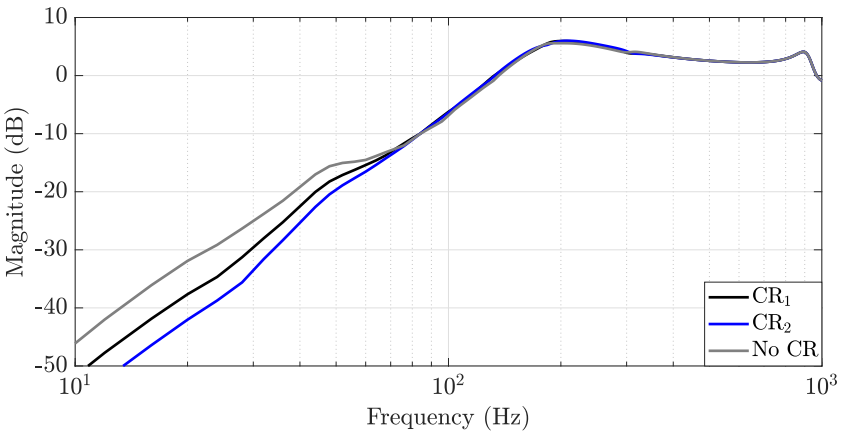

Figure 10.6: Pseudo-sensitivity magnitudes computed through the approximate method (Theorem 14) of the closed-loop system with G_1 as the plant, PID_1 as the PID controller, PCI as $\mathscr{R}$ and without CR architecture, with CR_1 or CR_2 respectively, discretized at 8 kHz.

50 Hz disturbance frequency. The improvement in performance resulting from the lower HOSIDFs at ω_{dis} introduced by the CR architecture, is clearly to be seen. While the peak at 50 Hz in the CPSD remains almost identical, showing that the SIDF does not change, the peaks at 150 Hz and 250 Hz decrease with decreasing $H_\varsigma(\omega_{dis}, n)$. The simulation

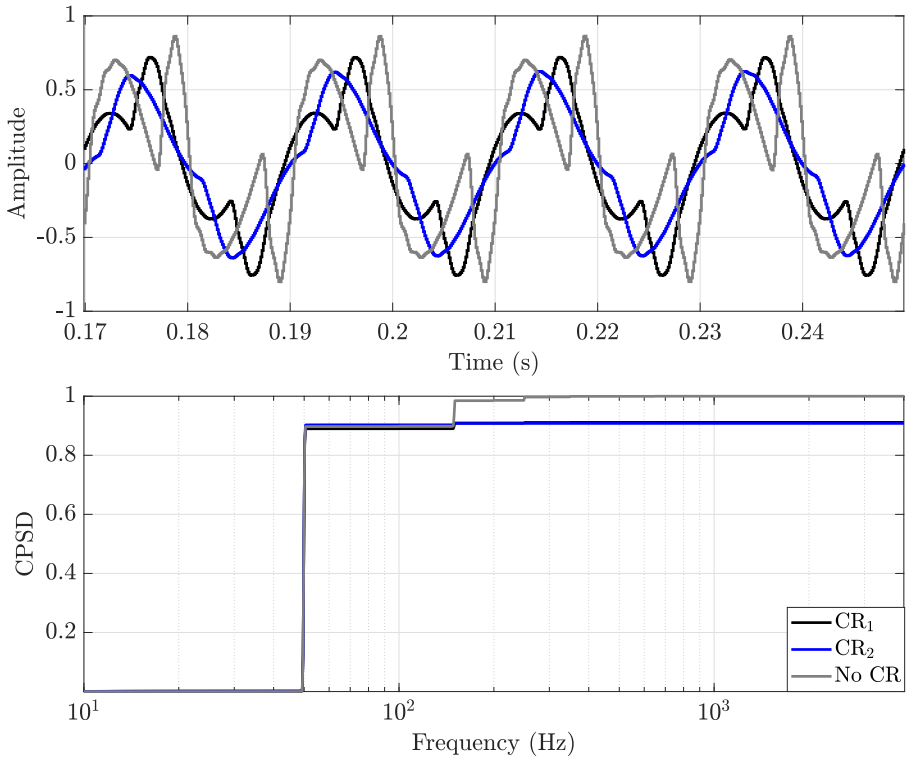

Figure 10.7: Normalized closed-loop steady state error signal (only four periods shown) resulting from a Simulink simulation of a system with G_1 as the plant, PID_1 as the PID controller, PCI as $\mathscr{R}$ and without CR architecture, with CR_1 or with CR_2 respectively. The inputs to the system are $r(t) = 0$, $n(t) = 0$, $d(t) = \sin(\omega_{dis} t)$, where $\omega_{dis} = 50$ Hz.

shown in Fig. 10.7 is repeated with n being white noise in Fig. 10.8. It can be seen that an increase in $H_\varsigma(\omega_{dis}, n)$ still results in lower excitation of higher order harmonics, however in this case, three signals have a different suppression of the disturbance frequency itself, confirming that the SIDF is less reliable in the presence of noise.

10.4. PARALLEL CR PCI-PID

With the CR architecture HOSIDFs can be successfully reduced in a certain frequency range, without affecting the SIDF. Nevertheless, the architecture suffers from limitations, caused by the effect of amplifying the high-frequent power content in the error signal through F_l. To avoid this, a novel parallel CR architecture is proposed. The block diagram of the structure is depicted in Fig. 10.9. In order to make use of the performance

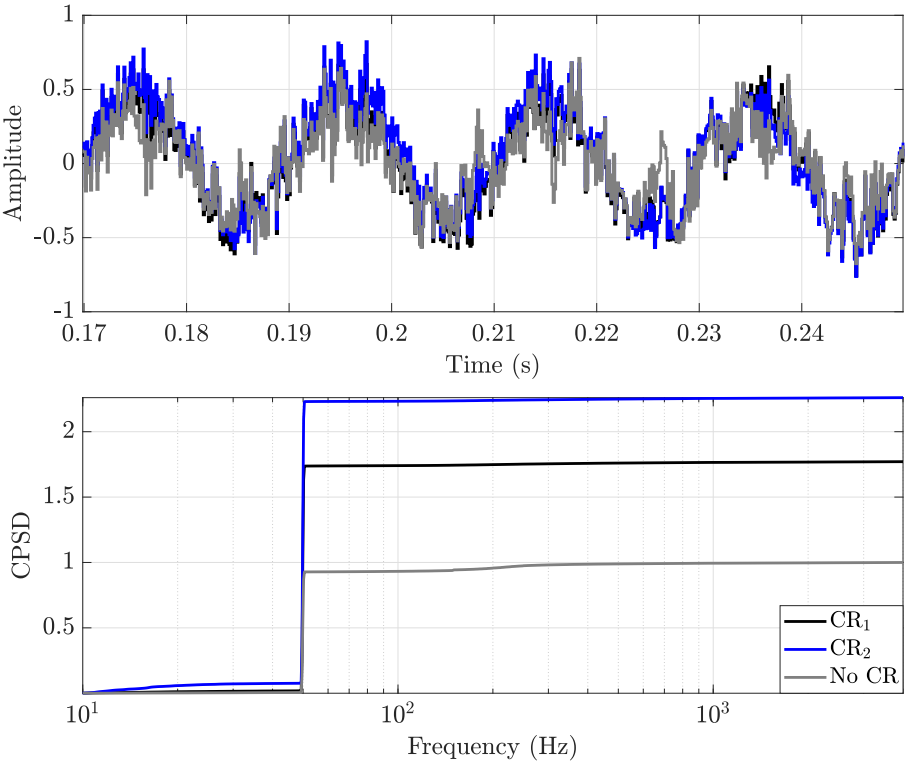

Figure 10.8: Normalized closed-loop steady state error signal (only four periods shown) resulting from a Simulink simulation of a system with G_1 as the plant, PID_1 as the PID controller, PCI as $\mathscr{R}$ and without CR architecture, with CR_1 or CR_2 respectively. The inputs to the system are $r(t) = 0$, $n(t)$ is white noise with power 1×10^{-5} m^2/Hz, $d(t) = \sin(\omega_{dis} t)$, where $\omega_{dis} = 50$ Hz.

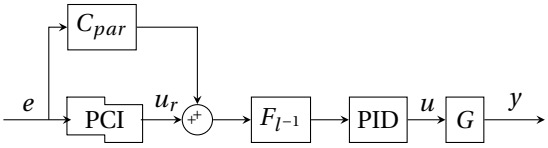

Figure 10.9: Parallel CR PCI-PID block diagram.

analysis methods presented in Section 10.2, the parallel CR architecture must be able to be represented using (10.1). It is possible to describe a reset system $\mathscr{R}$ in parallel with

C_{par}, as given in Fig. 10.9, by augmenting $\mathscr{R}$ and A_ρ as

$$\begin{aligned} A_r &= \begin{bmatrix} \hat{A}_r & 0 \\ 0 & A_{C_{par}} \end{bmatrix}, & B_r &= \begin{bmatrix} \hat{B}_r \\ B_{C_{par}} \end{bmatrix} \\ C_r &= \begin{bmatrix} \hat{C}_r & C_{C_{par}} \end{bmatrix}, & D_r &= \begin{bmatrix} \hat{D}_r + D_{C_{par}} \end{bmatrix} \\ A_\rho &= \begin{bmatrix} \hat{A}_\rho & 0 \\ 0 & I^{n_{C_{par}} \times n_{C_{par}}} \end{bmatrix}, & C_1 &= 1, \end{aligned} \tag{10.17}$$

with $\hat{A}_r, \hat{B}_r, \hat{C}_r, \hat{D}_r, \hat{A}_\rho$ the state-space matrices of the resetting part of $\mathscr{R}$ (e.g. a PCI) and $n_{C_{par}} \in \mathbb{Z}^+$ the number of states of C_{par}. Using this definition all theorems presented in Section 10.2 hold.

For a fully LTI system (i.e. $\mathscr{R} = R$), one can observe that the parallel CR architecture is equivalent to the series CR architecture when choosing $C_{par}(s) = R(s)\big(F_l(s) - 1\big)$. However, when resetting is introduced, this is no longer true. Therefore, in case $\mathscr{R}$ is a PCI, an approximation with

$$C_{par}(s) = \mathrm{PI}_{par}(s)\big(F_l(s) - 1\big), \mathrm{PI}_{par}(s) = 1 + \frac{\omega_{i_{par}}}{s}, \tag{10.18}$$

can be utilized instead. When $\mathscr{R} \neq R$, the open-loop SIDF is not identical to the equivalent system without CR, contrary to the conventional series CR architecture. This is confirmed in Fig. 10.10, where the PCI in series with CR_2 is compared to a parallel CR architecture with the same parameters, thus with $\omega_{i_{par}} = \omega_r$. For low frequencies the parallel CR structure approximates the series structure. For $\lim_{\omega\to 0} |C_{par}| = \frac{2\omega_{i_{par}}(\omega_t - \omega_d)}{\omega_d \omega_t}$, which is negligible compared to $\lim_{\omega\to 0} |\mathrm{PCI}| = \infty$. For $\lim_{\omega\to\infty} |C_{par}| = \frac{\omega_t^2 - \omega_d^2}{\omega_d^2}$, which is dominant over $\lim_{\omega\to\infty} |\mathrm{PCI}| = 1$. Since $\lim_{\omega\to\infty} |{F_l}^{-1}| = \left(\frac{\omega_d}{\omega_t}\right)^2$, for high frequencies the magnitude of the parallel architecture approaches $\frac{\omega_t^2 - \omega_d^2}{\omega_t^2}$. For low ω_d this is a good approximation for the series architecture, which instead approaches 1. However, in the mid-frequency range the parallel architecture has a smaller gain and lower phase. Furthermore, the HOSIDFs are also different between the two structures, with the parallel architecture having significantly lower HOSIDFs in the frequency range $\omega > \omega_d$. This is due to the fact that in a series CR architecture, the magnitude of the HOSIDFs depends on $|C_1(j\omega)|$, whereas in a parallel CR architecture it is not dependent on $|C_{par}(j\omega)|$, as it contributes only to the first harmonic. In fact, for a parallel CR system such as the one shown in Fig. 10.9, with $C_2 = F_l^{-1}\mathrm{PID}$, (10.9) becomes

$$\begin{aligned} u(t) = |C_{par}(j\omega)||C_2(j\omega)|\hat{e}\sin\big(\omega t + \varphi_e + \angle C_{par}(j\omega) + \\ \angle C_2(j\omega)\big) + \sum_{n=1}^{\infty} |H_n(\omega)||C_2(jn\omega)|\hat{e}\sin\big(n(\omega t + \varphi_e) + \\ \angle H_n(\omega) + \angle C_2(jn\omega)\big) \end{aligned} \tag{10.19}$$

Since the HOSIDFs in the parallel CR architecture are significantly lower than the series CR architecture in the range $\omega > \omega_d$, it allows for γ to be lowered while still maintaining lower HOSIDFs in the range of interest compared to a PCI-PID without CR. The effect of γ on the parallel CR architecture is portrayed in Fig. 10.12. The HOSIDFs increase over the entire frequency range, while the SIDF increases in the low- and mid-frequency range. The proposed tuning procedure for a parallel CR PCI-PID is thus as follows:

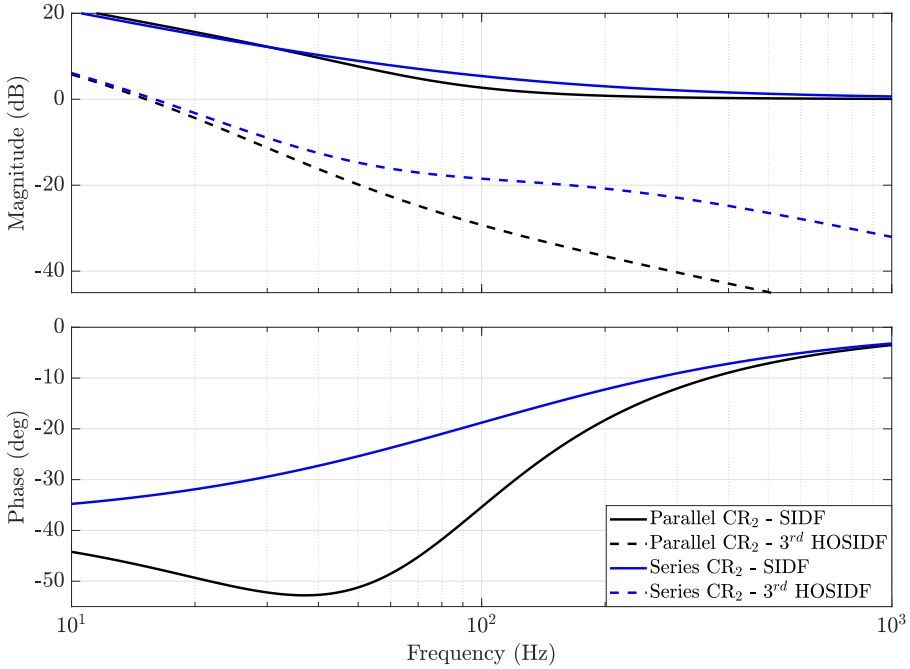

Figure 10.10: Magnitude and phase characteristics of the SIDF and 3rd harmonic of the PCI in the series CR_2 architecture and a parallel CR_2 architecture with $PI_{par} = R$, without the PID and plant.

Tuning Procedure 1 (Parallel CR PCI-PID)**.**

1. *Tune a series CR PCI-PID first according to [20]. Initially choose* $n_l = 1$.
2. *Choose* $\omega_{i_{par}} = \omega_r$ *as an initial guess and compute* C_{par} *using* (10.18).
3. *Transform the series CR PCI-PID into a parallel CR PCI-PID, by setting* $C_1 = 1$ *and adding* C_{par} *in parallel of* $\mathscr{R}$.
4. *Lower* γ *until the difference between the SIDF and the HOSIDFs (in dB) over the entire frequency range of interest (i.e. where expected disturbances are located) is the same or greater than with the series CR architecture.*
5. *Lower* $\omega_{i_{par}}$ *until the phase at* ω_{BW} *is the same as with the series CR architecture.*
6. *Adjust gain* k_p *to set the cross-over frequency at* ω_{BW}.
7. *In case the peak of the pseudo-sensitivity magnitude must be decreased further (i.e. it is higher than the acceptable level, e.g., 6 dB), return to step 5, however aiming at obtaining a higher phase at* ω_{BW}.
8. *In case the peak of the pseudo-sensitivity magnitude can be increased further (i.e. it is lower than the acceptable level, e.g., 6 dB), return to step 5, however aiming at obtaining a lower phase at* ω_{BW}.

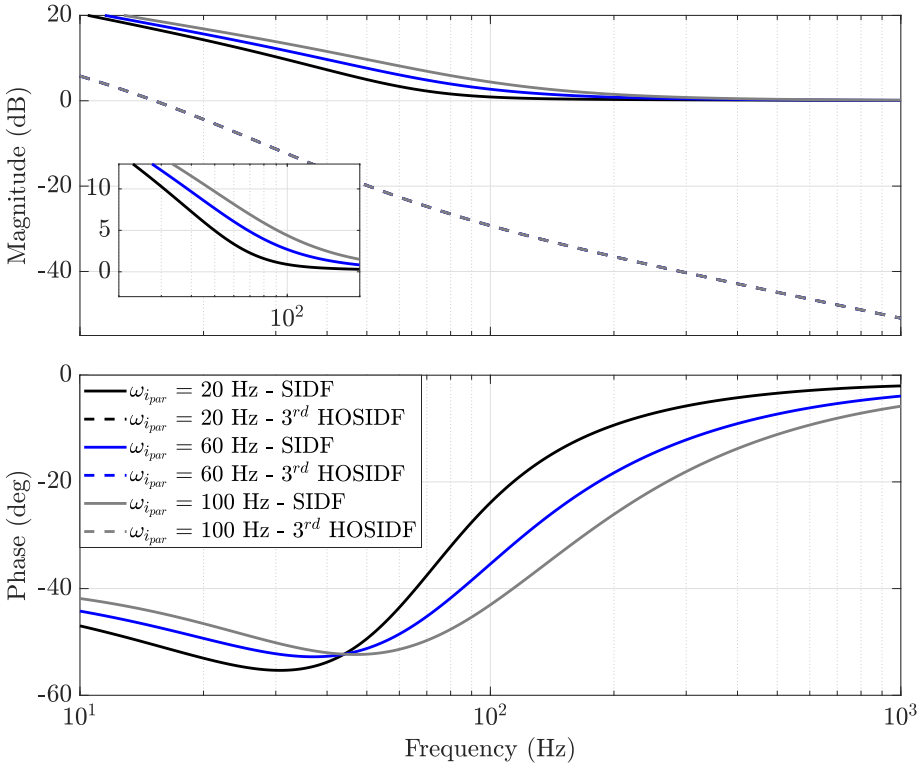

Figure 10.11: Magnitude and phase characteristics of the SIDF and 3$^{\text{rd}}$ harmonic of the PCI in the parallel CR$_2$ architecture for different values of $\omega_{i_{par}}$ without PID or a plant. All 3$^{\text{rd}}$ harmonics are identical and therefore plotted on top of each other.

9. *Increase n_l and repeat steps 2-8. Choose the controller whose pseudo-sensitivity results in the lowest gain at the desired frequency range.*

The tuning procedure was performed to convert the series CR$_2$ PCI-PID controller into a parallel CR controller. The gain was adjusted to keep the 200 Hz cross-over frequency such that $\omega_{i_{par}} = 30$ Hz and $\gamma = -0.3$ were found. The controller's SIDF and HOSIDFs are depicted in Fig. 10.13 where an LTI PI controller with the same phase at the cross-over frequency as the two CR PCI controllers is also shown. For the same phase margin and a greater difference between the first and 3$^{\text{rd}}$ harmonic in the range $\omega > 50$ Hz, the parallel CR PCI-PID achieves a greater SIDF gain in the low-frequency range. However, in the range [70, 200] Hz, the series CR architecture provides a slightly greater gain. Nevertheless, compared to the LTI system, the parallel CR system still has a larger gain. Furthermore at higher frequencies the series CR PCI has a slightly lower SIDF and thus provides better noise and disturbance suppression.

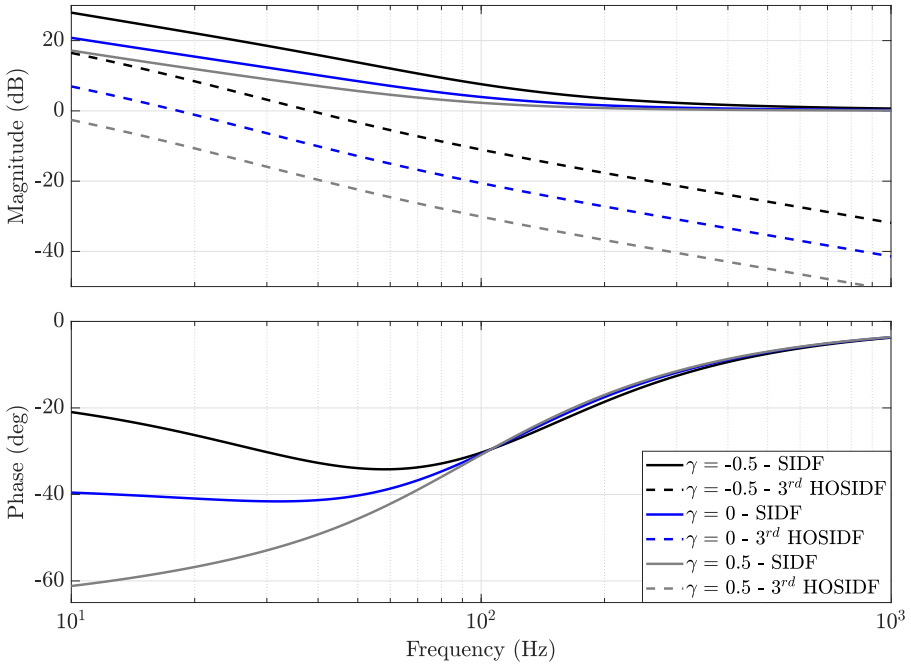

Figure 10.12: Magnitude and phase characteristics of the SIDF and 3$^{\text{rd}}$ harmonic of the PCI in the parallel CR$_2$ architecture for different values of γ, without PID or a plant.

10.5. PRACTICAL IMPLEMENTATION OF A RESET CONTROLLER

So far it was assumed that the reset controller acts in the continuous time domain. However, in reality a discrete time reset controller is implemented in the physical system. In order to describe the dynamics of a discrete time reset controller, (10.1) was modified to

$$\tilde{\mathscr{R}} = \begin{cases} x_{r_{k+1}} = \tilde{A}_r x_{r_k} + \tilde{B}_r e_{r_k}, & \text{if } (e_{r_k}, e_{r_{k-1}}) \notin \tilde{\mathscr{M}}, \\ x_{r_{k+1}} = \tilde{A}_r A_\rho x_{r_k} + \tilde{B}_r e_{r_k}, & \text{if } (e_{r_k}, e_{r_{k-1}}) \in \tilde{\mathscr{M}}, \\ u_{r_k} = \tilde{C}_r x_{r_k} + \tilde{D}_r e_{r_k}, & \text{if } (e_{r_k}, e_{r_{k-1}}) \notin \tilde{\mathscr{M}}, \\ u_{r_k} = \tilde{C}_r A_\rho x_{r_k} + \tilde{D}_r e_{r_k}, & \text{if } (e_{r_k}, e_{r_{k-1}}) \in \tilde{\mathscr{M}}, \end{cases} \tag{10.20}$$

with

$$\tilde{\mathscr{M}} := \{e_{r_k} e_{r_{k-1}} \leq 0\}, \tag{10.21}$$

where $\tilde{A}_r$, $\tilde{B}_r$, $\tilde{C}_r$, $\tilde{D}_r$ are the state-space matrices of the discretized BLS, and $k \in \mathbb{N}$ is the sample index. Resetting is based on the condition that e_r in the current sample changes sign compared to the previous sample, as in (10.21). Therefore, the sampling time imposes a time-regularization constraint, as in-between samples no resetting can occur. The condition is beneficial as it avoids the occurrence of Zenoness, a cause of ill-posedness, defined as the presence of infinite reset actions in a finite time [32].

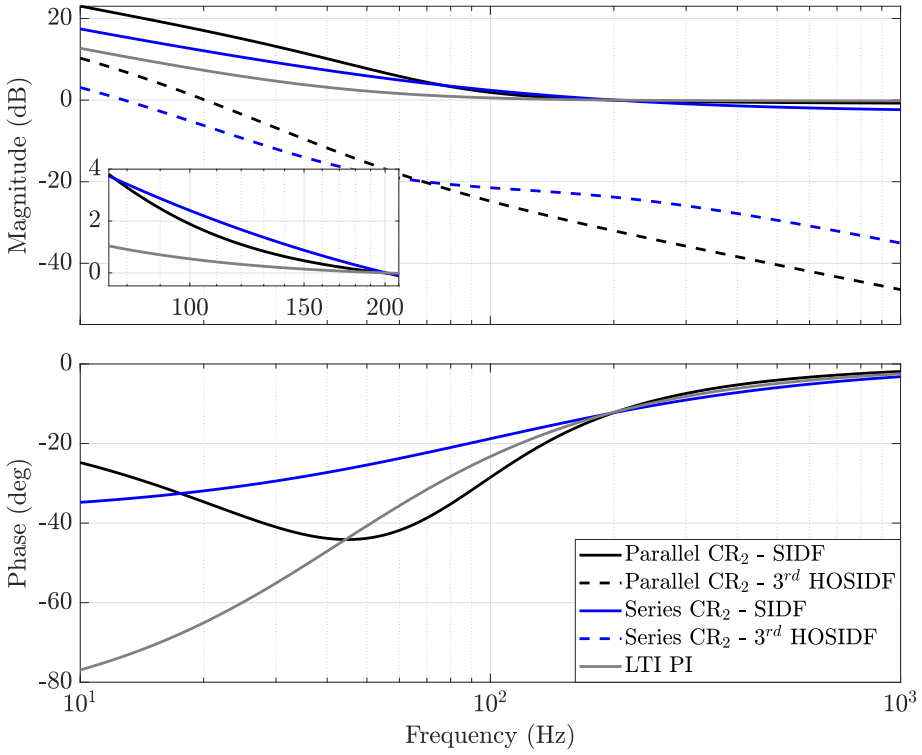

Figure 10.13: Magnitude and phase characteristics of the SIDF and the 3rd harmonic of the PCI in the series CR_2 architecture, a parallel CR_2 architecture with $\omega_{i_{par}} = 30$ Hz and $\gamma = -0.3$ as well as an LTI PI element with equivalent phase lag at 200 Hz.

10.6. EXPERIMENTAL SETUP AND RESULTS

10.6.1. EXPERIMENTAL SETUP

To experimentally validate the results obtained in this work, the isolated motion stage of a wire-bonding machine (Figure 10.14a, Figure 10.14b) is utilized. The wire bonder's motion platform is subdivided into an X-, a Y- and a Z-stage, allowing the end-effector to translate in three degrees of freedom. The positions of the three stages are measured by high-resolution optical encoders, resulting in low measurement noise levels compared with the error signals. The motion platform is designed and calibrated in such a manner that each motion axis can be assumed to be SISO LTI within its operating regime. In this work, only the X-stage is utilized, which represents the plant G in Fig. 10.1. The non-parametric plant model of the X-stage is given in Fig. 10.15, which shows the identified FRF from the actuator current that is applied to the X-stage to its measured encoder position. The FRF from the actuator of the Y-stage to the X-stage encoder position is also portrayed in the figure, which shows that the influence of cross-couplings can be neglected until beyond the aimed control bandwidth frequency. One can also observe

(a) (b)

Figure 10.14: (a) ASMPT wire bonder whose motion stage was utilized in this work. (b) Isolated XYZ-motion platform of the wire bonder.

that the system suffers from a transport delay, which limits the control system's bandwidth [33]. Due to confidentiality, the frequency-axis in the figure has been scaled by an arbitrary constant α.

Currently, SISO LTI feedback and feedforward control are employed to regulate the motion of each of the three stages. The feedforward controller ensures that errors during transient are reduced to acceptable levels. However, the base-frame that connects the stage to the ground is excited during motion, which results in undesired low-frequent disturbance forces that are acting on the system in steady-state. The resulting positioning error has to be compensated by means of feedback control. After the end of motion, high-precision wirebonding processes have to take place. By reducing the positioning error, these processes can start faster and wirebonding becomes more accurate. Therefore, improving the feedback controller is crucial for the system's overall performance.

10.6.2. EXPERIMENTAL RESULTS

An LTI PI-PID controller was tuned first using the tuning procedure from [34], which requires first selecting a bandwidth frequency ω_{BW} based on the plant's resonances and phase lag, as seen from its FRF (Fig. 10.15), and then assigning the PID parameters given in (10.14) based on rules of thumb. A PI was then added, which decreased the phase margin. This was recompensated by increasing the D-action, thus slightly decreasing ω_d and slightly increasing ω_t. A notch filter was also added to suppress plant's resonance. The PID parameters were adjusted until a high bandwidth and a peak of sensitivity of 6 dB were assured. The PI was then converted into a PCI. Due to the lower phase lag, it was

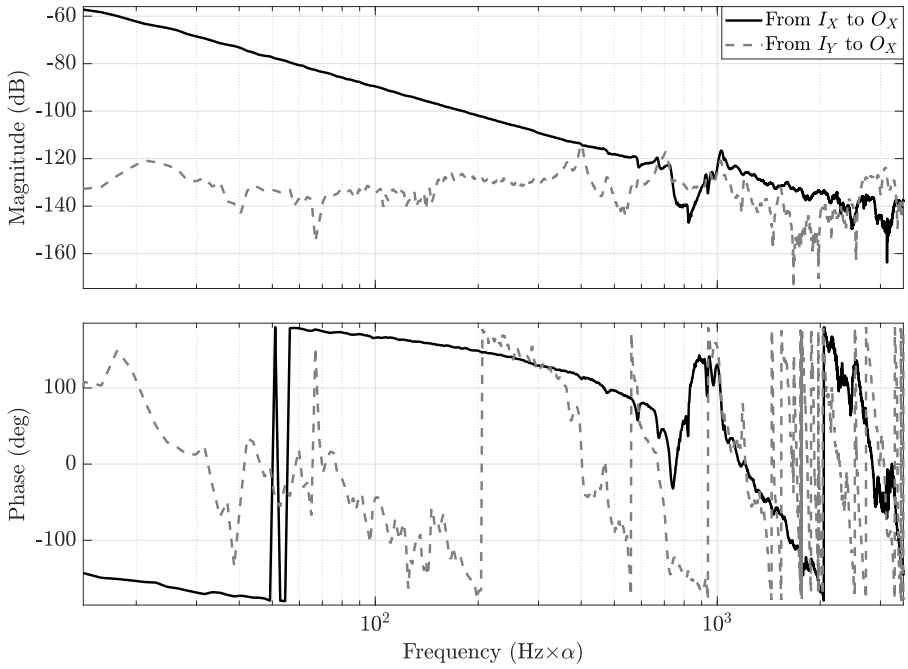

Figure 10.15: Identified FRF between X- (I_X) and Y-stages (I_Y) actuator current and X-stage encoder position (O_X) at the center position.

possible to increase the PCI's ω_i, thus the low frequency gain, without affecting the peak of sensitivity. A series CR PCI-PID was tuned next following the tuning procedure in [20]. It was then converted to a parallel CR PCI-PID using the tuning procedure in Tuning Procedure 1. The controllers' parameter values are not revealed due to confidentiality. The scaled open-loop FRF plots are portrayed in Fig. 10.16, whereas the respective magnitude plots of the pseudo-sensitivities, computed through the approximate method, are plotted in Fig. 10.17. It can be appreciated that for the same magnitude-peak of the pseudo-sensitivity, all reset systems have greater open-loop gain at low frequencies compared to the LTI system. Moreover, as expected, the parallel CR system has a larger open-loop magnitude compared to the respective series CR systems with the same F_l. However, for the case without CR the larger open-loop gain – compared to the LTI system – does not translate into a lower magnitude of the pseudo-sensitivitiy in a part of the low-frequency range. This is caused by the excitation of higher-order harmonics, and as expected, is reduced significantly by utilizing the series CR architecture. By utilizing the parallel CR system the magnitude of the pseudo-sensitivity can be lowered even further compared to the series CR architecture. Nevertheless, in a certain range before ω_{BW}, the magnitude of pseudo-sensitivities of the system controlled by the parallel CR PCI-PID is higher compared to the system controlled by the respective series CR PCI-PID. This is related to the trade-off of the magnitude of parallel CR architecture in the mid-frequency range already mentioned in Section 10.4.

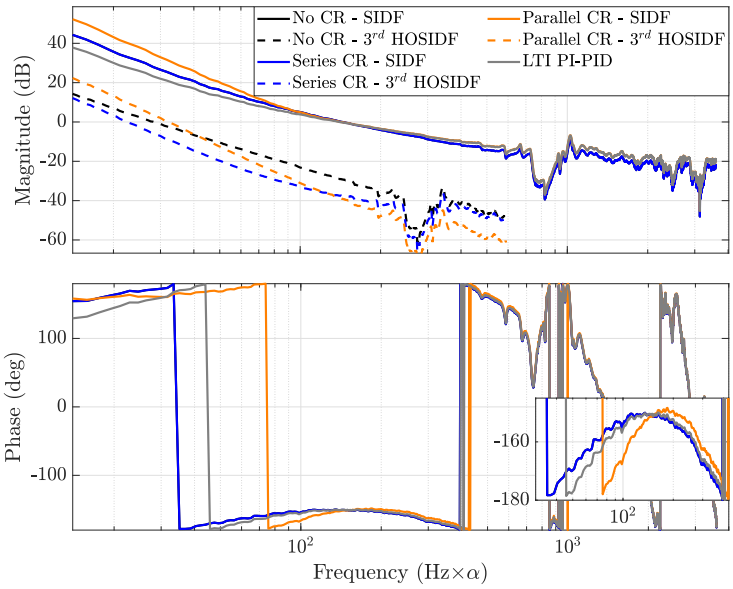

Figure 10.16: Magnitude and phase characteristics of the SIDF and 3rd harmonic of the open-loop system with the wire bonder's X-stage (at the center position) as the plant and different reset control structures. The SIDFs of the series CR and No CR PCI-PID are identical and therefore plotted on top of each other.

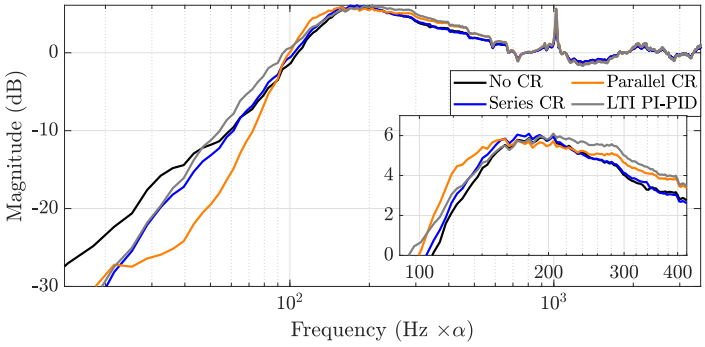

Figure 10.17: Magnitude characteristics of the pseudo-sensitivities for the closed-loop system (Fig. 10.1) with the wire bonder's X-stage (at the center position) as the plant and different reset control structures.

The scaled resulting error signals, for a typical reference trajectory, are portrayed in Fig. 10.18. The reference trajectory consists of a smooth forward and backward move from 0 to r_{max} and from r_{max} back to 0, which primarily contains energy below the control bandwidth frequency. Fig. 10.18 also shows the CPSDs of the error signal in the steady-state phase. This phase is defined as the period between sample $k_{set} \in \mathbb{N}$, the sample at which the reference signal reaches 0 after the backward move and the final sample. The Root-Mean-

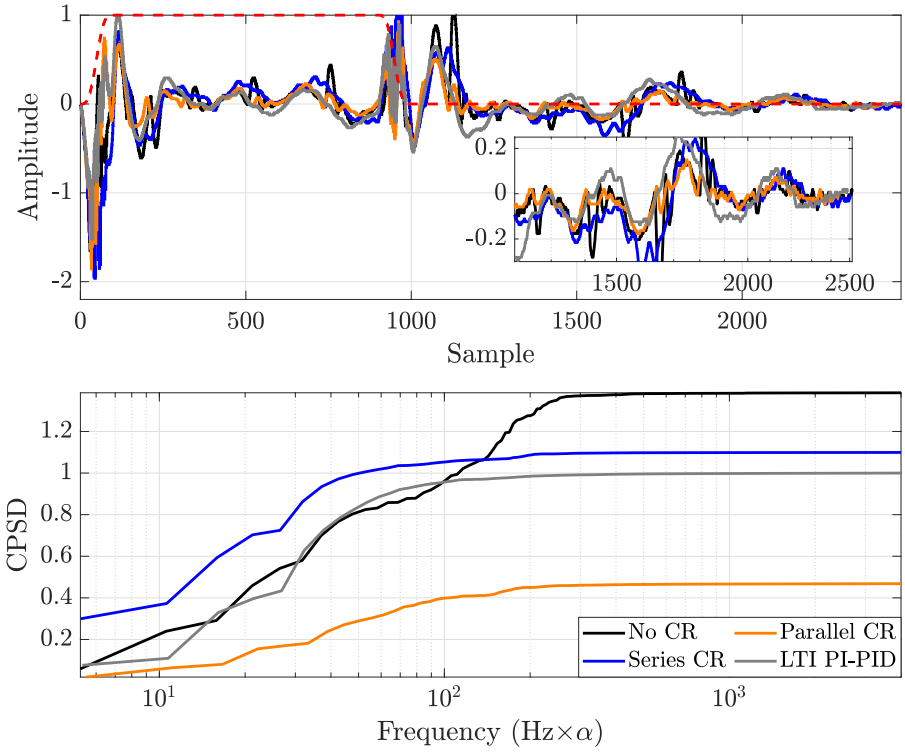

Figure 10.18: Normalized error signals and CPSDs of the steady-state phase obtained from experiments for a typical reference trajectory (the reference is scaled).

Square (RMS) of the steady-state phase of the error, is defined as

$$e_{RMS} = \sqrt{\frac{1}{1+k_n-k_{set}}\left(\sum_{k=k_{set}}^{k_n} e_k^2\right)}, \tag{10.22}$$

where $k_n \in \mathbb{N}$ is the total number of samples. The resulting RMS errors, normalized with respect to the e_{RMS} resulting from the LTI PI-PID system, are given in Table 10.2. The PCI-PID system without CR has a greater e_{RMS} than the fully LTI system due to the prevalence of HOSIDFs. This is accounted for partially using the series CR architecture which shows significantly lower power in the higher frequencies. However, at the same time it results in increased power at the first harmonic. This shows that the noise present in the system is amplified by this architecture to the point where performance deteriorates. Finally, the highest suppression of the first harmonic is achieved by the parallel CR structure. The parallel CR architectures reduces the steady-state RMS error by 32% compared to the LTI system.

Remark 15. *The feedback control output that is generated by reset controllers can in some cases be significantly larger than for an LTI controller [20], which can potentially lead to actuator saturation. However, note that in this application the feedforward controller*

Table 10.2: Normalized e_{RMS} obtained in experiments with different controller structures.

	No CR	series CR	parallel CR	LTI
e_{RMS}	1.1763	1.0491	0.6839	1

takes up the majority of the control output. Therefore, the control effort that is desired by the reset controller is not an issue.

10.7. CONCLUSION

In this work, a novel parallel CR architecture is developed. Furthermore, tuning guidelines for a parallel CR PCI-PID controller, based on loopshaping, are presented. These are obtained by employing open- and closed-loop HOSIDFs as a frequency-domain based steady-state performance-prediction tool. The parallel CR architecture allows to overcome a practical limitation of the existing series CR architecture: high-frequency noise amplification. This is achieved by avoiding using a lead filter before the reset element as in the series CR architecture, which causes amplification of the high-frequent power content in the error signal.

The findings are validated through experiments, consisting of tracking a typical reference signal on a wirebonding machine, in presence of both feedforward and feedback control. The PCI-PID system without CR architecture shows how the systems main disturbance is suppressed more effectively compared to a PI-PID system with the same bandwidth and peak of (pseudo)sensitivity. However, excitation of higher order harmonics of the disturbance frequency led to a significant decrease in performance. The series CR PCI-PID demonstrated its effectiveness at lowering the excitation of higher order harmonics. However, it shows an overall worse performance compared to the LTI PI-PID system, evidencing that when tuned inappropriately the noise can cause significant performance degradation in systems employing the series CR architecture. The parallel CR architecture achieves the best performance, with a 32% reduction in the RMS of the steady-state error when compared to the LTI PI-PID controller.

Although this work highlights the potential of the parallel CR architecture, it should be noted that existing stability analysis tools that apply to parallel CR systems, such as the classical H_β-condition, require a parametric plant description. Recently, the so-called Nyquist Stability Vector (NSV) [11] method has been proposed for some types of reset systems that are similar to the ones containing a parallel CR architecture. This method is equivalent to the H_β-condition but also allows to use a non-parametric plant description (FRF). A recommendation for future work is thus to augment the NSV method to include the parallel CR architecture. In fact, an augmented NSV method for a reset element with a similar structure as (10.17), was already presented in [11]. A further limitation in the design of reset controllers is given by the assumptions required to use the approximate method to compute pseudo-sensitivities (Theorem 14). Especially when HOSIDFs are high, the method can result in inaccurate results. For this reason, it would be beneficial to improve the current method in future works. Finally, it is of particular interest to study the transient performance of the proposed control architecture in more detail.

BIBLIOGRAPHY

[1] S. B. Joseph, E. G. Dada, A. Abidemi, D. O. Oyewola, and B. M. Khammas, "Metaheuristic algorithms for pid controller parameters tuning: Review, approaches and open problems", *Heliyon*, vol. 8, no. 5, e09399, 2022, ISSN: 2405-8440.

[2] K. Åström and R. Murray, *Feedback Systems: An Introduction for Scientists and Engineers*. Princeton University Press, 2010, ISBN: 9781400828739.

[3] H. W. Bode, *Network analysis and feedback amplifier design*. Van Nostrand, 1945.

[4] S. Skogestad and I. Postlethwaite, *Multivariable feedback control: Analysis and Design*. John Wiley, 2005.

[5] D. van Dinther, B. Sharif, S. J. A. M. van den Eijnden, H. Nijmeijer, M. F. Heertjes, and W. P. M. H. Heemels, "Overcoming performance limitations of linear control with hybrid integrator-gain systems", *IFAC-PapersOnLine*, vol. 54, no. 5, pp. 289–294, 2021, 7th IFAC Conference on Analysis and Design of Hybrid Systems ADHS 2021.

[6] G. Zhao, D. Nešić, Y. Tan, and C. Hua, "Overcoming overshoot performance limitations of linear systems with reset control", *Automatica*, vol. 101, pp. 27–35, 2019.

[7] B. G. B. Hunnekens, N. van de Wouw, and D. Nešić, "Overcoming a fundamental time-domain performance limitation by nonlinear control", *Automatica*, vol. 67, pp. 277–281, 2016.

[8] K. Åström and T. Hägglund, "The future of pid control", *Control Engineering Practice*, vol. 9, no. 11, pp. 1163–1175, 2001.

[9] M. Heertjes and M. Steinbuch, "Stability and performance of a variable gain controller with application to a dvd storage drive", *Automatica*, vol. 40, no. 4, pp. 591–602, 2004.

[10] N. Saikumar, K. Heinen, and S. H. HosseinNia, "Loop-shaping for reset control systems: A higher-order sinusoidal-input describing functions approach", *Control Engineering Practice*, vol. 111, p. 104 808, 2021.

[11] A. A. Dastjerdi, "Frequency-domain analysis of "constant in gain lead in phase (cglp)" reset compensators", Ph.D. dissertation, Delft University of Technology, 2021.

[12] L. F. van Eijk, S. Beer, R. M. J. van Es, D. Kostić, and H. Nijmeijer, "Frequency-domain properties of the hybrid integrator-gain system and its application as a nonlinear lag filter", *IEEE Transactions on Control Systems Technology*, vol. 31, no. 2, pp. 905–912, 2023.

[13] V. Utkin and A. Poznyak, "Adaptive sliding mode control", in *Advances in Sliding Mode Control*, Springer, 2013.

[14] J. C. Clegg, "A nonlinear integrator for servomechanisms", *Transactions of the American Institute of Electrical Engineers, Part II: Applications and Industry*, vol. 77, no. 1, pp. 41–42, 1958.

[15] Y. Chait and C. V. Hollot, "On horowitz's contributions to reset control", *International Journal of Robust and Nonlinear Control*, vol. 12, no. 4, pp. 335–355, 2002.

[16] N. Saikumar, R. K. Sinha, and S. H. HosseinNia, ""constant in gain lead in phase" element– application in precision motion control", *IEEE/ASME Transactions on Mechatronics*, vol. 24, no. 3, pp. 1176–1185, 2019.

[17] N. Karbasizadeh, N. Saikumar, and S. Hossein Nia Kani, "Fractional-order single state reset element", *Nonlinear Dynamics*, vol. 104, no. 1, pp. 413–427, 2021.

[18] N. Karbasizadeh, A. A. Dastjerdi, N. Saikumar, and S. H. HosseinNia, "Band-passing nonlinearity in reset elements", *IEEE Transactions on Control Systems Technology*, vol. 31, no. 1, pp. 333–343, 2023.

[19] E. Akyüz, N. Saikumar, and S. H. HosseinNia, "Reset control for vibration disturbance rejection", *IFAC-PapersOnLine*, vol. 52, no. 15, pp. 525–530, 2019.

[20] N. Karbasizadeh and S. H. HosseinNia, "Continuous reset element: Transient and steady-state analysis for precision motion systems", *Control Engineering Practice*, vol. 126, p. 105 232, 2022.

[21] L. Zaccarian, D. Nesic, and A. Teel, "First order reset elements and the clegg integrator revisited", in *Proceedings of the American Control Conference*, vol. 1, 2005, pp. 563–568.

[22] J. A. G. Prieto, A. Barreiro, and S. Dormido, "Frequency domain properties of reset systems with multiple reset anticipations", *IET Control Theory & Applications*, vol. 7, no. 6, pp. 796–809, 2013.

[23] Y. Guo, Y. Wang, and L. Xie, "Frequency-domain properties of reset systems with application in hard-disk-drive systems", *IEEE Transactions on Control Systems Technology*, vol. 17, no. 6, pp. 1446–1453, 2009.

[24] P. Nuij, O. Bosgra, and M. Steinbuch, "Higher-order sinusoidal input describing functions for the analysis of non-linear systems with harmonic responses", *Mechanical Systems and Signal Processing*, vol. 20, no. 8, pp. 1883–1904, 2006.

[25] M. Vidyasagar, *Nonlinear Systems Analysis (2nd Ed.)* Prentice-Hall, Inc., 1993.

[26] D. Rijlaarsdam, P. Nuij, J. Schoukens, and M. Steinbuch, "A comparative overview of frequency domain methods for nonlinear systems", *Mechatronics*, vol. 42, pp. 11–24, 2017.

[27] N. Saikumar, K. Heinen, and S. H. HosseinNia, "Corrigendum to "loop-shaping for reset control systems: A higher-order sinusoidal-input describing functions approach" [control engineering practice 111 (2021) 104808]", *Control Engineering Practice*, vol. 137, p. 105 565, 2023.

[28] A. A. Dastjerdi, A. Astolfi, N. Saikumar, N. Karbasizadeh, D. Valério, and S. H. HosseinNia, "Closed-loop frequency analysis of reset control systems", *IEEE Transactions on Automatic Control*, vol. 68, no. 2, pp. 1146–1153, 2023.

[29] A. A. Dastjerdi, N. Saikumar, and S. HosseinNia, "Tuning of a class of reset elements using pseudo-sensitivities", in *European Control Conference (ECC)*, 2021, pp. 1187–1192.

[30] A. Barreiro, A. Baños, S. Dormido, and J. A. González-Prieto, "Reset control systems with reset band: Well-posedness, limit cycles and stability analysis", *Systems and Control Letters*, vol. 63, pp. 1–11, 2014.

[31] O. Beker, "Analysis of reset control systems", Ph.D. dissertation, University of Massachusetts Amherst, 2001.

[32] A. Baños and A. Barreiro, *Reset Control Systems*. Springer, Oct. 2012, vol. 9.

[33] L. van Eijk, *Nonlinear motion control designs and performance evaluation on an industrial motion stage*, Master's Thesis, Eindhoven University of Technology, 2021.

[34] R. Munnig Schmidt, G. Schitter, and J. van Eijk, *The design of high performance mechatronics. High-tech functionality by multidisciplinary system integration.* Netherlands: IOS Press, 2011.

11

CONCLUSION

The main objective in this dissertation was to shape non-linearities in order to realise complex-order controllers and specifically having application in precision motion control in mind. In pursuit of this objective, different methods were presented as research questions, and each chapter not only has tried to answer these questions but has also explored various aspects of reset control and a number of contributions have been made in the field of reset control for linear time-invariant systems.

One of the keywords repeated in this dissertation was the waterbed effect, which was mentioned to be inherent for linear control systems. Either this dissertation could break or overcome this limitation needs further discussion. The answer to the question of breaking the waterbed effect is no. The explanation is rather straightforward, reset control in specific and nonlinear controllers in general cannot be represented fully in frequency domain; one can only make an approximation. Therefore, the Bode's sensitivity integral cannot be defined for them, and thus there will be no waterbed effect to begin with. Leaving this mathematical point of view aside, this dissertation looked from the mechatronics point of view into the question and interpreted the waterbed effect in terms of practical limitations for linear control systems. Making approximations in frequency domains using HOSIDF and pseudo-sensitivity techniques or focusing on the trade-off of transient and steady-state response, this dissertation introduced systematic approaches to design nonlinear controllers which can over-perform the linear controllers which are bound by waterbed effect.

Throughout the dissertation it was shown that reset controllers have a first-order harmonic behaviour which can be very favorable to create complex-order behaviour and improve the performance of the controller with respect to the linear controllers. However, the dissertation showed that higher-order harmonics as a direct result of nonlinearity have a significant role in reset control systems and cannot be neglected. However, they can be shaped to our benefit.

Chapter 2 explored the possibility of augmenting the reset state in a Clegg integrator and showed in a clear example that it is feasible to shape the higher-order harmonics of the reset controller while trying to keep the favorable first-order harmonic intact. Although the chapter itself used optimisation to tune the parameters of augmented controller, the observed results put a foundation for further steps toward understanding the reset elements shaping higher-order harmonics for better performance. Another important observation was that better performance was achieved when the latter states were more linear (γ closer to 1), which indicates that a lag element after a reset element can improve performance by reducing the higher-order harmonics in amplitude. The main disadvantage of this approach besides using optimisation instead of an analytic method was the presence of multiple resetting states in series. Resetting these series states specifically makes the analysis much harder.

The approaches used in the subsequent chapters to shape the nonlinearity of reset control systems can be categorized into two categories.
The first approach was to use the concept of ψ, i.e., the linear domain phase difference between the output of the reset element and the signal that determines the resets. By defining this phase difference, a clear understanding was achieved regarding how the reset elements behave and how by manipulating and shaping ψ, the nonlinearity can be shaped.

Chapter 3 showed a method for shaping ψ and consequently higher-order harmonics. It showed that when ψ crosses zero, all higher-order harmonics will be zero and thus the reset element behaves linearly in a specific frequency. FOSRE, the element proposed in this chapter, used a fractional-order lag element in combination with a reset integrator to do so. Comparison of the FOSRE CgLp with conventional CgLp clearly showed improvement in terms of steady-state precision. The concept of shaping ψ in this chapter was solely focused on zero-crossings of ψ and tuning the frequency of linear behaviour. Chapter 4, also not only falls under the category of ψ-shaping methods, but also provides a comprehensive framework for analysing and utilizing this concept in a simpler architecture. In this architecture, the inner feedback loop of the FOSRE is not present, which gives more freedom in design and makes the implementation easier. Using the method provided in this chapter, the higher-order harmonics can be suppressed in a desired range instead of a single frequency. Keeping ("band-passing") the nonlinearity to the bandwidth region, steady-state performance could be further improved. The main contribution of this chapter was the systematic method in shaping ψ.

In Chapter 5, the main contribution is providing a method based on the concept of shaping ψ to desired non-flat positive phase slopes around bandwidth region which provides another step in realization of the complex-order controller. This addition to the previous chapter also came with a different implementation; instead of using a pre- and post-filer for reset element, a filter was added on the reset line. In this architecture, the noise filtering from the reset line and the ψ-shaping can be done using one filter.
The second category of approaches was called "Continuous Reset". The subsequent chapters fell under this category. The main differences with the ψ-shaping method can

be categorized into transient and steady state.

Firstly, the ψ-shaping method focuses on steady-state performance and lacks an approach to improve the transient response. Although in many precision motion applications, feed-forward controller takes care of the transient and not much is left for feedback to deal with, improving transient response of feedback controller can still be useful in some applications. CR had a clear advantage here and it was achieved by introducing a lead element as a pre-filter for reset element.

Secondly, there was also a difference in terms of steady-state performance, the ψ-shaping approach was to confine the nonlinearity to a specific range and thus change the first-order harmonic behaviour of the reset element outside the range. However, it was proven in Chapter 6 that, using the CR approach, the first-order harmonic remains completely intact and the higher-order harmonics are reduced in the whole range of frequencies. However, they will not be zero unless ψ is shaped to cross zero. This makes the choice between the methods an application-based decision.

Chapter 6 also showed the reason for naming this approach as it showed that using a lag element as a post-filter not only reduces the higher-order harmonics but also makes the output of the reset element continuous as opposed to conventional reset elements. This was shown to have benefits in terms of practical implementation of the controller.

The waterbed effect can also be seen as a trade-off between transient and steady-state performance, using the CR method; both can be improved to the point that a non-overshoot performance could be achieved with 4 stacked integrators. This was seen in Chapter 7, while comparing to the linear counterparts, the overshoot increased with each stacked integrator. Especially in precision motion control, the necessity of the demand for having higher gains at lower frequencies is increasing and this chapter showed a way forward for dealing with the drawbacks associated with it.

The analytical approach in studying the transient response of the reset controllers is very complex and complexity grows with the number of states in the system. However, such an analysis even for a simple system can guide the way towards better understanding. Chapter 8, served this purpose by investigating the underlying mechanics of the improved transient response in CR architectures.

The main drawback in architecture presented in Chapter 6 was noise. Introduction of the lead element as a pre-filter of the reset element will amplify the high-frequency constant of the signal and create excessive unnecessary rest instants that can deteriorate the performance of the controller.

Chapter 9 proposed two approaches to serve this end. In both of them the architecture was conserved and the problem was mitigated by either increasing the order of the lead and lag elements serving as pre- and post-filter or using an observer-based filter to filter the reset line. The chapter also proposed an analytical framework to study the

deterioration of performance due to model inaccuracy of the observer used for filtering the reset line in open loop.

As previously mentioned in the current chapter, the transient response is not necessarily important for all precision motion applications because of the presence of the feedforward controller. The CR approach significantly benefits us in steady-state performance. Chapter 10 introduced a parallel architecture in which the lead pre-filter was moved to a parallel branch, solving the noise amplification by removing its root cause. This will deprive us of the transient performance improvement of the CR but still the continuity of steady-state precision improvements remains. Chapter 10 also illustrated the results of implementation of the proposed CR controller in an industrial precision motion stage and showed the superiority of it over its linear counterparts.

Looking back at all of the chapters of this dissertation, first and foremost a clearer and better understanding of how reset elements work was achieved. Higher-order harmonics were seen to play a very important role in the performance of these elements and cannot be neglected. The complex-order behaviour of first-order harmonics of reset elements can only be helpful if one takes into account the higher-order harmonics and design based on them. The principles of such a design were introduced. It was shown that the nonlinearity of the reset elements can be shaped. This shaping can be utilized to provide significant improvements in terms of steady-state and transient responses of reset controllers. Many of the architectures were implemented in practice, and the practicality of their implementation was shown. However, depending on the application, one may surpass the others. Choosing between the multiple architectures presented in this dissertation is heavily application-dependent. However, this dissertation tried to present an understanding and guidelines to choose one.

Although this dissertation showed the great potential of reset controllers, there are some areas that were not touched upon and can be interesting topics for future research. All reset control systems studied in this dissertation were satisfying the H_β stability criteria. This essentially means that the Lyapunov defined for them was decreasing during the linear regime and also at reset instants. But it is known that H_β condition is conservative. Reset control systems with an unstable base linear system can also be stable if the decrease of Lyapunov function at reset instants makes the overall Lyapunov function decrease. Or the other way around, if the decrease of the Lyapunov function in linear regime compensates the jump of the Lyapunov function at reset instants, the overall reset control system will be stable. The performance study of the latter two types of reset control systems can be an interesting topic for investigation.

The study of the reset control systems in this dissertation was done in continuous time. Practical implementation examples of this dissertation were done in discrete time, like almost all of the controllers in the industry. However, the impact of discretisation on stability and performance is not present, as it was assumed that the sampling frequency is large enough to make this impact negligible. Although this is common practice in linear control, a more in-depth study for reset control systems can be worthwhile.

The last suggestion can be towards the MIMO systems. The investigation in this dissertation focused on SISO systems. The study in Chapter 10 showed that even the reset controller that was designed and studied from the SISO point of view showed a significant performance improvement on a stage suffering from coupling of degrees of freedom. However, this example was indication that in industry most of the systems are MIMO and continuation of this research with MIMO focus can be beneficial for industrial applications.

ACKNOWLEDGEMENTS

As I look back at the pages of this dissertation, my heart overflows with gratitude and emotion. It is impossible to find the right words to show the depth of appreciation I feel for the extraordinary individuals who have been my pillars of strength, guiding lights, and sources of love and support throughout this academic voyage.

Hassan, you've been more than a supervisor; you've been a friend. Your kindness, endless energy, and your talent for generating brilliant ideas, along with your constructive criticism, have played a pivotal role in shaping not just this dissertation or me as a researcher, but also my growth as a person. From the first moment we met in person at 9:00, on 3 December 2018, until now through all the coffees we had together, all the friendly chats and scientific discussions, and all the fun moments we had, you showed me that being a successful person is not only about hard work, but savouring every moment of life. I am truly indebted to you. I wish you best of luck next to **Elaheh**.

And **Just**, your kindness, openness, and profound wisdom have been a guiding light on this path to its end. Born of years of dedicated research and scholarship, your views enriched my understanding and sharpened my critical thinking. Your presence has been instrumental, and I want to express my deepest gratitude for your invaluable contributions to my academic growth.

Throughout the course of this research, I had the privilege of collaborating with a group of exceptional fellow researchers who shared this journey with me: **Ali, Niranjan, Duarte, Marcin, Xinxin** and **Luke**. Your invaluable insights and contributions are an integral part of this research. In every sense, this dissertation is also yours.

I also want to acknowledge and appreciate the contributions of the user committee members of the CLOC project because the valuable insights they provided.

During four years of my PhD I enjoyed coaching eight master students. **Daniel, Tiis, Mees, Aldo, Dennis, Shrinath, Mohammed,** and **Tingting**, it was my first experience of coaching and leading a scientific team, through our interaction you taught me how to be a better one. I am proud of your efforts. I have to specifically recognize and appreciate **Daniel, Tiis, Mees,** and **Aldo**, since you contributed directly to this dissertation.

The PhD journey is often seen as a solo job, where you tackle a complex project and strive to become an independent researcher. Just like any adventure, there are moments of pure joy and satisfaction when you solve a challenges or have that eureka moment. These moments truly make you feel alive. However, as with any journey, there are also challenges to face. There are times of stress, disappointment, feeling lost, and frustration. Fortunately, I had the incredible support of my fellow PhD and postdoc colleagues – **Ali Amooz, Saleh, Ad, Malte, Jelle, Francesco, Dave, Marcin, Abdullah,** and **Xixin**. You all created such a positive and supportive environment, and I'm truly grateful for that.

Ali Amooz, I want to take a moment to single you out from our amazing colleagues. You were not just a colleague to me; we shared a unique bond sitting side by side for three years. It was a true privilege to be able to converse in Persian with you, as there's nothing

quite like expressing oneself in their mother tongue.

Receiving admission to a PhD program at TUDelft wouldn't have been possible without the guidance of my master's supervisor, **Mehdi Tale Masouleh**. You led me through my initial research project and taught me how to write scientific papers. You probably can see some of your writing style in the text of this dissertation! More importantly, you showed me the persistence and hard work required in academia. It was truly an honor to be your student.

One of the most profound lessons I gained throughout my PhD journey was that it's not just about acquiring knowledge in a specific field but also about personal growth, developing character, and nurturing independent thinking and judgment. **Farshid** and **Soroush**, our regular trilateral discussions played a pivotal role in shaping my perspective of the incredible world we live in. It is not a long time that I know you **Soheib**, but you already made your mark, by showing to me that it is never late for new experiences.

I embarked on my PhD journey as an immigrant, and immigration itself is a significant challenge. Integration becomes essential, and it all begins with learning the language. **Tiny** and **René**, you graciously opened your home to us and dedicated countless hours to help us learn Dutch and integrate into Dutch society. To Delaram and me, you've become far more than just "taalmaatjes". Nogmaals bedankt voor jullie liefde!

Soheib & Mojdeh, Farshid & Sepideh, Mostafa & Zahra, Saeed & Mahsa, Erfan, Fatima & Mandana, Milad, Shokoufeh & Niki, Majid & Shabnam, Ali & Shahrzad, Ali, Azar & Amirali, Saleh & Mahnaz, Pooyan & Masoumeh and **Ramin**, I cannot write individually about these names, for that would require another book in itself, I want to convey that simply mentioning your names is a way of saying that you made me feel truly at home. We shared numerous joyful moments, and each and every one of you holds a special place in my heart.

Beyond the academic sphere, I am grateful for the support and love I've received from my in-laws, **Marzieh**, **Hossein**, **Shakiba**, and **Ali**. Your warmth and acceptance have made me feel like a part of the family from the very beginning. Your encouragement has been a source of strength. The moments we've shared together, whether celebrating milestones or simply enjoying each other's company, have created cherished memories that I will hold dear.

Vajiheh, I want to to express my deep gratitude for the significant role you've played in shaping my educational path. From the time I was just a child, you recognized my curiosity. I'll never forget how you introduced me to those fun educational games that sparked my fascination with electronics or the moments during my junior high school years, when we sat to solve optics homeworks together. Your constant encouragement during my education and academic pursuits, has been a driving force for me. Your influence has left an enduring mark on my journey.

Turning to my parents **Hamidreza** and **Elaheh**, I am at a loss of words to express the depth of my feelings about them, as love can never be expressed in words.

چون قلم اندر نوشتن می‌شتافت

چون به عشق آمد قلم بر خود شکافت

Your continuous concern for my future and success your unceasing encouragement for higher education have been nothing short of extraordinary. Your presence alone has been the cornerstone upon which I've built my life. It's clear to me that your sole dream has always been the success and happiness of me, **Sina** and **Parsa**. I can't begin to imagine how you sacrificed so selflessly over the years. Your love and dedication in making that dream a reality have shaped who I am today.
Sina and **Parsa**, we grew up together, remember that I always care about you. I wish that the determination you have makes you successful and happy in your lives as your hapiness fills my heart with joy.
I've saved this part for the end to to carefully craft my words for my love, friend and wife, **Delaram**. You are bold, determined, and courageous. You love breaking the fictional paradigms of the mind. This was what I loved the most about you. Together we put many bricks together to build a life. It is no secret that we are here because we were together. Every moment spent with you is a reminder of the depth of love and happiness you've brought into my life. I cherish every moment of it.

آن که دلارام دید از دلش آرام رفت
چشم ندارد خلاص آن که در این دام رفت

Nima Karbasizadeh
Rosmalen, September 2023

CURRICULUM VITÆ

Nima KARBASIZADEH ESFAHANI

23-12-1989 Born in Esfahan, Iran.

EDUCATION

2018–2023 **PhD.** in Mechatronic System Design
Department of Precision and Microsystems Engineering
Delft University of Technology, Delft, The Netherlands

Dissertation: Shaping Nonlinearity in Reset Control Systems to Realize Complex-Order Controllers

Promotors: Prof.dr.ir. J.L. Herder, Dr. S.H. HosseinNia

2014–2017 **M.Sc.** in Mechatronics Engineering
University of Tehran, Tehran, Iran

Thesis: Dynamic Identification and Model Feed-Forward Control of a Haptic Device and Design of a Virtual Environment for Dental Training

Supervisors: Dr. M. Tale Masouleh, Dr. A. Kalhor

2008–2013 **B.Sc.** in Mechanical Engineering
Isfahan University of Technology, Esfahan, Iran

EXPERIENCE

2022– present Mechatronics Engineer
ASML, Eindhoven, the Netherlands

2017–2018 Mechatronics Engineer
Tiam Networks, Tehran, Iran

AWARDS

2018 Top graduate student
Iran's Elites Foundation

List of Publications

Journal Publications

- D. Valério, N. Saikumar, A. A. Dastjerdi, **N. Karbasizadeh**, and S. H. HosseinNia, *"Reset control approximates complex order transfer functions,"* in Nonlinear Dynamics **97**, 2323-2337 (2019).
- **N. Karbasizadeh**, N. Saikumar, and S. H. HosseinNia, *"Fractional-order single state reset element,"* in Nonlinear Dynamics **104**, 413-427 (2021).
- **N. Karbasizadeh**, and S. H. HosseinNia, *"Continuous reset element: Transient and steady-state analysis for precision motion systems,"* in Control Engineering Practice **126**, 105232 (2022).
- **N. Karbasizadeh**, A. A. Dastjerdi, N. Saikumar, and S. H. HosseinNia, *"Band-Passing Nonlinearity in Reset Elements,"* in IEEE Transactions on Control Systems Technology **31**, 333-343 (2023).
- A. A. Dastjerdi, A. Astolfi, N. Saikumar, **N. Karbasizadeh**, D. Valério, and S. H. HosseinNia, *"Closed-Loop Frequency Analysis of Reset Control Systems,"* in IEEE Transactions on Automatic Control **68**, 1146-1153 (2023).
- D. Caporale, L. F. van Eijk, **N. Karbasizadeh**, S. Beer, D. Kostic, and S. H. HosseinNia, *"Practical Implementation of a Reset Controller to Improve Performance of an Industrial Motion Stage,"* in IEEE Transactions on Control Systems Technology *(Conditionally accepted for publication)*, (2023).
- **N. Karbasizadeh**, T. van der Werf, and S. H. HosseinNia, *"Improving the Noise Robustness of Continuous Reset Control Systems," (Under preparation for submission)*, (2023).
- M. Vanderbroeck, **N. Karbasizadeh**, and S. H. HosseinNia, *"Damping Analysis of Transient Response in Reset Control Systems: an Analytical Approach," (Under preparation for submission)*, (2023).

Conference Publications

- M. S. Bahnamiri, **N. Karbasizadeh**, A. A. Dastjerdi, N. Saikumar, and S. H. HosseinNia, *"Tuning of CgLp based reset controllers: Application in precision positioning systems,"* in 21st IFAC World Congress: Berlin, Germany, 8997-9004 (2020).

- **N. Karbasizadeh**, A. A. Dastjerdi, N. Saikumar, D. Valério, and S. H. HosseinNia, *"Benefiting from Linear Behaviour of a Nonlinear Reset-Based Element at Certain Frequencies,"* in Australian and New Zealand Control Conference (ANZCC), Gold Coast, QLD, Australia, 226-231 (2020).

- A. Sebastian, **N. Karbasizadeh**, N. Saikumar and S. H. HosseinNia, *"Augmented Fractional-order Reset Control: Application in Precision Mechatronics,"* in IEEE/ASME International Conference on Advanced Intelligent Mechatronics (AIM), Delft, Netherlands, 231-238 (2021).

- **N. Karbasizadeh**, and S. H. HosseinNia, *"Complex-order Reset Control System,"* in IEEE/ASME International Conference on Advanced Intelligent Mechatronics (AIM), Sapporo, Japan, 427-433 (2022).

- **N. Karbasizadeh**, and S. H. HosseinNia, *"Stacking Integrators Without Sacrificing the Overshoot in Reset Control Systems,"* in American Control Conference (ACC), Atlanta, GA, USA, 893-899 (2022).